

Mapping the Thermal Climate of the H. J. Andrews Experimental  
Forest, Oregon

by  
Jonathan W. Smith

A THESIS

submitted to

Oregon State University

in partial fulfillment of  
the requirements for the  
degree of

Master of Science

Presented April 23, 2002

Commencement June 2002

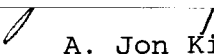
AN ABSTRACT FOR THE THESIS OF

Jonathan W. Smith for the degree of Master of Science in Geography presented on April 23, 2002.

Title: Mapping the Thermal Climate of the H. J. Andrews Experimental Forest, Oregon.

Signature redacted for privacy.

ABSTRACT APPROVED: \_\_\_\_\_

  
A. Jon Kimerling

The H. J. Andrews Experimental Forest in the Cascades of central Oregon provides a unique opportunity to study spatial climate patterns on a relatively small scale. Historical records at the 64 square-kilometer site provide a spatially-dense 30-year dataset. Thermal regimes at the H. J. Andrews are generally known but the effects of its complex topography and canopy cover on temperatures have been poorly understood. In this study, 1971-2000 mean monthly maximum and minimum temperature maps of the H. J. Andrews were created over a 50-meter grid, accounting for several environmental factors affecting microclimates in forested, mountainous terrain. The effects of elevation, forest canopy, cloudiness, and topographic shading on radiation regimes were assumed to be the primary factors and the datasets were adjusted to account for them. Specifically, it was assumed that maximum temperatures were affected by shortwave daytime radiation regimes, and minimum temperatures were affected by surface longwave radiation emission at night. The Image-Processing Workbench (IPW) was used to estimate incoming shortwave solar radiation at all climate station sites, taking into account

elevation, cloudiness and topographic shading. Using IPW, fisheye photographs, and the HemiView program, proportions of solar radiation and sky view factors blocked by the tree canopy were calculated at each site, and accounted for when calculating daily shortwave radiation values for each month. Sky view factors were calculated at each site accounting for canopy and surrounding topography. Specific site pairs were then analyzed by plotting observed monthly temperature differences against simulated radiation and sky view factors and computing monthly regression functions. Monthly maximum temperature/shortwave radiation regression functions were used to adjust maximum temperatures onto 'open, flat' terrain, (leaving only elevation effects on temperatures), and monthly minimum temperature/sky view factor regression functions were used to adjust minimum temperatures. Temperatures were spatially interpolated over the H. J. Andrews using the Parameter-elevation Regressions on Independent Slopes Model (PRISM) program, which calculates spatially-varying temperature/elevation gradients. Topographic effects of shortwave radiation and sky view factors were reintroduced to the PRISM temperature grids using the appropriate regression functions. To make the resulting maps as useful and applicable as possible for future research, temperatures were modeled to simulate open siting conditions common in NWS station networks. Overall, temperatures were most sensitive to elevation and topographic position. Maximum temperature was sensitive to variations in shortwave radiation, especially in winter when solar radiation loads were small. Minimum temperature was sensitive to variations in sky view factors, particularly during clear summer months. Factors not accounted for in the project include small-scale effects of cold-air drainage, forest edge effects, topographic scale

effects, and stream effects. These and other issues are summarized in a set of recommendations for future climate mapping research in the H. J. Andrews.

Master of Science thesis of Jonathan W. Smith presented on  
April 23, 2002.

APPROVED:

Signature redacted for privacy.

---

Major Professor, representing Geography

Signature redacted for privacy.

---

Head of the Department of Geosciences

---

Dean of the Graduate School

I understand that my thesis will become part of the permanent collection of Oregon State University libraries. My signature below authorizes release of my thesis to any reader upon request.

Signature redacted for privacy.

---

Jonathan W. Smith, Author

## ACKNOWLEDGMENTS

The author expresses sincere and heartfelt appreciation to Professor Christopher Daly for his technical expertise, positive attitude, and friendship. Professor Julia Jones provided ever-thoughtful input and motivation. Professors A. Jon Kimerling, Jones, and Daly all provided invaluable assistance in the preparation of this document. In addition, I also thank John Moreau of the H. J. Andrews LTER organization for his eternally positive attitude and never-ending assistance with field issues. Don Henshaw at the Forest Science Laboratory helped with the compilation of the datasets, for which I am grateful. David Garen at the USDA-NRCS National Water and Climate Center assisted greatly with the Image Processing Workbench. Amy Smith has been a constant loving source of support. This research was supported by National Science Foundation grant DEB-96-32921 (H. J. Andrews Long-term Ecological Research [LTER]).

## TABLE OF CONTENTS

	<u>Page</u>
1. INTRODUCTION .....	1
1.1 Overview and impetus behind the study .....	1
1.2 Goals and objectives .....	2
2. THE STUDY AREA .....	3
2.1 Description of the study area .....	3
2.2 Large-scale influences on H. J. Andrews climate .....	5
2.3 Small-scale influences on H. J. Andrews climate .....	6
3. BACKGROUND AND LITERATURE REVIEW .....	8
3.1 Elements of microclimate in mountainous terrain .....	8
3.1.1 General effects of topography .....	8
3.1.2 Radiation budgets of mountain microclimates .....	9
3.1.3 Vegetation effects on temperature regimes .....	11
3.1.4 Nocturnal temperature regimes in complex terrain .....	15
3.1.5 Modeling solar radiation in complex terrain .....	17
3.1.6 Stream microclimates .....	18
3.2 Spatially interpolating temperature in mountainous terrain .....	19
3.3 Related studies .....	22
3.4 Summary .....	24

TABLE OF CONTENTS (Continued)

	<u>Page</u>
4. METHODS .....	26
4.1 History and management of climate data at the H. J. Andrews .....	26
4.2 The datasets .....	28
4.3 Initial adjustments to datasets .....	30
4.4 Temporal adjustments to datasets .....	35
4.5 Radiation adjustments to datasets .....	37
4.5.1 Topographic adjustments .....	43
4.5.2 Canopy adjustments .....	56
4.5.3 Calculation of regression functions .....	65
4.6 Mapping methods .....	78
4.6.1 PRISM logic and features .....	78
4.6.2 Using PRISM to map H. J. Andrews temperatures .....	80
5. RESULTS .....	88
5.1 PRISM temperature grids with no radiation/ sky view factor effects .....	88
5.2 IPW radiation and sky view factor grids .....	97
5.3 PRISM temperature grids showing effects of radiation and sky view factors .....	98
6. DISCUSSION .....	117
6.1 Hypotheses behind methodology .....	117
6.2 Sources of uncertainty .....	118

TABLE OF CONTENTS (Concluded)

	<u>Page</u>
7. CONCLUSIONS .....	124
7.1 Summary of project and results .....	124
7.2 Recommendations for future work .....	125
BIBLIOGRAPHY .....	130
APPENDICES .....	141
Appendix A: Maximum temperature correlation coefficients between long-term sites ...	142
Appendix B: Processed hemispherical fisheye images of all sites .....	144
Appendix C: PRISM temperature maps with no radiation/sky view factor effects .....	164
Appendix D: IPW monthly radiation maps .....	178
Appendix E: Sky view factor map .....	186
Appendix F: Detailed descriptions of all sites used in the study .....	188

## LIST OF FIGURES

<u>Figure</u>	<u>Page</u>
2.1 Map of the H. J. Andrews showing locations of all historical climate stations	4
4.1 Data inventory of all historical climate stations in the H. J. Andrews LTER network	27
4.2 Differences between adjusted and actual mean monthly maximum temperatures for long-term sites	36
4.3 Differences between adjusted and actual mean monthly minimum temperatures for long-term sites	36
4.4 Observed and modeled solar radiation at UPLMET	46
4.5 Differences in simulated radiation and observed maximum temperatures for site pairs and regression lines for each month	68
4.6 Slopes of maximum temperature regression trendlines and modeled radiation at UPLMET for each month	71
4.7 Slopes of monthly maximum temperature regression trendlines plotted against modeled radiation at UPLMET	71
4.8 Differences in simulated sky view factors and observed minimum temperatures for site pairs and regression lines for each month	72
4.9 Slopes of minimum temperature regression trendlines and cloud factors for each month	74

LIST OF FIGURES (Continued)

<u>Figure</u>	<u>Page</u>
4.10 Slopes of minimum temperature regression trendlines plotted against monthly cloud factors	74
4.11 Plot of mean maximum temperatures and elevation for January	84
4.12 Plot of mean maximum temperatures and elevation for July	84
4.13 Plot of mean minimum temperatures and elevation for January	85
4.14 Plot of mean minimum temperatures and elevation for July	85
4.15 Summary of all maximum and minimum temperature adjustments taken to create the final maps	87
5.1 Map of the H. J. Andrews showing locations of all historical climate stations	89
5.2 Maps showing (a) PRISM September maximum temperatures with no radiation effects, (b) radiation for September, (c) PRISM September maximum temperatures with radiation effects, and (d) differences between (a) and (c)	90
5.3 Maps showing (a) PRISM September minimum temperatures with no sky view factor effects, (b) sky view factors, (c) PRISM September maximum temperatures with sky view factor effects, and (d) differences between (a) and (c)	92

LIST OF FIGURES (Concluded)

<u>Figure</u>	<u>Page</u>
5.4 PRISM monthly maximum temperature-elevation regression slopes for layers 1 and 2 compared with values used by Rosentrater (1997)	95
5.5 PRISM monthly minimum temperature-elevation regression slopes for layers 1 and 2 compared with values used by Rosentrater (1997)	95
5.6 PRISM estimated mean monthly maximum and minimum temperature maps for all months showing topographic effects of radiation and sky view factors	104

## LIST OF TABLES

<u>Table</u>	<u>Page</u>
4.1 Percentages of months with temperature data for all sites during the 30-year period of record	31
4.2 Specifications of sites used in the study	32
4.3 Original mean monthly maximum temperatures for historical climate stations (°C)	33
4.4 Original mean monthly minimum temperatures for historical climate stations (°C)	34
4.5 Correlation coefficients between short-term sites and long-term sites used for temporal correction	38
4.6 Original (U) and temporally-adjusted (A) mean monthly maximum temperatures for each climate station (°C)	39
4.7 Original (U) and temporally-adjusted (A) mean monthly minimum temperatures for each climate station (°C)	41
4.8 Observed and modeled monthly solar radiation variables at UPLMET (MJ/m <sup>2</sup> ·day)	47
4.9 Summary of steps taken to create solar radiation grids	50
4.10 Observed and modeled monthly solar radiation for MET sites (MJ/m <sup>2</sup> ·day)	51

LIST OF TABLES (Continued)

<u>Table</u>		<u>Page</u>
4.11	Modeled horizontal-surface, cloud-adjusted monthly solar radiation at each climate station (MJ/m <sup>2</sup> ·day)	52
4.12a	Differences between modeled horizontal-surface, cloud-adjusted and horizontal-surface, cloud/horizon-adjusted monthly solar radiation at each climate station (MJ/m <sup>2</sup> ·day)	53
4.12b	Differences between modeled horizontal-surface, cloud/horizon-adjusted and sloped-surface, cloud/horizon-adjusted monthly solar radiation at each climate station (MJ/m <sup>2</sup> ·day)	54
4.13	Modeled sloped-surface, cloud/horizon-adjusted monthly solar radiation at each climate station (MJ/m <sup>2</sup> ·day)	55
4.14	Proportions of total solar radiation blocked by canopy and topography at each climate station	59
4.15	Sky view factors at each climate station	60
4.16	Proportions of total solar radiation blocked by topography at each climate station	62
4.17	Proportions of total solar radiation blocked by canopy at each climate station	63
4.18	Modeled sloped-surface, cloud/canopy/topography-adjusted monthly solar radiation at each climate station (MJ/m <sup>2</sup> ·day)	64

LIST OF TABLES (Continued)

<u>Table</u>		<u>Page</u>
4.19	Summary of sites considered for adjustment pairs	67
4.20	Site pairs used for maximum temperature adjustments and their temperature/radiation differences	69
4.21	Monthly regression functions and R-squared values for maximum temperature adjustments	69
4.22	Site pairs used for minimum temperature adjustments and their temperature/sky view factor differences	73
4.23	Monthly regression functions and R-squared values for minimum temperature adjustments	73
4.24	Cloud/canopy/topography-adjusted mean monthly maximum temperatures at each climate station (°C)	76
4.25	Cloud/canopy/topography-adjusted mean monthly minimum temperatures at each climate station (°C)	77
4.26	Summary of sites used for final mapping and those discarded	82
5.1	PRISM mean monthly temperatures for the H. J. Andrews in the absence of vegetation, with and without the effects of radiation (RADN) and sky view factors (SVF), (°C)	101

LIST OF APPENDIX FIGURES

<u>Figure</u>	<u>Page</u>
B.1 Processed hemispherical fisheye images with suntracks at each climate station used in the study	145
C.1 PRISM estimated mean monthly maximum and minimum temperature maps for all months with no radiation or sky view factor effects	165
D.1 IPW mean daily solar radiation maps for each month	179
E.1 Sky view factor map	187

LIST OF APPENDIX TABLES

<u>Table</u>	<u>Page</u>
A.1 Maximum temperature correlation coefficients between long-term sites	143
F.1 Detailed site descriptions of climate stations used in the study	189

# MAPPING THE THERMAL CLIMATE OF THE H. J. ANDREWS EXPERIMENTAL FOREST, OREGON

## 1. INTRODUCTION

### 1.1 OVERVIEW AND IMPETUS BEHIND THE STUDY

The H. J. Andrews Experimental Forest is an important environmental research area in the Pacific Northwest. It is part of the Long-Term Ecological Research (LTER) network and attracts researchers worldwide from a variety of ecological and scientific fields. Although the climate of the H. J. Andrews (hereafter referred to as the HJA) is generally understood (Bierlmaier and McKee, 1989), few studies have looked at the myriad of environmental factors affecting its local microclimates and none have quantified these factors to spatially predict its temperature regimes.

There is a great need for accurate temperature maps of the HJA. Most scientific research is carried out in areas with little or no instrumentation and knowledge of local temperature regimes has been virtually nonexistent. Accurate temperature data are needed for research involving a range of subjects from animal habitats to hydrologic cycles to forest management practices.

A 30-year temperature dataset now exists from a dense spatial network of sites at the HJA. Current Geographic Information System (GIS) capabilities allowed us to take full advantage of this dataset, and advanced computer software (Dozier and Frew, 1990; Delta-T Devices, Ltd, 1999) is now available to quantify and analyze effects of topography and vegetation cover on microclimate. This project also provided

an opportunity to use a reliable temperature interpolation model (Daly et al., 1994) that was well-suited to the complex HJA geography.

## 1.2 GOALS AND OBJECTIVES

The primary goal of this study was to provide the most accurate spatial representation of temperature regimes in the HJA given the datasets and tools currently available. The maps depict mean monthly maximum and minimum temperatures over the entire HJA on a 50-meter grid taking into account as many factors affecting local climates as possible. The effects of topography and forest canopy on solar radiation, and hence temperature, were the primary factors considered in this study. To make the products applicable to a wide range of users, temperatures were modeled with the effects of vegetation removed, simulating the standard siting conditions of National Weather Service weather stations. Vegetation-free maps also provide a dataset modeling uniformly open conditions, a 'universal' starting point for various projects that may use these data as input.

This project had several secondary objectives. Monthly mean radiation maps were produced that explicitly take into account topography and cloudiness, and their effects on direct and diffuse radiation. Historical temperature datasets and site specifications were quality-checked and inventoried, and site radiation regimes were summarized with hemispherical fisheye photographs. Regression functions were developed for quantifying the effects of topography and canopy on maximum and minimum temperatures.

## 2. THE STUDY AREA

### 2.1 DESCRIPTION OF THE STUDY AREA

The HJA is a 64 square-kilometer research area 130 kilometers east of Eugene in the central Oregon Cascades. It encompasses the entire Lookout Creek watershed and varies in elevation from about 410 meters at the southwest corner to over 1600 meters at the top of Lookout Mountain (Figure 2.1).

The HJA is one of 21 LTER (Long-term Ecological Research) sites funded by the National Science Foundation. Established as a USFS (United States Forest Service) Experimental Forest in 1948, it has been a major center for analysis of forest and stream ecosystems in the Pacific Northwest for over 50 years. Several dozen university and federal scientists use the site as a common meeting ground, working together to gain an understanding of ecosystems and applications of developments in land management policy (HJA/LTER website, 2002). Logging has taken place in the HJA since 1949, and young stands cover 25% of the watershed (Jones and Grant, 1996). The area is biologically diverse and almost half of it is occupied by old growth forest over 400 years old.

Vegetation patterns in the HJA are typical of mountainous areas in the Pacific Northwest. Below 1050 meters forest stands are dominated by Douglas Fir, Western Hemlock, and Western Red Cedar, while near and above this height Douglas Fir, Pacific Silver Fir, and Mountain Hemlock are more common. Understories of forest stands are typically composed of rhododendrons and young conifers throughout the area (Dyrness et al., 1976).

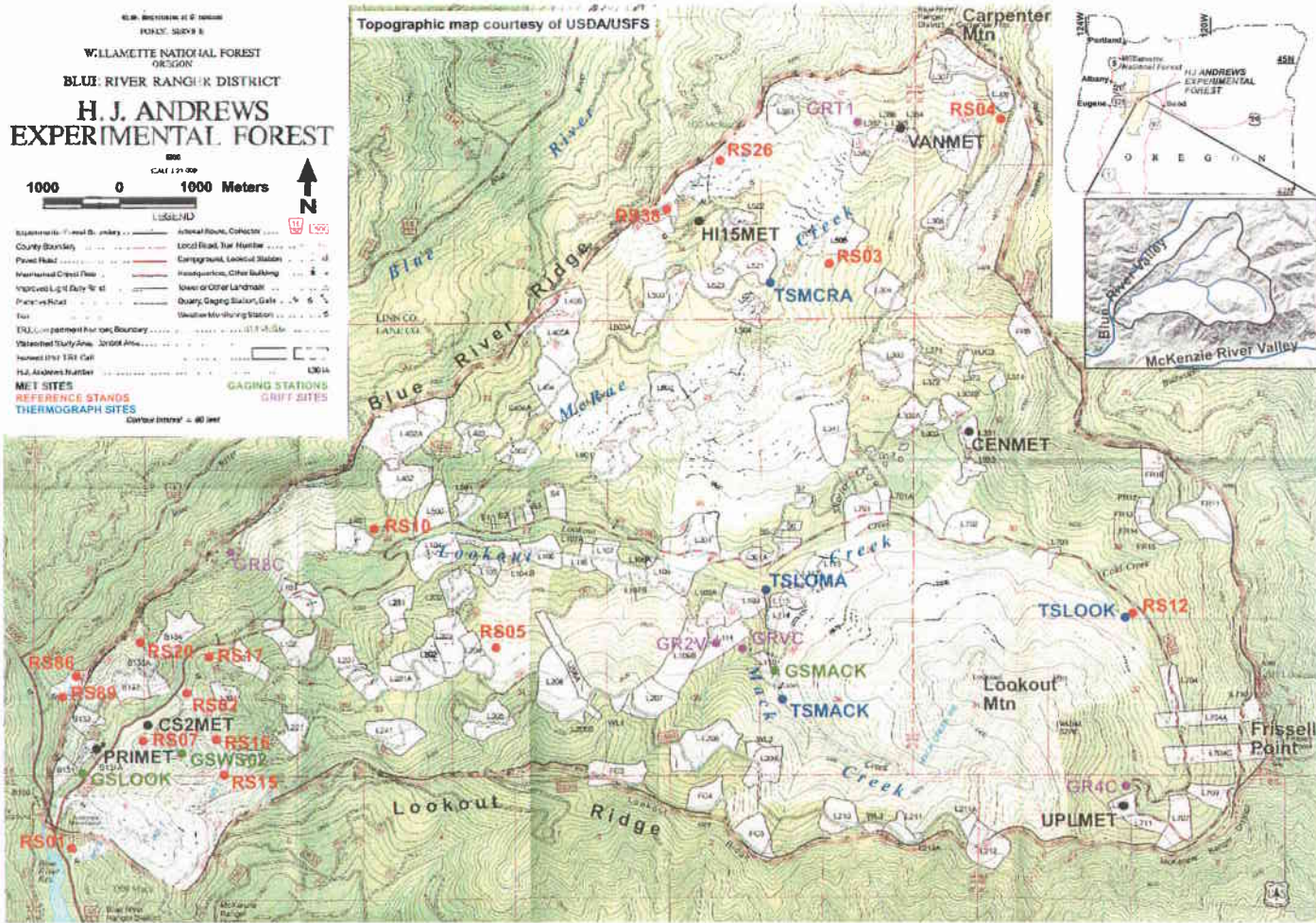


Figure 2.1. Map of the H. J. Andrews showing locations of all historical climate stations.

## 2.2 LARGE-SCALE INFLUENCES ON H. J. ANDREWS CLIMATE

The HJA's proximity to the Pacific Ocean, its latitude, and its position relative to the crest of the Cascade Mountain Range all play a role in determining its climate. Located on the western slopes of the Cascade Range 150 kilometers from the Pacific coast, the HJA is generally under a maritime influence, affected mainly by subtropical, Pacific, and Gulf of Alaska air masses depending upon the season (Taylor and Hannan, 1999). The polar jet stream shifts throughout the year between 40° north (winter months) and 60° north (summer months), acting as a steering mechanism for low pressure systems and frontal storms in the PNW. When the polar jet begins its seasonal shift southward in late autumn, the HJA (latitude 44° north) experiences the onset of its winter, characterized by an abundance of precipitation and cloudiness mainly from cold and occluded oceanic fronts. The Cascades force topographic uplifting of moisture-laden air from the Pacific and slow the easterly-moving storms, resulting in rain events that are of long duration and low intensity (Bierlmaier and McKee, 1989). Its location just 30 kilometers west of the Cascade crest often results in the HJA receiving the maximum precipitation possible from these storms. During summer the absence of the polar jet allows a ridge of high pressure to form along the coast, increasing atmospheric stability, which results in relatively sunny, dry weather for much of Oregon (Bierlmaier and McKee, 1989).

These large-scale factors have the net effect of giving the HJA a 'quasi-Mediterranean' climate; winters are mild and moist, while summers are warm and dry. July is usually the sunniest, driest month and December is the cloudiest and

wettest. Historical mean monthly temperatures range from 17.8°C in July to 0.6°C in January, and annual precipitation is over 200 centimeters. Seasonal precipitation differences are striking, with 71% of yearly rainfall occurring from November through March, compared with only 6% from June through August (Bierlmaier and McKee, 1989).

### 2.3 SMALL-SCALE INFLUENCES ON H. J. ANDREWS CLIMATE

Topography and vegetation affect nearly all aspects of local climate in the HJA. Accounting for their effects on temperature regimes is the essence of this study.

The HJA is divided topographically by Lookout Creek, with the northern and southern boundaries defined by major east-west ridges (Blue River Ridge and Lookout Ridge, respectively), and the eastern boundary defined by a ridge extending from Carpenter Mountain to Frissell Point (Figure 2.1). A smaller east-west ridge extending from the confluence of McRae Creek and Lookout Creek to the eastern boundary is also notable (Figure 2.1). The resulting elevation variations largely determine local precipitation variations in the HJA; limited data suggest that the northern half of the watershed is drier than the southern half possibly because of a rain shadow caused by Lookout Ridge at its southern edge (C. Daly, pers. comm.). The smaller central ridge further shields its north side from rainfall, suggesting that the McRae Creek valley may be the driest place in the HJA. Annual precipitation amounts estimated from the PRISM (Parameter-elevation Regressions on Independent Slopes Model) model range from 230 centimeters at low elevations in the HJA to over 350 centimeters at the highest point (Daly, 1995). Elevation is

naturally the main determinant of snow levels. Persistent winter snowpacks are common above 1000-1200 meters, and snow depths up to 5 meters in the highest elevation forests are not unusual (Waring et al., 1978).

The HJA's terrain patterns also divide it into regions of high (south-facing slopes) and low (north-facing slopes) potential solar radiation, again with Lookout Creek comprising the boundary between them (Greenland, 1994a). Absorbed solar radiation is crucial in determining the diurnal temperature regime of a surface; this in turn depends strongly on the slope, aspect, and amount of vegetation cover on the surface (Gieger, 1965). Forest cover in the HJA is highly variable and thus has a great effect on temperatures. Terrain-induced nighttime temperature inversions due to cold air drainage are common in the HJA both in summer and winter, often causing strong temperature inversions, especially above the lower Lookout Creek valley (Rosentrater, 1997). Nighttime temperature patterns are further complicated by the resulting thermal belts at mid-elevations along the sides of valleys in the HJA (Rosentrater, 1997).

Microclimates in the HJA are complex because of its varied topography and vegetation. The climate of the HJA is representative of the northern Cascades in particular and the Pacific Northwest in general (Greenland, 1994b). Thus, further study of the climate of the HJA is of both local and regional interest. This project investigates monthly temperature variations in the HJA by quantifying as many small-scale influences on its climate as possible.

### 3. BACKGROUND AND LITERATURE REVIEW

Much scientific research has been devoted to understanding the many factors affecting microclimates in forested, mountainous terrain. Accurate modeling of temperature regimes in the HJA's complex geography requires not only an understanding of these factors, but also how they interact. This chapter provides background on these factors and summarizes the current state of knowledge about them. A summary of spatial temperature interpolation techniques is also presented, and the chapter concludes with a description of relevant research and the scientific angle from which this study was conducted.

#### 3.1 ELEMENTS OF MICROCLIMATE IN MOUNTAINOUS TERRAIN

##### 3.1.1 General effects of topography

Evaluating local climate in areas of complex terrain can be very difficult. Varying slopes and aspects of surfaces have a great effect on solar radiation inputs which are major determinants of climate (Geiger, 1965; Oke, 1987). Ridges and valleys also modify airflow. Because topography is less relevant to longwave radiation outputs, topographic influences on temperatures are generally more noticeable during the day than at night, although nocturnal phenomena such as cold air drainage are also significant. Local precipitation patterns are highly dependent upon topography, which in turn affects humidity and temperature patterns (Geiger, 1965). Although

topography affects nearly every aspect of mountain microclimates, the influence of elevation alone is the most encompassing (Geiger, 1965; Pielke and Mehring, 1977; McCutchan and Fox, 1986; Oke, 1987; Barry and Chorley, 1992; Daly et al., 2002).

### 3.1.2 Radiation budgets of mountain microclimates

Since radiation is the most important of all meteorological parameters, it is useful to review the earth-atmosphere radiation budget. This interaction is often affected profoundly by the physical geography of mountainous areas.

The law of conservation of energy states that the amount of outgoing radiation cannot exceed the amount of incoming radiation for any body. Solar energy is absorbed by the earth during the day as shortwave radiation and emitted at night as longwave radiation. A simple equation governing this process can be given as

$$IS + IL = OS + OL \quad (1)$$

where IS = incoming shortwave radiation (direct and diffuse solar radiation), IL = incoming longwave radiation (emitted by the atmosphere), OS = outgoing (reflected) shortwave radiation, and OL = outgoing longwave radiation (emitted blackbody irradiance at a certain temperature given by the Stefan-Boltzmann Law) (Geiger, 1965). Incoming shortwave radiation always occurs during the day, with variations in the relative amounts of direct and diffuse depending upon cloudiness and other atmospheric conditions. Incoming

longwave radiation from the atmosphere plays a relatively insignificant role in the overall radiation budget, so shortwave radiation dominates the balance during the day.

Amounts of reflected shortwave and outgoing longwave radiation depend upon surface characteristics. Shortwave solar radiation reflected by a surface depends upon its albedo and the angle at which beam radiation strikes it. More shortwave radiation absorbed and stored by the earth during the day (sunny weather) results in higher longwave radiation loss at night, especially if the night is clear. Since the radiation balance must hold for all times, with incoming and outgoing shortwave radiation relevant only during the day, the nighttime heat balance of the earth's surface is thus dominated by outgoing longwave radiation (Geiger, 1965). As a result of these processes, the temperature of air adjacent to the surface and affected by it (the 'boundary layer') generally decreases with height by day and increases with height at night (Oke, 1987).

Slope and aspect of a surface greatly affect the amount of solar radiation absorbed, as previously mentioned. At mid-latitudes in the northern hemisphere, south-facing slopes can receive up to three times more solar radiation than north-facing slopes on clear days. The resulting differential heating between these slopes can produce local slope winds, further affecting temperature patterns (Oke, 1987).

The radiation balance is also affected by elevation and the amount of sky visible over a surface ('sky view factor'). The amount of solar radiation which is able to penetrate through the atmosphere is determined by the atmosphere's transmissivity. The higher the surface, the less atmosphere the radiation must pass through to reach it and hence less radiation is attenuated (Barry and Chorley, 1992). At night,

a location with more visible sky (a high sky view factor) experiences greater loss of longwave radiation and colder minimum temperatures than a location whose sky view factor is lowered by vegetation or nearby terrain. Clouds, which are often induced by topography itself, can also limit the amount of longwave radiation lost at night and hence raise a site's minimum temperature (Oke, 1987).

### 3.1.3 Vegetation effects on temperature regimes

Vegetation characteristics are vitally important in determining microclimates in heavily forested areas such as the HJA. Because of the highly variable radiation environment created by shading inside forest stands, the nature of a forest canopy greatly affects the microclimate of the forest floor below it. Stand height, species and density affect the radiation balances inside forests (Oke, 1987), and are highly variable in the HJA. Significant portions of the HJA have been logged, and uneven regeneration of planted trees has resulted in different ages and densities of forest stands. Some openings have been maintained for various periods of time near climate stations and roads. Boundaries between relatively dense forests (closed canopies) and relatively open areas are significant climatological determinants (Geiger, 1965; Chen et al., 1993, Saunders et al., 1999).

A forest canopy alters the radiation balance near the forest floor by affecting the amount of direct (beam) and diffuse incoming shortwave sky radiation that reaches the floor and by scattering this direct and diffuse radiation (Black et al., 1991). These effects are lessened in cloudy weather when less solar energy is transmitted through the

direct beam. Old stand canopies with low sky view factors can prevent over 80% of incoming radiation from reaching the forest floor. The needles of evergreen branches act to effectively scatter the direct beam, giving it more diffuse properties under the canopy (Oke, 1987). Solar zenith angle is especially important under discontinuous canopies where direct radiation reaches the forest floor only during certain times of day. Carlson and Groot (1997) and Morecroft et al. (1998) have quantified the effect of canopy gaps on radiation and microclimate in forest stands.

Evergreen forests are excellent absorbers and emitters of solar energy. Coniferous trees have the lowest albedos of any vegetation type (ranging from 0.05 to 0.15) and some of the highest emissivity values (0.97 to 0.99). This is due mainly to the tightly packed structure of their dark needles and the varying orientation of needles on branches, characteristics that also explain why forests are such effective windbreaks (Oke, 1987). Downward-directed longwave radiation from the bottom of the canopy is a factor in the radiation balance, especially at night. Nighttime forest temperatures are commonly warmer than in open areas because of this downward radiation and the blocking effects of the canopy on the outgoing longwave radiation from the ground. The relative magnitude of downward-directed longwave radiation from the bottom of the canopy is not enough to keep temperatures inside the forest higher than in open areas during the day, however. Transpiration of foliage and the ability of forests to retain from 15-40% of precipitation as interception storage increases levels of relative humidity during the day and night. The overall effect of these factors is that in the daytime the air inside forests is relatively

cool, humid and calm, while at night the air is relatively warm, moist, and still (Oke, 1987).

There are other unique factors in the heat balance specific to forests. Plant metabolism requires energy for photosynthesis, and the differing thermal capacities between tree trunks, branches, leaves, and needles give rise to heat exchange. The air mass in the trunk area of a forest can affect heat transport in the stand. However, all of these factors are relatively insignificant in the overall heat budget of a forest (Geiger, 1965).

Understory and surface vegetation also play a role in forest heat exchange. However, their effects are relatively small compared to those of the canopy. The mass of plants taking part in heat exchange with the environment has a very small thermal capacity, and shortwave radiation passes relatively unimpeded through it (Geiger, 1965). Since many HJA climate sites have small amounts of insolation reaching the surface and most are maintained to keep the ground beneath the sensors relatively clear of vegetation, surface conditions play a negligible role in this climate study.

Much more important to the microclimates of the HJA are the effects of forest clearings, both natural and artificial. Figure 2.1 clearly shows the checkerboard patterns resulting from logging, and nearly every climate station in the area has a clearing near it. The most obvious effect of an opening is to increase forest temperatures during the day and decrease them at night, due to the diurnal radiation characteristics of forests as discussed above. Daytime maximum temperatures can be 5°C to 7°C warmer in clearings during summer months (Morecroft et al., 1998), whereas nighttime minimum temperatures can be 2°C to 3°C warmer inside a forest stand (Raynor, 1971; Karlsson, 2000). These differences are much

less extreme and often negligible during cloudy winter months. Overall, harvesting a site greatly reduces its total net radiation because of the removal of the canopy and understory, two crucial components of radiation storage and emission within the stand (Holbo and Childs, 1987).

The boundary between a clearing and forest is such an important transition zone that it virtually creates its own unique climate (Geiger, 1965; Chen et al., 1993, Saunders et al., 1999). These 'edge effects' on microclimates in adjacent forests and clearings have been studied extensively. Radiation balances are altered at edges, in part because the increased albedo of a clearing relative to a forest reflects shortwave radiation into the highly absorbent forest wall (Geiger, 1965). This altered radiation regime can dramatically increase the diurnal ranges of both temperature and humidity at the edge. Daily maximum and minimum temperatures can be affected as far as 230 meters and 60 meters, respectively, into a coniferous forest from the edge (Chen et al., 1995; Saunders et al 1999). The orientation of the edge is an important parameter in determining its microclimate, with seasonal variations in radiation loading affecting other climate variables (Geiger, 1965, Chen et al., 1995). Forest edge effects have also been studied by Chen and Franklin (1990), Cadenasso et al. (1997), and Malcolm (1998).

It is likely that edge effects are a significant factor in determining temperature patterns in the HJA. Most climate monitoring stations are well within effective distances of edges. Due to the complex nature of edge effects and the ever-changing locations of edges in this actively-logged area, their effects on temperature cannot be directly addressed in this study. However, open and closed canopy differences and

their effects on radiation and temperature can be quantified and constitute a major facet of this study.

#### 3.1.4 Nocturnal temperature regimes in complex terrain

Diurnal patterns of the radiation balance in mountainous terrains were described in section 2.1.1. Variables affecting temperature patterns are completely different at night and are discussed in detail here.

The phenomenon most affecting nocturnal temperatures in hilly areas is cold air drainage (Geiger, 1965; Bergen, 1969; Hocevar and Martsolf, 1971; Miller et al., 1983; Gustavsson, 1998). Relatively dense cold air flows toward the lowest local elevations, resulting in lower minimum temperatures in valley bottoms. This effect is often so pronounced that valley bottoms can be up to 6°C colder than surrounding hilltops at night (Bootsma, 1976). Less daylight and the reduction of turbulent heat exchange in a valley bottom also contribute to colder minimum temperatures (Geiger, 1965). Thus, temperatures in a valley at night often increase with height up to a certain elevation. Such inversions are very common in mountainous areas and may be hundreds of meters deep, depending on topography and weather conditions. Just above the inversion temperatures begin to decrease with height, resulting in a thin layer of warmer temperatures ('thermal belt') at mid-valley elevations (Geiger 1965; Oke, 1987). Therefore, a location's height above a valley bottom becomes an important variable in determining its mean minimum temperature (Tabony, 1985).

Cold air drainage, inversions, and thermal belts can have profound effects on mountain microclimates and are well

documented. Clouds and wind reduce their occurrence by blocking outgoing longwave radiation and increasing turbulent mixing. Cold air drainage and its effects are thus more common in clear, calm conditions (Hovecar and Martsolf, 1971; Bootsma, 1976; Laughlin, 1982; Lindkvist et al., 1999).

The relative orientation of a valley can be a controlling factor on cold air drainage. Tributaries most closely aligned with the main canyon in a watershed have been found to more efficiently transport cold air at night than those tributaries more perpendicularly aligned to it (Coulter et al., 1991).

Though not as comprehensively studied, forest cover also affects cold air drainage. Forested sites with low sky view factors are more likely to retain longwave radiation at night and have low wind speeds. However, sites sheltered by either topography or forest (or both) tend to begin cooling earlier in the evening, possibly resulting in earlier and more pronounced initial cold air movement (Gustavsson et al., 1998). Height of inversions and density flows can be affected by forest cover because of their dependence on surface roughness (Hovecar and Martsolf, 1971; Miller et al., 1983).

Minimum temperatures in the HJA are greatly affected by cold air drainage, inversions, and thermal belts. A thorough understanding of these phenomena is essential to the production of accurate minimum temperature maps, and every reasonable attempt has been made to account for them in this study.

### 3.1.5 Modeling solar radiation in complex terrain

Accurate predictions of solar radiation in areas lacking instrumentation are extremely valuable to climatologists. In general, solar radiation is not observed as often as temperature and precipitation, a fact which has motivated much research into radiation modeling. Solar radiation modeling is numerically complex and has developed mainly since the advent of the computer.

Topography has the second greatest influence on solar radiation at a surface, after clouds (Dubayah, 1994). Predicting radiation in areas of uneven terrain is complicated, involving separate calculations of direct and diffuse components on surfaces of varying elevation, slope, and aspect (Williams et al., 1971). Radiation models thus rely heavily on both Digital Elevation Models (DEMs) and surface or satellite measurements.

Dozier and Frew (1990) developed a concise set of terrain parameters to be taken into account when modeling solar radiation. Since the effect of a slope on solar irradiation is due to varying angles and shadowing, calculations must involve slope, azimuth, surface illumination angle, horizons, and sky view factors. Other important parameters are surface albedo, albedo of surrounding terrain, and atmospheric transmissivity (Dozier and Frew, 1990). In their spatial modeling of solar radiation, Dubayah et al. (1990) also found the choice of grid spacing to be an important parameter.

Bristow and Campbell (1985) developed an equation for separating total daily solar radiation into its direct and diffuse components. Variation in the proportion of diffuse to direct radiation depends mostly upon cloudiness, with a higher

ratio in overcast conditions. The direct component of incoming radiation is more affected by the slope and aspect of a surface. However, the diffuse component can also be affected, especially on steep slopes where the sky view factor is lowered (Bristow and Campbell, 1985).

Some studies have explicitly linked solar radiation modeling with other climate variable modeling. Bristow and Campbell (1983) described a method relating solar radiation to daily temperature ranges, and Thornton et al. (2000) devised algorithms for estimating daily radiation and humidity from observations of temperature and precipitation. Other studies combining both radiation modeling and climate modeling include those by Richardson (1981), Thornton et al. (1997), Goodale et al. (1998) and Thornton and Running (1999).

#### 3.1.6 Stream microclimates

Other factors affect microclimates in mountain areas, playing a small but probably significant role in the mean monthly temperature regimes of the HJA. Of these, stream effects are the most important.

Comprising the entire Lookout Creek watershed, the HJA is highly dissected by streams. Most carry a small volume of water during summer but in winter and spring their flows are significant. Since air temperatures over water are affected by water surface temperatures, the presence of a cold stream can significantly cool the air above it (Geiger, 1965). This is especially true in the HJA during winter and spring, when melting snow at high elevations provides a constant source of very cold water below. There is a strong correlation between stream temperatures and air temperatures above 0°C (Mohseni

and Stefan, 1999), and average daily temperatures in the HJA are rarely this low in the winter. Air temperatures over streams are also very susceptible to edge effects (see section 2.1.2). Research into buffer zones around streams in actively-logged forests shows that clearcuts affect the air temperature above streams as far as 72 meters on either side of the stream (Dong et al., 1998). Many clearcuts in the HJA are closer than this to streams.

Like edge effects in upland areas discussed previously, edge effects on riparian areas are very complex in the HJA and are not considered here. Although air temperature datasets exist for many stream sites in the HJA, a distance-temperature function could not be developed to quantify stream effects on the climate monitoring network because of the lack of nearby non-stream sites with which to compare them.

### 3.2 SPATIALLY INTERPOLATING TEMPERATURE IN MOUNTAINOUS TERRAIN

Spatially interpolating climate variables in areas with little or no data has been a concern of climatologists for decades. Considerable effort has been expended to develop ways of using of station (point) data and other spatial datasets to estimate patterns of climate (Richardson, 1981; Running and Nemani, 1987; Daly et al., 1994; Dodson and Marks, 1995; Thornton et al., 1997; Bolstad et al., 1998; Goodale et al., 1998; Nalder and Wein, 1998; Jarvis and Stuart, 2000).

Historical climate mapping methods fall into two distinct categories. Until the 1970s, the discipline was largely geographic in nature, involving manual preparation of maps based on the correlation of point and topographic data.

Since the 1970s and the advent of computer technology, climate mapping has been more quantitative, relying on statistical algorithms to quantify specific parameters (Daly and Johnson, 1999). The following discussion will focus on statistical methods of mapping temperature distributions.

All statistical temperature mapping methods are similar in that they use a calculated or prescribed numerical function to weight irregularly spaced temperature point data on a regularly spaced prediction grid (Daly et al., 2002). General interpolation functions are of the form

$$F[r(j)] = z(j) \quad j = 1, 2, \dots, N \quad (2)$$

where  $z(j)$  are the predicted temperature values,  $r(j)$  are points where temperature is measured, and  $N$  is the number of known temperature values in the dataset (Jarvis and Stuart, 2001).

Several techniques have been proposed and used for temperature interpolation. Inverse-distance weighting is a simple statistical interpolation method that considers distance between points as the primary determinant of station weight. Kriging is based on semi-variogram models that best fit the data to calculate optimum station weights for interpolation (Daly et al., 2002). Other techniques include thin-plate smoothing splines, polynomial regression and trend-surface analysis.

All of these methods have been applied to temperature mapping. Richardson (1981) modeled temperature in the Midwestern United States using a multivariate model with variables conditioned by precipitation data. Dodson and Marks (1995) used inverse-distance weighting to model potential temperature in the Pacific Northwest, and Thornton et al.

(1997) used a Gaussian weighting filter to model several climate variables in the northwestern United States.

Comparison studies between techniques have been carried out, with varying results. Bolstad et al. (1998) found regional polynomial regression to be the most accurate temperature interpolator in the Southern Appalachian Mountains. However, Goodale et al. (1998) found little difference between the accuracy of polynomial regression and simple inverse-distance weighting interpolation in Ireland. Nalder and Wein (1998) combined multiple linear regression and distance weighting to achieve the best results in Western Canada, and Jarvis and Stuart (2001) found splining to be the best method for modeling temperatures in Great Britain. The best method apparently depends on the geographic scale and climatological characteristics of the region one wishes to model, as well as the amount of available data for the region.

Selection of appropriate physical parameters to consider in temperature mapping is essential and should not be overlooked. Interpolation is best guided by indices that influence climatic conditions and should relate land-cover and topography to achieve the best results (Jarvis and Stuart, 2001). Thus, selection of physical parameters influencing temperature in the HJA is an important step in this study.

With so many interpolation methods in use, the most accurate procedure may be one that combines the best attributes of each method. Daly et al. (2002) provide such a model that is an effective combination of statistical and geographic methods. The Parameter-elevation Regressions on Independent Slopes Model (PRISM) is an elevation-based hybrid approach using a combination of other methods and allows the user to dictate model parameters based on observations and knowledge of the climate of the study area (Daly et al.,

2002). It uses a unique two-layer atmosphere model to account for temperature inversions. The PRISM model was selected to map temperature regimes in the HJA, and will be discussed in more detail in Chapter 4.

### 3.3 RELATED STUDIES

Very few studies have addressed climatology in the HJA. Mapping temperatures in a small, mountainous, heavily forested watershed such as the HJA presents a unique set of parameters to consider.

Running and Nemani (1987) describe a method for modeling temperature, precipitation, humidity, and solar radiation. 'MTCLIM' initially was developed as a one-dimensional point model combining climatological and topographic parameters to simulate these variables. Specifically, it takes into account elevation, slope, aspect, and albedo of the surface in question. Originally developed to assess the relationship between tree photosynthesis/transpiration and topography (Running and Nemani, 1985), it has been used to predict microclimate differences between north-facing and south-facing slopes on a small scale (Running and Nemani, 1987). Thornton et al. (1997) extended MTCLIM to a two-dimensional spatially-explicit model to generate precipitation, temperature, humidity, and radiation maps over several scales in the northwestern United States.

Though MTCLIM accounts for many parameters, it is significantly different from the effort described in this study. It applies general summer and winter lapse rates (instead of monthly lapse rates) to correct for elevation effects on temperatures. Radiation is derived from daily

temperature ranges according to the procedure developed by Bristow and Campbell (1984) instead of observations as in this study, and it does not take into account topographic shading on a surface as in this study (Thornton et al., 1997). Variable monthly cloudiness is not taken into account and forest canopy effects are considered by applying a simple multiplier based on the leaf area index (LAI) of the study site (Running and Nemani, 1997). In short, MTCLIM is best suited to larger-scale applications where precise meteorology is not as important as regional characterization. It does not consider topographically-driven phenomena such as cold air drainages, frost pockets, and temperature inversions that are so important in HJA climatology (Glassy and Running, 1994).

Few studies examine the adjustment of climate variables to account for the effects of forest. Xia et al. (1999) established mathematical functions to transform temperature data from open-site regional climate stations to temperatures in a forest environment. However, neither forest characteristics, topography, nor cloudiness were taken into account. Garen and Marks (2001) describe a method to correct solar and thermal radiation in snowy terrain to account for the presence of forest canopy. The canopy adjustment is based on a land-cover classification (Link and Marks, 1999) and is thus a very general estimate of solar attenuation due to tree shading. Both of these studies employ one-dimensional point models and do not address two-dimensional spatial interpolation of these variables.

The only other temperature modeling study conducted in the HJA uses MTCLIM for its interpolation method (Rosentrater, 1997). In that study, canopy attenuation was not quantified, and the varying effects of seasonal solar radiation were not considered (Rosentrater, 1997).

Greenland (1996) created maps of potential solar insolation for the HJA but did not take into account cloudiness, canopy cover, or longwave radiation effects such as sky view factors. Other studies at the HJA have examined spatial radiation distribution over the area but none have explicitly accounted for canopy cover or used such estimates to predict climate variables (Greenland, 1996).

### 3.4 SUMMARY

There are several characteristics of this temperature mapping project that make it unique. The small scale of the study differentiates it from other mapping studies. The approach explicitly takes into account topographic effects on solar radiation such as terrain shading, slope, aspect and elevation to map their effects on temperatures at this scale. The effects of forest canopy and topography on both direct and diffuse solar radiation are quantified in making temperature adjustments through the use of fisheye photography. Monthly cloudiness attenuation based on observations is also considered in this study. The 30-year HJA dataset, with a high spatial density of sites and year-round data, is a rich source of data matched in few spatial climate studies. Thus we have an opportunity to improve upon previous temperature mapping work at the HJA with a longer, high resolution dataset and more comprehensive tools at our disposal. The final maps represent the temperature regime of the HJA in the absence of vegetation, which allows the results to be applied in a wide range of studies requiring temperature data for their analyses. The mapping model effectively combines several proven interpolation methods and is the only one that uses a

two-layer model to spatially predict temperatures accounting for inversions, known to be prevalent in the HJA.

## 4. METHODS

### 4.1 HISTORY AND MANAGEMENT OF CLIMATE DATA AT THE H. J. ANDREWS

Meteorological datasets at the HJA provide a lengthy and reliable period of record. Climate variables have been measured at the HJA for about half a century since the establishment of the first precipitation and temperature sensors in 1952 and 1959, respectively (Bierlmaier and McKee, 1989).

The majority of long-term sensors were established in the early 1970s as part of a 'reference stand' network. These climate station sites were originally selected to represent specific vegetation zones and habitat types in the HJA (Hawk et al., 1978). In 1972 the first comprehensive weather station (the primary meteorological station, or 'PRIMET') was constructed near HJA headquarters. Providing high temporal-resolution air temperature, dew point temperature, wind speed and precipitation data, PRIMET served as the only standard weather station at the HJA until the 1990s when four other fully-equipped weather stations were established. Many other sites have come and gone since the early 1970s, resulting in a temporal patchwork of data over the years (Figure 4.1). Currently there are 32 functioning climate stations in the HJA LTER network. Seven of these are outside the boundaries of the HJA.

Site instrumentation has been upgraded over the years, with new sensors and recording devices installed at various times. During the 1970s and 1980s temperature data were

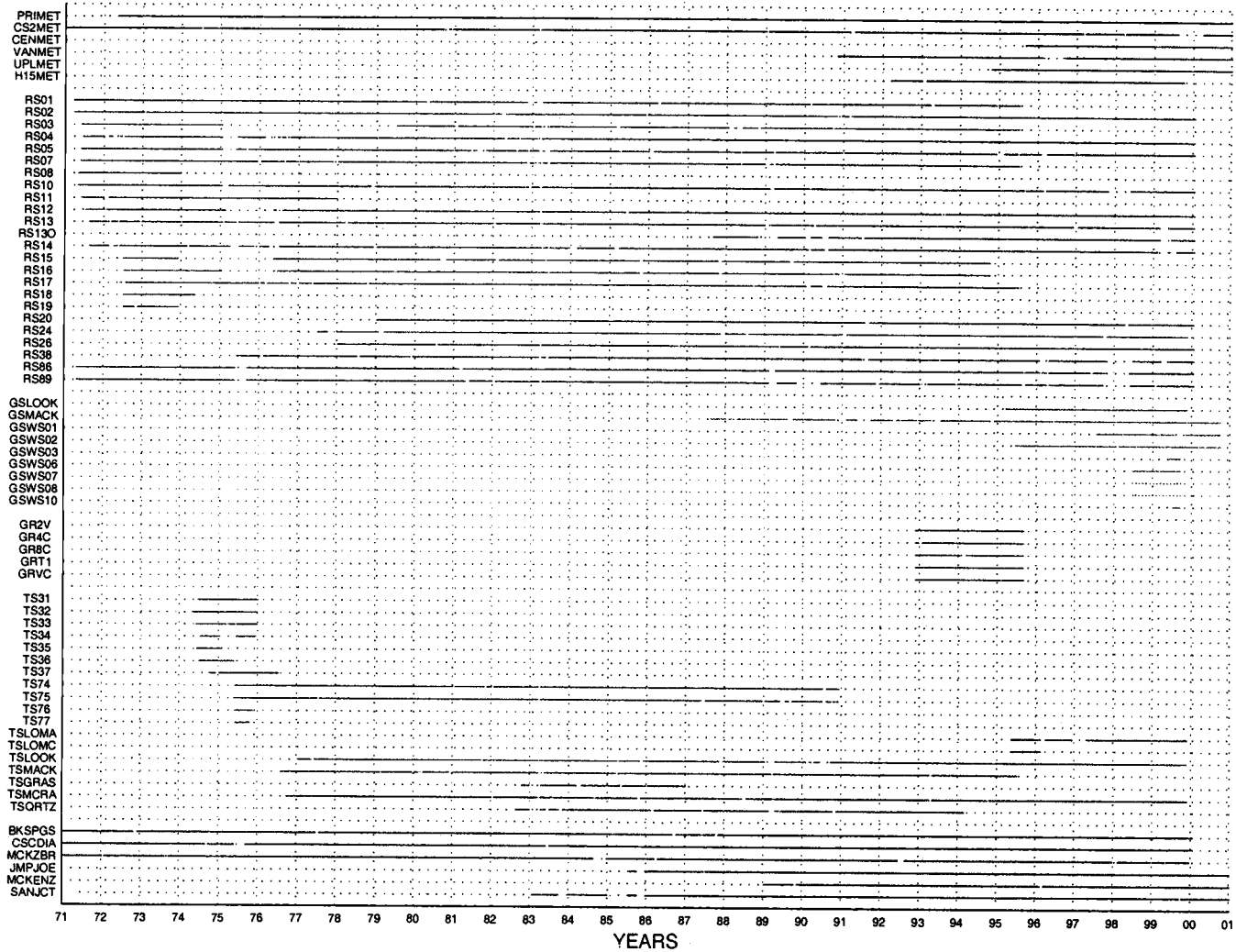


Figure 4.1. Data inventory of all historical climate stations in the H. J. Andrews LTER network.

recorded using mercury bulb thermometers with circular Partlow charts and were processed by hand. Sites were upgraded with thermistors and Campbell Scientific CR-10 digital data loggers starting in the late 1980s (Rosentrater, 1997). By the mid-1990s, all of the sites had been equipped with thermistor/CR-10 units. Since then, raw data have been digitally downloaded in the field every few weeks and transferred to a permanent medium at HJA headquarters (J. Moreau, pers. comm.). 'Pre-digital' data were digitized and made compatible with newer formats in the early 1990s (D. Henshaw, pers. comm.).

Climate data at the HJA are managed by the Forest Science Data Bank, a collaboration between Oregon State University's Department of Forest Science and the U.S. Forest Service's Northwest Research Station in Corvallis (HJA/LTER website, 2002).

#### 4.2 THE DATASETS

The original dataset (Figure 4.1) contained data from every climate station known to have operated in the HJA LTER network during its history. Thus, a large number of sites having highly variable physical and temporal characteristics were initially considered.

The uneven spatial distribution of sites across the HJA is due to the fact that they often operate as part of specific (often temporary) research projects. Sites are naturally more numerous in areas that are easily accessible year-round, such as the vicinity of HJA headquarters (Figure 2.1). The nomenclature applied to each group of sites reflects the patchwork nature of the network.

PRIMET was joined by the four other benchmark meteorological stations in the late 1980s and early 1990s. All five of the 'MET' sites have thermister towers recording air temperatures at 1.5, 2.5, 3.5, and 4.5 meters above the ground. They are the only sites in the HJA whose site conditions approximate NWS standards, surrounded by maintained clearings with negligible blockage of solar radiation from nearby forests. CS2MET is categorized as a MET site because it provides air/dew point temperature, humidity and precipitation data and is in a maintained clearing (though it is affected by nearby trees and does not have a tower). PRIMET's temperature dataset is unique in that the long-term sensor is the only one in the HJA enclosed in a cotton shelter box.

As mentioned previously, the reference stand (RS) sites comprise the majority of the long-term dataset, and are typically located in deep forests. Many of the 'gaging stations' (GSWS) have been only recently placed and are all located directly over streams, sometimes under dense forest canopy. Most of the 'thermograph sites' (TS) are also located over streams. The 'griff sites' (GR) operated for a relatively short period of time under various canopy types. Three sites each from the National Weather Service's Cooperative Observer's Network (National Climatic Data Center, 2000) and the National Resources Conservation Service's Snow-Telemetry network (United States Department of Agriculture, 2000) were included in the initial datasets.

Though instrumentation standards among sites have varied throughout the period of record, there have been important consistencies. Thermometers and thermisters at each site were/are shielded above with a half-PVC pipe cut lengthwise, and sensor heights above the ground have been close enough to

the standard 1.5 meters for variations to have a negligible effect on long-term monthly mean temperatures.

It is important to realize that the HJA climate station network was never designed to provide a comprehensive spatial dataset. Thus, the initial steps of the project involved taking inventory of datasets and piecing together data from different studies into one database.

#### 4.3 INITIAL ADJUSTMENTS TO DATASETS

Original datasets consisted of daily mean, maximum and minimum temperatures that had been quality-checked and processed into a consistent format. Missing data were indicated and questionable values were flagged according to a number of conditions (Bierlmaier, pers. comm.) Any value flagged in any way during this first filtering process was immediately discarded from the database and transformed into a missing value for that day. Daily temperatures were graphed and visually analyzed again on monthly and yearly scales to check for erroneous values possibly missed during the first filtering process. Again, any questionable values were discarded, ensuring the most reliable possible dataset. For the MET sites with variable sensor heights, the 1.5 meter values were used unless that value was missing, in which case the next lower sensor (2.5 meters) was used. A complete inventory of the resulting data is shown in Table 4.1.

After filtering twice, any site left with less than three years of data (10% of the 30-year period) was discarded. The GR sites were an exception to this rule because of their strategic locations in underrepresented areas or next to open MET sites (making them ideal for open/closed canopy

Table 4.1. Percentages of months with temperature data for all sites during the 30-year period of record.

	JAN	FEB	MAR	APR	MAY	JUN	JUL	AUG	SEP	OCT	NOV	DEC	ALL
PRIMET	90.1	92.7	92.7	92.7	94.3	94.4	94.5	93.4	94.0	96.5	95.1	93.2	93.6
CS2MET	89.4	90.4	83.3	96.7	95.8	97.6	95.8	94.8	92.8	86.9	91.3	91.3	92.2
CENMET	16.5	16.7	16.7	16.7	16.7	16.7	16.7	17.6	19.9	20.0	19.8	20.0	17.8
VANMET	32.7	32.5	29.9	30.0	29.9	29.8	29.0	31.2	32.9	32.5	35.3	36.5	31.8
UPLMET	20.0	20.0	19.7	20.0	20.0	20.0	19.8	19.8	19.8	21.9	22.9	23.1	20.6
H15MET	19.9	20.6	25.3	26.3	26.7	26.3	26.7	26.6	26.4	23.2	23.3	22.0	24.5
RS01	78.7	74.6	75.1	74.6	82.5	82.7	81.0	79.1	79.9	78.9	76.7	73.4	78.1
RS02	90.0	89.4	89.8	93.1	96.0	95.9	96.6	96.3	96.7	96.6	92.7	92.7	93.9
RS03	57.3	58.4	58.3	59.4	60.2	65.9	67.6	66.6	64.8	64.8	66.1	66.3	63.0
RS04	87.5	86.2	84.7	81.9	83.8	92.7	94.5	94.7	94.0	95.4	96.3	95.4	90.6
RS05	81.1	81.2	79.8	82.9	87.0	89.8	92.9	91.1	91.0	92.4	93.1	85.1	87.3
RS07	70.3	75.5	74.8	76.7	77.1	79.0	77.2	76.3	78.0	78.9	75.6	69.8	75.8
RS08	6.7	6.7	6.7	6.9	10.0	10.0	10.0	10.0	10.0	10.0	10.0	10.0	8.9
RS10	86.6	78.5	82.8	86.7	94.0	94.1	93.2	93.8	96.0	91.4	89.8	89.2	89.7
RS11	17.6	18.5	19.9	20.0	20.3	23.3	22.5	23.3	23.3	23.3	23.3	23.3	21.6
RS12	89.6	88.8	85.1	84.7	87.4	85.6	83.8	90.0	92.4	93.2	93.2	93.3	88.9
RS13	83.1	83.8	83.3	84.3	86.9	88.1	92.7	93.9	96.1	96.6	93.8	89.5	89.4
RS130	34.4	32.0	32.3	33.2	36.0	35.2	34.9	37.6	42.7	41.8	40.0	39.7	36.7
RS14	86.0	79.4	82.5	81.0	82.2	83.4	85.7	91.9	96.0	95.6	94.1	87.1	87.1
RS15	61.7	61.4	62.9	63.1	63.4	64.6	68.5	68.0	64.1	62.9	62.8	62.5	63.8
RS16	65.2	66.5	66.2	66.7	67.2	67.8	71.6	73.0	73.0	67.5	65.2	65.9	68.1
RS17	72.6	73.0	75.1	76.0	74.5	77.3	70.6	76.0	75.1	71.4	76.0	74.6	74.3
RS18	6.7	6.6	6.7	6.7	4.0	3.6	6.7	6.7	6.7	6.7	6.7	6.6	6.2
RS19	3.3	3.3	3.3	3.3	3.3	3.3	6.7	6.6	6.7	4.9	5.7	4.4	4.6
RS20	69.7	69.6	69.0	67.4	68.9	68.7	66.7	65.9	69.2	70.0	70.0	70.0	68.8
RS24	66.5	69.5	71.7	72.3	73.0	73.7	73.3	76.0	73.2	70.1	68.3	66.1	71.2
RS26	74.8	70.2	71.9	72.8	71.7	72.3	70.3	73.3	73.3	71.8	73.2	72.4	72.4
RS38	74.9	70.6	68.5	70.7	72.4	79.7	77.4	80.0	83.3	79.9	78.2	77.8	76.1
RS86	88.0	86.0	83.9	88.9	93.2	92.7	92.6	92.3	94.0	93.2	82.8	91.7	90.8
RS89	79.1	81.0	79.5	80.6	85.5	92.2	90.5	90.6	91.6	88.6	86.2	87.8	86.1
GSL00K	13.3	13.3	15.6	16.7	16.6	16.4	16.7	16.7	16.7	16.7	15.7	13.3	15.6
GSMACK	40.1	41.7	43.0	39.4	37.2	35.6	39.5	40.2	43.4	42.4	35.1	38.2	36.2
GSWS01	9.9	9.2	8.8	9.9	9.9	10.0	10.9	10.0	10.0	10.2	10.0	10.0	6.6
GSWS02	15.4	16.5	16.7	16.6	16.6	18.3	20.0	20.0	20.0	16.9	16.7	16.7	14.1
GSWS03	0.0	0.0	0.0	0.0	2.8	3.3	3.3	3.3	2.2	0.0	0.0	0.0	1.3
GSWS06	3.3	3.3	3.3	3.3	3.3	5.8	6.7	6.7	5.6	3.3	3.3	3.3	4.3
GSWS07	3.3	3.3	3.3	3.3	3.5	6.6	6.7	6.7	5.6	3.3	3.3	3.3	4.4
GSWS08	3.3	3.3	3.3	3.3	3.3	3.4	6.5	6.3	5.6	3.3	3.3	3.3	4.0
GSWS10	0.0	0.0	0.0	0.0	0.0	1.0	3.3	3.3	2.2	0.0	0.0	0.0	0.8
GR2V	9.6	8.8	10.0	10.0	9.9	10.0	10.0	9.5	7.2	6.7	6.0	10.0	9.0
GR4C	8.5	9.9	9.7	9.9	10.0	10.0	9.9	9.9	7.3	6.7	7.8	9.7	9.1
GR8C	9.9	6.4	9.6	9.9	9.7	12.2	7.7	9.0	7.0	6.2	7.8	9.9	8.8
GRT1	10.0	9.7	10.0	9.7	10.0	10.0	10.0	10.0	6.9	6.7	7.6	10.0	9.2
GRVC	9.6	8.0	10.0	9.9	9.9	9.9	9.9	9.8	7.3	6.3	6.9	10.0	9.0
TS31	4.3	3.3	3.3	3.3	3.3	4.4	6.7	6.7	6.7	6.7	6.7	6.7	5.2
TS32	3.3	3.3	3.3	4.2	6.7	6.6	6.7	6.7	6.7	6.7	6.0	6.1	5.5
TS33	3.3	3.3	1.6	1.6	3.5	4.4	6.7	6.7	6.7	6.7	6.7	6.7	4.8
TS34	0.0	0.0	0.0	0.0	0.0	2.1	5.7	6.7	6.7	6.7	6.7	5.2	3.3
TS35	3.3	0.7	0.0	0.0	0.0	2.3	3.3	3.3	3.3	3.3	3.3	3.3	2.2
TS36	3.3	3.3	3.3	3.3	2.9	0.0	3.1	3.3	3.3	3.3	3.3	3.2	3.0
TS37	5.9	6.7	6.7	6.7	6.6	6.7	4.8	3.3	3.3	6.7	6.7	4.2	5.7
TS74	45.7	49.9	48.3	48.7	49.5	52.3	49.0	52.5	53.0	52.9	52.0	49.1	50.2
TS75	49.7	49.8	48.4	48.6	49.2	46.7	46.8	51.0	50.0	51.1	52.3	48.5	49.3
TS76	0.0	0.0	0.0	0.0	0.2	3.3	3.3	3.3	3.3	3.3	2.0	0.0	1.6
TS77	0.0	0.0	0.0	0.0	0.0	2.9	3.3	3.3	2.7	2.5	0.0	0.0	1.2
TSLOMA	10.0	8.4	6.7	12.0	16.2	16.4	16.7	16.7	16.7	16.7	15.6	11.3	13.6
TSLOMC	3.2	1.7	0.0	0.0	2.6	3.2	3.3	3.3	3.3	3.3	3.3	3.3	2.6
TSLOOK	72.4	68.2	68.5	69.9	74.3	71.4	72.3	74.3	72.6	74.3	70.0	70.8	71.6
TSMACK	61.5	57.5	55.1	56.6	58.7	61.0	58.6	60.6	61.2	61.7	62.0	58.6	59.4
TSGRAS	9.1	9.7	9.2	5.8	11.5	13.0	12.6	13.3	13.3	15.9	16.7	14.2	12.0
TSMCRA	73.5	73.3	71.4	71.8	72.6	72.6	73.1	71.4	76.3	74.3	76.3	75.6	73.7
TSQRTZ	35.5	32.0	30.0	33.7	34.5	32.3	36.5	38.3	37.8	33.5	39.1	37.2	35.0

Table 4.2. Specifications of sites used in the study.

SITE	UTM ZONE 10		ELEV (m)	ASPECT (°)	SLOPE (°)
	EASTING	NORTHING			
PRIMET	559563	4895461	430	-	0
CS2MET	560044	4895780	460	355	5
CENMET	568680	4899065	1018	260	12
VANMET	567832	4902239	1273	180	13
UPLMET	570331	4895053	1294	72	13
H15MET	565859	4901219	922	240	15
RS01	559434	4894296	490	200	41
RS02	560513	4896132	490	285	22
RS03	567175	4900777	945	315	5
RS04	568985	4902368	1310	270	27
RS05	563769	4896670	880	10	12
RS07	560023	4895655	460	1	19
RS10	562474	4897908	610	170	6
RS12	570409	4897130	1007	282	11
RS15	560821	4895184	760	350	33
RS16	560694	4895527	640	202	29
RS17	560767	4896468	490	315	14
RS20	559997	4896597	683	180	34
RS26	565992	4901852	1040	180	20
RS38	565480	4901379	977	170	15
RS86	559377	4896330	653	215	28
RS89	559227	4896106	475	315	37
GSLOOK	559438	4895195	436	230	1
GSMACK	566590	4896416	756	350	7
GSWS02	560444	4895513	561	340	13
GR2V	566112	4896700	872	55	15
GR4C	570404	4895251	1268	60	13
GR8C	560999	4897637	756	135	25
GRT1	567437	4902252	1277	190	12
GRVC	566366	4896704	805	90	17
TSLOMA	566547	4897293	652	-	0
TSLOOK	570293	4897091	988	315	5
TSMACK	566697	4896231	780	330	7
TSMCRA	566568	4900583	829	225	3

Table 4.3. Original mean monthly maximum temperatures for historical climate stations (°C).

	JAN	FEB	MAR	APR	MAY	JUN	JUL	AUG	SEP	OCT	NOV	DEC	ANN
PRIMET	5.0	7.7	11.5	15.4	19.4	23.4	28.0	28.2	24.9	16.9	8.0	4.2	16.1
CS2MET	3.6	5.2	7.9	12.8	18.3	22.8	27.7	26.5	19.5	12.5	6.4	3.4	13.9
CENMET	6.1	7.3	9.7	12.8	15.5	21.2	27.3	27.2	23.4	15.4	9.5	6.8	15.2
VANMET	5.6	7.2	8.7	10.2	15.4	18.5	24.6	25.3	23.2	15.1	7.3	5.3	13.9
UPLMET	4.2	6.0	6.6	9.9	12.6	17.7	23.4	23.4	20.2	12.4	6.7	4.8	12.3
H15MET	4.7	5.1	8.6	10.9	17.0	20.5	26.2	24.9	21.2	12.9	6.5	3.4	13.5
RS01	6.0	8.4	10.6	13.5	17.7	21.4	25.7	26.2	23.6	17.1	8.1	5.4	15.3
RS02	4.3	6.2	9.3	12.6	17.2	21.2	26.0	25.8	21.7	14.5	7.1	4.1	14.2
RS03	2.8	4.3	5.9	8.9	14.7	18.3	22.9	23.5	19.0	12.3	4.9	2.6	11.7
RS04	1.9	2.4	3.4	5.7	9.5	14.4	19.2	19.1	15.6	9.9	3.4	1.7	8.9
RS05	3.0	4.6	6.1	9.0	13.1	17.1	21.6	21.4	17.8	12.4	5.5	3.1	11.2
RS07	4.0	6.0	8.3	11.5	16.0	19.8	24.3	24.1	20.0	13.7	6.6	3.8	13.2
RS10	4.7	6.8	8.9	11.9	16.2	20.0	24.9	24.9	21.5	15.4	7.2	4.3	13.9
RS11	3.3	5.2	4.3	7.8	13.2	17.8	23.3	22.6	19.5	12.7	6.1	3.4	11.6
RS12	2.2	3.1	4.5	7.3	13.0	17.7	22.8	21.7	16.7	11.0	4.4	2.0	10.5
RS13	1.9	2.3	2.9	4.8	8.8	13.7	18.4	18.4	15.5	10.4	3.6	1.7	8.5
RS130	4.5	7.2	9.3	11.2	14.2	17.2	22.0	22.2	21.1	14.7	6.6	3.8	12.8
RS14	2.0	2.3	3.4	5.4	9.0	13.8	18.3	18.3	15.3	10.3	3.7	1.9	8.6
RS15	4.1	5.3	6.5	9.4	13.4	17.5	21.6	21.6	17.6	12.8	5.9	3.6	11.6
RS16	4.6	6.6	8.7	12.0	15.8	19.8	23.9	24.2	20.9	15.1	6.9	4.4	13.6
RS17	3.8	5.9	8.1	11.4	16.2	20.6	24.4	24.0	20.0	13.5	6.4	3.6	13.2
RS20	5.7	7.2	9.3	11.8	16.1	19.6	24.4	24.8	21.8	15.3	7.4	5.0	14.0
RS24	5.8	6.8	8.8	11.0	14.8	18.2	22.0	22.3	19.2	14.1	7.2	4.9	12.9
RS26	4.0	4.9	6.4	8.4	12.7	16.6	21.3	21.6	18.5	12.9	5.6	3.7	11.4
RS38	6.7	8.0	9.9	12.1	16.1	20.2	24.7	25.2	22.3	16.1	7.9	6.0	14.6
RS86	7.1	9.0	11.6	14.6	19.1	23.3	27.9	28.2	25.1	18.1	9.1	6.3	16.6
RS89	4.7	7.1	10.5	14.0	19.8	24.2	29.1	29.0	23.8	15.8	7.3	3.9	15.8
TS74	6.0	7.5	9.8	13.8	17.5	21.6	25.7	26.1	21.9	16.1	7.6	5.6	14.9
TS75	5.3	6.8	9.1	13.0	16.4	20.1	24.4	24.6	20.3	14.7	7.4	4.9	13.9
TSCMA	4.5	4.4	6.3	12.6	16.9	20.2	26.5	26.0	20.9	12.4	8.4	4.0	13.6
TSLOOK	1.5	2.1	3.2	5.6	11.2	16.2	20.1	19.0	14.4	9.4	4.0	1.4	9.0
TSMACK	2.4	3.1	4.6	7.0	12.6	16.8	20.5	19.5	14.2	9.9	4.6	2.5	9.8
TSGRAS	3.8	5.9	9.8	12.6	16.7	21.3	24.6	26.1	19.1	13.7	4.8	2.1	13.4
TSMCRA	2.3	3.4	5.7	9.3	15.1	20.2	24.9	23.3	17.6	11.6	5.1	2.2	11.7
TSQRTZ	4.8	7.0	9.9	13.2	17.2	21.0	23.9	24.5	19.5	14.1	7.0	3.4	13.8
GSLOOK	5.5	6.5	10.6	14.3	17.7	21.1	26.7	26.9	23.2	14.8	9.5	4.8	15.1
GSMACK	2.8	3.9	5.9	10.1	15.6	21.0	26.1	25.7	19.0	11.5	6.3	2.9	12.6
GSWS02	4.0	4.9	6.6	10.2	13.8	18.3	22.3	21.1	17.5	11.6	8.3	4.5	11.9
GR2V	6.9	0.0	12.2	13.0	19.3	20.9	25.7	25.4	25.5	15.6	5.8	4.3	14.6
GR4C	2.9	2.6	5.0	5.7	11.5	13.5	17.8	17.3	17.5	10.2	1.3	0.9	8.9
GR8C	4.2	6.5	8.8	9.6	15.8	17.2	20.4	20.4	20.9	12.6	3.8	3.7	12.0
GRT1	2.5	3.1	5.6	5.5	11.9	13.8	18.6	18.2	19.7	11.6	2.6	2.5	9.6
GRVC	3.9	4.3	6.8	9.5	17.0	17.9	22.3	21.7	20.1	12.6	3.9	3.1	11.9
BKSPGS	4.1	6.8	10.2	13.7	18.3	22.5	27.4	27.5	24.2	17.2	8.1	3.7	15.3
CSCDIS	7.7	0.4	12.7	15.1	18.4	21.5	25.6	26.3	23.5	17.9	10.6	6.9	15.6
MCKZBR	6.1	9.5	13.4	17.2	22.1	25.9	30.1	30.1	25.9	17.9	9.5	5.6	17.8
JMPJOE	4.4	6.1	9.1	11.8	15.0	19.4	23.5	23.9	21.3	15.1	7.7	4.4	13.5
MCKENZ	4.2	0.5	9.7	10.0	13.5	17.2	21.3	22.5	20.0	13.1	5.7	4.3	11.8
SANJCT	4.7	6.1	8.7	11.0	14.9	19.1	24.1	25.1	21.4	15.2	6.6	4.0	13.4

Table 4.4. Original mean monthly minimum temperatures for historical climate stations (°C).

	JAN	FEB	MAR	APR	MAY	JUN	JUL	AUG	SEP	OCT	NOV	DEC	ANN
PRIMET	-0.9	-0.3	0.7	2.4	5.0	7.5	9.3	9.1	6.5	3.4	1.2	-1.0	3.6
CS2MET	-0.8	0.0	1.0	2.7	5.8	8.6	10.8	10.7	8.0	4.6	1.5	-0.6	4.4
CENMET	-1.4	-1.1	-1.3	0.9	3.6	6.4	9.8	9.8	8.1	3.9	1.7	-0.9	3.3
VANMET	-1.7	-0.7	-0.8	0.4	3.7	6.0	9.4	10.0	8.5	4.0	0.0	-2.0	3.1
UPLMET	-2.2	-2.0	-2.2	-0.5	2.0	5.2	9.2	9.2	7.4	2.6	-0.2	-2.1	2.2
H15MET	-0.2	-1.1	0.4	1.9	5.1	7.2	10.3	10.6	8.8	4.6	1.1	-1.1	4.0
RS01	0.3	1.3	1.9	3.4	6.4	9.4	11.9	11.9	9.4	6.2	2.5	0.4	5.4
RS02	-0.4	0.2	1.2	2.7	5.6	8.5	10.9	10.8	8.0	4.6	1.9	-0.2	4.5
RS03	-0.3	0.5	1.2	2.4	5.7	8.5	11.8	12.3	10.1	6.4	1.6	-0.5	5.0
RS04	-2.1	-1.7	-1.2	0.2	2.7	6.1	10.0	10.7	8.3	4.3	-0.4	-2.1	2.9
RS05	-0.6	0.3	1.0	2.6	5.4	8.5	11.8	12.1	9.7	6.2	1.8	-0.3	4.9
RS07	-0.5	0.7	1.6	3.3	5.9	8.9	11.0	11.0	8.3	4.8	2.0	0.0	4.8
RS10	0.0	0.8	1.6	3.1	6.0	9.1	11.8	11.8	9.3	5.7	2.4	0.2	5.2
RS11	-1.1	0.1	-0.8	0.7	4.3	7.9	11.9	12.2	10.2	5.6	1.8	-0.6	4.4
RS12	-1.1	-0.9	-0.2	1.0	3.8	6.8	9.9	10.0	7.7	4.5	0.8	-1.2	3.4
RS13	-2.5	-2.1	-2.0	-0.8	2.2	5.8	9.8	10.3	8.0	4.3	-0.6	-2.5	2.5
RS130	-2.2	-1.3	-1.2	0.0	2.8	5.6	10.0	10.1	9.1	4.4	0.0	-2.5	2.9
RS14	-2.7	-2.3	-1.8	-0.4	2.3	6.0	9.8	10.3	7.9	4.2	-0.7	-2.5	2.5
RS15	0.6	1.4	1.9	3.4	6.1	9.5	12.3	12.5	10.3	7.0	2.3	0.3	5.6
RS16	0.4	1.1	1.9	3.6	6.5	9.6	12.1	12.5	10.2	6.9	2.5	0.7	5.7
RS17	-0.2	0.7	1.7	3.4	6.5	9.3	11.4	11.4	8.6	5.0	2.1	0.1	5.0
RS20	0.4	0.9	1.5	3.1	5.9	8.8	11.7	11.8	9.9	6.1	2.1	0.1	5.2
RS24	1.4	1.4	2.2	3.4	6.1	8.9	11.5	12.0	10.0	6.7	2.5	0.6	5.6
RS26	-0.4	-0.1	0.5	1.7	4.6	7.7	11.3	11.7	9.7	5.9	1.1	-0.6	4.4
RS38	-0.2	0.3	0.6	2.0	4.6	7.7	10.5	10.8	8.9	5.5	1.5	-0.4	4.3
RS86	-0.5	0.2	1.1	2.7	5.4	8.6	11.1	11.2	8.9	5.4	1.9	-0.4	4.6
RS89	-0.5	0.5	1.2	2.7	5.9	8.6	10.6	10.8	7.8	4.6	1.8	-0.5	4.5
TS74	0.9	1.3	2.2	4.1	6.7	10.0	12.4	12.9	10.5	7.0	2.6	1.0	6.0
TS75	0.3	0.7	1.9	3.9	6.2	8.9	11.2	11.7	9.0	5.5	2.3	0.4	5.2
TSOMA	0.7	0.1	0.3	2.4	4.8	7.2	10.3	9.9	7.7	4.2	3.3	-0.2	4.2
TSLOOK	-0.9	-0.6	0.0	1.2	4.0	7.2	9.8	9.9	7.5	4.6	1.1	-0.9	3.6
TSMACK	0.5	0.9	1.8	3.1	6.0	9.2	11.8	12.0	9.5	6.5	2.1	0.4	5.3
TSGRAS	-1.1	-0.6	0.9	2.5	4.0	6.2	7.6	7.9	4.5	2.7	-0.3	-1.9	2.7
TSMCRA	-0.9	-0.5	0.4	1.8	4.3	7.2	9.5	9.7	7.5	4.3	1.1	-0.6	3.7
TSQRTZ	0.8	1.7	2.1	3.7	6.0	9.2	10.9	11.0	8.7	6.2	2.8	-0.3	5.2
GSLOOK	0.7	0.2	1.2	2.7	5.8	8.3	11.5	11.1	8.2	4.4	3.8	0.2	4.8
GSMACK	-0.5	-0.1	0.3	2.2	4.7	7.7	10.7	10.6	8.9	5.3	2.3	-0.3	4.3
GSWS02	0.7	0.7	1.3	3.3	6.2	9.1	12.1	11.7	9.5	5.4	4.1	0.6	5.4
GR2V	0.9	1.2	2.4	3.7	7.4	8.8	11.4	10.6	11.2	6.2	-0.4	-0.6	5.2
GR4C	-0.1	-1.5	0.4	1.1	4.3	5.8	9.5	9.2	9.9	5.1	-2.2	-2.0	3.3
GR8C	0.9	1.4	3.1	3.9	7.6	9.2	11.4	10.7	11.3	6.3	0.2	0.7	5.6
GRT1	-0.9	-0.6	1.5	1.4	5.2	6.6	10.4	10.1	12.0	5.9	-1.2	-0.9	4.1
GRVC	0.8	0.7	2.4	4.0	8.5	9.4	12.4	12.1	11.8	7.5	0.6	0.7	5.9
BKSPGS	-2.4	-1.6	-0.5	2.4	3.9	7.0	9.4	9.2	6.5	3.3	0.5	-1.9	3.0
CSCDIS	-0.3	0.5	1.6	3.1	5.4	8.0	9.6	9.1	6.5	3.7	2.2	0.1	4.1
MCKZBR	-1.7	-0.9	0.4	2.1	4.6	7.4	9.5	9.0	6.3	3.0	0.7	-1.2	3.3
JMPJOE	-1.6	-1.8	-1.0	0.9	3.5	6.1	8.9	9.4	7.6	4.5	1.9	-1.0	3.1
MCKENZ	-6.9	-2.3	-4.3	-3.8	-2.0	0.4	4.5	3.0	1.0	-2.4	-4.1	-7.9	-2.1
SANJCT	-5.3	-4.9	-3.8	-2.1	0.5	3.6	5.6	5.4	3.7	0.4	-2.7	-5.5	-0.4

comparisons). Most discarded sites are in areas that are adequately represented spatially by long-term sites.

A summary of site specifications is shown in Table 4.2, with more detailed descriptions given in Appendix F. Mean monthly values for maximum and minimum temperatures were computed for the sites remaining in the database and are shown in Tables 4.3 and 4.4.

#### 4.4 TEMPORAL ADJUSTMENTS TO DATASETS

Daily temperature datasets with periods of record ranging from just under three years to over 28 years were used to calculate monthly mean temperatures. To eliminate the effects of temporal warm or cold biases in the data, corrections were made to adjust the short-term temperature datasets (with data for less than 22.5 years, or 75% of the period of record) to the full 30-year period.

Tests were conducted to determine the most suitable methods for adjusting these short-term sites. Each long-term site (with data for at least 75% of the 30-year period) in the database was systematically sub-sampled to a theoretical short-term site with periods of record ranging from one to 28 years, spanning every possible time period from 1971-2000. Each of these sites was then temporally adjusted according to similarities in temperatures with its top (most closely) correlated site. For every month in the short-term dataset, the difference in temperatures between the 30-year mean and the month in question was calculated for the long-term dataset, and this difference was applied to the short-term dataset to approximate what the 30-year mean temperature would be for that month. Figures 4.2 and 4.3 show the results from

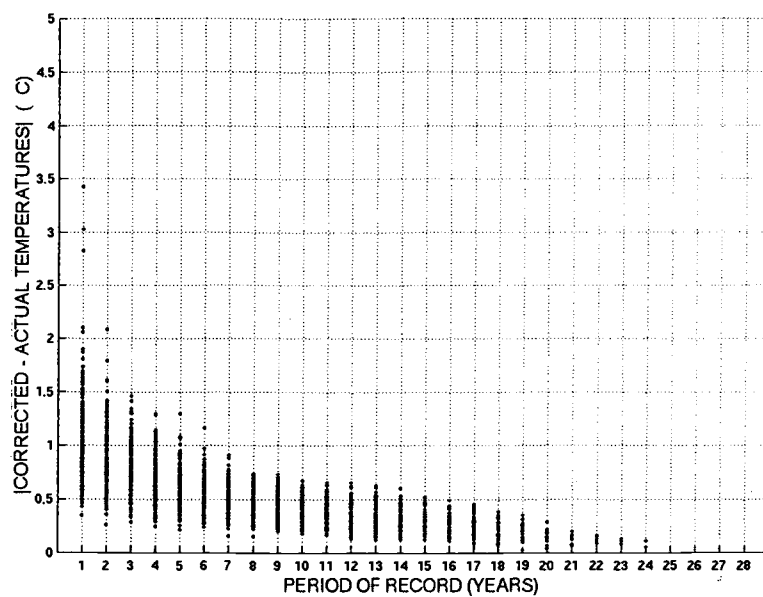


Figure 4.2. Differences between adjusted and actual mean monthly maximum temperatures for long-term sites.

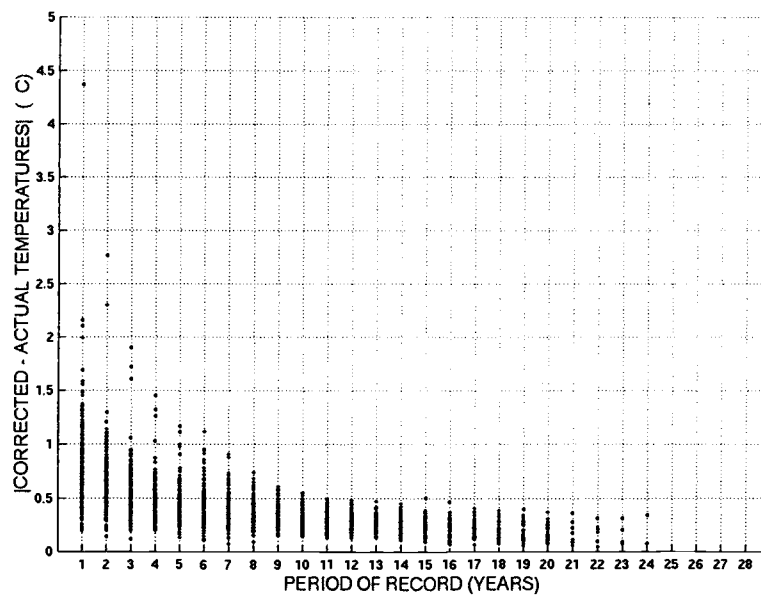


Figure 4.3. Differences between adjusted and actual mean monthly minimum temperatures for long-term sites.

adjusting these theoretical short-term sites with their single highest-correlated sites. Attempts to adjust a site with less than three years of data were deemed unreliable (hence the decision to discard any site with less than three years of original data). The figures also show how it is somewhat easier to accurately adjust short-term maximum temperatures datasets than those for minimum temperatures.

Sites with the highest correlated maximum temperatures were used to correct both maximum and minimum temperature short-term datasets (Table 4.5). For a given short-term site, the same long-term site was found to give the highest correlation coefficient in almost every case for both maximum and minimum temperatures. For those site pairs that were not the same, the differences in correlation coefficients were negligible.

Only short-term sites were adjusted. Details of the short-term sites that were adjusted and the long-term sites used to correct them are shown on Table 4.5. Maximum temperature correlation matrices for long-term sites are shown in Appendix A. Note that all correlation coefficients are generally high (above 0.97), a fact that reflects the relatively small geographic extent of the HJA. 30-year adjusted temperatures are shown in Tables 4.6 and 4.7, with original unadjusted values shown for comparison.

#### 4.5 RADIATION ADJUSTMENTS TO DATASETS

Once the temperature datasets were adjusted for temporal biases, the effects of radiation exposure were quantified. The two major determinants of radiation in the HJA are terrain shading and forest canopy, so each of these had to be taken

Table 4.5. Correlation coefficients between short-term sites and long-term sites used for temporal correction.

<u>CORRECTED</u> <u>SHORT-TERM</u>		<u>LONG-TERM SITE</u>	
<u>SITE</u>	<u>% DATA</u>	<u>USED FOR</u> <u>CORRECTION</u>	<u>CORRELATION</u> <u>COEFFICIENT</u>
CENMET	17.8	RS10	0.994
VANMET	31.8	RS04	0.989
UPLMET	20.6	RS04	0.994
H15MET	24.5	RS02	0.995
RS03	63.0	RS10	0.985
RS130	36.7	RS01	0.977
RS15	63.8	RS05	0.984
RS16	68.1	RS01	0.986
RS17	74.3	RS07	0.988
RS20	68.8	RS02	0.980
RS26	72.4	RS04	0.991
GSLOOK	15.6	RS89	0.996
GSMACK	36.2	RS12	0.988
GSWS02	14.1	RS12	0.995
GR2V	9.0	RS10	0.988
GR4C	9.1	RS04	0.991
GR8C	8.8	RS10	0.985
GRT1	9.2	RS01	0.985
GRVC	9.0	RS07	0.994
TSLOMA	13.6	RS02	0.995
TSLOOK	71.6	RS12	0.984
TSMACK	59.4	RS12	0.975
TSMCRA	73.7	RS07	0.978

Table 4.6. Original (U) and temporally-adjusted (A) mean monthly maximum temperatures for each climate station (°C).

	JAN		FEB		MAR		APR		MAY		JUN	
	U	A	U	A	U	A	U	A	U	A	U	A
PRIMET*	5.0	5.0	7.7	7.7	11.5	11.5	15.4	15.4	19.4	19.4	23.4	23.4
CS2MET*	3.6	3.6	5.2	5.2	7.9	7.9	12.8	12.8	18.3	18.3	22.8	22.8
CENMET	6.1	7.5	7.3	8.8	9.7	10.9	12.8	14.0	15.5	17.4	21.2	21.9
VANMET	5.6	5.3	7.2	6.3	8.7	7.7	10.2	10.3	15.4	13.6	18.5	18.6
UPLMET	4.2	4.5	6.0	5.9	6.6	6.6	9.9	10.0	12.6	12.1	17.7	17.6
H15MET	4.7	3.7	5.1	5.2	8.6	7.4	10.9	10.2	17.0	14.7	20.5	19.3
RS01*	6.0	6.0	8.4	8.4	10.6	10.6	13.5	13.5	17.7	17.7	21.4	21.4
RS02*	4.3	4.3	6.2	6.2	9.3	9.3	12.6	12.6	17.2	17.2	21.2	21.2
RS03	2.8	2.9	4.3	4.7	5.9	5.6	8.9	8.7	14.7	14.3	18.3	18.5
RS04*	1.9	1.9	2.4	2.4	3.4	3.4	5.7	5.7	9.5	9.5	14.4	14.4
RS05*	3.0	3.0	4.6	4.6	6.1	6.1	9.0	9.0	13.1	13.1	17.1	17.1
RS07*	4.0	4.0	6.0	6.0	8.3	8.3	11.5	11.5	16.0	16.0	19.8	19.8
RS10*	4.7	4.7	6.8	6.8	8.9	8.9	11.9	11.9	16.2	16.2	20.0	20.0
RS12*	2.2	2.2	3.1	3.1	4.5	4.5	7.3	7.3	13.0	13.0	17.7	17.7
RS15	4.1	3.9	5.3	5.2	6.5	6.3	9.4	9.0	13.4	13.3	17.5	17.5
RS16	4.6	4.5	6.6	6.6	8.7	8.4	12.0	11.5	15.8	15.8	19.8	19.6
RS17	3.8	3.5	5.9	5.7	8.1	8.3	11.4	11.3	16.2	16.4	20.6	20.5
RS20	5.7	5.6	7.2	7.3	9.3	9.1	11.8	11.2	16.1	15.8	19.6	19.7
RS26	4.0	4.0	4.9	5.0	6.4	6.2	8.4	8.6	12.7	12.5	16.6	16.8
RS38*	6.7	6.7	8.0	8.0	9.9	9.9	12.1	12.1	16.1	16.1	20.2	20.2
RS86*	7.1	7.1	9.0	9.0	11.6	11.6	14.6	14.6	19.1	19.1	23.3	23.3
RS89*	4.7	4.7	7.1	7.1	10.5	10.5	14.0	14.0	19.8	19.8	24.2	24.2
GSLOOK	5.5	4.9	6.5	7.3	10.6	10.5	14.3	10.5	17.7	18.6	21.1	22.8
GSMACK	2.8	2.4	3.9	3.8	5.9	5.5	10.1	5.5	15.6	15.0	21.0	19.8
GWS02	4.0	4.1	4.9	5.2	6.6	6.9	10.2	6.9	13.8	14.1	18.3	17.1
GR4C	2.9	2.7	2.6	2.1	5.0	3.4	5.7	3.4	11.5	8.8	13.5	13.8
GR8C	4.2	5.1	6.5	6.7	8.8	8.2	9.6	8.2	15.8	15.0	17.2	18.9
GRT1	2.5	2.6	3.1	3.4	5.6	4.7	5.5	4.7	11.9	10.6	13.8	15.7
GRVC	3.9	4.3	4.3	4.9	6.8	7.0	9.5	7.0	17.0	16.3	17.9	19.4
TSLOMA	4.5	3.9	4.4	5.2	6.3	7.3	12.6	7.3	16.9	16.1	20.2	19.0
TSLOOK	1.5	1.2	2.1	1.7	3.2	3.0	5.6	3.0	11.2	11.3	16.2	16.4
TSMACK	2.4	2.1	3.1	2.9	4.6	4.4	7.0	4.4	12.6	12.6	16.8	17.2
TSMCRA	2.3	1.9	3.4	3.2	5.7	5.6	9.3	5.6	15.1	15.5	20.2	20.2

\* Denotes long-term sites

Table 4.6. (Concluded).

	JUL		AUG		SEP		OCT		NOV		DEC		ANN	
	U	A	U	A	U	A	U	A	U	A	U	A	U	A
PRIMET*	28.0	28.0	28.2	28.2	24.9	24.9	16.9	16.9	8.0	8.0	4.2	4.2	16.1	16.1
CS2MET*	27.7	27.7	26.5	26.5	19.5	19.5	12.5	12.5	6.4	6.4	3.4	3.4	13.9	13.9
CENMET	27.3	26.0	27.2	27.0	23.4	22.9	15.4	17.3	9.5	8.4	6.8	6.8	15.2	15.7
VANMET	24.6	23.6	25.3	24.3	23.2	21.2	15.1	14.6	7.3	6.3	5.3	5.3	13.9	13.1
UPLMET	23.4	21.4	23.4	22.3	20.2	18.8	12.4	12.6	6.7	5.5	4.8	4.5	12.3	11.8
H15MET	26.2	24.3	24.9	23.4	21.2	19.8	12.9	13.4	6.5	6.3	3.4	3.6	13.5	12.6
RS01*	25.7	25.7	26.2	26.2	23.6	23.6	17.1	17.1	8.1	8.1	5.4	5.4	15.3	15.3
RS02*	26.0	26.0	25.8	25.8	21.7	21.7	14.5	14.5	7.1	7.1	4.1	4.1	14.2	14.2
RS03	22.9	23.2	23.5	23.5	19.0	19.1	12.3	12.3	4.9	5.4	2.6	2.9	11.7	11.8
RS04*	19.2	19.2	19.1	19.1	15.6	15.6	9.9	9.9	3.4	3.4	1.7	1.7	8.9	8.9
RS05*	21.6	21.6	21.4	21.4	17.8	17.8	12.4	12.4	5.5	5.5	3.1	3.1	11.2	11.2
RS07*	24.3	24.3	24.1	24.1	20.0	20.0	13.7	13.7	6.6	6.6	3.8	3.8	13.2	13.2
RS10*	24.9	24.9	24.9	24.9	21.5	21.5	15.4	15.4	7.2	7.2	4.3	4.3	13.9	13.9
RS12*	22.8	22.8	21.7	21.7	16.7	16.7	11.0	11.0	4.4	4.4	2.0	2.0	10.5	10.5
RS15	21.6	22.0	21.6	21.7	17.6	18.0	12.8	12.2	5.9	5.9	3.6	3.8	11.6	11.6
RS16	23.9	23.9	24.2	24.1	20.9	21.0	15.1	14.7	6.9	6.5	4.4	4.2	13.6	13.4
RS17	24.4	24.8	24.0	24.2	20.0	20.0	13.5	13.4	6.4	6.3	3.6	3.4	13.2	13.2
RS20	24.4	24.5	24.8	24.7	21.8	21.6	15.3	15.4	7.4	7.4	5.0	5.0	14.0	13.9
RS26	21.3	21.5	21.6	21.7	18.5	18.5	12.9	12.5	5.6	5.5	3.7	3.7	11.4	11.4
RS38*	24.7	24.7	25.2	25.2	22.3	22.3	16.1	16.1	7.9	7.9	6.0	6.0	14.6	14.6
RS86*	27.9	27.9	28.2	28.2	25.1	25.1	18.1	18.1	9.1	9.1	6.3	6.3	16.6	16.6
RS89*	29.1	29.1	29.0	29.0	23.8	23.8	15.8	15.8	7.3	7.3	3.9	3.9	15.8	15.8
GSLOOK	26.7	26.9	26.9	27.8	23.2	23.0	14.8	15.8	9.5	8.1	4.8	4.5	15.1	15.4
GSMACK	26.1	25.1	25.7	24.8	19.0	17.2	11.5	11.2	6.3	5.3	2.9	2.5	12.6	11.8
GSWS02	22.3	20.0	21.1	19.3	17.5	16.3	11.6	12.5	8.3	6.5	4.5	4.0	11.9	11.3
GR4C	17.8	18.1	17.3	18.0	17.5	15.1	10.2	9.4	1.3	2.0	0.9	1.2	8.9	8.4
GR8C	20.4	22.3	20.4	21.7	20.9	19.3	12.6	13.4	3.8	6.1	3.7	5.5	12.0	12.7
GRT1	18.6	20.7	18.2	19.2	19.7	17.8	11.6	11.8	2.6	4.1	2.5	2.5	9.6	9.9
GRVC	22.3	24.4	21.7	22.9	20.1	18.3	12.6	13.2	3.9	6.3	3.1	4.6	11.9	12.7
TSLOMA	26.5	23.9	26.0	24.7	20.9	20.0	12.4	13.2	8.4	6.6	4.0	3.8	13.6	13.0
TSLOOK	20.1	20.5	19.0	19.1	14.4	14.4	9.4	9.5	4.0	4.1	1.4	1.4	9.0	9.0
TSMACK	20.5	21.4	19.5	20.2	14.2	14.5	9.9	9.6	4.6	4.9	2.5	2.4	9.8	9.9
TSMCRA	24.9	25.6	23.3	23.4	17.6	17.9	11.6	11.3	5.1	4.9	2.2	2.3	11.7	11.7

\* Denotes long-term sites

Table 4.7. Original (U) and temporally-adjusted (A) mean monthly minimum temperatures for each climate station (°C).

	JAN		FEB		MAR		APR		MAY		JUN	
	U	A	U	A	U	A	U	A	U	A	U	A
PRIMET*	-0.9	-0.9	-0.3	-0.3	0.7	0.7	2.4	2.4	5.0	5.0	7.5	7.5
CS2MET*	-0.8	-0.8	0.0	0.0	1.0	1.0	2.7	2.7	5.8	5.8	8.6	8.6
CENMET	-1.4	-1.4	-1.1	-0.7	-1.3	-0.6	0.9	1.2	3.6	4.1	6.4	6.9
VANMET	-1.7	-1.9	-0.7	-1.1	-0.8	-1.1	0.4	0.7	3.7	2.8	6.0	6.3
UPLMET	-2.2	-2.2	-2.0	-1.8	-2.2	-1.7	-0.5	0.0	2.0	1.9	5.2	5.6
H15MET	-0.2	-0.7	-1.1	-0.5	0.4	0.4	1.9	1.7	5.1	4.5	7.2	7.4
RS01*	0.3	0.3	1.3	1.3	1.9	1.9	3.4	3.4	6.4	6.4	9.4	9.4
RS02*	-0.4	-0.4	0.2	0.2	1.2	1.2	2.7	2.7	5.6	5.6	8.5	8.5
RS03	-0.3	-0.2	0.5	0.4	1.2	1.1	2.4	2.4	5.7	5.6	8.5	8.6
RS04*	-2.1	-2.1	-1.7	-1.7	-1.2	-1.2	0.2	0.2	2.7	2.7	6.1	6.1
RS05*	-0.6	-0.6	0.3	0.3	1.0	1.0	2.6	2.6	5.4	5.4	8.5	8.5
RS07*	-0.5	-0.5	0.7	0.7	1.6	1.6	3.3	3.3	5.9	5.9	8.9	8.9
RS10*	0.0	0.0	0.8	0.8	1.6	1.6	3.1	3.1	6.0	6.0	9.1	9.1
RS12*	-1.1	-1.1	-0.9	-0.9	-0.2	-0.2	1.0	1.0	3.8	3.8	6.8	6.8
RS15	0.6	0.4	1.4	1.3	1.9	1.7	3.4	3.0	6.1	5.9	9.5	9.3
RS16	0.4	0.3	1.1	1.1	1.9	1.4	3.6	3.0	6.5	6.1	9.6	9.2
RS17	-0.2	-0.2	0.7	0.5	1.7	1.7	3.4	3.2	6.5	6.5	9.3	9.2
RS20	0.4	0.3	0.9	1.0	1.5	1.5	3.1	3.1	5.9	5.9	8.8	9.1
RS26	-0.4	-0.4	-0.1	0.1	0.5	0.4	1.7	1.9	4.6	4.5	7.7	7.7
RS38*	-0.2	-0.2	0.3	0.3	0.6	0.6	2.0	2.0	4.6	4.6	7.7	7.7
RS86*	-0.5	-0.5	0.2	0.2	1.1	1.1	2.7	2.7	5.4	5.4	8.6	8.6
RS89*	-0.5	-0.5	0.5	0.5	1.2	1.2	2.7	2.7	5.9	5.9	8.6	8.6
GSLOOK	0.7	-0.3	0.2	0.3	1.2	1.4	2.7	2.8	5.8	5.5	8.3	8.3
GSMACK	-0.5	-0.8	-0.1	0.1	0.3	0.5	2.2	1.9	4.7	4.7	7.7	7.5
GSWS02	0.7	-0.1	0.7	0.6	1.3	1.6	3.3	3.0	6.2	5.9	9.1	9.0
GR4C	-0.1	-0.4	-1.5	-1.4	0.4	-1.0	1.1	0.6	4.3	2.4	5.8	6.2
GR8C	0.9	0.4	1.4	1.5	3.1	2.2	3.9	3.2	7.6	6.4	9.2	9.8
GRT1	-0.9	-1.2	-0.6	-0.5	1.5	0.1	1.4	0.9	5.2	3.3	6.6	7.0
GRVC	0.8	0.9	0.7	1.5	2.4	2.4	4.0	3.9	8.5	7.3	9.4	9.9
TSLOMA	0.7	-0.5	0.1	0.3	0.3	0.7	2.4	2.3	4.8	4.5	7.2	7.2
TSLOOK	-0.9	-1.1	-0.6	-1.0	0.0	0.0	1.2	1.2	4.0	4.1	7.2	7.3
TSMACK	0.5	0.2	0.9	0.8	1.8	1.2	3.1	2.3	6.0	5.5	9.2	8.8
TSMCRA	-0.9	-1.2	-0.5	-0.5	0.4	0.0	1.8	1.4	4.3	4.0	7.2	7.1

\* Denotes long-term sites

Table 4.7. (Concluded).

	JUL		AUG		SEP		OCT		NOV		DEC		ANN	
	U	A	U	A	U	A	U	A	U	A	U	A	U	A
PRIMET*	9.3	9.3	9.1	9.1	6.5	6.5	3.4	3.4	1.2	1.2	-1.0	-1.0	3.6	3.6
CS2MET*	10.8	10.8	10.7	10.7	8.0	8.0	4.6	4.6	1.5	1.5	-0.6	-0.6	4.4	4.4
CENMET	9.8	9.4	9.8	9.8	8.1	7.8	3.9	4.7	1.7	0.3	-0.9	-1.1	3.3	3.4
VANMET	9.4	9.0	10.0	9.8	8.5	7.3	4.0	4.2	0.0	-0.5	-2.0	-1.7	3.1	2.8
UPLMET	9.2	8.2	9.2	8.9	7.4	6.6	2.6	3.4	-0.2	-1.1	-2.1	-2.2	2.2	2.1
H15MET	10.3	10.3	10.6	10.8	8.8	8.4	4.6	5.1	1.1	1.2	-1.1	-1.0	4.0	4.0
RS01*	11.9	11.9	11.9	11.9	9.4	9.4	6.2	6.2	2.5	2.5	0.4	0.4	5.4	5.4
RS02*	10.9	10.9	10.8	10.8	8.0	8.0	4.6	4.6	1.9	1.9	-0.2	-0.2	4.5	4.5
RS03	11.8	12.0	12.3	12.5	10.1	10.3	6.4	6.4	1.6	2.1	-0.5	-0.4	5.0	5.1
RS04*	10.0	10.0	10.7	10.7	8.3	8.3	4.3	4.3	-0.4	-0.4	-2.1	-2.1	2.9	2.9
RS05*	11.8	11.8	12.1	12.1	9.7	9.7	6.2	6.2	1.8	1.8	-0.3	-0.3	4.9	4.9
RS07*	11.0	11.0	11.0	11.0	8.3	8.3	4.8	4.8	2.0	2.0	0.0	0.0	4.8	4.8
RS10*	11.8	11.8	11.8	11.8	9.3	9.3	5.7	5.7	2.4	2.4	0.2	0.2	5.2	5.2
RS12*	9.9	9.9	10.0	10.0	7.7	7.7	4.5	4.5	0.8	0.8	-1.2	-1.2	3.4	3.4
RS15	12.3	12.4	12.5	12.4	10.3	10.3	7.0	6.4	2.3	2.3	0.3	0.4	5.6	5.5
RS16	12.1	12.1	12.5	12.5	10.2	10.1	6.9	6.5	2.5	2.4	0.7	0.4	5.7	5.4
RS17	11.4	11.7	11.4	11.5	8.6	8.6	5.0	4.9	2.1	2.4	0.1	0.1	5.0	5.0
RS20	11.7	12.0	11.8	12.2	9.9	10.0	6.1	6.2	2.1	2.2	0.1	0.1	5.2	5.3
RS26	11.3	11.3	11.7	11.8	9.7	9.7	5.9	5.6	1.1	1.2	-0.6	-0.6	4.4	4.4
RS38*	10.5	10.5	10.8	10.8	8.9	8.9	5.5	5.5	1.5	1.5	-0.4	-0.4	4.3	4.3
RS86*	11.1	11.1	11.2	11.2	7.9	8.9	5.4	5.4	1.9	1.9	-0.4	-0.4	4.6	4.6
RS89*	10.6	10.6	10.8	10.8	7.8	7.8	4.6	4.6	1.8	1.8	-0.5	-0.5	4.5	4.5
GSLOOK	11.5	10.8	11.1	10.8	8.2	7.9	4.4	4.6	3.8	2.0	0.2	0.0	4.8	4.5
GSMACK	10.7	10.5	10.6	10.9	8.9	8.3	5.3	5.1	2.3	1.5	-0.3	-0.6	4.3	4.1
GSWS02	12.1	11.5	11.7	11.5	9.5	9.3	5.4	5.3	4.1	2.3	0.6	0.3	5.4	5.0
GR4C	9.5	9.7	9.2	10.1	9.9	7.5	5.1	4.8	-2.2	-0.8	-2.0	-1.7	3.3	3.0
GR8C	11.4	11.8	10.7	11.6	11.3	9.9	6.3	6.0	0.2	2.2	0.7	0.8	5.6	5.5
GRT1	10.4	10.6	10.1	11.0	12.0	9.6	5.9	5.7	-1.2	0.2	-0.9	-0.6	4.1	3.8
GRVC	12.4	13.1	12.1	13.6	11.8	10.7	7.5	7.6	0.6	2.5	0.7	1.1	5.9	6.2
TSLOMA	10.3	9.6	9.9	9.6	7.7	7.4	4.2	4.4	3.3	1.5	-0.2	-0.4	4.2	3.9
TSLOOK	9.8	10.2	9.9	10.1	7.5	7.7	4.6	4.6	1.1	1.3	-0.9	-0.8	3.6	3.6
TSMACK	11.8	11.8	12.0	11.9	9.5	9.3	6.5	6.0	2.1	2.0	0.4	0.3	5.3	5.0
TSMCRA	9.5	9.6	9.7	9.7	7.5	7.5	4.3	4.0	1.1	1.1	-0.6	-0.8	3.7	3.5

\* Denotes long-term sites

into account. However, the procedure hinged upon analysis of hemispherical fisheye photographs which make no distinction between sky blocked by canopy and topography, so separating the effects of these two factors was crucial to the analysis. The goal of analyzing radiation regimes at each site was to determine the monthly regression functions for maximum and minimum temperatures to correct them 'out of the canopy' onto simulated open, flat terrain.

#### 4.5.1 Topographic adjustments

In order to account for the effects of topography on temperature, radiation estimates were made for each site in the HJA. The Image Processing Workbench (IPW) was used to create radiation grids. IPW is a UNIX-based portable image-processing program designed to map solar radiation in mountainous terrain (Dozier and Frew, 1990). It lets the user specify several parameters it considers essential to radiation regimes in complex topography and calculates radiation maps based on user input values and a Digital Elevation Model (DEM). IPW produces topography-induced radiation coverages only and does not account for canopy effects.

IPW simulates solar radiation with the two-stream model that uses a multiple-scattering approximation of the radiative transfer equation to predict the scattering and absorption of light by the clear atmosphere and clouds (Dubayah et al., 1990; Dubayah, 1994). The program operates under the assumption that, within the solar spectrum, a slope is irradiated from three sources: direct beam from the sun, diffuse from the sky, and direct and diffuse reflected by nearby terrain. Calculations were made over the entire HJA

50-meter grid every 20 minutes during daylight hours on the 15<sup>th</sup> of each month, then summed together to get a daily total. This daily total was taken to be the average daily radiation for that month.

IPW assumes that topographic effects on solar irradiance are due mainly to variations in the sunbeam angle and shadowing from local horizons, and uses a relevant set of parameters which can be specified by the user (Dozier and Frew, 1990). Single-scattering albedo and scattering asymmetry parameters are related to radiation extinction in the atmosphere (Dubayah, 1990). We used recommended values for these parameters of 0.8 and 0.6 respectively (David Garen, pers. comm.). Since coniferous forests have albedo values between 0.05 and 0.15 (Oke, 1987), 0.10 was used as a constant surface albedo over the entire HJA. An optical depth value of 0.42 was used based on tests using observed solar radiation in the HJA (described below).

Unless otherwise noted, the above values were used for all IPW calculations. Other parameters such as solar zenith angles and extraterrestrial radiation are based on solar geometry throughout the year and hard-coded within IPW. Sky view factors and terrain configuration factors (geometric radiation effects between each pixel and other mutually visible pixels), calculated within IPW, are also important in the procedure.

The first step in the process was to calculate direct and diffuse clear sky radiation over the HJA for each month. The direct beam at each pixel was attenuated by multiplying the incoming value by a horizon mask, calculated with solar geometry and the DEM. Diffuse radiation was reduced at each pixel according to its sky view factor, also calculated from the DEM. These direct and diffuse components were then

recombined to give clear sky radiation values at each pixel treating them as horizontal surfaces. Horizontal surfaces were modeled here because radiometers measure radiation over a hemisphere leveled horizontally.

Since IPW is sensitive to optical depth ( $t$ ) specifications, care was taken to determine the optimal value to use. Daily solar radiation data from UPLMET's level radiometer for the period 1995-2000 was plotted against IPW's monthly clear sky predictions for UPLMET's pixel using various values for  $t$ . Visual comparison between UPLMET's clear sky envelope and IPW's theoretical curve revealed the optimal value of  $t$  to be 0.42 (Figure 4.4). UPLMET was chosen from the five MET sites because its site is open and had the most reliable radiation data. Shading from any nearby trees would cause discrepancies between observed and IPW-predicted values, and UPLMET's data quality was superior to other MET sites. IPW-predicted radiation at UPLMET is least accurate during winter months (Figure 4.4). This may be due to higher albedo values from snow cover which we did not account for using IPW.

Next, we determined the amount of attenuation from clouds for each month by dividing UPLMET's historical monthly radiation averages by IPW's theoretical clear sky values at UPLMET. The HJA is small enough to consider these monthly 'cloud factors' as constant over its area, although there are undoubtedly some differences across the watershed. Resulting cloud factors range from just under 50% in cloudy January to less than 17% in sunny August (Table 4.8d). IPW's horizontal-surface radiation coverages were then multiplied by these cloud factors to get twelve monthly horizontal-surface cloud-adjusted radiation maps of the HJA. Dividing these maps by IPW's computed extraterrestrial (potential) radiation over the HJA gives monthly 'transmittance coefficients' for every pixel

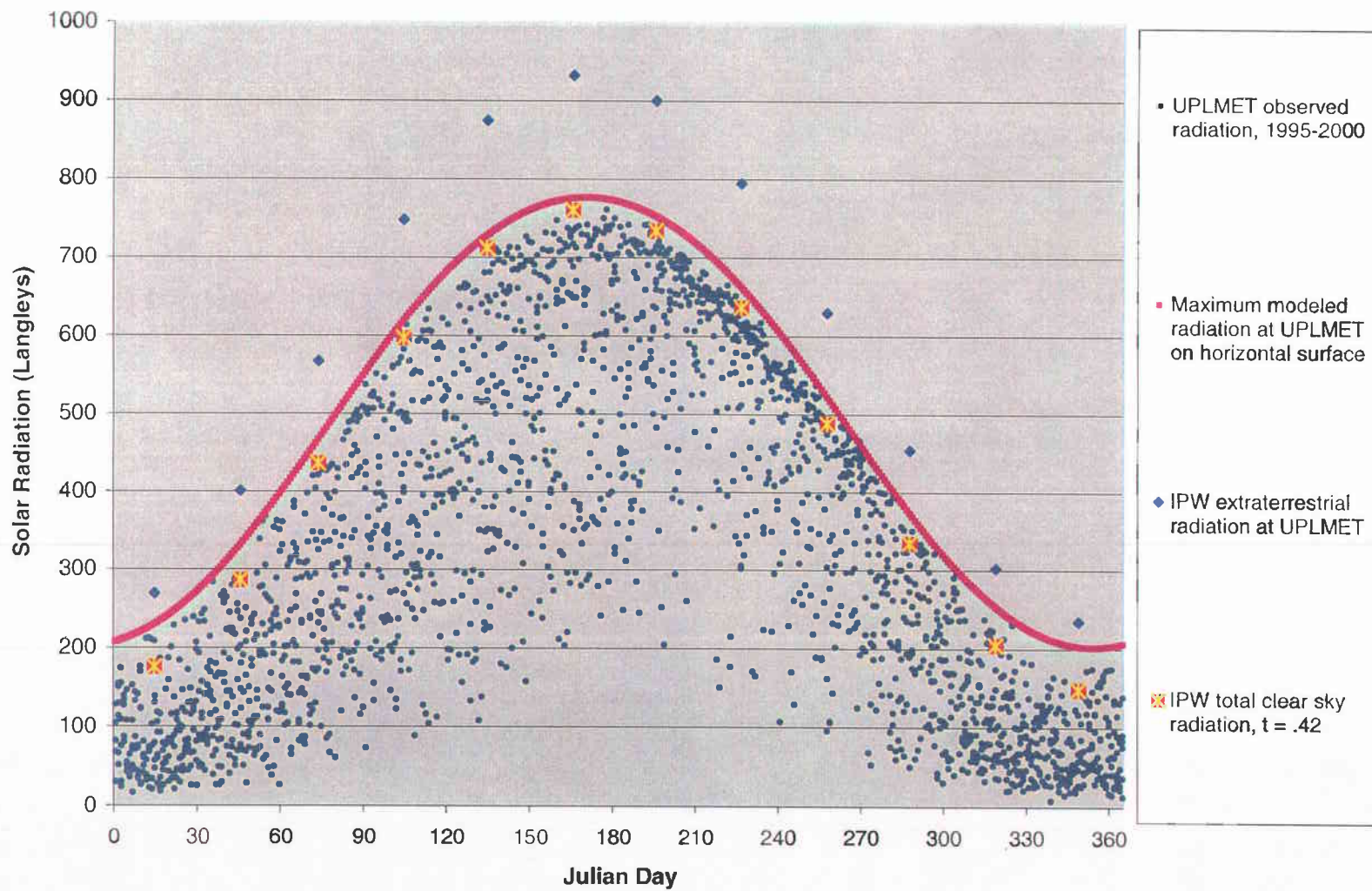


Figure 4.4. Observed and modeled solar radiation at UPLMET.

Table 4.8. Observed and modeled monthly solar radiation variables at UPLMET (MJ/m<sup>2</sup>·day).

	JAN	FEB	MAR	APR	MAY	JUN	JUL	AUG	SEP	OCT	NOV	DEC
a) Observed radiation 1995-2000	3.74	6.63	10.92	16.24	19.65	23.42	24.88	22.19	16.51	9.28	4.55	3.24
b) IPW clear-sky radiation (horizontal surface)	7.38	12.00	18.23	25.03	29.79	31.84	30.77	26.67	20.50	13.99	8.58	6.25
c) IPW extraterrestrial radiation	11.06	16.34	23.17	30.62	35.84	38.19	36.92	32.36	25.60	18.57	12.41	9.44
d) Cloud factors (1-a/b)	0.49	0.45	0.40	0.35	0.34	0.26	0.19	0.17	0.19	0.34	0.47	0.48
e) Transmission coefficients (a/c)	0.34	0.41	0.47	0.53	0.55	0.61	0.67	0.69	0.65	0.50	0.37	0.35
f) Proportion diffuse radiation	0.86	0.77	0.67	0.59	0.56	0.47	0.38	0.37	0.42	0.63	0.82	0.85
g) Final IPW-modeled radiation (horizontal surface)	3.69	6.54	10.77	16.12	19.48	23.28	24.81	22.18	16.46	9.20	4.47	3.18
h) Final IPW-modeled radiation (sloped surface)	3.52	6.21	10.35	15.47	18.69	22.45	23.97	21.37	15.84	8.74	4.27	3.01

based on the daily value for the 15<sup>th</sup> of each month.

These coefficients are essential for the next step, which uses Bristow and Campbell's (1985) equation for determining the percentage of diffuse radiation from total radiation. Monthly values for direct and diffuse fractions of total radiation are important because as they change, the effect of topography on total radiation (and hence temperature) changes. For example, on a cloudy day when the fraction of diffuse radiation is high, there will be less of a radiation difference between a north-facing and a south-facing slope, resulting in a small temperature difference. Monthly fractions of direct and diffuse radiation to represent cloudiness are not taken into account in most radiation models. Most models increase or decrease clear sky radiation to account for cloudiness, but in this study, direct and diffuse fractions were entered into IPW, allowing it to explicitly evaluate topographic effects.

The general form of the Bristow-Campbell equation is

$$T_d = T_t [1 - \exp\{0.6(1 - B/T_t)/(B - 0.4)\}] \quad (3)$$

where  $T_t$  = daily total transmittance on a horizontal surface,  $T_d$  = daily diffuse transmittance on a horizontal surface, and  $B$  = maximum clear sky transmissivity (Bristow and Campbell, 1985). We used  $B = 1.0$ , a value used in other Northwest regional studies (David Garen, pers. comm.), giving the simplified Bristow-Campbell equation

$$T_d = T_t [1 - \exp(1 - 1/T_t)] \quad (4)$$

Calculated proportions of diffuse radiation at UPLMET range from over 0.85 in winter to just under 0.37 in summer (Table

4.8f). Bristow and Campbell's diffuse percentage of total radiation over the high desert of eastern Washington during summer was around 0.14 (Bristow and Campbell, 1985). The higher value for UPLMET is not surprising given the cloudy maritime climate of the Oregon Cascades.

Finally, we multiplied the cloud-adjusted horizontal-surface radiation coverages by the appropriate diffuse and direct proportions, and reintroduced slope and aspect into the procedure. The results are twelve radiation maps taking into account cloudiness, proportions of direct and diffuse radiation, terrain shading, and slope/aspect/elevation effects for each month (Appendix D). It is important to remember that the final radiation values for each pixel assume their surfaces to be sloped according to the DEM, not the value a leveled radiometer would record.

Table 4.9 summarizes all of the steps taken to produce these radiation maps. Table 4.10 shows observed and modeled radiation values for the three MET sites with the most reliable radiation datasets. Note that IPW's predicted radiation for UPLMET is slightly lower than the observed values for that site. This is because IPW is modeling UPLMET's radiation on a gentle northeast-facing slope, while the observed values are taken over a hemisphere which is horizontally leveled. In all cases the predicted values are higher than observed values because radiation at these sites is affected to some degree by adjacent forests.

Table 4.11 shows modeled cloud-adjusted radiation at each site on a horizontal surface, with no horizon shading present. Table 4.12a lists the amounts of radiation blocked at each site from horizon shading, and Table 4.12b shows radiation adjustments when transforming the horizontal surface to a sloped surface. Table 4.13 shows the final sloped-

Table 4.9. Summary of steps taken to create solar radiation grids.

1. Model direct and diffuse components of clear sky radiation.
2. Multiply direct radiation by horizon mask and diffuse radiation by sky view factor.
3. Add components together to get total clear sky radiation on horizontal surface.
4. Compare modeled clear sky radiation to historical observations at UPLMET.
5. Repeat steps 1-4 for varying optical depth values to determine optimal value that gives the best match between modeled and observed radiation.
6. Compute cloud factors for each month by dividing mean observed radiation at UPLMET by theoretical clear sky radiation at UPLMET.
7. Multiply clear sky radiation over the HJA by monthly cloud factors to get cloud-corrected radiation.
8. Use Bristow and Campbell's equation to determine proportions of direct and diffuse radiation for each month.
9. Apply effects of topography to make final radiation maps.

Table 4.10. Observed and modeled monthly solar radiation for MET sites (MJ/m<sup>2</sup>·day).

	JAN	FEB	MAR	APR	MAY	JUN	JUL	AUG	SEP	OCT	NOV	DEC
a) PRIMET observed radiation 1995-1998	2.70	5.67	9.50	13.69	17.09	20.82	22.14	19.52	13.48	7.38	3.38	1.94
b) PRIMET IPW-modeled radiation (horizontal surface)	2.84	5.40	9.66	14.71	17.80	21.49	22.97	20.55	14.98	8.04	3.55	2.51
c) CENMET observed radiation 1995-2000	3.09	4.97	8.76	12.69	15.21	20.65	23.17	19.85	14.42	8.00	3.83	3.03
d) CENMET IPW-modeled radiation (horizontal surface)	3.41	6.07	10.06	15.07	18.56	22.37	23.80	21.07	15.44	8.54	4.20	2.99
e) UPLMET observed radiation 1995-2000	3.74	6.63	10.92	16.24	19.65	23.42	24.88	22.19	16.51	9.28	4.55	3.24
f) UPLMET IPW-modeled radiation (horizontal surface)	3.69	6.54	10.77	16.12	19.48	23.28	24.81	22.18	16.46	9.20	4.47	3.18

Table 4.11. Modeled horizontal-surface, cloud-adjusted monthly solar radiation at each climate station (MJ/m<sup>2</sup>·day).

	ELEV (m)	JAN	FEB	MAR	APR	MAY	JUN	JUL	AUG	SEP	OCT	NOV	DEC
PRIMET	430	3.76	6.67	11.03	16.38	19.77	23.56	25.02	22.36	16.68	9.33	4.50	3.27
CS2MET	460	3.76	6.67	11.05	16.38	19.79	23.56	25.02	22.38	16.69	9.36	4.58	3.27
CENMET	1018	3.85	6.80	11.23	16.61	20.06	23.87	25.35	22.68	16.96	9.51	4.68	3.36
VANMET	1273	3.91	6.85	11.32	16.72	20.17	23.99	25.50	22.83	17.08	9.60	4.74	3.41
UPLMET	1294	3.91	6.85	11.32	16.72	20.19	24.02	25.50	22.84	17.08	9.60	4.75	3.40
H15MET	922	3.85	6.78	11.19	16.56	20.00	23.82	25.28	22.63	16.91	9.48	4.68	3.36
RS01	490	3.77	6.68	11.05	16.39	19.80	23.57	25.01	22.38	16.69	9.36	4.58	3.27
RS02	490	3.76	6.67	11.05	16.38	19.79	23.56	25.02	22.38	16.68	9.36	4.58	3.27
RS03	945	3.85	6.79	11.21	16.59	20.03	23.83	25.31	22.65	16.92	9.50	4.68	3.37
RS04	1310	3.91	6.86	11.32	16.72	20.20	24.03	25.50	22.85	17.07	9.61	4.74	3.41
RS05	880	3.85	6.78	11.18	16.56	20.00	23.82	25.27	22.63	16.90	9.48	4.68	3.35
RS07	460	3.78	6.68	11.06	16.38	19.82	23.59	25.06	22.43	16.71	9.38	4.59	3.28
RS10	610	3.79	6.71	11.09	16.44	19.85	23.65	25.09	22.47	16.77	9.39	4.62	3.31
RS12	1007	3.85	6.79	11.22	16.60	20.05	23.86	25.32	22.67	16.96	9.51	4.68	3.36
RS15	760	3.80	6.74	11.15	16.48	19.93	23.72	25.19	22.54	16.83	9.44	4.63	3.32
RS16	640	3.80	6.72	11.11	16.48	19.89	23.70	25.15	22.51	16.81	9.41	4.63	3.32
RS17	490	3.78	6.68	11.06	16.38	19.82	23.59	25.06	22.43	16.71	9.38	4.59	3.29
RS20	683	3.80	6.71	11.11	16.47	19.89	23.70	25.15	22.51	16.80	9.42	4.63	3.32
RS26	1040	3.87	6.80	11.25	16.62	20.07	23.91	25.37	22.72	16.97	9.53	4.70	3.36
RS38	977	3.85	6.79	11.21	16.60	20.02	23.83	25.31	22.66	16.92	9.50	4.68	3.36
RS86	653	3.79	6.71	11.09	16.44	19.87	23.66	25.09	22.46	16.78	9.39	4.62	3.31
RS89	475	3.78	6.68	11.06	16.38	19.82	23.59	25.06	22.43	16.72	9.38	4.59	3.27
GSLOOK	436	3.76	6.67	11.03	16.37	19.79	23.56	25.02	22.36	16.68	9.34	4.57	3.27
GSMACK	756	3.81	6.74	11.15	16.49	19.93	23.73	25.19	22.56	16.84	9.45	4.64	3.32
GSWS02	561	3.79	6.70	11.09	16.44	19.85	23.64	25.08	22.45	16.75	9.38	4.61	3.30
GR4C	1268	3.91	6.85	11.30	16.70	20.17	23.99	25.48	22.82	17.06	9.60	4.74	3.40
GR8C	756	3.80	6.74	11.15	16.48	19.93	23.72	25.19	22.54	16.83	9.44	4.63	3.32
GRT1	1277	3.91	6.85	11.31	16.71	20.18	24.01	25.50	22.84	17.08	9.60	4.74	3.40
GRVC	805	3.82	6.75	11.16	16.53	19.95	23.76	25.21	22.59	16.84	9.46	4.65	3.32
TSLOMA	652	3.79	6.71	11.10	16.46	19.89	23.70	25.14	22.50	16.79	9.41	4.63	3.32
TSLOOK	988	3.85	6.79	11.21	16.61	20.03	23.83	25.32	22.68	16.94	9.50	4.68	3.36
TSMACK	780	3.82	6.76	11.15	16.51	19.93	23.76	25.21	22.57	16.84	9.44	4.64	3.32
TSMCRA	829	3.83	6.76	11.17	16.53	19.97	23.77	25.23	22.59	16.87	9.46	4.65	3.33

Table 4.12a. Differences between modeled horizontal-surface, cloud-adjusted and horizontal-surface, cloud/horizon-adjusted monthly solar radiation at each climate station (MJ/m<sup>2</sup>·day).

	ELEV (m)	JAN	FEB	MAR	APR	MAY	JUN	JUL	AUG	SEP	OCT	NOV	DEC
PRIMET	430	0.92	1.27	1.37	1.67	1.97	2.07	2.05	1.81	1.70	1.29	0.95	0.76
CS2MET	460	0.73	0.86	1.02	1.18	1.41	1.40	1.32	1.22	1.26	0.98	0.72	0.86
CENMET	1018	0.44	0.73	1.17	1.54	1.50	1.50	1.55	1.61	1.52	0.97	0.48	0.37
VANMET	1273	0.17	0.22	0.36	0.40	0.49	0.47	0.48	0.41	0.36	0.28	0.22	0.18
UPLMET	1294	0.22	0.31	0.55	0.60	0.71	0.74	0.69	0.66	0.62	0.40	0.28	0.22
H15MET	922	0.25	0.37	0.61	0.71	0.89	1.06	0.78	0.73	0.67	0.47	0.29	0.25
RS01	490	0.52	0.90	1.29	1.77	2.08	2.10	2.18	1.96	1.61	1.10	0.63	0.52
RS02	490	0.81	0.82	1.08	1.44	1.50	1.65	1.58	1.52	1.19	0.92	0.80	0.84
RS03	945	0.23	0.37	0.53	0.69	0.74	0.68	0.73	0.71	0.57	0.45	0.29	0.27
RS04	1310	0.59	0.85	1.09	1.27	1.75	1.44	1.71	1.52	1.46	1.16	0.56	0.59
RS05	880	0.49	0.29	0.30	0.35	0.45	0.46	0.47	0.36	0.34	0.33	0.36	0.71
RS07	460	0.87	0.77	0.74	0.86	1.00	0.97	0.94	0.86	0.84	0.88	0.96	0.66
RS10	610	0.15	0.26	0.35	0.37	0.48	0.53	0.41	0.42	0.33	0.27	0.22	0.25
RS12	1007	0.81	1.26	1.58	1.92	2.33	2.60	2.42	2.16	1.75	1.27	0.94	0.74
RS15	760	0.30	0.53	0.92	1.11	1.31	1.67	1.42	1.25	1.02	0.65	0.35	0.30
RS16	640	0.30	0.51	0.88	1.11	1.27	1.65	1.38	1.22	1.00	0.62	0.35	0.30
RS17	490	2.14	2.14	2.01	1.71	1.88	1.71	1.63	1.54	1.75	2.26	2.34	1.79
RS20	683	1.20	1.20	1.59	1.83	2.20	2.67	2.27	2.21	1.83	1.57	1.41	1.38
RS26	1040	0.48	0.62	0.92	0.90	1.02	1.12	1.05	0.98	0.96	0.75	0.53	0.51
RS38	977	0.16	0.26	0.37	0.45	0.57	0.56	0.55	0.48	0.42	0.31	0.18	0.18
RS86	653	0.04	0.08	0.14	0.16	0.21	0.20	0.13	0.07	0.10	0.08	0.06	0.08
RS89	475	0.06	0.16	0.19	0.23	0.36	0.27	0.31	0.22	0.21	0.20	0.09	0.11
GSLOOK	436	0.04	0.12	0.21	0.19	0.33	0.29	0.30	0.20	0.25	0.16	0.09	0.07
GSMACK	756	0.96	1.44	2.11	2.83	2.78	2.98	2.98	2.69	2.48	1.87	1.45	0.87
GSWS02	561	0.93	1.46	1.83	2.04	2.12	2.65	2.29	2.15	2.25	1.57	1.17	0.94
GR4C	1268	1.40	1.65	2.02	2.23	2.32	2.30	2.26	2.35	2.38	2.04	1.27	1.44
GR8C	756	2.24	1.89	1.94	2.12	2.52	2.79	2.63	2.20	2.28	2.19	2.54	1.91
GRT1	1277	0.49	0.51	0.62	0.72	0.83	0.86	0.85	0.80	0.74	0.57	0.51	0.44
GRVC	805	0.25	0.40	0.66	0.85	1.03	1.32	1.24	0.91	0.88	0.50	0.29	0.21
TSLOMA	652	0.01	0.02	0.03	0.04	0.04	0.03	0.07	0.07	0.06	0.02	0.00	0.00
TSLOOK	988	0.45	0.64	0.82	0.91	0.96	0.96	0.94	0.90	0.97	0.72	0.48	0.97
TSNACK	780	0.62	0.93	1.12	1.16	1.13	1.22	1.10	1.03	1.16	1.19	0.96	0.47
TSMCRA	829	1.09	1.67	1.73	1.91	2.08	2.29	2.34	2.13	2.02	1.94	1.33	0.95

Table 4.12b. Differences between modeled horizontal-surface, cloud/horizon-adjusted and sloped-surface, cloud/horizon-adjusted monthly solar radiation at each climate station (MJ/m<sup>2</sup>·day).

	SLOPE (°)	ASPECT (°)	JAN	FEB	MAR	APR	MAY	JUN	JUL	AUG	SEP	OCT	NOV	DEC
PRIMET	0	-	-0.05	-0.10	-0.14	-0.17	-0.14	-0.13	-0.15	-0.18	-0.23	-0.15	-0.03	-0.05
CS2MET	5	355	0.48	1.05	1.76	2.30	2.20	2.48	3.04	3.53	3.38	1.85	0.68	0.37
CENMET	12	260	0.27	0.41	0.49	0.70	1.00	1.19	1.02	0.60	0.35	0.37	0.31	0.25
VANMET	13	180	0.08	-0.01	-0.04	0.22	0.80	1.07	0.77	-0.18	-0.97	-0.49	-0.05	0.03
UPLMET	13	72	0.17	0.33	0.42	0.65	0.79	0.83	0.84	0.81	0.62	0.46	0.20	0.17
H15MET	15	240	0.19	0.16	0.18	0.53	1.06	1.26	1.11	0.15	-0.60	-0.20	0.13	0.14
RS01	41	200	0.87	1.40	2.11	3.09	3.76	4.45	4.39	3.63	2.63	1.70	1.01	0.73
RS02	22	285	0.36	0.70	1.15	1.55	1.65	1.87	2.16	2.12	1.92	1.11	0.47	0.28
RS03	5	315	0.15	0.27	0.43	0.60	0.55	0.67	0.67	0.73	0.67	0.39	0.18	0.14
RS04	27	270	0.58	0.94	1.43	1.99	2.03	2.56	2.47	2.36	1.96	1.20	0.68	0.47
RS05	12	10	0.05	0.12	0.18	0.22	0.19	0.22	0.20	0.32	0.34	0.18	0.07	0.03
RS07	19	1	0.80	1.79	3.00	4.02	4.13	4.74	5.43	5.83	5.31	2.87	1.06	0.75
RS10	6	170	-0.05	-0.26	-0.28	-0.21	0.02	0.08	-0.02	-0.56	-0.85	-0.55	-0.11	-0.09
RS12	11	282	0.19	0.15	0.16	0.41	0.63	0.78	0.64	0.07	-0.22	0.03	0.17	0.13
RS15	33	350	2.67	3.74	5.14	6.61	7.16	7.56	8.54	8.87	7.99	5.15	3.11	2.26
RS16	29	202	1.36	1.35	1.76	2.46	3.23	3.54	3.48	2.64	1.77	1.56	1.55	1.46
RS17	14	315	-1.31	-0.78	0.08	0.70	0.52	0.87	1.26	1.80	1.61	-0.13	-1.34	-0.98
RS20	34	180	-0.71	-0.66	-0.80	-0.33	0.29	0.43	0.46	-1.02	-1.95	-1.50	-0.94	-0.97
RS26	20	180	-0.10	-0.24	-0.35	0.16	0.88	1.23	0.90	-0.30	-1.34	-0.78	-0.21	-0.21
RS38	15	170	0.13	0.13	0.14	0.44	0.96	1.31	0.97	-0.01	-0.74	-0.35	0.11	0.09
RS86	28	215	0.96	1.45	2.10	3.10	4.14	4.83	4.64	3.37	2.00	1.45	1.14	0.80
RS89	37	315	2.01	3.32	5.25	7.21	7.85	9.00	9.45	9.20	7.76	4.74	2.63	1.72
GSL00K	1	230	0.83	1.26	1.47	1.68	1.69	2.24	1.87	1.72	1.74	1.26	1.01	0.82
GSMACK	7	350	0.47	0.37	0.13	-0.33	-0.20	-0.37	-0.31	0.13	0.33	0.45	-0.12	0.60
GSWS02	13	340	1.49	0.96	1.07	1.42	1.71	1.54	1.94	1.98	1.88	1.58	1.60	1.08
GRAC	13	60	-0.34	-0.01	0.36	0.76	0.73	1.01	1.38	1.68	1.40	0.32	-0.03	-0.50
GR8C	25	135	-1.61	-0.95	-0.58	-0.08	0.17	0.39	0.29	-0.31	-1.14	-1.36	-1.88	-1.39
GRT1	12	190	-0.45	-0.51	-0.63	-0.57	-0.18	-0.06	-0.32	-0.99	-1.47	-0.90	-0.48	-0.33
GRVC	17	90	0.40	0.62	0.76	0.89	0.82	0.65	0.77	1.27	1.22	0.84	0.45	0.84
TSLOMA	0	-	0.54	0.72	0.75	0.78	1.00	1.15	1.03	0.54	0.37	0.81	0.87	0.41
TSLOOK	5	315	0.69	1.11	1.01	1.11	1.25	1.46	1.53	1.34	1.17	1.33	0.92	0.04
TSMACK	7	330	1.11	0.74	1.30	1.71	1.80	1.73	1.84	1.76	1.70	0.74	0.99	1.27
TSMCRA	3	225	-0.01	-0.88	-0.68	-0.70	-0.67	-0.80	-0.94	-0.95	-0.87	-0.98	-0.65	-0.11

Table 4.13. Modeled sloped-surface, cloud/horizon-adjusted monthly solar radiation at each climate station (MJ/m<sup>2</sup>·day).

	SLOPE (°)	ASPECT (°)	JAN	FEB	MAR	APR	MAY	JUN	JUL	AUG	SEP	OCT	NOV	DEC
PRIMET	0	-	2.89	5.50	9.80	14.88	17.94	21.62	23.12	20.73	15.21	8.19	3.58	2.56
CS2MET	5	355	2.55	4.76	8.27	12.90	16.18	19.68	20.66	17.63	12.05	6.53	3.18	2.04
CENMET	12	260	3.14	5.66	9.57	14.37	17.56	21.18	22.78	20.47	15.09	8.17	3.89	2.74
VANMET	13	180	3.66	6.64	11.00	16.10	18.88	22.45	24.25	22.60	17.69	9.81	4.57	3.20
UPLMET	13	72	3.52	6.21	10.35	15.47	18.69	22.45	23.97	21.37	15.84	8.74	4.27	3.01
H15MET	15	240	3.41	6.25	10.40	15.32	18.05	21.50	23.39	21.75	16.84	9.21	4.26	2.97
RS01	41	200	2.38	4.38	7.65	11.53	13.96	17.02	18.44	16.79	12.45	6.56	2.94	2.02
RS02	22	285	2.59	5.15	8.82	13.39	16.64	20.04	21.28	18.74	13.57	7.33	3.31	2.15
RS03	5	315	3.47	6.15	10.25	15.30	18.74	22.48	23.91	21.21	15.68	8.66	4.21	2.96
RS04	27	270	2.74	5.07	8.80	13.46	16.42	20.03	21.32	18.97	13.65	7.25	3.50	2.35
RS05	12	10	3.31	6.37	10.70	15.99	19.36	23.14	24.60	21.95	16.22	8.97	4.25	2.61
RS07	19	1	2.11	4.12	7.32	11.50	14.69	17.88	18.69	15.74	10.56	5.63	2.57	1.87
RS10	6	170	3.69	6.71	11.02	16.28	19.35	23.04	24.70	22.61	17.29	9.67	4.51	3.15
RS12	11	282	2.85	5.38	9.48	14.27	17.09	20.48	22.26	20.44	15.43	8.21	3.57	2.49
RS15	33	350	0.83	2.47	5.09	8.76	11.46	14.49	15.23	12.42	7.82	3.64	1.17	0.76
RS16	29	202	2.14	4.86	8.47	12.91	15.39	18.51	20.29	18.65	14.04	7.23	2.73	1.56
RS17	14	315	2.95	5.32	8.97	13.97	17.42	21.01	22.17	19.09	13.35	7.25	3.59	2.48
RS20	34	180	3.31	6.17	10.32	14.97	17.40	20.60	22.42	21.32	16.92	9.35	4.16	2.91
RS26	20	180	3.49	6.42	10.68	15.56	18.17	21.56	23.42	22.04	17.35	9.56	4.38	3.06
RS38	15	170	3.56	6.40	10.70	15.71	18.49	21.96	23.79	22.19	17.24	9.54	4.39	3.09
RS86	28	215	2.79	5.18	8.85	13.18	15.52	18.63	20.32	19.02	14.68	7.86	3.42	2.43
RS89	37	315	1.71	3.20	5.62	8.94	11.61	14.32	15.30	13.01	8.75	4.44	1.87	1.44
GSLOOK	1	230	2.89	5.29	9.35	14.50	17.77	21.03	22.85	20.44	14.69	7.92	3.47	2.38
GSMACK	7	350	2.38	4.93	8.91	13.99	17.35	21.12	22.52	19.74	14.03	7.13	3.31	1.85
GSWS02	13	340	1.37	4.28	8.19	12.98	16.02	19.45	20.85	18.32	12.62	6.23	1.84	1.28
GR4C	13	60	2.85	5.21	8.92	13.71	17.12	20.68	21.84	18.79	13.28	7.24	3.50	2.46
GR8C	25	135	3.17	5.80	9.79	14.44	17.24	20.54	22.27	20.65	15.69	8.61	3.97	2.80
GRT1	12	190	3.87	6.85	11.32	16.56	19.53	23.21	24.97	23.03	17.81	9.93	4.71	3.29
GRVC	17	90	3.17	5.73	9.74	14.79	18.10	21.79	23.20	20.41	14.74	8.12	3.91	2.27
TSLOMA	0	-	3.26	6.01	10.32	15.64	18.85	22.52	24.18	22.03	16.48	8.58	3.76	2.91
TSLOOK	5	315	2.71	5.04	9.38	14.59	17.82	21.41	22.85	20.44	14.80	7.45	3.28	2.35
TEMACK	7	330	2.09	5.09	8.73	13.64	17.00	20.81	22.27	19.78	13.98	7.51	2.69	1.58
TEMCRA	3	225	2.75	5.97	10.12	15.32	18.56	22.28	23.83	21.41	15.72	8.50	3.97	2.49

surface, cloud/horizon adjusted solar radiation at each site, using the values given in Tables 4.12a and 4.12b to adjust Table 4.11. Note how sites in topographically-sheltered areas, such as PRIMET, experience a greater reduction in radiation from horizon shading than sites that are more open. Sites with north-facing slopes such as RS07 experienced a reduction in radiation when transformed from a horizontal surface to a sloped surface. Some sites on south-facing slopes, such as RS20, did not necessarily see an increase in radiation when going from a horizontal to a sloped surface, because other elements such as sky view factor and proportions of direct and diffuse radiation were also considered. Note that flat sites such as PRIMET and TSLOMA experience a non-zero adjustment when introducing slope and aspect into the process. This is because their slope and aspect pixel values on the 50-meter DEM were not exactly  $0^\circ$ . The effects of elevation on solar radiation (Table 4.11) are slight compared to the topographic effects of horizon shading and slope and aspect.

#### 4.5.2 Canopy adjustments

After cloud-adjusted, topographically-correct radiation had been estimated at each site, the next step was to quantify the effects of the forest canopy on each site's radiation regime.

Hemispherical 'fisheye' photographs were taken and analyzed at every climate station in the HJA. Such photography has long been used in forest research and is an effective tool for characterizing forest light regimes (Chan

et al., 1986; Vales and Bunnell, 1988; Easter and Spies, 1994).

Photographs were taken using a Cannon AE-1 camera body with a 7.5 millimeter fisheye lens mounted on a tripod. Great care was taken to level the plane of the camera and a magnetic compass was used to orient the top of the image with true north. The most common problem with hemispherical photography in forests is getting the proper relative exposure between sky and vegetation, a problem which is magnified under high contrast (sunny) conditions (Chen et al., 1986). For this reason, photographs were taken as early or as late in the day as possible or under overcast skies, when lighting was mostly diffuse. Several photographs with variable combinations of shutter speeds and f-stop were taken at each site to ensure the best images possible. Black and white film was used, and reference photographs of site surroundings and surface characteristics were taken.

For analysis of fisheye photographs the HemiView software program was used (Delta-T Devices Ltd, 1999). HemiView allows the user to specify a gray-level threshold to discriminate between sky and vegetation in digital fisheye images. This valuable feature allowed a different threshold for each site's image based on its exposure characteristics to best differentiate between vegetation and sky on an image-by-image basis. Since HemiView's primary function is to 'visually' analyze photographs, it was used strictly to ascertain the percentage of direct and diffuse radiation blocked by each site's canopy, not to predict actual radiation amounts. IPW emphasizes explicit modeling of incoming solar radiation and was used for this purpose. Together, the two programs provided an effective tandem for radiation analysis in the HJA.

Several parameters could be specified to optimize HemiView's output. The most important input variable was the percentage of diffuse radiation for each month which was obtained using the Bristow-Campbell equation and IPW. Percentages of direct and diffuse radiation represent monthly variation of cloudiness. HemiView was able to calculate blocked amounts of direct and diffuse radiation differently and independent of one another. A constant clear-sky transmissivity value of 0.77 was specified. This value was obtained by dividing IPW clear-sky radiation at UPLMET by the extraterrestrial radiation above the HJA for each month and taking the average over all months. These monthly values are similar to those used in previous HJA radiation studies (Greenland, 1994). Our analysis used the Uniform Overcast Sky Model which assumes equal amounts of diffuse radiation from all sky sectors, selected to match IPW specifications and cloudiness regimes at the HJA. Each site was treated as if it were at sea level in order for transmissivity values to remain constant for all sites. It should be noted that with the exception of diffuse radiation percentages, varying all of these parameters changed results so slightly as to be negligible, well within the margin of error inherent in the fisheye photographs. HemiView was used to obtain proportions only, not actual radiation values.

Hemispherical photographs do not separate the effects of vegetation and topography or provide information on the relative distances of objects from the camera. For most HJA sites (except for the MET sites), the density of the surrounding forest is such that surrounding terrain is not visible anyway. Proportions of blocked radiation calculated by HemiView are shown in Table 4.14 and sky view factors for each site are listed on Table 4.15.

Table 4.14. Proportions of total solar radiation blocked by canopy and topography at each climate station.

	JAN	FEB	MAR	APR	MAY	JUN	JUL	AUG	SEP	OCT	NOV	DEC
PRIMET	0.255	0.214	0.174	0.151	0.142	0.135	0.128	0.126	0.139	0.171	0.215	0.257
CS2MET	0.731	0.760	0.797	0.697	0.627	0.630	0.628	0.618	0.713	0.809	0.760	0.734
CENMET	0.176	0.171	0.154	0.124	0.102	0.091	0.086	0.091	0.120	0.155	0.171	0.177
VANMET	0.069	0.062	0.054	0.052	0.043	0.036	0.033	0.037	0.047	0.052	0.062	0.068
UPLMET	0.141	0.120	0.108	0.079	0.084	0.113	0.113	0.079	0.075	0.110	0.121	0.143
H15MET	0.604	0.635	0.631	0.580	0.527	0.419	0.413	0.537	0.595	0.645	0.635	0.608
RS01	0.817	0.808	0.820	0.842	0.777	0.740	0.736	0.780	0.856	0.823	0.809	0.819
RS02	0.903	0.913	0.927	0.916	0.850	0.824	0.820	0.847	0.925	0.932	0.913	0.904
RS03	0.952	0.957	0.965	0.948	0.902	0.923	0.920	0.896	0.952	0.967	0.957	0.953
RS04	0.904	0.913	0.924	0.930	0.921	0.879	0.879	0.930	0.939	0.928	0.913	0.905
RS05	0.930	0.933	0.936	0.903	0.885	0.907	0.905	0.878	0.904	0.938	0.933	0.931
RS07	0.895	0.906	0.913	0.904	0.888	0.911	0.914	0.892	0.912	0.918	0.906	0.896
RS10	0.918	0.909	0.906	0.912	0.926	0.952	0.953	0.925	0.908	0.905	0.909	0.917
RS12	0.943	0.949	0.948	0.926	0.904	0.900	0.897	0.899	0.926	0.950	0.949	0.944
RS13	0.821	0.833	0.826	0.807	0.764	0.728	0.724	0.759	0.815	0.830	0.834	0.822
RS130	0.433	0.412	0.306	0.266	0.290	0.273	0.264	0.266	0.239	0.301	0.414	0.434
RS15	0.924	0.932	0.943	0.931	0.901	0.909	0.909	0.901	0.938	0.946	0.932	0.925
RS16	0.951	0.953	0.925	0.907	0.947	0.968	0.969	0.943	0.898	0.924	0.953	0.951
RS17	0.897	0.908	0.909	0.882	0.873	0.882	0.883	0.872	0.884	0.913	0.908	0.898
RS20	0.900	0.898	0.874	0.829	0.840	0.854	0.851	0.827	0.816	0.873	0.899	0.900
RS26	0.865	0.851	0.824	0.846	0.848	0.867	0.867	0.846	0.840	0.821	0.851	0.866
RS38	0.864	0.847	0.792	0.779	0.825	0.862	0.864	0.823	0.766	0.791	0.847	0.865
RS86	0.451	0.419	0.343	0.329	0.434	0.537	0.537	0.407	0.289	0.329	0.419	0.447
RS89	0.902	0.912	0.901	0.828	0.852	0.850	0.846	0.846	0.818	0.907	0.912	0.903
GSLOOK	0.921	0.929	0.930	0.930	0.912	0.879	0.876	0.911	0.933	0.932	0.929	0.921
GSMACK	0.634	0.647	0.581	0.515	0.504	0.481	0.473	0.492	0.506	0.585	0.648	0.637
GSWS02	0.876	0.890	0.908	0.889	0.855	0.797	0.794	0.858	0.899	0.914	0.890	0.877
GR4C	0.910	0.918	0.922	0.913	0.868	0.845	0.841	0.868	0.918	0.926	0.918	0.911
GR8C	0.875	0.874	0.872	0.870	0.860	0.899	0.902	0.860	0.877	0.874	0.875	0.876
GRT1	0.936	0.942	0.946	0.930	0.909	0.897	0.896	0.909	0.931	0.949	0.942	0.937
GRVC	0.906	0.916	0.927	0.941	0.940	0.940	0.943	0.948	0.947	0.930	0.916	0.907
TSLOMA	0.871	0.860	0.839	0.841	0.838	0.906	0.911	0.835	0.842	0.839	0.861	0.873
TSLOOK	0.961	0.965	0.967	0.961	0.958	0.937	0.937	0.959	0.964	0.968	0.965	0.962
TSMACK	0.891	0.898	0.902	0.846	0.876	0.882	0.884	0.877	0.843	0.908	0.899	0.892
TSMCRA	0.805	0.828	0.845	0.822	0.787	0.804	0.804	0.787	0.832	0.850	0.828	0.806

Table 4.15. Sky view factors at each climate station.

<b>PRIMET</b>	0.568
<b>CS2MET</b>	0.194
<b>CENMET</b>	0.672
<b>VANMET</b>	0.777
<b>UPLMET</b>	0.718
<b>H15MET</b>	0.314
<b>RS01</b>	0.159
<b>RS02</b>	0.073
<b>RS03</b>	0.037
<b>RS04</b>	0.079
<b>RS05</b>	0.064
<b>RS07</b>	0.096
<b>RS10</b>	0.066
<b>RS12</b>	0.048
<b>RS15</b>	0.066
<b>RS16</b>	0.034
<b>RS17</b>	0.081
<b>RS20</b>	0.095
<b>RS26</b>	0.090
<b>RS38</b>	0.124
<b>RS86</b>	0.383
<b>RS89</b>	0.085
<b>GSLOOK</b>	0.057
<b>GSMACK</b>	0.270
<b>GSWS02</b>	0.100
<b>GR4C</b>	0.082
<b>GR8C</b>	0.101
<b>GRT1</b>	0.048
<b>GRVC</b>	0.076
<b>TSLOMA</b>	0.115
<b>TSLOOK</b>	0.031
<b>TSMACK</b>	0.092
<b>TSMCRA</b>	0.134

Proportions of total radiation blocked by canopy and topography were then separated into their respective components. IPW was used to calculate cloud and topography-adjusted total radiation values for each site, treating the surfaces as open and horizontal. Dividing these values by the total radiation value at each site with no topography present (Table 4.11) and subtracting this value from 1.0 gives the proportion of radiation blocked by topography only at each site. These proportions are shown in Table 4.16. Once these values were found, it was straightforward to determine the amount of radiation blocked by canopy only. This was done by subtracting the proportion blocked by topography from the proportion blocked by canopy and topography. Table 4.17 shows the proportions of total radiation blocked by canopy only for each site in the HJA.

The margin of error present in the fisheye images can be significant. The photographs show only a recent snapshot of the canopy over each site and obviously give no indication of vegetation changes over the periods of record ranging from three to 28 years in the HJA. Some climate stations in the HJA are located in clearcuts that have completely grown over since the site was established, so that canopy effects on these datasets was impossible to ascertain (these sites were discarded from the analysis). Photographs at defunct sites were taken from 'best guess' locations that were often unreliable for short-term sites that operated years ago.

Table 4.18 shows the final cloud/topography/canopy-adjusted radiation values at each site in the HJA. Fisheye images of all sites, processed and complete with suntrack diagrams, can be found in Appendix B.

Table 4.16. Proportions of total solar radiation blocked by topography at each climate station.

	JAN	FEB	MAR	APR	MAY	JUN	JUL	AUG	SEP	OCT	NOV	DEC
PRIMET	0.245	0.190	0.124	0.102	0.100	0.088	0.082	0.081	0.102	0.138	0.211	0.232
CS2MET	0.194	0.129	0.092	0.072	0.071	0.059	0.053	0.055	0.075	0.105	0.157	0.263
CENMET	0.114	0.107	0.104	0.093	0.075	0.063	0.061	0.071	0.090	0.102	0.103	0.110
VANMET	0.043	0.032	0.032	0.024	0.024	0.020	0.019	0.018	0.021	0.029	0.046	0.053
UPLMET	0.056	0.045	0.049	0.036	0.035	0.031	0.027	0.029	0.036	0.042	0.059	0.065
H15MET	0.065	0.055	0.055	0.043	0.045	0.045	0.031	0.032	0.040	0.050	0.062	0.074
RS01	0.138	0.135	0.117	0.108	0.105	0.089	0.087	0.088	0.096	0.118	0.138	0.159
RS02	0.215	0.123	0.098	0.088	0.076	0.070	0.063	0.068	0.071	0.098	0.175	0.257
RS03	0.060	0.054	0.047	0.042	0.037	0.029	0.029	0.031	0.034	0.047	0.062	0.080
RS04	0.151	0.124	0.096	0.076	0.087	0.060	0.067	0.067	0.086	0.121	0.118	0.173
RS05	0.127	0.043	0.027	0.021	0.023	0.019	0.019	0.016	0.020	0.035	0.077	0.212
RS07	0.230	0.115	0.067	0.053	0.050	0.041	0.038	0.038	0.050	0.094	0.209	0.201
RS10	0.040	0.039	0.032	0.023	0.024	0.022	0.016	0.019	0.020	0.029	0.048	0.076
RS12	0.210	0.186	0.141	0.116	0.116	0.109	0.096	0.095	0.103	0.134	0.201	0.220
RS13	0.105	0.097	0.098	0.082	0.078	0.082	0.068	0.068	0.075	0.086	0.097	0.109
RS130	0.105	0.097	0.098	0.082	0.078	0.082	0.068	0.068	0.075	0.086	0.097	0.109
RS15	0.568	0.326	0.188	0.110	0.100	0.078	0.070	0.073	0.111	0.246	0.514	0.548
RS16	0.316	0.180	0.143	0.112	0.111	0.113	0.090	0.098	0.109	0.166	0.305	0.416
RS17	0.103	0.075	0.066	0.040	0.039	0.034	0.030	0.031	0.042	0.064	0.092	0.134
RS20	0.029	0.027	0.024	0.019	0.022	0.018	0.016	0.015	0.018	0.024	0.028	0.042
RS26	0.031	0.025	0.027	0.020	0.020	0.019	0.016	0.015	0.017	0.023	0.030	0.039
RS38	0.034	0.040	0.030	0.027	0.028	0.021	0.022	0.020	0.024	0.034	0.038	0.060
RS86	0.018	0.024	0.024	0.016	0.021	0.016	0.015	0.013	0.021	0.022	0.030	0.033
RS89	0.246	0.207	0.183	0.166	0.135	0.120	0.114	0.114	0.141	0.192	0.305	0.251
GSLOOK	0.239	0.214	0.160	0.120	0.104	0.109	0.089	0.092	0.131	0.164	0.247	0.278
GSMACK	0.341	0.228	0.168	0.122	0.104	0.086	0.078	0.093	0.128	0.200	0.252	0.410
GWSO2	0.588	0.276	0.170	0.127	0.123	0.115	0.100	0.094	0.131	0.227	0.547	0.573
GR4C	0.125	0.074	0.054	0.043	0.041	0.035	0.033	0.034	0.042	0.059	0.108	0.129
GR8C	0.061	0.058	0.058	0.049	0.051	0.054	0.048	0.038	0.052	0.051	0.058	0.063
GRT1	0.028	0.018	0.021	0.017	0.016	0.014	0.011	0.012	0.013	0.022	0.023	0.024
GRVC	0.110	0.089	0.069	0.050	0.044	0.037	0.033	0.036	0.052	0.072	0.097	0.280
TSLOMA	0.156	0.131	0.096	0.067	0.055	0.049	0.041	0.043	0.066	0.123	0.205	0.142
TSLOOK	0.288	0.250	0.158	0.120	0.107	0.099	0.096	0.098	0.123	0.208	0.291	0.292
TSMACK	0.448	0.244	0.214	0.171	0.146	0.123	0.118	0.125	0.167	0.200	0.412	0.521
TSMCRA	0.272	0.108	0.090	0.066	0.064	0.054	0.050	0.049	0.066	0.101	0.142	0.249

Table 4.17. Proportions of total solar radiation blocked by canopy at each climate station.

	JAN	FEB	MAR	APR	MAY	JUN	JUL	AUG	SEP	OCT	NOV	DEC
PRIMET	0.010	0.024	0.050	0.049	0.042	0.047	0.046	0.045	0.037	0.032	0.004	0.024
CS2MET	0.537	0.631	0.704	0.625	0.556	0.570	0.575	0.563	0.637	0.705	0.603	0.471
CENMET	0.062	0.063	0.050	0.032	0.027	0.028	0.025	0.020	0.030	0.053	0.069	0.067
VANMET	0.025	0.030	0.022	0.028	0.019	0.016	0.014	0.020	0.026	0.023	0.016	0.016
UPLMET	0.085	0.075	0.060	0.044	0.049	0.082	0.086	0.050	0.039	0.069	0.062	0.078
H15MET	0.539	0.580	0.577	0.537	0.483	0.374	0.382	0.505	0.555	0.596	0.573	0.534
RS01	0.679	0.674	0.703	0.734	0.672	0.651	0.649	0.692	0.760	0.705	0.671	0.660
RS02	0.687	0.790	0.829	0.828	0.775	0.754	0.757	0.779	0.854	0.833	0.738	0.647
RS03	0.892	0.903	0.917	0.907	0.865	0.894	0.891	0.865	0.918	0.920	0.895	0.872
RS04	0.753	0.789	0.828	0.854	0.834	0.819	0.812	0.864	0.853	0.807	0.795	0.732
RS05	0.803	0.890	0.909	0.882	0.863	0.887	0.887	0.862	0.884	0.904	0.856	0.719
RS07	0.665	0.791	0.846	0.851	0.838	0.870	0.877	0.853	0.861	0.824	0.697	0.695
RS10	0.878	0.870	0.875	0.889	0.902	0.929	0.937	0.906	0.888	0.876	0.862	0.842
RS12	0.733	0.763	0.807	0.810	0.787	0.791	0.801	0.804	0.823	0.816	0.748	0.724
RS13	0.716	0.736	0.728	0.725	0.685	0.646	0.656	0.691	0.741	0.744	0.737	0.713
RS130	0.328	0.315	0.208	0.184	0.211	0.191	0.196	0.198	0.164	0.215	0.317	0.325
RS15	0.356	0.606	0.754	0.822	0.801	0.832	0.839	0.828	0.827	0.700	0.418	0.377
RS16	0.635	0.773	0.782	0.795	0.836	0.856	0.879	0.845	0.789	0.758	0.649	0.535
RS17	0.794	0.834	0.843	0.842	0.834	0.848	0.853	0.841	0.843	0.849	0.817	0.765
RS20	0.871	0.872	0.849	0.810	0.818	0.836	0.836	0.812	0.798	0.849	0.871	0.858
RS26	0.834	0.826	0.798	0.826	0.828	0.848	0.851	0.832	0.823	0.798	0.821	0.827
RS38	0.830	0.807	0.761	0.752	0.797	0.841	0.842	0.803	0.742	0.758	0.809	0.805
RS86	0.432	0.395	0.319	0.313	0.413	0.521	0.523	0.394	0.268	0.306	0.389	0.414
RS89	0.656	0.706	0.719	0.662	0.717	0.729	0.733	0.732	0.677	0.715	0.607	0.652
GSLOOK	0.682	0.714	0.770	0.810	0.808	0.770	0.786	0.818	0.803	0.768	0.681	0.643
GSMACK	0.293	0.419	0.413	0.393	0.400	0.395	0.395	0.399	0.378	0.385	0.396	0.227
GWS02	0.288	0.614	0.739	0.762	0.732	0.683	0.694	0.764	0.768	0.687	0.343	0.305
GR4C	0.785	0.844	0.868	0.870	0.828	0.810	0.808	0.834	0.876	0.866	0.810	0.782
GR8C	0.814	0.817	0.813	0.822	0.809	0.845	0.853	0.821	0.825	0.823	0.817	0.812
GRT1	0.908	0.924	0.925	0.912	0.893	0.883	0.884	0.898	0.918	0.927	0.918	0.913
GRVC	0.796	0.827	0.858	0.890	0.896	0.902	0.910	0.912	0.895	0.858	0.819	0.627
TSLOMA	0.716	0.729	0.742	0.774	0.783	0.857	0.870	0.792	0.776	0.716	0.656	0.731
TSLOOK	0.673	0.715	0.809	0.841	0.852	0.838	0.841	0.861	0.840	0.760	0.675	0.670
TSMACK	0.443	0.654	0.688	0.675	0.731	0.759	0.765	0.752	0.676	0.707	0.487	0.371
TSMCRA	0.534	0.720	0.756	0.756	0.723	0.749	0.755	0.738	0.766	0.749	0.686	0.557

Table 4.18. Modeled sloped-surface, cloud/canopy/topography-adjusted monthly solar radiation at each climate station (MJ/m<sup>2</sup>·day).

	JAN	FEB	MAR	APR	MAY	JUN	JUL	AUG	SEP	OCT	NOV	DEC
PRIMET	2.86	5.37	9.31	14.15	17.18	20.61	22.06	19.79	14.65	7.93	3.56	2.50
CS2MET	1.18	1.76	2.45	4.84	7.19	8.46	8.78	7.70	4.37	1.93	1.26	1.08
CENMET	2.95	5.30	9.09	13.92	17.09	20.59	22.21	20.05	14.63	7.74	3.62	2.56
VANMET	3.57	6.44	10.75	15.64	18.52	22.08	23.92	22.16	17.23	9.58	4.50	3.15
UPLMET	3.22	5.75	9.73	14.80	17.78	20.61	21.91	20.29	15.23	8.14	4.01	2.77
H15MET	1.57	2.62	4.40	7.09	9.34	13.46	14.46	10.76	7.49	3.72	1.82	1.39
RS01	0.76	1.43	2.27	3.07	4.58	5.93	6.47	5.17	2.99	1.93	0.97	0.69
RS02	0.81	1.08	1.51	2.31	3.75	4.93	5.18	4.13	1.98	1.22	0.87	0.76
RS03	0.37	0.60	0.85	1.43	2.53	2.38	2.61	2.86	1.28	0.70	0.44	0.38
RS04	0.68	1.07	1.52	1.97	2.73	3.63	4.01	2.59	2.00	1.40	0.72	0.63
RS05	0.65	0.70	0.97	1.89	2.66	2.61	2.79	3.02	1.88	0.86	0.61	0.73
RS07	0.71	0.86	1.13	1.71	2.39	2.32	2.31	2.31	1.46	0.99	0.78	0.57
RS10	0.45	0.87	1.38	1.81	1.90	1.63	1.56	2.12	1.93	1.20	0.62	0.50
RS12	0.76	1.27	1.83	2.70	3.63	4.29	4.42	4.00	2.74	1.51	0.90	0.69
RS15	0.53	0.97	1.25	1.56	2.28	2.44	2.45	2.13	1.35	1.09	0.68	0.47
RS16	0.78	1.10	1.85	2.65	2.52	2.67	2.46	2.90	2.97	1.75	0.96	0.72
RS17	0.61	0.89	1.40	2.21	2.89	3.20	3.26	3.03	2.10	1.09	0.66	0.58
RS20	0.43	0.79	1.55	2.85	3.17	3.38	3.68	4.00	3.42	1.41	0.54	0.41
RS26	0.58	1.12	2.16	2.71	3.13	3.28	3.50	3.71	3.07	1.94	0.78	0.53
RS38	0.61	1.23	2.55	3.90	3.75	3.50	3.76	4.38	4.45	2.31	0.84	0.60
RS86	1.58	3.14	6.03	9.05	9.11	8.93	9.70	11.53	10.74	5.45	2.09	1.42
RS89	0.59	0.94	1.58	3.02	3.28	3.88	4.09	3.49	2.83	1.27	0.73	0.50
GSLOOK	0.92	1.51	2.15	2.75	3.42	4.83	4.88	3.71	2.90	1.84	1.11	0.85
GSMACK	1.68	2.87	5.23	8.49	10.41	12.79	13.62	11.87	8.73	4.38	2.00	1.43
GSWS02	0.98	1.65	2.14	3.09	4.30	6.17	6.39	4.32	2.93	1.95	1.21	0.89
GR4C	0.61	0.81	1.17	1.78	2.95	3.93	4.19	3.13	1.64	0.97	0.66	0.54
GR8C	0.59	1.06	1.83	2.57	3.29	3.18	3.27	3.69	2.75	1.52	0.73	0.53
GRT1	0.36	0.52	0.85	1.45	2.09	2.71	2.88	2.36	1.46	0.72	0.38	0.29
GRVC	0.65	0.99	1.38	1.62	1.89	2.12	2.09	1.79	1.54	1.15	0.71	0.85
TSLOMA	0.93	1.63	2.66	3.53	4.09	3.22	3.15	4.58	3.69	2.43	1.29	0.78
TSLOOK	0.89	1.44	1.79	2.32	2.65	3.46	3.64	2.84	2.37	1.79	1.07	0.78
TSMACK	1.16	1.76	2.72	4.43	4.57	5.01	5.23	4.91	4.53	2.20	1.38	0.99
TSMCRA	1.28	1.67	2.47	3.73	5.13	5.59	5.85	5.60	3.68	2.13	1.25	1.10

#### 4.5.3 Calculation of regression functions

The next step was to adjust mean monthly temperatures to simulate flat open site conditions. Once solar radiation was modeled for each site, monthly regression functions could be calculated to correct each site's temperatures to what they would be if the site were flat and open. Procedures for calculating regression equations for maximum and minimum temperatures were different because of the physical factors affecting them; maximum temperatures are driven largely by solar radiation regimes during the day while minimum temperatures are determined primarily by longwave radiation loss at night. Thus, incoming radiation for maximum temperatures and site sky view factors for minimum temperatures were the primary variables used to adjust the temperature datasets.

Both procedures first involved the careful selection of site pairs for comparison. The premise behind this step was that different monthly radiation and sky view factor regimes between two sites would result in differences in monthly maximum and minimum temperatures, respectively. By selecting enough site pairs for comparison, these differences could be quantified.

Rules governing what sites to use for maximum and minimum temperature adjustments were similar in many respects. Site pairs had to be within 50 meters elevation of one another and physically located either within the HJA borders or very close to them, to avoid elevational or regional biases. No stream sites were used because of the localized cooling effects of running water and cold air drainage. Except in the case of the lower Lookout Creek Valley where inversions exist throughout the year, sites near streams were discarded if they

could possibly be affected by cold-air drainage. If a defunct site's location was especially vague, that site could not be used in a pair. Any other factors capable of creating local biases in a dataset eliminated that site from consideration.

Certain sites were included in maximum temperature but not minimum temperature analysis, and vice-versa. This is because temperatures at a site can be affected differently by local phenomenon between day and night. For example, PRIMET and CS2MET were not included in maximum temperature pairs because their historical temperatures are unusually cool, a fact probably attributable to localized cold air drainage at both sites during certain months of the year. However, they were included in minimum temperature pairs because they are clearly under a year-round nighttime inversion which is well-documented by other nearby sites in the bottom of the Lookout Creek valley. VANMET was used in maximum temperature pairs but not minimum temperature pairs because of suspected anomalous radiant heat loss tendencies of its surrounding terrain at night. Roughly an equal number of pairs below and above the minimum temperature inversion were used to determine minimum temperature adjustments, deemed appropriate because of the significance of this phenomenon year-round in the HJA. Table 4.19 summarizes the sites eliminated from consideration and the remaining sites that were included in site pairs.

To determine maximum temperature adjustments, total radiation and temperature differences between seven site pairs were graphed on a scatterplot, and regression functions were generated for each month (Figure 4.5). Maximum temperature site pairs, with their temperature and radiation differences, are listed in Table 4.20, with corresponding equations and regression correlation coefficients (R-squared values) shown in Table 4.21. Seasonal effects are immediately apparent from

Table 4.19. Summary of sites considered for adjustment pairs.

SITE	CONSIDERED FOR MAXIMUM TEMPERATURE CORRECTION PAIRS?	CONSIDERED FOR MINIMUM TEMPERATURE CORRECTION PAIRS?
PRIMET		Y
CS2MET		Y
CENMET	Y	Y
VANMET	Y	
UPLMET	Y	Y
H15MET	Y	Y
RS01		
RS02	Y	Y
RS03	Y	Y
RS04	Y	Y
RS05	Y	Y
RS07	Y	Y
RS10	Y	Y
RS12		
RS15		
RS16		
RS17	Y	Y
RS20	Y	Y
RS26	Y	Y
RS38		
RS86	Y	Y
RS89		
GSLOOK		
GSMACK		
GSWS02		
GR4C		
GR8C		
GRT1		
GRVC		
TSLOMA		
TSLOOK		
TSMACK		
TSMCRA		

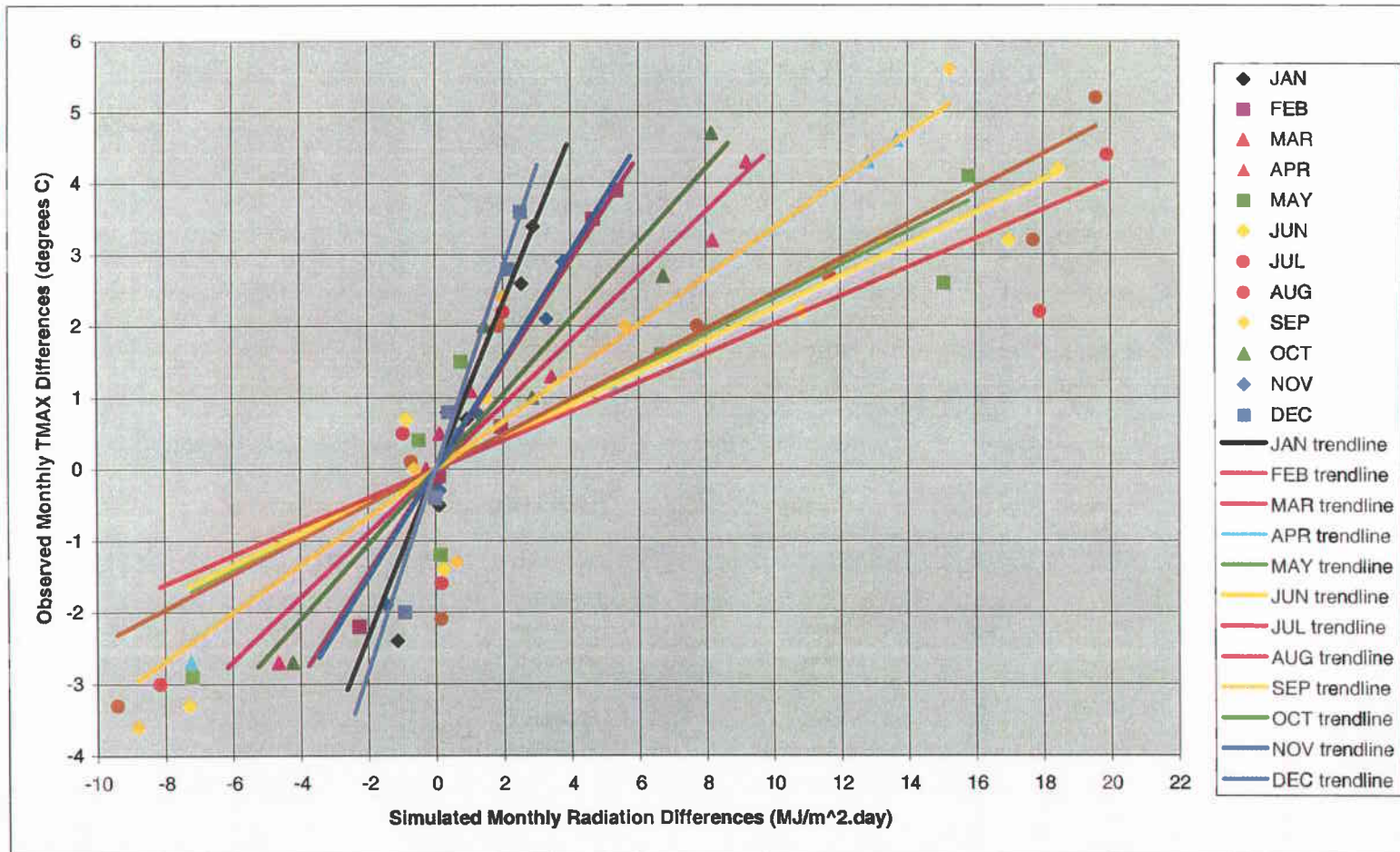


Figure 4.5. Differences in simulated radiation and observed maximum temperatures for site pairs and regression lines for each month.

Table 4.20. Site pairs used for maximum temperature adjustments and their temperature/radiation differences.

MJ.m-2.day-1	JAN	FEB	MAR	APR	MAY	JUN	JUL	AUG	SEP	OCT	NOV	DEC
VANMET - UPLMET RADN	0.35	0.70	1.02	0.85	0.74	1.47	2.01	1.87	2.00	1.44	0.49	0.38
UPLMET - RS04 RADN	2.55	4.67	8.22	12.82	15.06	16.98	17.90	17.71	13.22	6.74	3.29	2.14
H15MET - RS05 RADN	0.92	1.92	3.43	5.20	6.68	10.85	11.67	7.74	5.61	2.86	1.21	0.65
RS07 - RS17 RADN	0.10	-0.02	-0.28	-0.50	-0.50	-0.87	-0.95	-0.72	-0.64	-0.10	0.12	-0.01
RS10 - RS86 RADN	-1.14	-2.27	-4.65	-7.24	-7.20	-7.30	-8.14	-9.41	-8.81	-4.25	-1.47	-0.93
VANMET - RS04 RADN	2.89	5.37	9.24	13.67	15.79	18.46	19.91	19.57	15.22	8.18	3.78	2.52
RS05 - RS03 RADN	0.28	0.10	0.12	0.46	0.13	0.22	0.17	0.16	0.60	0.17	0.17	0.36

Table 4.21. Monthly regression functions and R-squared values for maximum temperature adjustments.

	JAN	FEB	MAR	APR	MAY	JUN	JUL	AUG	SEP	OCT	NOV	DEC
TMAX REGRESSION FUNCTION	y=1.17x	y=0.73x	y=0.45x	y=0.33x	y=0.24x	y=0.22x	y=0.20x	y=0.25x	y=0.34x	y=0.52x	y=0.76x	y=1.41x
R-SQUARED	0.91	0.96	0.96	0.99	0.82	0.84	0.74	0.82	0.87	0.91	0.92	0.95

NOTE: y = difference in maximum temperature  
x = difference in radiation

the graph. During the winter months when sun angles and radiation levels are low, slopes of regression lines were highest. During the months of maximum radiation, slopes are relatively low. Thus, a  $\text{MJ}/\text{m}^2 \cdot \text{day}$  radiation difference had a much greater effect on maximum temperatures during winter than summer. Figures 4.6 and 4.7 depict this seasonal variation, with an inverse relationship between solar radiation and trendline slopes year-round. The positive slopes of the regression lines reflect the cooling effects of canopy and topography on maximum temperatures. Regression lines for all months show fairly high R-squared values. Lowest R-squared values occur in the summer (July R-squared = 0.74), because trendline slopes are lowest during that time of year when radiation differences result in relatively small temperature differences. Maximum temperature regression slopes vary throughout the year because of varying solar radiation (Figures 4.6 and 4.7).

For minimum temperatures, sky view factors and monthly temperature differences between fourteen site pairs are related on a scatterplot in Figure 4.8. The negative slopes of these lines show the warming effects on minimum temperatures of canopy and topography. The fourteen pairs with their temperature and sky view factor differences are shown in Table 4.22. Table 4.23 shows monthly regression functions and their R-squared values. Like maximum temperature functions, minimum temperature trendlines in Figure 4.8 show dramatic seasonal differences. The steepest regression lines (brown, orange, and red) occur during the summer months (July, August, and September) when clear skies facilitated greater longwave radiation loss at night. By contrast, adjustment factors during winter months were lower due to the insulating effects of clouds and high humidity on

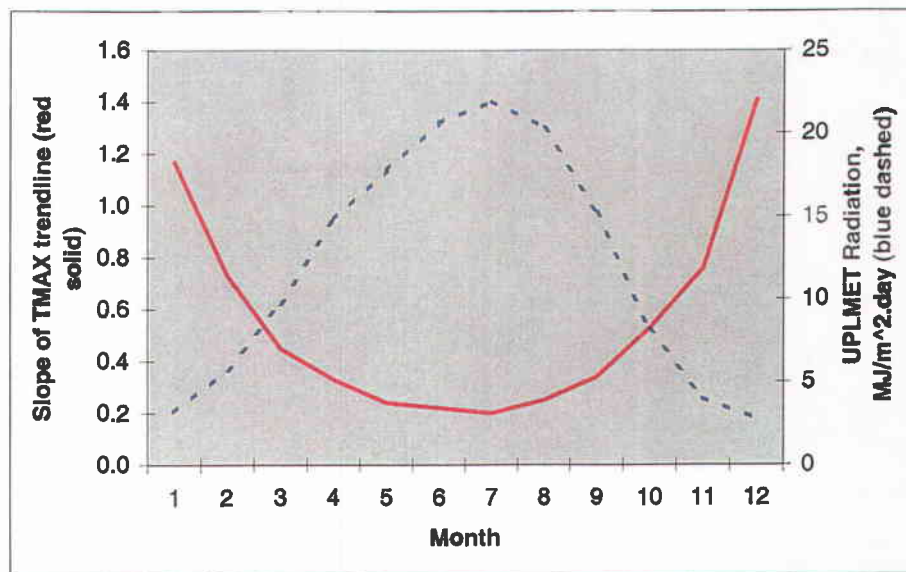


Figure 4.6. Slopes of maximum temperature regression trendlines and modeled radiation at UPLMET for each month.

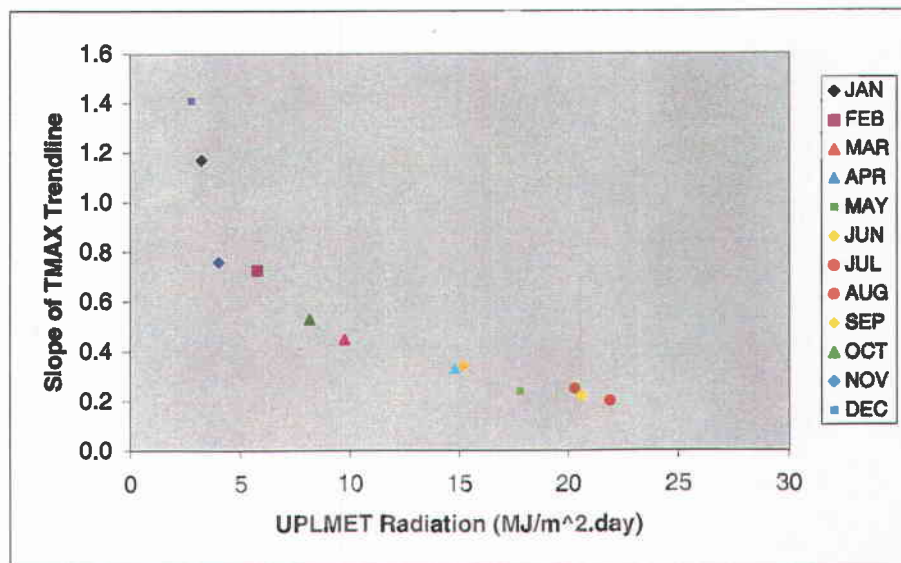


Figure 4.7. Slopes of monthly maximum temperature regression trendlines plotted against modeled radiation at UPLMET.

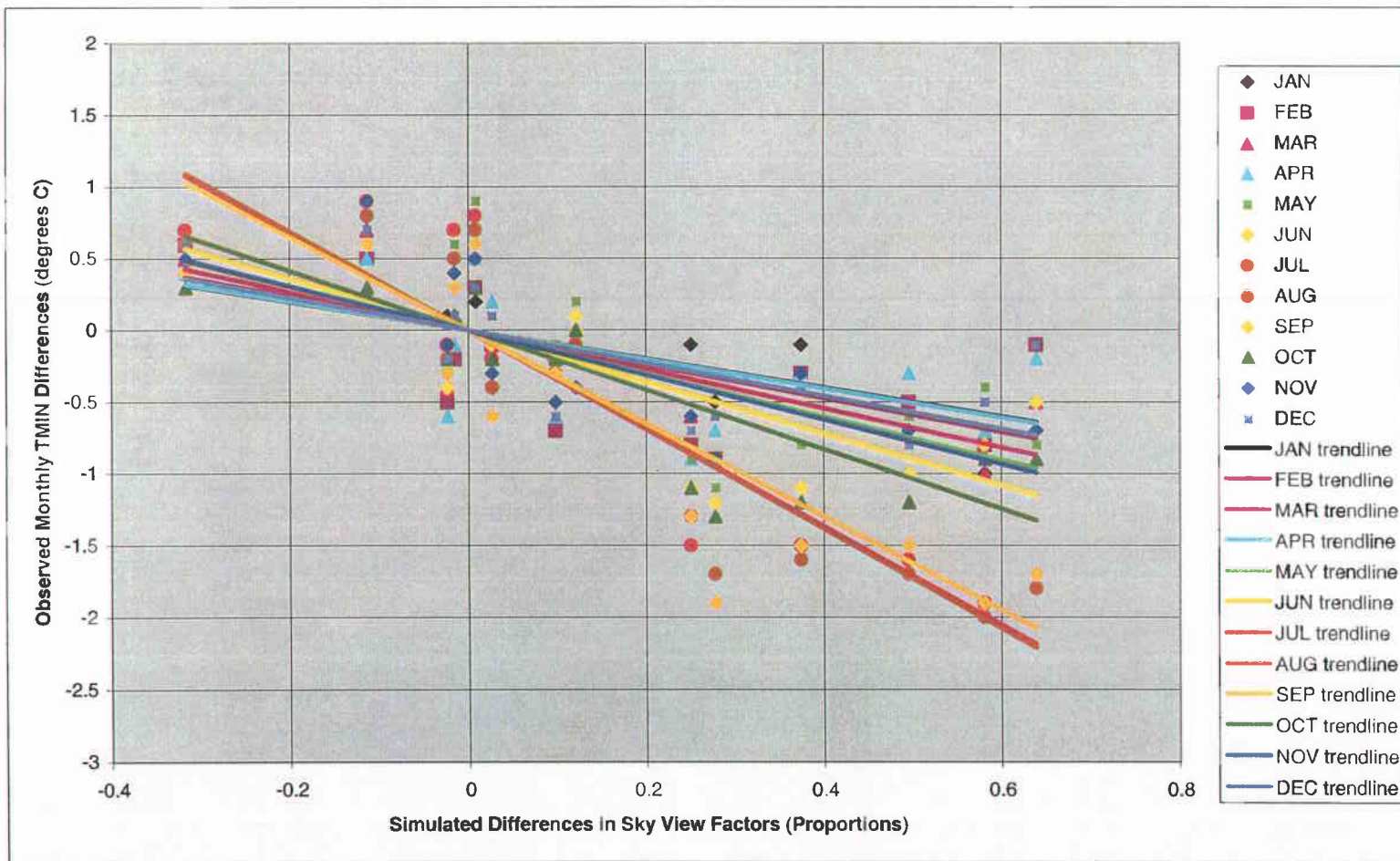


Figure 4.8. Differences in simulated sky view factors and observed minimum temperatures for site pairs and regression lines for each month.

Table 4.22. Site pairs used for minimum temperature adjustments and their temperature/sky view factor differences.

Degrees C													SKY VIEW
	JAN	FEB	MAR	APR	MAY	JUN	JUL	AUG	SEP	OCT	NOV	DEC	FACTOR
CS2MET- RS02 TMIN	-0.4	-0.2	-0.2	0.0	0.2	0.1	-0.1	-0.1	0.0	0.0	-0.4	-0.4	0.12
UPLMET - RS04 TMIN	-0.1	-0.1	-0.5	-0.2	-0.8	-0.5	-1.8	-1.8	-1.7	-0.9	-0.7	-0.1	0.64
H15MET - RS05 TMIN	-0.1	-0.8	-0.6	-0.9	-0.9	-1.1	-1.5	-1.3	-1.3	-1.1	-0.6	-0.7	0.25
RS17 - RS07 TMIN	0.3	-0.2	0.1	-0.1	0.6	0.3	0.7	0.5	0.3	0.1	0.4	0.1	-0.02
RS10 - RS86 TMIN	0.5	0.6	0.5	0.4	0.6	0.5	0.7	0.6	0.4	0.3	0.5	0.6	-0.32
PRIMET - CS2MET TMIN	-0.1	-0.3	-0.3	-0.3	-0.8	-1.1	-1.5	-1.6	-1.5	-1.2	-0.3	-0.4	0.37
PRIMET - RS02 TMIN	-0.5	-0.5	-0.5	-0.3	-0.6	-1.0	-1.6	-1.7	-1.5	-1.2	-0.7	-0.8	0.50
CS2MET - RS07 TMIN	-0.3	-0.7	-0.6	-0.6	-0.1	-0.3	-0.2	-0.3	-0.3	-0.2	-0.5	-0.6	0.10
RS17 - CS2MET TMIN	0.6	0.5	0.7	0.5	0.7	0.6	0.9	0.8	0.6	0.3	0.9	0.7	-0.11
CENMET - RS26 TMIN	-1.0	-0.8	-1.0	-0.7	-0.4	-0.8	-1.9	-2.0	-1.9	-0.9	-0.9	-0.5	0.58
H15MET - RS03 TMIN	-0.5	-0.9	-0.7	-0.7	-1.1	-1.2	-1.7	-1.7	-1.9	-1.3	-0.9	-0.6	0.28
RS02 - RS07 TMIN	0.1	-0.5	-0.4	-0.6	-0.3	-0.4	-0.1	-0.2	-0.3	-0.2	-0.1	-0.2	-0.02
RS17 - RS02 TMIN	0.2	0.3	0.5	0.5	0.9	0.7	0.8	0.7	0.6	0.3	0.5	0.3	0.01
RS05 - RS03 TMIN	-0.4	-0.1	-0.1	0.2	-0.2	-0.1	-0.2	-0.4	-0.6	-0.2	-0.3	0.1	0.03

Table 4.23. Monthly regression functions and R-squared values for minimum temperature adjustments.

	JAN	FEB	MAR	APR	MAY	JUN	JUL	AUG	SEP	OCT	NOV	DEC
TMIN REGRESSION FUNCTION	y=-1.00x	y=-1.18x	y=-1.36x	y=-1.01x	y=-1.51x	y=-1.8x	y=-3.41x	y=-3.46x	y=-3.25x	y=-2.07x	y=-1.56x	y=-1.14x
R-SQUARED	0.49	0.33	0.58	0.31	0.5	0.55	0.81	0.83	0.75	0.66	0.63	0.47

NOTE: y = difference in minimum temperature  
x = difference in sky view factor

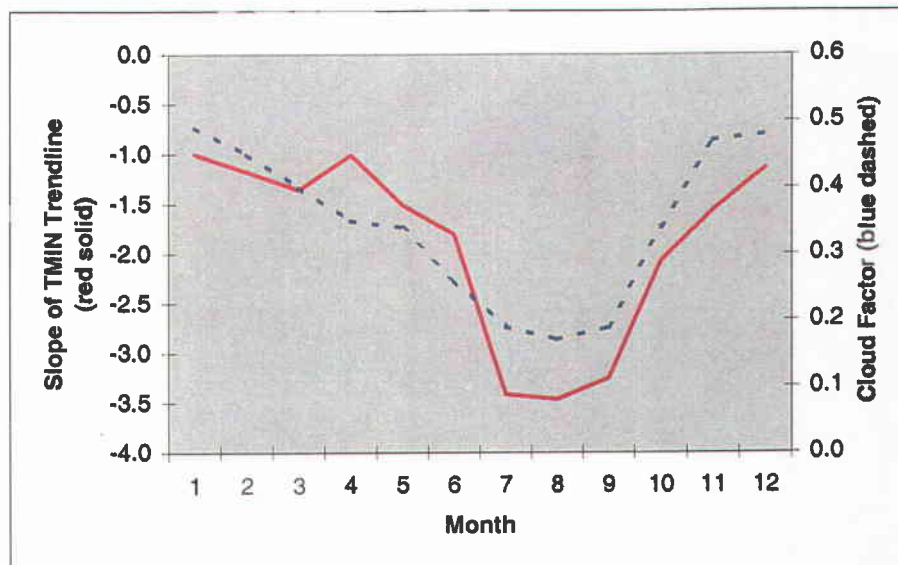


Figure 4.9. Slopes of minimum temperature regression trendlines and cloud factors for each month.

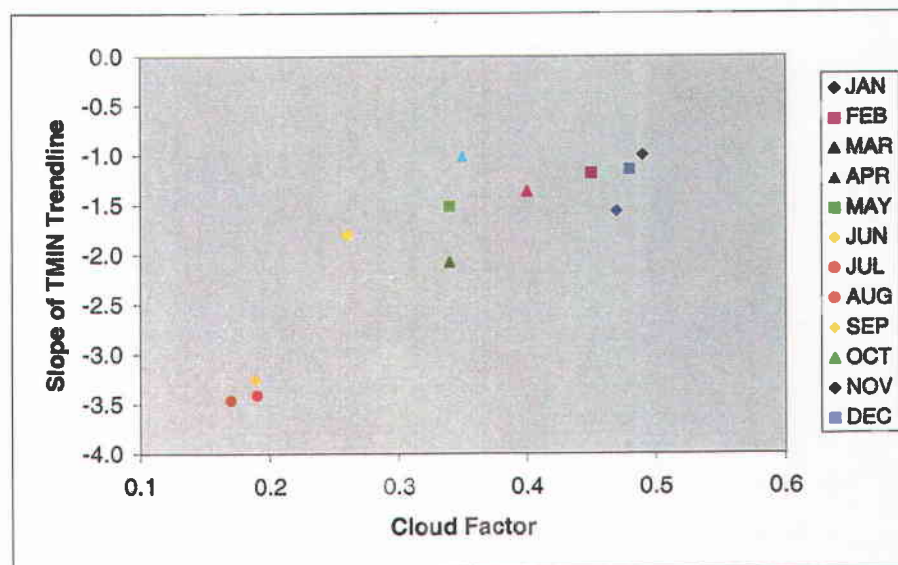


Figure 4.10. Slopes of minimum temperature regression trendlines plotted against monthly cloud factors.

thermal heat loss. Figures 4.9 and 4.10 show the close relationship between minimum temperature regression slopes and seasonal cloudiness in the HJA.

Minimum temperature regression functions showed less predictive skill than those for maximum temperature. R-squared values were lowest in the winter, highest during summer (opposite the seasonal trends for maximum temperatures), and never exceeded 0.83 for any month.

After these regression functions were finalized, it was a relatively simple process to adjust the datasets. For maximum temperatures, each site's final radiation value (Table 4.18) was subtracted from its theoretical flat/open radiation value (Table 4.11) and the appropriate amount added to its temporally-adjusted temperature dataset based on the monthly regression function. For minimum temperatures, each site's sky view factor was subtracted from 1.0 and its 30-year temperatures adjusted according to the monthly regression functions.

Tables 4.24 and 4.25 show the final maximum and minimum temperature datasets adjusted for cloudiness with the effects of topography and canopy removed. These were the final temperature datasets imported into PRISM.

Table 4.24. Cloud/canopy/topography-adjusted mean monthly maximum temperatures at each climate station (°C).

	JAN	FEB	MAR	APR	MAY	JUN	JUL	AUG	SEP	OCT	NOV	DEC	ANN
PRIMET	6.1	8.6	12.3	16.1	20.0	24.1	28.6	28.8	25.6	17.6	8.7	5.3	16.8
CS2MET	6.6	8.8	11.8	16.7	21.3	26.2	31.0	30.1	23.6	16.4	8.9	6.5	17.3
CENMET	8.6	9.9	11.9	14.9	18.1	22.6	26.6	27.6	23.7	18.2	9.2	7.9	16.6
VANMET	5.7	6.6	8.0	10.7	14.0	19.0	23.9	24.5	21.2	14.6	6.5	5.7	13.4
UPLMET	5.3	6.7	7.3	10.6	12.7	18.4	22.1	22.9	19.4	13.4	6.1	5.4	12.5
H15MET	6.4	8.2	10.5	13.4	17.2	21.6	26.5	26.3	23.0	16.4	8.5	6.4	15.4
RS01	9.5	12.2	14.5	17.9	21.3	25.4	29.4	30.4	28.2	21.0	10.8	9.0	19.2
RS02	7.7	10.3	13.6	17.3	21.0	25.4	30.0	30.3	26.6	18.8	9.9	7.6	18.2
RS03	7.0	9.2	10.3	13.8	18.5	23.3	27.8	28.4	24.3	16.9	8.6	7.1	16.3
RS04	5.7	6.6	7.8	10.6	13.7	19.0	23.5	24.1	20.7	14.2	6.5	5.6	13.2
RS05	6.7	9.0	10.7	13.9	17.2	21.9	26.1	26.2	22.8	16.9	8.6	6.8	15.6
RS07	7.6	10.2	12.8	16.4	20.1	24.6	28.9	29.0	25.1	18.1	9.5	7.6	17.5
RS10	8.6	11.1	13.3	16.8	20.5	24.9	29.7	29.9	26.5	19.7	10.2	8.3	18.3
RS12	5.8	7.1	8.7	11.9	16.9	22.1	27.0	26.3	21.5	15.2	7.3	5.8	14.6
RS15	7.7	9.4	10.8	14.0	17.5	22.3	26.6	26.7	23.2	16.6	8.9	7.8	16.0
RS16	8.0	10.7	12.6	16.1	19.9	24.3	28.5	28.9	25.6	18.7	9.3	7.9	17.5
RS17	7.2	9.9	12.6	16.0	20.4	25.1	29.2	29.0	24.9	17.8	9.3	7.2	17.4
RS20	9.5	11.6	13.4	15.8	19.8	24.3	28.8	29.2	26.1	19.6	10.5	9.1	18.1
RS26	7.8	9.1	10.3	13.2	16.5	21.4	25.9	26.4	23.2	16.5	8.5	7.7	15.5
RS38	10.5	12.0	13.8	16.3	20.0	24.8	29.1	29.7	26.5	19.9	10.8	9.9	18.6
RS86	9.7	11.6	13.9	17.1	21.7	26.6	31.0	30.9	27.1	20.2	11.0	9.0	19.1
RS89	8.4	11.3	14.8	18.5	23.7	28.6	33.3	33.6	28.5	20.1	10.2	7.8	19.9
GSLOOK	8.2	11.1	14.5	19.2	22.5	27.0	31.0	32.4	27.6	19.7	10.7	7.9	19.3
GSMACK	4.9	6.6	8.2	11.7	17.3	22.3	27.4	27.4	19.9	13.9	7.3	5.2	14.3
GSWS02	7.4	8.9	10.9	13.6	17.8	21.0	23.8	23.7	20.9	16.4	9.1	7.4	15.1
GR4C	6.6	6.5	8.0	10.9	12.9	18.3	22.4	22.8	20.3	13.9	5.1	5.2	12.7
GR8C	8.9	10.8	12.4	14.9	19.0	23.5	26.7	26.3	24.0	17.6	9.1	9.4	16.9
GRT1	6.8	8.0	9.4	10.9	14.9	20.5	25.3	24.2	23.0	16.5	7.4	6.9	14.5
GRVC	8.0	9.1	11.4	15.8	20.6	24.3	29.1	28.0	23.4	17.6	9.3	8.1	17.0
TSLOMA	7.2	8.9	11.1	16.3	19.9	23.6	28.3	29.1	24.4	16.9	9.1	7.4	16.9
TSLOOK	4.7	5.6	7.2	10.3	15.4	21.0	24.9	24.0	19.3	13.5	6.8	5.0	13.1
TSMACK	5.2	6.5	8.2	10.9	16.2	21.4	25.4	24.5	18.6	13.4	7.4	5.7	13.6
TSMCRA	4.9	6.9	9.5	13.4	19.0	24.3	29.5	27.6	22.3	15.1	7.5	5.4	15.5

Table 4.25 Cloud/canopy/topography-adjusted mean monthly minimum temperatures at each climate station (°C).

	JAN	FEB	MAR	APR	MAY	JUN	JUL	AUG	SEP	OCT	NOV	DEC	ANN
PRIMET	-1.3	-0.8	0.1	2.0	4.3	6.7	7.8	7.6	5.1	2.5	0.5	-1.9	2.7
CS2MET	-1.6	-1.0	-0.1	1.9	4.6	7.2	8.0	7.9	5.4	2.9	0.2	-3.1	2.7
CENMET	-1.7	-1.1	-1.0	0.9	3.6	6.3	8.3	8.7	6.7	4.0	-0.2	-2.0	2.7
VANMET	-2.1	-1.4	-1.4	0.5	2.5	5.9	8.2	9.0	6.6	3.7	-0.8	-2.0	2.4
UPLMET	-2.5	-2.1	-2.1	-0.3	1.5	5.1	7.2	7.9	5.7	2.8	-1.5	-2.9	1.6
H15MET	-1.4	-1.3	-0.5	1.0	3.5	6.2	8.0	8.4	6.2	3.7	0.1	-3.3	2.5
RS01	-0.5	0.3	0.8	2.5	5.1	7.9	9.0	9.0	6.7	4.5	1.2	-2.5	3.7
RS02	-1.3	-0.9	-0.1	1.8	4.2	6.8	7.7	7.6	5.0	2.7	0.5	-3.1	2.6
RS03	-1.2	-0.7	-0.2	1.4	4.1	6.9	8.7	9.2	7.2	4.4	0.6	-3.8	3.0
RS04	-3.0	-2.8	-2.5	-0.7	1.3	4.4	6.9	7.5	5.3	2.4	-1.8	-5.3	1.0
RS05	-1.5	-0.8	-0.3	1.6	4.0	6.8	8.6	8.9	6.7	4.3	0.3	-3.3	2.9
RS07	-1.4	-0.4	0.4	2.4	4.5	7.3	7.9	7.9	5.4	2.9	0.6	-3.1	2.9
RS10	-0.9	-0.3	0.3	2.2	4.6	7.4	8.6	8.6	6.3	3.8	0.9	-3.0	3.2
RS12	-2.1	-2.0	-1.5	0.0	2.4	5.1	6.6	6.7	4.6	2.5	-0.7	-4.2	1.5
RS15	-0.5	0.2	0.4	2.1	4.5	7.6	9.2	9.2	7.3	4.5	0.8	-2.8	3.5
RS16	-0.7	0.0	0.1	2.0	4.6	7.5	8.8	9.2	7.0	4.5	0.9	-2.6	3.4
RS17	-1.1	-0.6	0.5	2.3	5.1	7.5	8.6	8.3	5.6	3.0	1.0	-3.0	3.1
RS20	-0.6	-0.1	0.3	2.2	4.5	7.5	8.9	9.1	7.1	4.3	0.8	-3.2	3.4
RS26	-1.3	-1.0	-0.8	1.0	3.1	6.1	8.2	8.7	6.7	3.7	-0.2	-3.8	2.5
RS38	-1.1	-0.7	-0.6	1.1	3.3	6.1	7.5	7.8	6.1	3.7	0.1	-3.5	2.5
RS86	-1.1	-0.5	0.3	2.1	4.5	7.5	9.0	9.1	6.9	4.1	0.9	-2.6	3.3
RS89	-1.4	-0.6	0.0	1.8	4.5	7.0	7.5	7.6	4.8	2.7	0.4	-3.7	2.5
GSLOOK	-1.2	-0.8	0.1	1.8	4.1	6.6	7.6	7.5	4.8	2.6	0.5	-2.8	2.6
GSMACK	-1.5	-0.8	-0.5	1.2	3.6	6.2	8.0	8.4	5.9	3.6	0.4	-2.8	2.6
GSWS02	-1.0	-0.5	0.4	2.1	4.5	7.4	8.4	8.4	6.4	3.4	0.9	-2.5	3.2
GR4C	-1.3	-2.5	-2.2	-0.3	1.0	4.6	6.6	6.9	4.5	2.9	-2.2	-5.0	1.1
GR8C	-0.5	0.4	1.0	2.3	5.0	8.2	8.7	8.5	7.0	4.1	0.8	-2.4	3.6
GRT1	-2.2	-1.6	-1.2	-0.1	1.9	5.3	7.3	7.7	6.5	3.7	-1.3	-4.2	1.8
GRVC	0.0	0.4	1.1	3.0	5.9	8.2	9.9	10.4	7.7	5.7	1.1	-1.7	4.3
TSLOMA	-1.4	-0.7	-0.5	1.4	3.2	5.6	6.6	6.5	4.5	2.6	0.1	-3.3	2.0
TSLOOK	-2.1	-2.1	-1.3	0.2	2.6	5.6	6.9	6.7	4.6	2.6	-0.2	-3.7	1.6
TSMACK	-0.7	-0.3	0.0	1.4	4.1	7.2	8.7	8.8	6.4	4.1	0.6	-2.4	3.2
TSMCRA	-2.1	-1.5	-1.2	0.5	2.7	5.5	6.6	6.7	4.7	2.2	-0.2	-3.3	1.7

## 4.6 MAPPING METHODS

### 4.6.1 PRISM logic and features

After mean monthly maximum and minimum temperature datasets were adjusted with regression functions to simulate open flat sites, they were imported into PRISM. PRISM uses a combination of geographic and statistical methods to spatially interpolate climate variables (Daly et al., 1994). It is a coordinated set of rules, decisions, and calculations (an 'inference engine') designed to mirror the decision-making process an expert climatologist would use in making a map (Daly and Johnson, 1999).

PRISM is based on the premise that climate varies with elevation. Elevation is an excellent predictor variable because it is often sampled at a greater spatial density than climate variables and is easily estimated on a regular grid (DEM) (Daly et al., 2002). By statistically and spatially analyzing elevation and point (station) data, PRISM estimates the temperature at every cell on the DEM. It does this by calculating a linear climate-elevation regression function over an area using data from surrounding stations within a user-defined radius. The general form of this simple regression formula is

$$y = (b')x + b'' \quad (7)$$

where  $y$  = the predicted temperature at the target cell,  $b'$  = the regression slope,  $b''$  = the regression intercept, and  $x$  = the DEM elevation at the target cell. A simple linear function is used because it is easier to control and interpret

than complex relationships between multiple independent variables and climate elements (Daly and Johnson, 1999). The inference engine interacts with the station database within PRISM to set weights for station points entering the regression functions.

Weights are assigned to the point data according to various factors. A station is downweighted when its elevation differs significantly from that of the target cell or is far from it geographically. The station's influence is further reduced if it is clustered with others (avoiding over-representation), or has a significantly different slope and aspect (topographic facet) than the target cell (Daly et al., 1997). When used on large areas, PRISM is able to consider a station's proximity to the ocean and the 'flatness' of an area to determine whether two-dimensional or three-dimensional estimates should be used (Daly and Johnson, 1999). These last two factors are not important in this study, because the HJA is a small area 150 kilometers from the nearest ocean and is hilly enough to require only the three-dimensional model.

PRISM is especially well-suited for modeling HJA temperatures because of its ability to divide stations into two vertical layers, one representing the boundary (lower) layer and the other the free atmosphere above it (upper layer). A station in the same layer as the target cell is given more weight than one in the other layer, thus limiting a station's ability to affect regression functions in another layer (Daly et al., 2002). PRISM allows a user-defined amount of 'cross-talk' (sharing of data points) between layers to best determine regression functions in each layer (Daly et al., 1997).

PRISM is an extremely flexible model in that it allows the user to specify precisely how and which different

climatological factors are accounted for. This 'knowledge-based system' (KBS) combines both human-expert and statistical interpolation methods. PRISM employs KBS logic by inferring solutions to problems based on a user's expert knowledge through a moving-window user-interface (Daly et al., 2002). This powerful feature allows a user of PRISM to quickly and easily interact with the model at all times and tailor it to best suit his or her needs. Results can be independently evaluated to assess their consistency with other spatial climate elements (Daly et al., 1997), a particularly valuable feature when mapping temperatures over small areas such as the HJA.

PRISM is a tested model that has successfully been used on different geographic scales and varying climate types. It has been used to update official temperature and precipitation maps of all 50 United States and to create detailed climate maps of Canada, China, Mongolia, and the European Alps (Daly et al., 2000). Its reliability and ability to take into account user-specified small-scale climate variables make it ideal for mapping temperature regimes in the HJA.

#### 4.6.2 Using PRISM to map H. J. Andrews temperatures

PRISM alone cannot create reliable temperature maps without close interaction with a knowledgeable user. Thus it is essential to carefully consider how best to use it in an area with such complex microclimates as the HJA. The use of the term 'grid' in the following discussions refers to the digital data (represented on a 50-meter grid, with a data value at each pixel), while 'map' refers to a cartographic representation of gridded data. Maps for this project were

created with ArcView GIS software (Environmental Systems Research Institute, Inc., 2000), using PRISM grids as input.

An iterative approach was taken in creating the gridded data for the temperature maps. With the exception of the stream sites, all canopy/topography-adjusted maximum and minimum temperature datasets were initially input into PRISM, using default parameters and a single-layer atmosphere model. The resulting grids clearly showed which sites to initially discard. For example, the unusually warm sites RS38, RS89, and H15MET were visually obvious as high temperature 'bull's eyes'. All GR sites were revealed to be anomalously warm and were also discarded. Other sites such as CS2MET, RS02 and RS86 were also discarded because of warm or cold spatial biases. Including RS01's data caused unusual temperature patterns due to the seasonal presence of Blue River Reservoir. From initial PRISM modeling and personal experience, VANMET was known to be anomalously warm and RS04 anomalously cool. In order to retain spatial representation in their area, a 'pseudo-site' was created at point between them on the DEM, with temperature values given as their averages for each month. Using this pseudo-site instead of VANMET and RS04 individually gave far more realistic temperatures on top of the northern peaks and ridges of the HJA. The National Climatic Data Center's 500-millibar (approximately 5200 meters) 2.5° global temperature grid was used as a high-level anchor 'site' over the HJA to ensure that the tops of the highest peaks and ridges in the area were modeled correctly. Table 4.26 summarizes the sites used in the final analysis. With the exception of the Mack Creek area, most regions within the HJA are fairly well-represented spatially, having a measurement station within about two kilometers.

Table 4.26. Summary of sites used for final mapping and sites discarded.

<u>USED FOR MAPPING</u>	<u>ELEVATION (m)</u>
PRIMET	430
CENMET	1018
UPLMET	1294
RS03	945
RS05	880
RS07	460
RS10	610
RS17	490
RS20	683
RS26	1040
VANMET/RS04	1239

<u>NOT USED FOR MAPPING</u>	<u>REASON</u>
CS2MET	Unusually cool historical temperatures
H15MET	Unusually warm historical temperatures
VANMET	Unusually warm historical temperatures
RS01	Lake effects from Blue River Reservoir
RS02	Unusually warm historical temperatures
RS04	Unusually cool historical temperatures
RS12	Stream/local cold air drainage effects
RS15	Unreliable location
RS16	Unreliable location
RS38	Unusually warm historical temperatures (emerging clearcut)
RS86	Unusually warm historical temperatures
RS89	Unusually warm historical temperatures
GSLOOK	Stream site
GSMACK	Stream site
GSWS02	Stream site
GR4C	Unreliable location
GR8C	Unreliable location
GRT1	Unreliable location
GRVC	Unreliable location
TSLOMA	Stream site
TSLOOK	Stream site
TSMACK	Stream site
TSMCRA	Stream site

PRISM was run again with the reduced set of sites. Since the number of sites had been decreased to 15, the radius of influence was specified to consider every point in the HJA when making cell estimates. Even using a single atmospheric layer model with this specification, a temperature inversion over the lower Lookout Creek Valley was evident during most months for both maximum and minimum temperatures. Figures 4.11 and 4.12 show mean maximum temperatures and site elevations for January and July, and Figures 4.13 and 4.14 show mean minimum temperatures and elevations for those months. The maximum temperature inversion is more defined in January (at an elevation of approximately 700 meters), with minimum temperature inversions well-defined in both January and July at approximately 720 meters. Taking the base elevation of the Lookout Creek valley to be 420 meters, depths of inversions over it were approximately 280 meters for maximum temperatures and 300 meters for minimum temperatures.

We thus switched to the two-atmosphere model in PRISM with these inversion height values specified. A certain amount of 'cross-talk' was allowed between layers to avoid an unnaturally abrupt transition between layers. Elevations were buffered by  $\pm 150$  meters for maximum temperature and  $\pm 120$  meters for minimum temperatures, reflecting the higher seasonal variation in minimum temperature inversion heights. Variable inversion heights with elevation were modeled such that the deepest inversions were found at the lowest elevations (over the lower Lookout Creek and McKenzie River valleys). The two-layer atmosphere model was used to model both maximum and minimum temperatures for every month.

All of the final parameter values used to make the grids were determined by varying them slightly in different combinations, then iteratively running PRISM and analyzing the

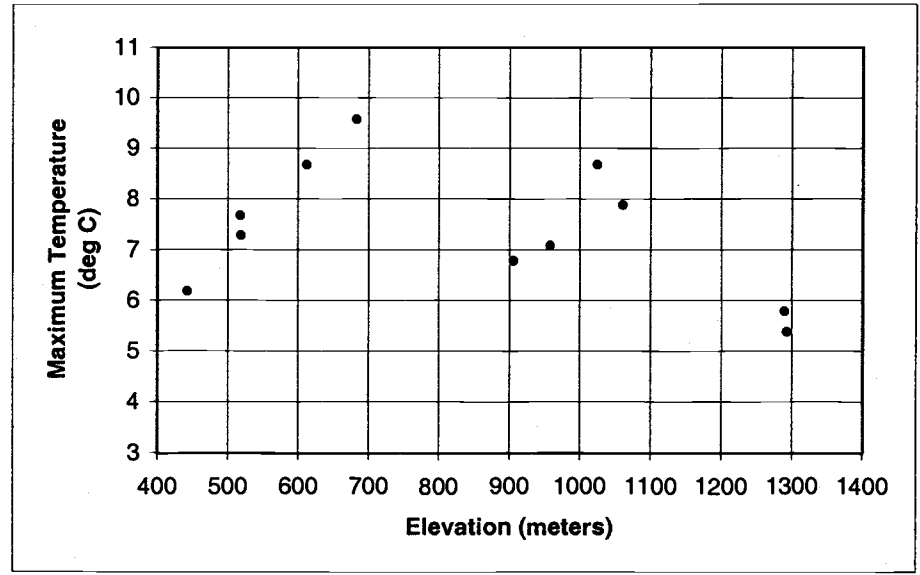


Figure 4.11. Plot of mean maximum temperatures and elevation for January.

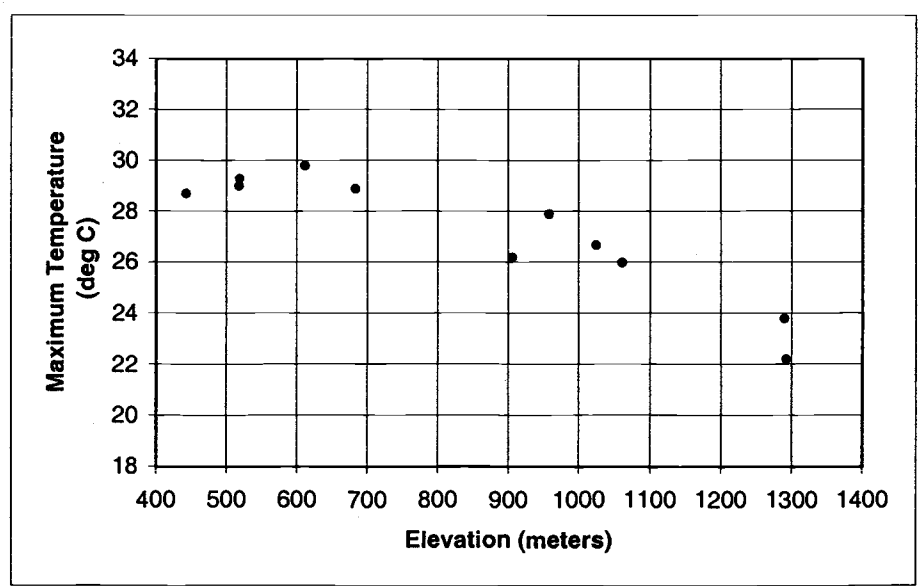


Figure 4.12. Plot of mean maximum temperatures and elevation for July.

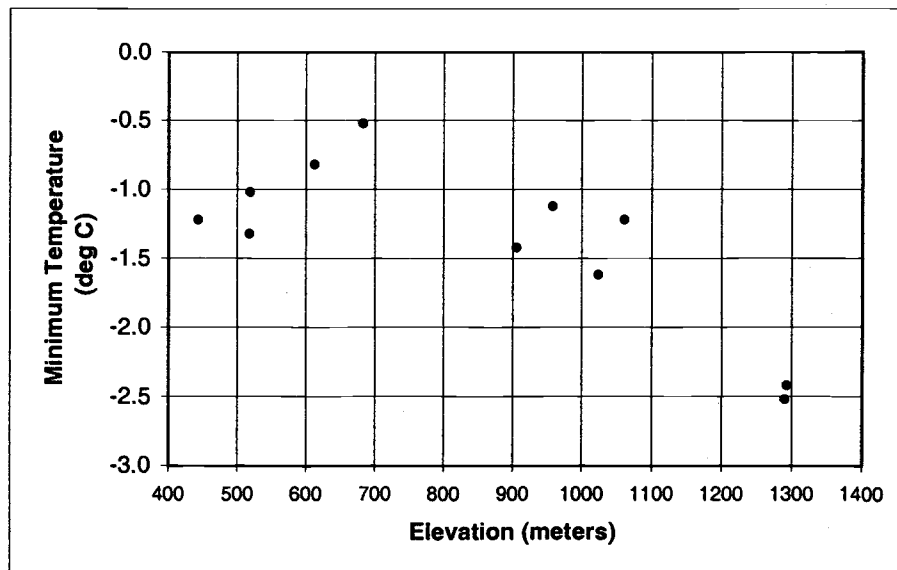


Figure 4.13. Plot of mean minimum temperatures and elevation for January.

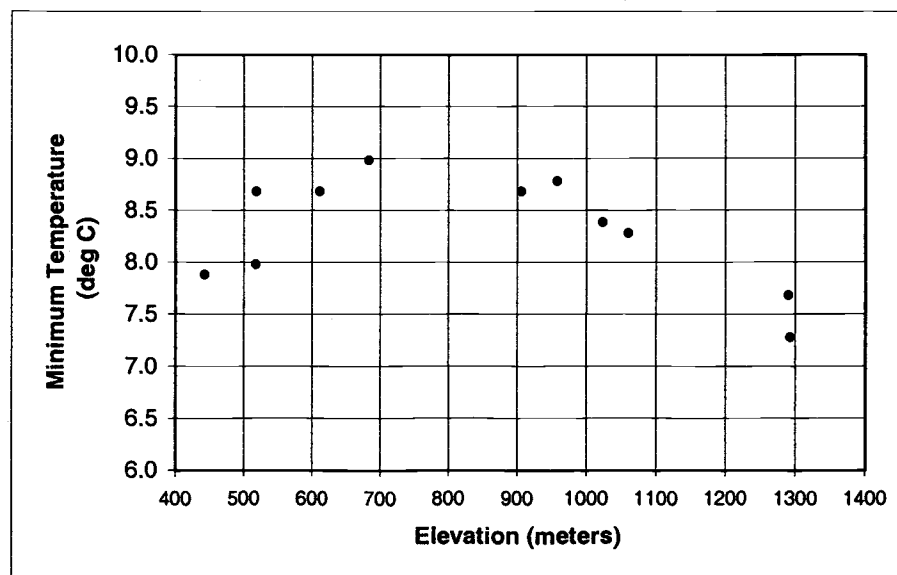


Figure 4.14. Plot of mean minimum temperatures and elevation for July.

results both statistically (with regression functions through the PRISM interface) or visually (with the temperature grids). In this way, knowledge of HJA microclimatology could be applied and combined with PRISM's statistical abilities to create maps that were not only numerically sound, but made sense physically.

After mean monthly temperature grids were generated with PRISM, the GRASS GIS program (United States Army - Construction Engineering Research Laboratory, 1992) was used to add the effects of radiation and sky view factors to them, using the IPW grids and original regression functions. Only topographic effects of radiation and sky view factors were applied; vegetation was not reintroduced to the process. For maximum temperatures, the difference between solar radiation on a flat open surface and the topographically-correct surface was calculated over each DEM pixel. Changes to monthly maximum temperatures were then applied over each grid based on the temperature/radiation regression functions (Table 4.21). For minimum temperatures, differences in the sky view factor between a flat open surface and the topographically correct surface were calculated over each pixel. Then changes to monthly minimum temperatures were applied over the grid according to the temperature/sky view factor regression functions (Table 4.23). Figure 4.15 provides a summary of the major steps taken to create the final temperature maps.

**Maximum Temperatures****Minimum Temperatures**

Temporal adjustment of initial  
temperature datasets to 1971-2000 period

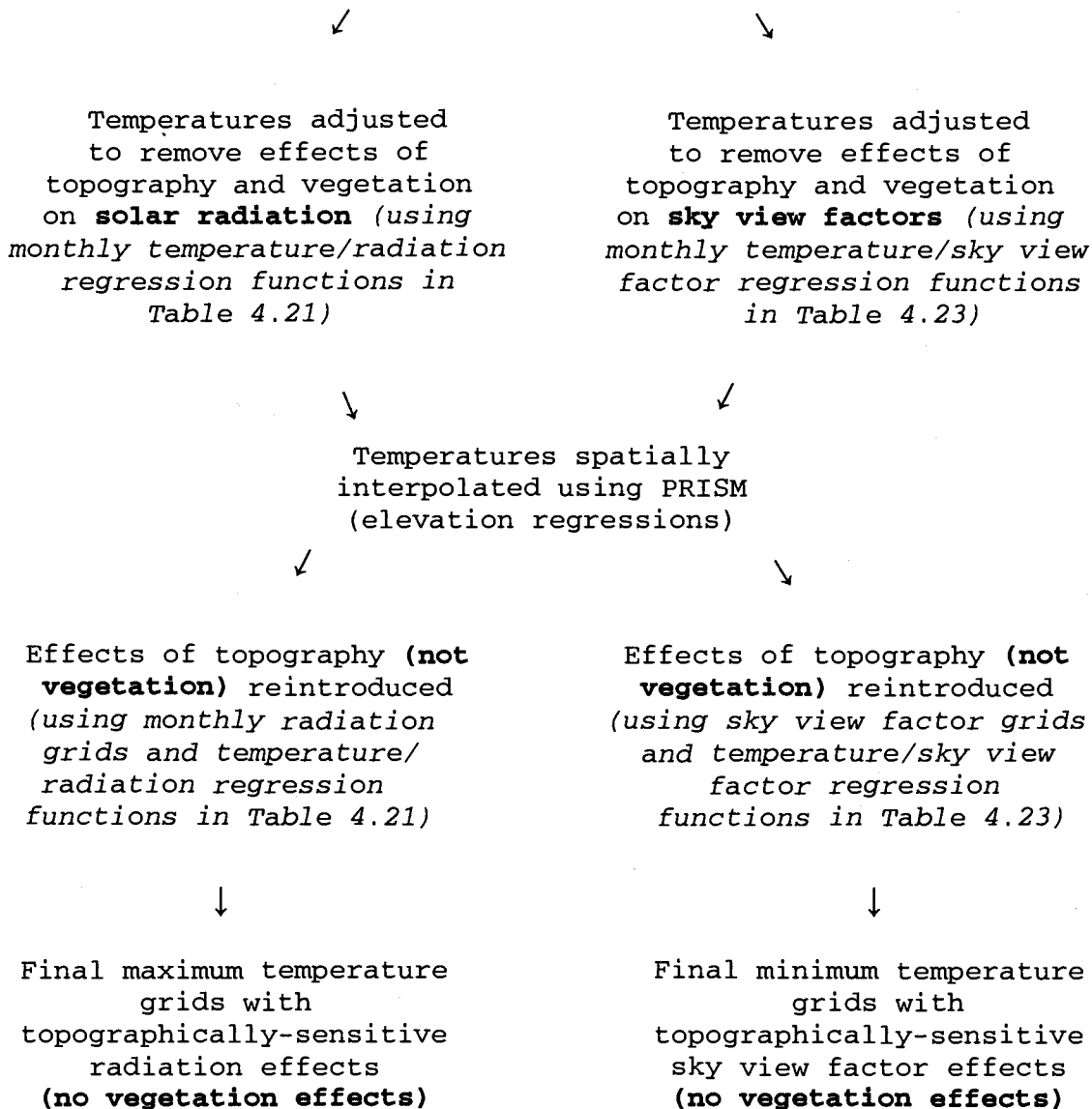


Figure 4.15. Summary of all maximum and minimum temperature adjustments taken to create the final maps.

## 5. RESULTS

An important aspect of this study is the quantitative and systematic adjustment of temperatures to account for the effects of solar radiation and sky view factors. It is thus helpful to discuss the results at each step in the process. Figure 5.2 shows visually how the PRISM maximum temperature maps changed to account for solar radiation effects, and Figure 5.3 shows how minimum temperatures changed when accounting for the effects of sky view factors. Regression functions used to adjust station temperatures 'into the open' (no topographic or vegetation effects) were described in Chapter 4. These same monthly regression functions were applied to the PRISM temperature grids to reintroduce the effects of radiation on maximum temperatures and sky view factors on minimum temperatures. A reference map of the HJA is provided in Figure 5.1. Pixel data on all grids were resampled from 50-meter to 10-meter resolution and presented as maps using the ArcView GIS program (Environmental Systems Research Institute, Inc., 2000).

### 5.1 PRISM TEMPERATURE GRIDS WITH NO RADIATION/SKY VIEW FACTOR EFFECTS

All temperature datasets input into PRISM were adjusted to remove the effects of both topography and vegetation, as discussed in Chapter 4. Since PRISM is an elevation-based climate interpolator, its output showed mainly the effects of terrain height, with temperature patterns generally following topographic patterns (Figures 5.2a and 5.3a). It does not

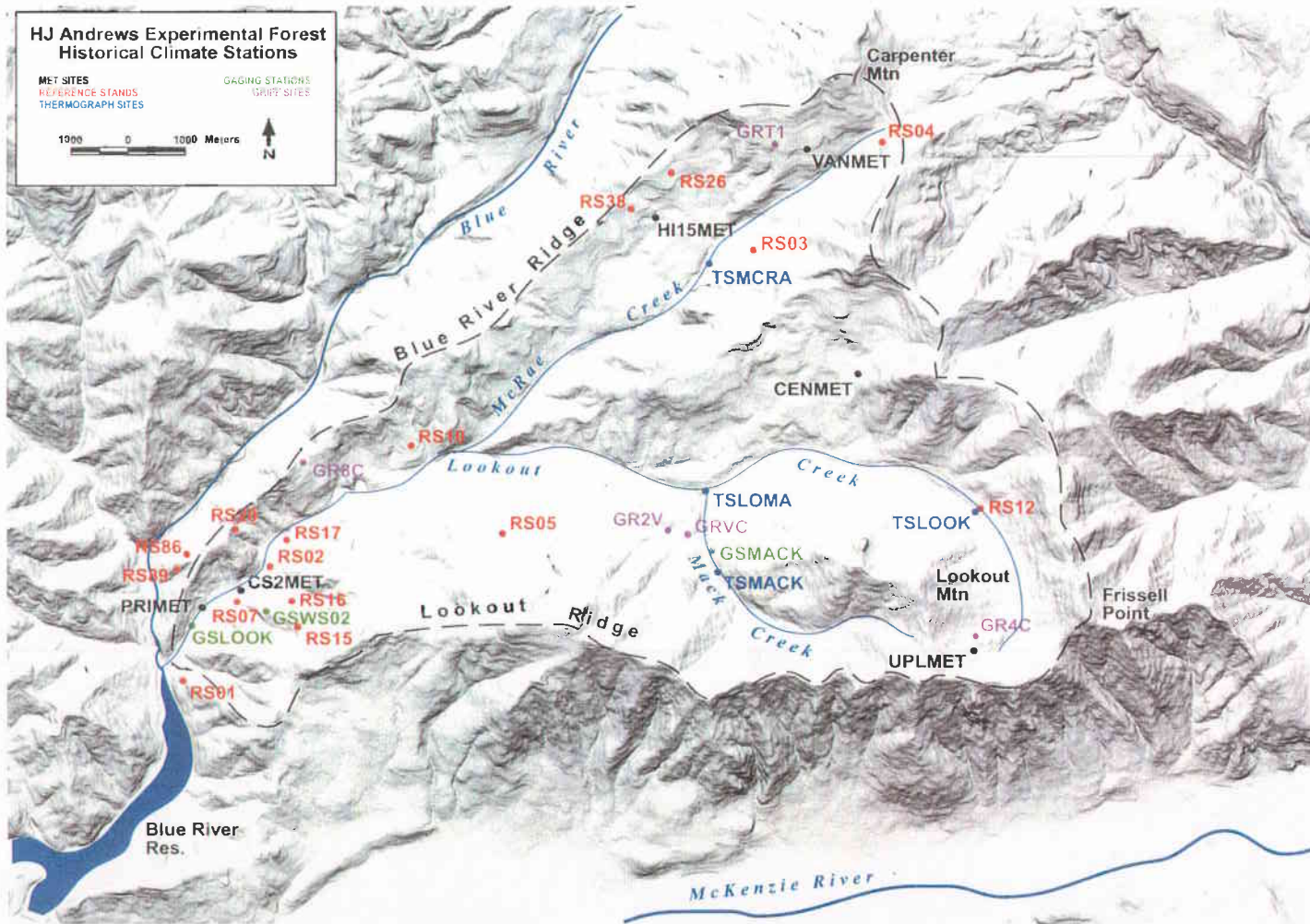


Figure 5.1. Map of the H. J. Andrews showing locations of all historical climate stations.

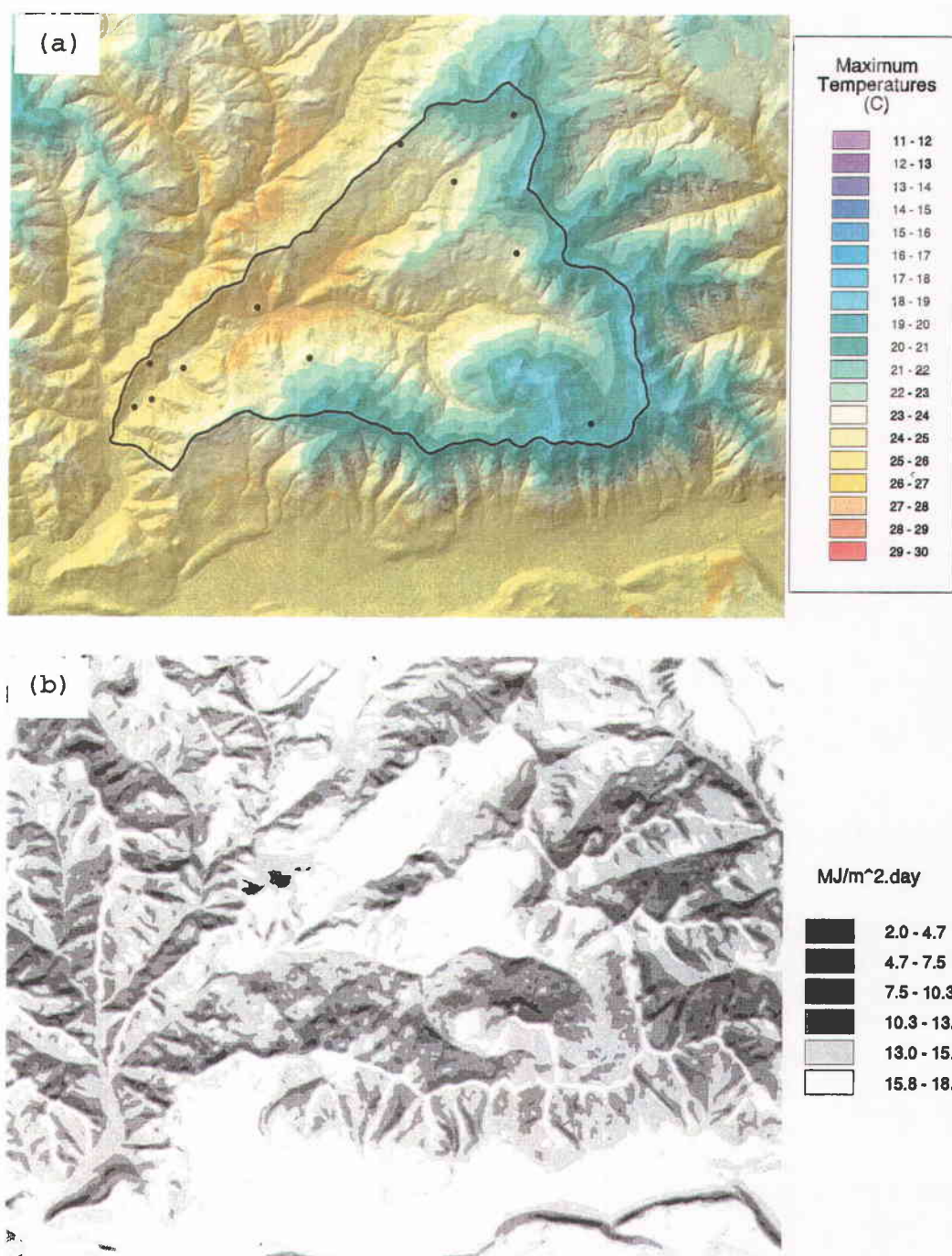


Figure 5.2. Maps showing (a) PRISM September maximum temperatures with no radiation effects, (b) radiation for September, (c) PRISM September maximum temperatures with radiation effects, and (d) differences between (a) and (c).

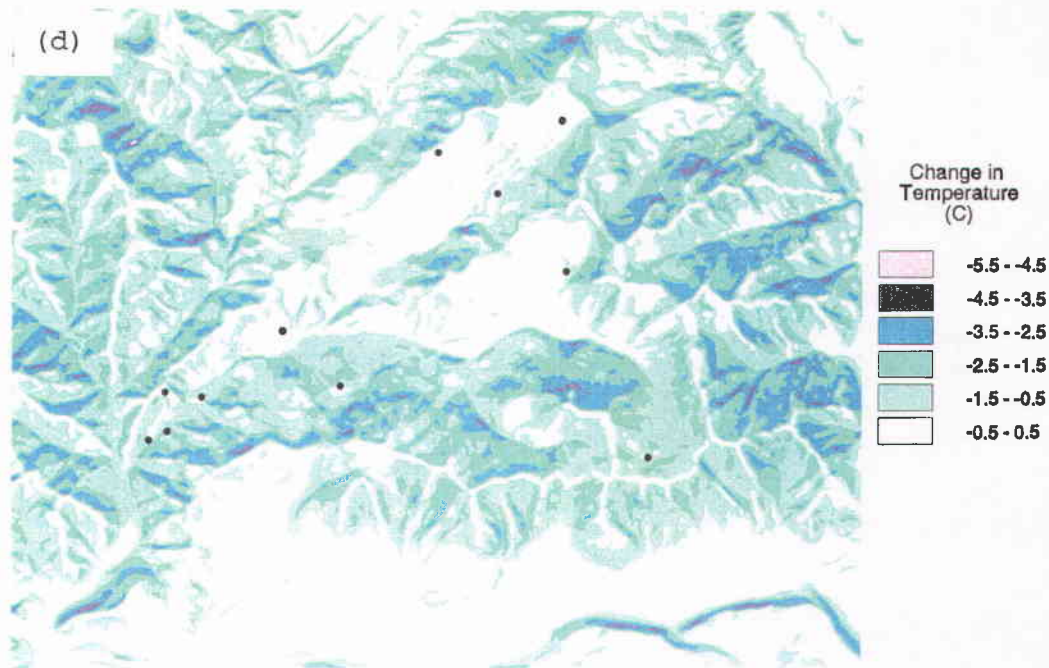


Figure 5.2. (Concluded).

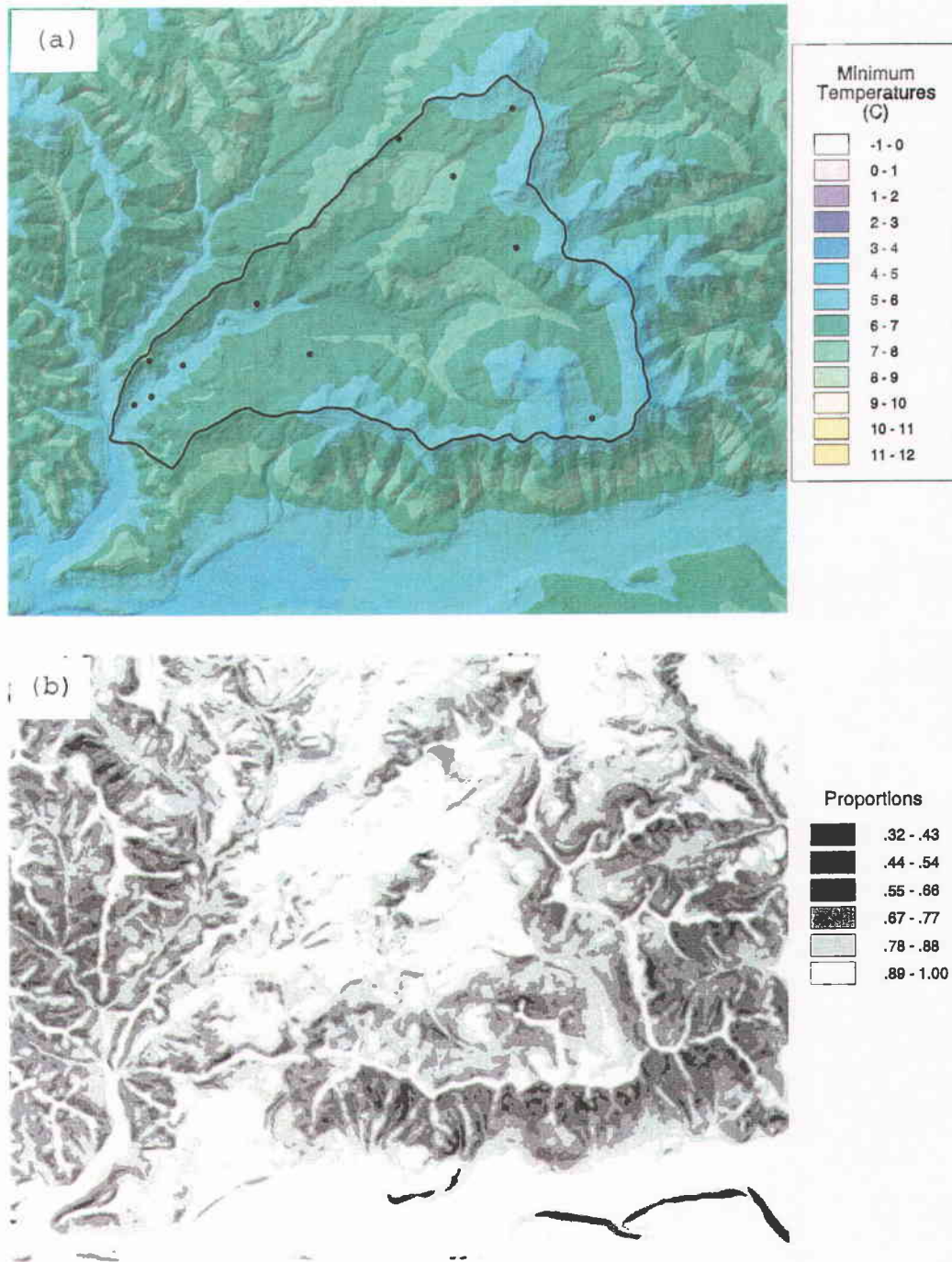


Figure 5.3. Maps showing (a) PRISM September minimum temperatures with no sky view factor effects, (b) sky view factors, (c) PRISM September minimum temperatures with sky view factor effects, and (d) differences between (a) and (c).

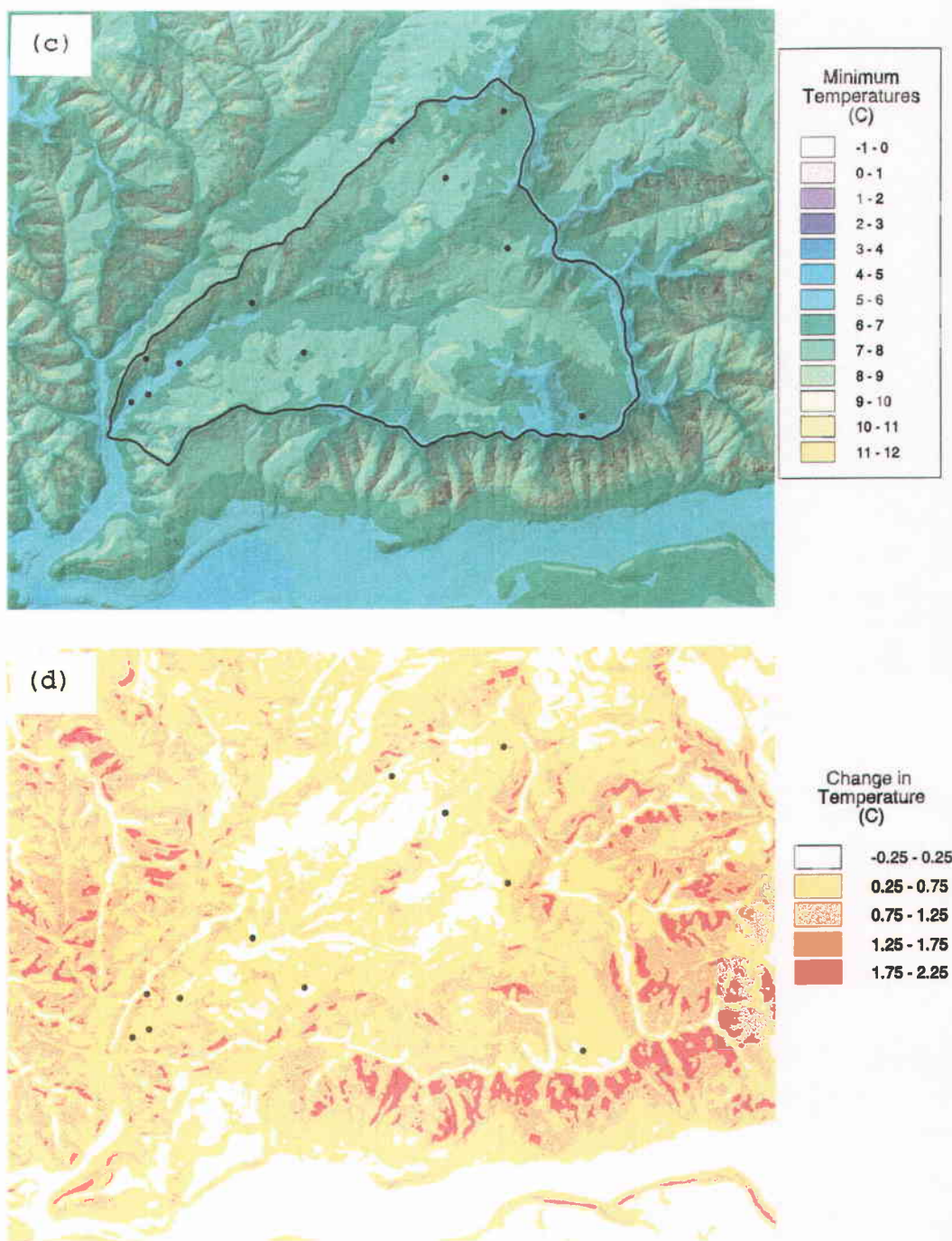


Figure 5.3. (Concluded).

explicitly account for radiation or sky view effects on maximum and minimum temperatures, so temperature differences between north and south-facing slopes or topographically-sheltered and open terrain were not depicted in its output. Cold air drainage effects are readily seen in Figure 5.3a, because PRISM accounts for inversions by modeling a two-layer atmosphere. September mean minimum temperatures in the lower McKenzie River and Blue River valleys were as low as temperatures at the highest elevations of the HJA (Figure 5.3).

At each pixel, PRISM calculates monthly temperature-elevation regression slopes both below (layer 1) and above (layer 2) the top of the inversion. Figures 5.4 and 5.5 show the average values calculated by PRISM and, for comparison, the values calculated in Rosentrater's (1997) HJA climate study. An increase in maximum temperature with height (inversion) was evident in layer 1 in all months except during the late spring and early summer, and minimum temperature inversions existed mainly in the late summer and early autumn. April and May were the only months for which there was a decrease in temperature with height (no inversion) for maximum and minimum temperatures. This was likely due to increased turbulent mixing of the atmosphere during the seasonal transition from spring to summer, which tends to minimize cold air drainage effects (Bergen, 1969; Bootsma, 1976; Lindqvist et al., 1999). Maximum temperature regression slopes differed dramatically between September and October in layer 1, reflecting the highly transitional nature of October's climate in the HJA from summer to autumn (Bierlmaier and McKee, 1989). PRISM's and Rosentrater's seasonal trends are generally in agreement for most months, with the exception of maximum winter temperatures in layer 1. PRISM's increases in maximum

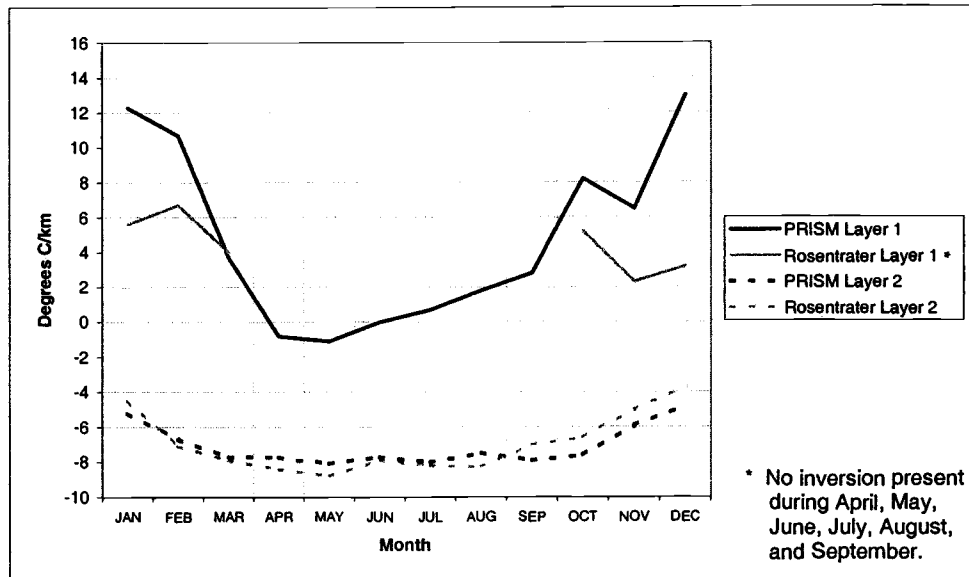


Figure 5.4. PRISM monthly maximum temperature-elevation regression slopes for layers 1 and 2 compared with values used by Rosentrater (1997).

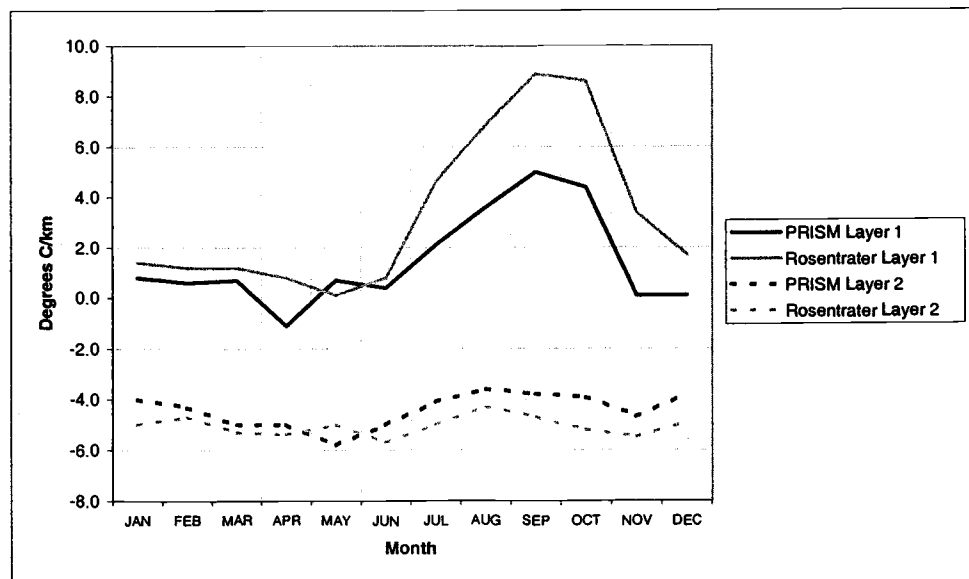


Figure 5.5. PRISM monthly minimum temperature-elevation regression slopes for layers 1 and 2 compared with values used by Rosentrater (1997).

temperature with height are much larger than Rosentrater's from November through January. This is because PRISM's input temperatures had been adjusted to remove the effects of topography and vegetation, raising them considerably; the steepest temperature-radiation regression slopes of the year (the largest adjustments) occurred during the winter months for maximum temperatures (Table 4.21). Sites near the top of the inversion were disproportionately warmed more than lower elevation sites because they were located on steeper slopes with lower sky view factors than lower sites, and received more diffuse radiation after adjusting them 'into the open' during these cloudy months.

The decrease in maximum and minimum temperature with height in layer 2 for all months approximates the accepted free-atmosphere rate of  $-6.0^{\circ}\text{C}/\text{km}$  (Geiger 1965; Oke, 1987). As discussed in Chapter 4, PRISM used variable inversion heights (based in the station data) over the HJA according to terrain elevation. Base inversion heights over the lower Lookout Creek valley were 700 and 720 meters for maximum and minimum temperatures, respectively, and increased somewhat over higher valleys. Rosentrater's inversion heights ranged from 650 meters for maximum temperatures to 700-800 meters for minimum temperatures, and were fixed over the entire area for each month.

The complete set of monthly temperature maps based on the PRISM grids with no radiation or sky view factor effects can be found in Appendix C.

## 5.2 IPW RADIATION AND SKY VIEW FACTOR GRIDS

The regression functions for bringing temperatures 'into the open' relied heavily on values from radiation and sky view factor grids. The process used to generate these gridded data was described in Chapter 4. Maps in all figures show radiation and sky view factors in the absence of vegetation, with only topographic features accounted for.

Figure 5.2b shows monthly radiation for September and Figure 5.3b shows sky view factor proportions for the HJA (constant for all months). Ridge tops clearly stand out in both maps. In the radiation map, ridge tops and open flat areas (not necessarily south-facing slopes) received the highest amounts of solar radiation. North-facing slopes often received as much and sometimes more radiation than south-facing slopes. This is because diffuse radiation is accounted for; a steeper south-facing slope may not receive as much diffuse radiation as a more topographically-open north-facing slope, because less sky is visible (a lower sky view factor). Even in relatively cloud-free September (Figure 5.2b), some pixels on the south side of Lookout Ridge received less radiation than pixels on the north side of the ridge because their sky view factors were so low, even though they had southern exposures. During winter months, when the cloud factors were high (a higher proportion of diffuse radiation), a site's sky view factor became more important in determining its radiation regime than its aspect. Some of the lowest sky view factors in the region were found in the steep south-facing gullies on Lookout Ridge near the bottom of the map (Figure 5.3b). During summer, east and west-facing slopes often received surprisingly large amounts of radiation,

because the sun rises in the northeast and sets in the northwest during those months.

Appendix D contains the complete set of IPW cloud-corrected monthly radiation maps, and Appendix E shows the sky view factor map for the HJA region.

### 5.3 PRISM TEMPERATURE GRIDS SHOWING EFFECTS OF RADIATION AND SKY VIEW FACTORS

Topographic effects of radiation and sky view factor were applied to the PRISM grids according to the procedure in Chapter 4. Figures 5.2c and 5.3c show the final temperature maps in the September sequence, and Figures 5.2d and 5.3d show the temperature differences between original PRISM maps and those incorporating radiation and sky view factor effects.

Maximum temperature patterns followed elevational patterns less closely after adding radiation effects to the grids (comparing Figures 5.2a and 5.2c). September's relatively cloud-free skies accentuated 'shading' effects on north-facing slopes, causing a reduction in maximum temperature of as much as 4.5-5.5°C. Areas affected most by radiation corresponded to the darkest spots on the radiation grid (Figure 5.2b). For example, the lowest temperatures in Figure 5.1c were seen on the high north side of Lookout Mountain (13-14°C), not at its summit (16-17°C). Instead of ridge tops being the coolest spots as in Figure 5.2a, slopes just below ridge tops showed the lowest temperatures in Figure 5.2c, because the reduced sky view factor at these sloped pixels lowered the amount of diffuse radiation received by them and hence their maximum temperatures. This was also true in narrow valleys (such as the Blue River valley), where

temperatures were lowered 1-2°C by radiation effects. Steeply sloped terrain was generally cooler on the grids incorporating radiation effects, because reducing the sky view factor lowered radiation values and maximum temperatures.

Like maximum temperatures, elevational minimum temperature patterns were reduced when sky view factor effects were introduced to the grids (Figure 5.3c). Minimum temperatures changed according to the sky view factor at each pixel (Figure 5.3b), a function of slope and topographic shading. Minimum temperatures on ridge tops and peak summits (the most open spots) were least affected by sky view factor effects, while sheltered areas in steep terrain were greatly affected by them. For example, September minimum temperatures in the steep ravines on the south side of Lookout Ridge were raised by as much as 2°C by sky view factor effects. Minimum temperatures in the Mack Creek valley rose by over 1°C and those on the north side of the central east-west ridge dividing McRae Creek and Lookout Creek were raised by 1-2°C (Figure 5.3d). In these areas, maximum temperatures were lowered because of radiation effects. Thermal belts (bands roughly corresponding to contour lines with the areas of highest minimum temperatures) that surrounded most ridges at mid-elevations in Figure 5.3a became more pronounced because of sky view factor effects, because the steepest slopes (where minimum temperatures were raised the most) on ridges were often found at these mid-elevations. The effects of sky view factors extended thermal belts in the sheltered upper valleys of Lookout Creek, McRae Creek, and Mack Creek to higher elevations.

The tendency for temperatures in steep narrow valleys to be raised may be misleading, because we did not account for stream effects which may have lowered minimum temperatures on

a smaller scale than is depicted here. However, on a larger scale, cold air drainage was a major characteristic of the minimum temperature map even after sky view factors were accounted for. Like the original PRISM-based map in Figure 5.3a, Figure 5.3c showed temperatures at the lowest elevations of the region to be as cold as those on top of Lookout Mountain.

Table 5.1 summarizes PRISM mean monthly maximum and minimum temperatures across the HJA. Maximum monthly temperatures were decreased by 0.8 to 1.5°C through radiation adjustments and minimum temperatures were increased by 0.1 to 0.5°C through sky view factor adjustments. As a result, overall monthly means were 0.1 to 0.6°C higher on the maps showing radiation and sky view factor effects (Table 5.1).

The complete set of final PRISM temperature maps without vegetation, showing the effects of radiation and sky view factors, is shown in Figure 5.6. Legend scales vary between summer and winter for both variables, with winter color scales used for November-April and summer scales used for May-October.

Maximum temperature patterns in the HJA were consistent from month to month. Throughout the year, the high, steep, north-facing slopes of Lookout Mountain (just below the summit) had the lowest maximum temperatures, which varied from 0-1°C in the winter to 19-20°C in July. During winter months (November through February), highest maximum temperatures (approximately 10°C) occurred between 600 and 650 meters in the central Lookout Creek valley. Highest maximum summer (July and August) temperatures, up to 30°C, often occurred in the central Lookout Creek valley near the confluence of Lookout Creek and Mack Creek, a relatively low elevation area receiving high amounts of solar radiation. The spatial range

Table 5.1. PRISM mean monthly temperatures for the H. J. Andrews in the absence of vegetation, with and without the effects of radiation (RADN) and sky view factors (SVF), (°C).

	A			C			E		
	MEAN MAXIMUM TEMPERATURE, NO RADN EFFECTS	MEAN MAXIMUM TEMPERATURE, W/RADN EFFECTS	DIFFERENCE (A-B)	MEAN MINIMUM TEMPERATURE, NO SVF EFFECTS	MEAN MINIMUM TEMPERATURE, W/SVF EFFECTS	DIFFERENCE (C-D)	MEAN TEMPERATURE, NO RADN, SVF EFFECTS	MEAN TEMPERATURE, W/RADN, SVF EFFECTS	DIFFERENCE (E-F)
JAN	7.2	5.9	1.3	-1.6	-1.5	-0.1	2.8	2.2	0.6
FEB	9.0	7.9	1.1	-1.1	-0.9	-0.2	4.0	3.5	0.5
MAR	10.6	9.6	1.0	-0.8	-0.5	-0.3	4.9	4.6	0.4
APR	13.8	12.8	1.0	1.1	1.2	-0.1	7.5	7.0	0.5
MAY	17.3	16.5	0.8	3.4	3.6	-0.2	10.4	10.1	0.3
JUN	22.0	21.2	0.8	6.4	6.7	-0.3	14.2	14.0	0.3
JUL	26.4	25.6	0.8	8.2	8.7	-0.5	17.3	17.2	0.1
AUG	26.9	25.9	1.0	8.6	9.1	-0.5	17.8	17.5	0.3
SEP	23.3	22.2	1.1	6.4	6.9	-0.5	14.9	14.6	0.3
OCT	16.9	15.8	1.1	3.7	4.0	-0.3	10.3	9.9	0.4
NOV	8.4	7.5	0.9	-0.1	0.1	-0.2	4.2	3.8	0.4
DEC	7.1	5.6	1.5	-1.7	-1.5	-0.2	2.7	2.1	0.7
ANN	15.7	14.7	1.0	2.7	3.0	-0.3	9.2	8.9	0.4

Note: Values refer to temperatures within the boundaries of the HJA only, and do not include the surrounding region depicted on the maps.

of maximum temperatures across the HJA was only slightly lower in winter (9-10°C) compared to summer (11-12°C). Though clearer skies created greater radiation differentials in summer than winter, temperature-radiation regression slopes were much lower in the summer (Table 4.21).

Inversions are evident in the maximum temperature maps from October through February (Figure 5.6). The highest maximum temperatures occurred between 600 and 650 meters and were often 3-5°C warmer than the valley floors at 400 to 600 meters. During winter months when these inversions occurred, progressively cooler temperatures appeared toward the lower elevations of the region. Thermal belts were least discernable on the northwest side of the lower Lookout Ridge, where slopes are dissected by many small steep gullies.

Though maximum temperature differences between north and south-facing slopes were noticeable during most months in the HJA, they were most pronounced during the winter. Differences were often as high as 4-5°C in December and January, and only 1-2°C in July and August (Figure 5.6). Again, the larger temperature-radiation regression slopes in the winter (seven times higher in December than July) accounted for this, offsetting the higher radiation differentials between north and south-facing slopes during the summer.

Like maximum temperatures, minimum temperature patterns were consistent throughout the year. Lowest minimum temperatures were almost always on peak summits and ridge tops, (the highest, most open surfaces), ranging from -4.0°C in the winter to approximately 7°C in the summer. Highest minimum temperatures, located within thermal belts, ranged from 0°C during the winter to 10-11°C during the summer. The warmest minimum temperatures in winter months were between 600 and 700 meters in the sheltered gullies on the northwest side

of the lower Lookout Ridge. In the summer, the elevation of the thermal belt's upper edge rose to as high as 850 meters, and with it the zone of warmest minimum temperatures.

Minimum temperature inversions occurred in all months, with variable intensities throughout the year. They were deepest and most pronounced (up to 400 meters deep above the lower Lookout Creek valley) from July through September, when temperatures in the thermal belts just above the inversion were 2-4°C higher than nearby valley floors. The relatively clear, calm atmospheric conditions during these summer months made these inversions the strongest of the year in the HJA. Inversions were least pronounced from March through May, when a relatively turbulent and well-mixed atmosphere characterizes the seasonal transition from spring to summer in the HJA and inhibits cold air drainage (Bergen, 1969; Bootsma, 1976; Lindqvist et al., 1999). As in the case of maximum temperatures, larger-scale minimum temperature cold air drainage was depicted by progressively colder temperatures at the lowest elevations in the region, especially during summer months.

Figure 5.6. PRISM estimated mean monthly maximum and minimum temperature maps for all months showing topographic effects of radiation and sky view factors.

*Note: Maps show hypothesized patterns of temperatures assuming unvegetated surfaces, accounting for the effects of elevation, cloudiness, and topography on radiation and temperature regimes.*

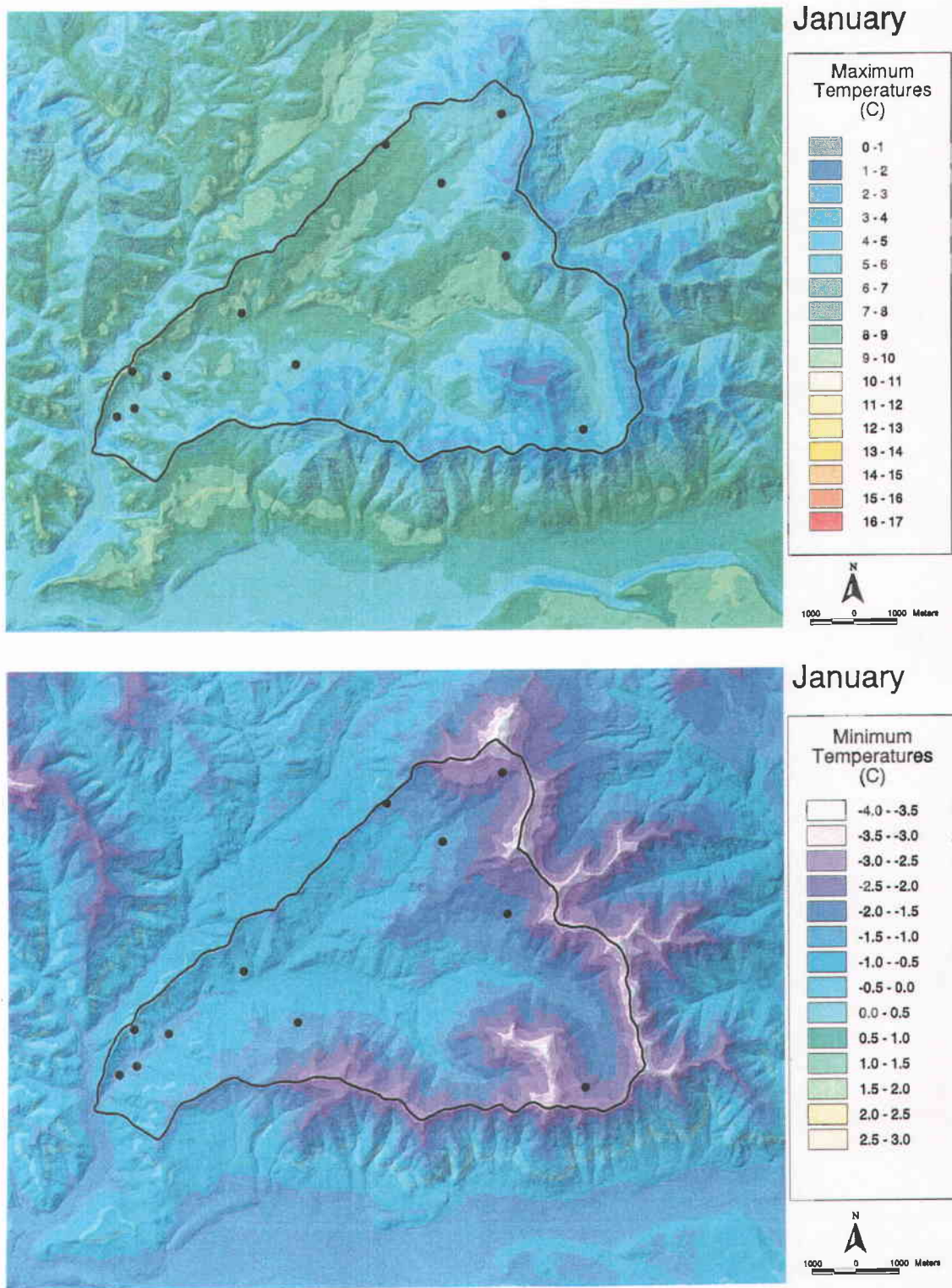


Figure 5.6. (Continued).

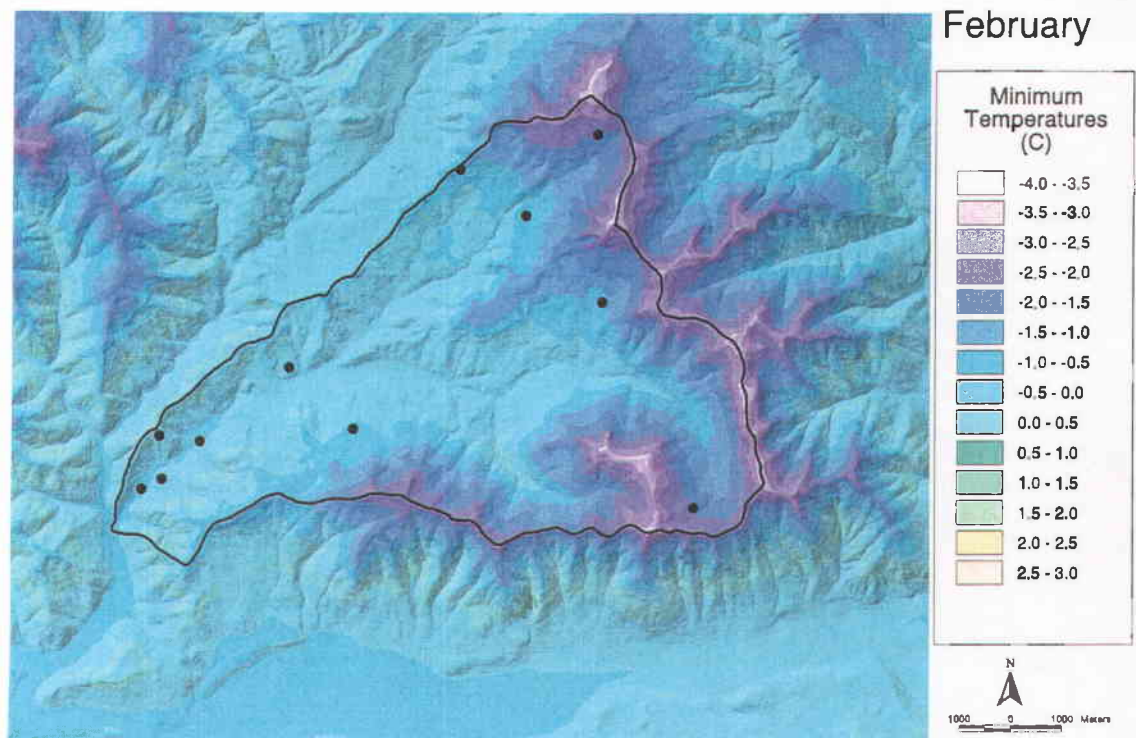


Figure 5.6. (Continued).

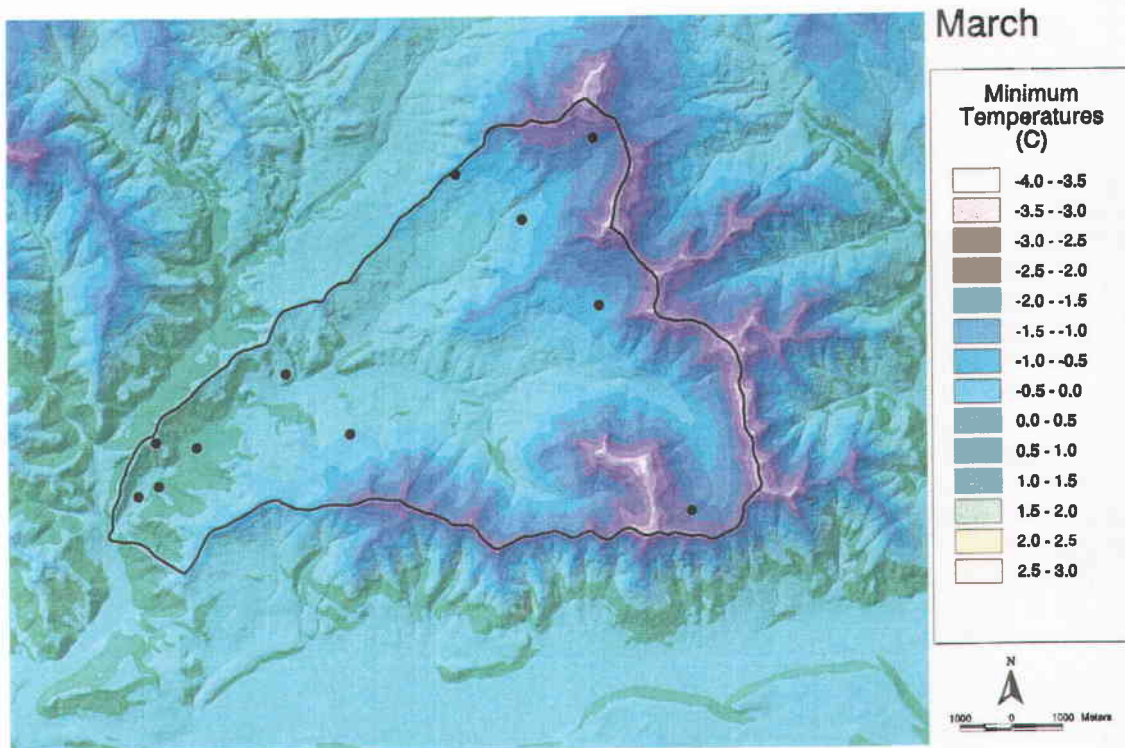
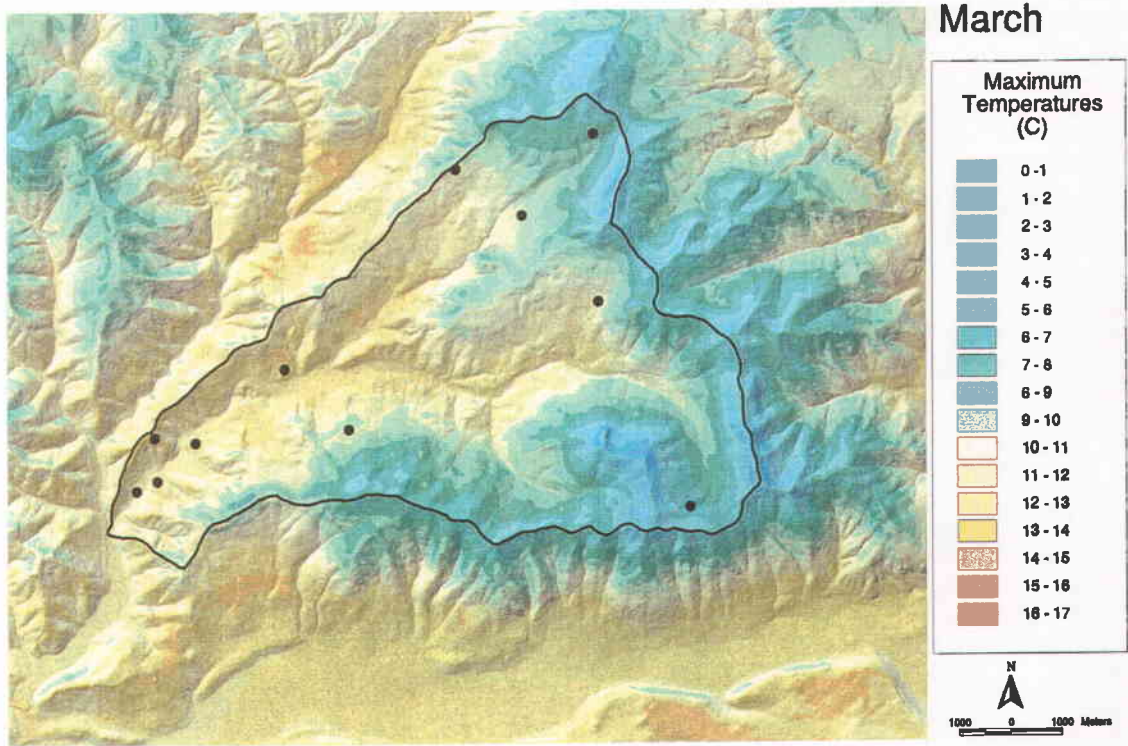


Figure 5.6. (Continued).

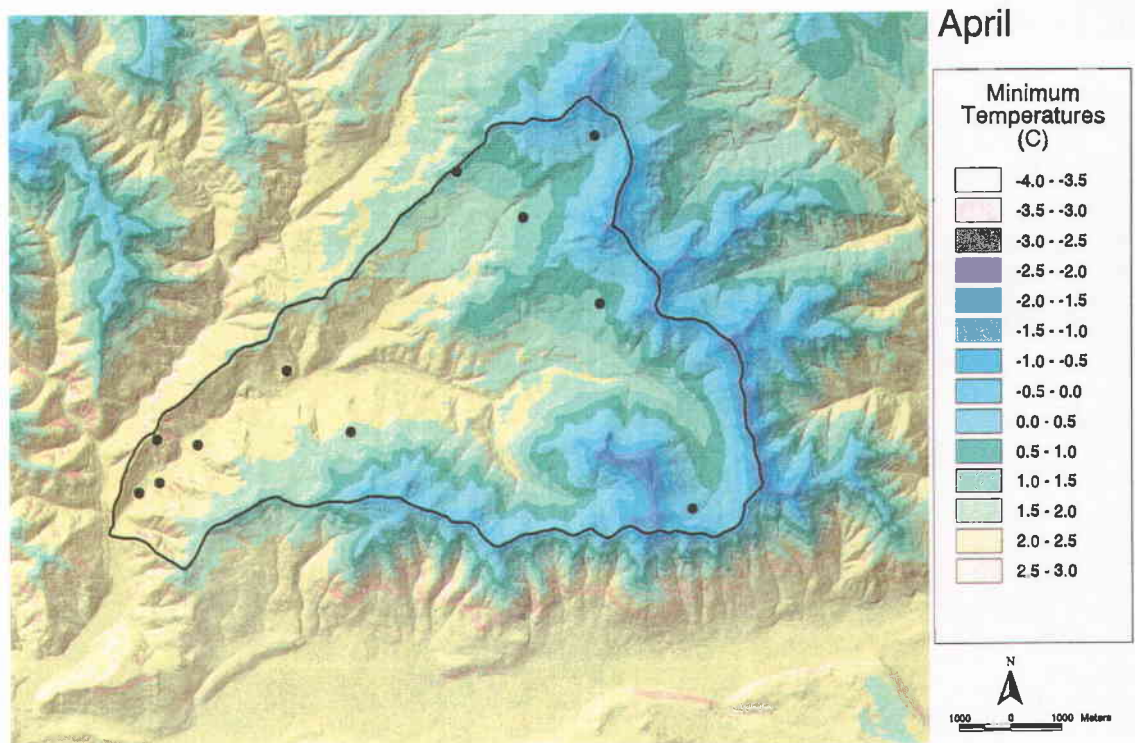
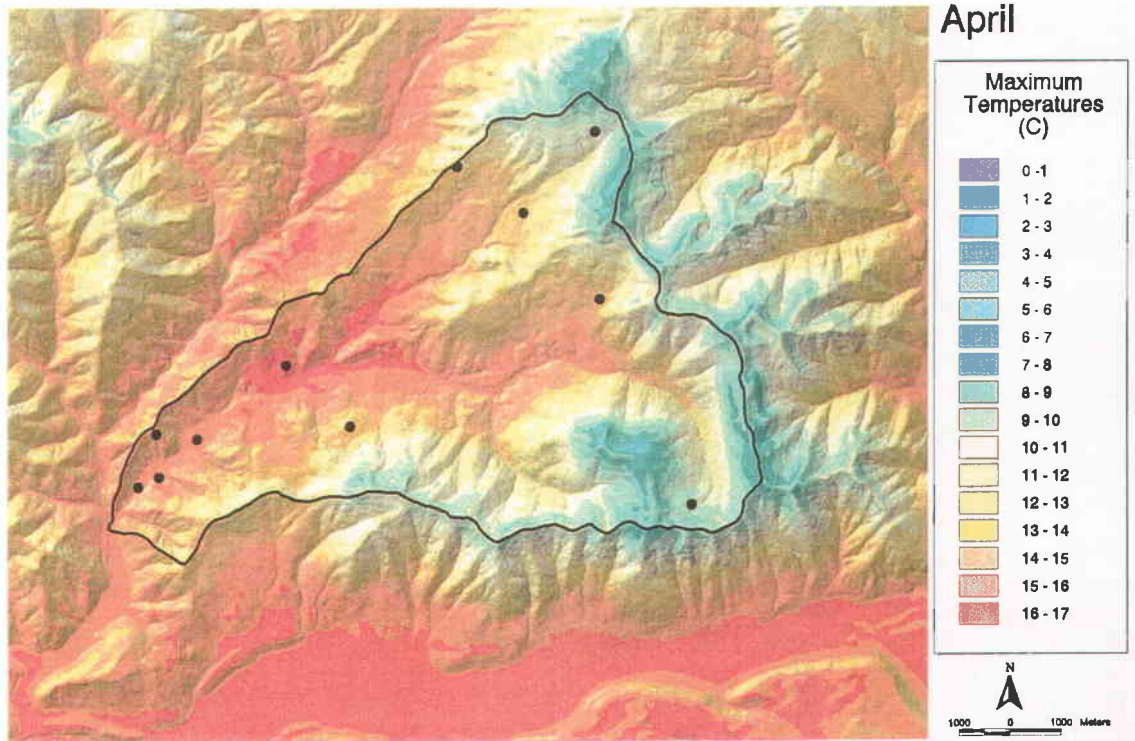


Figure 5.6. (Continued).

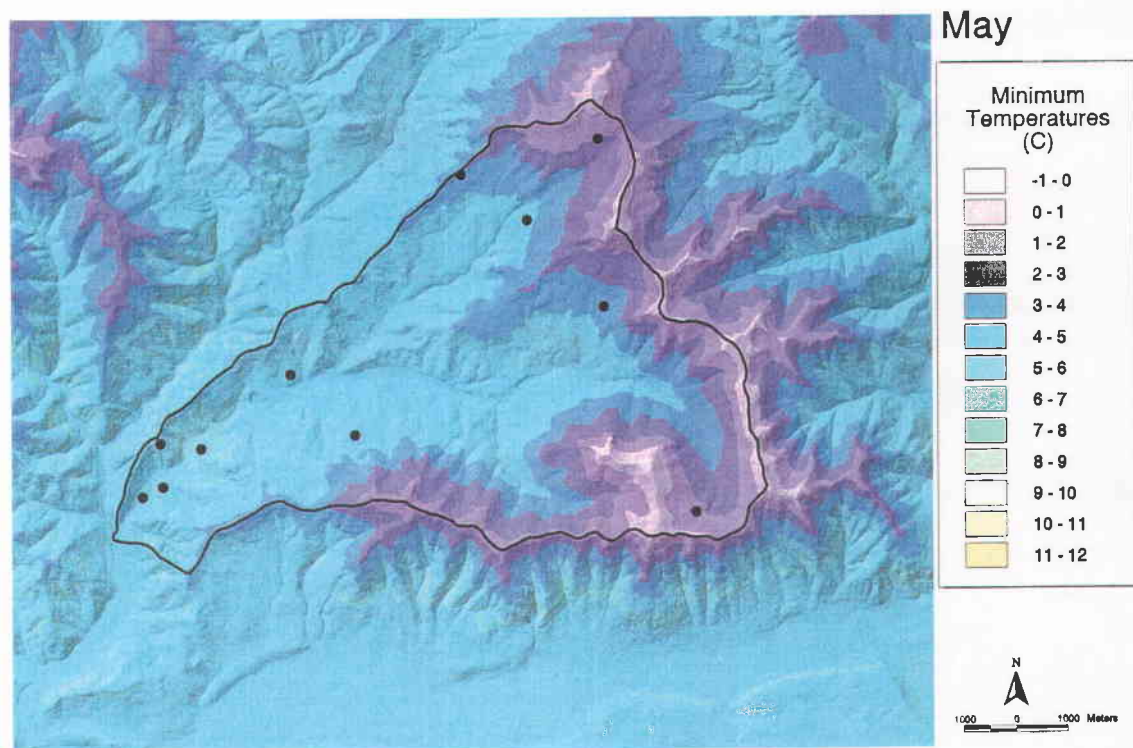
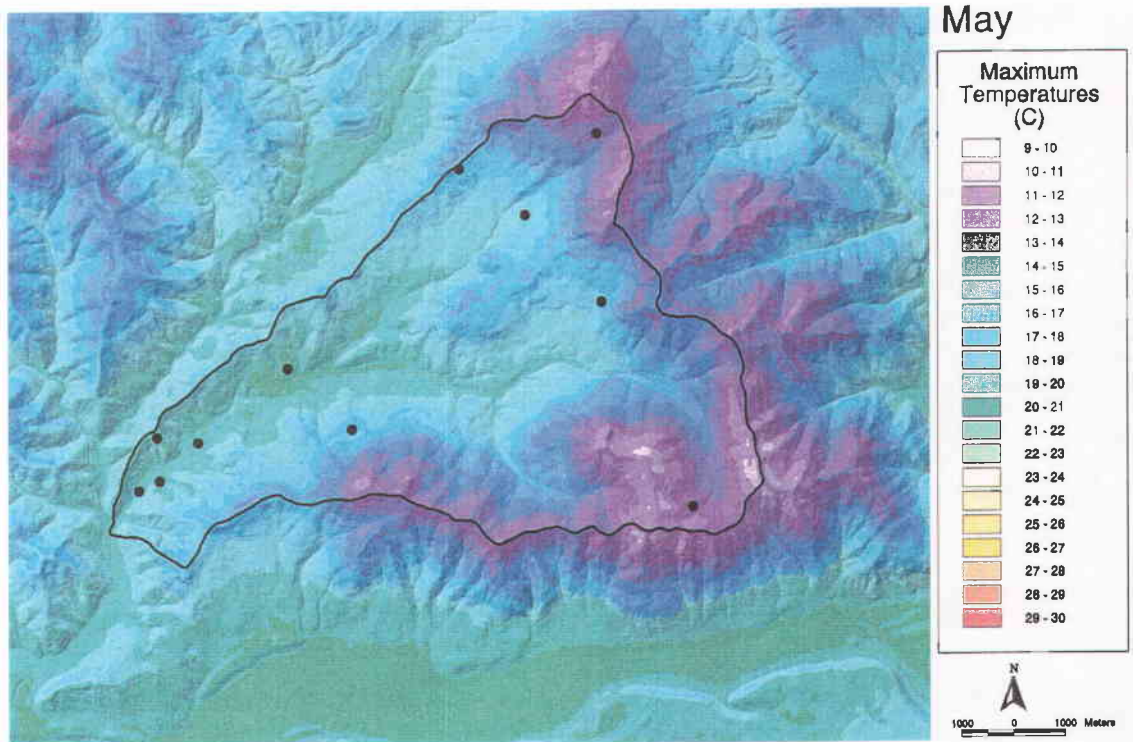


Figure 5.6. (Continued).

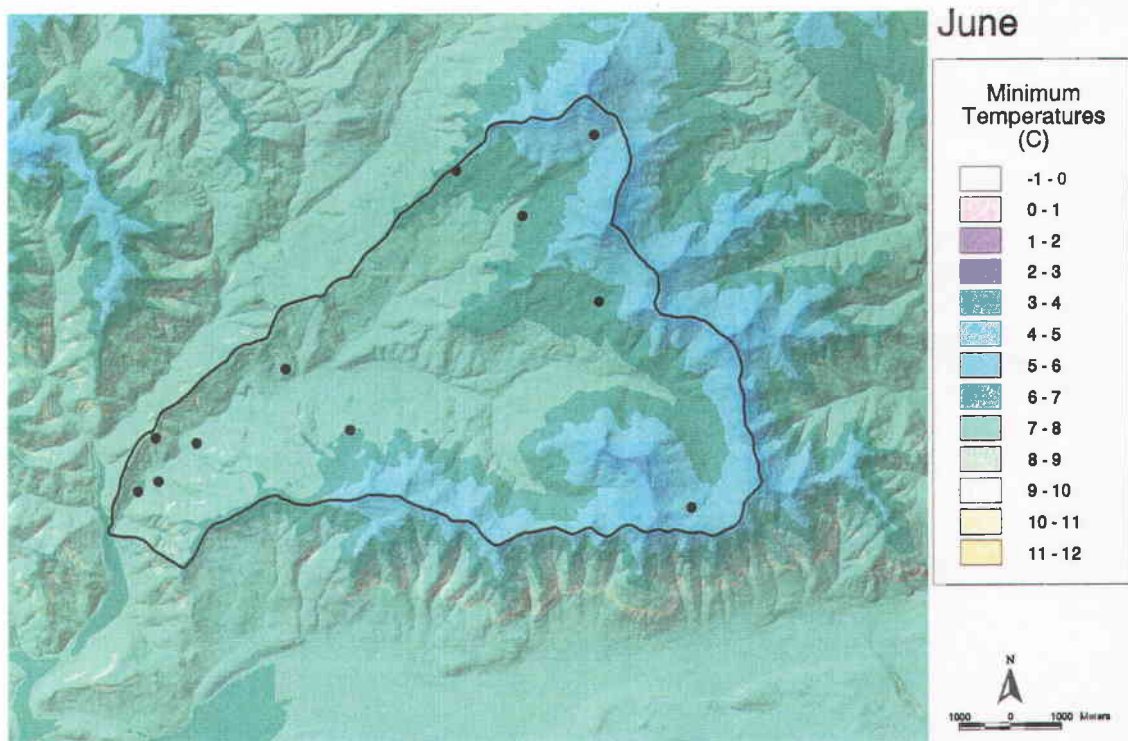
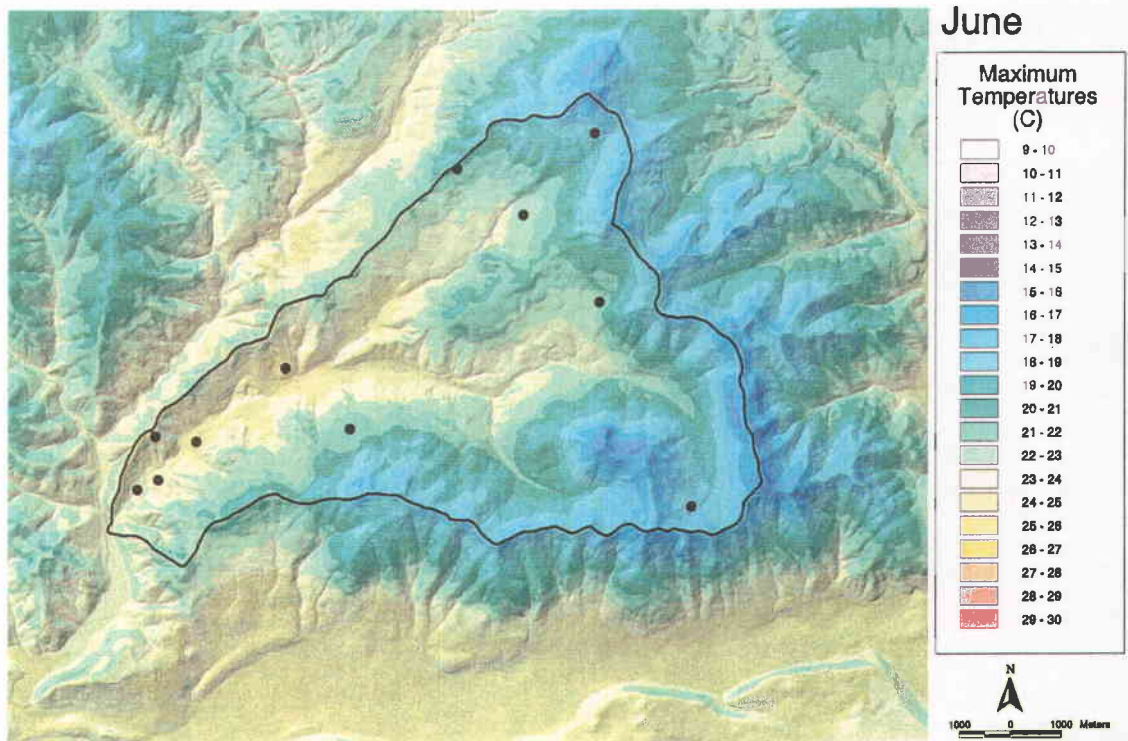


Figure 5.6. (Continued).

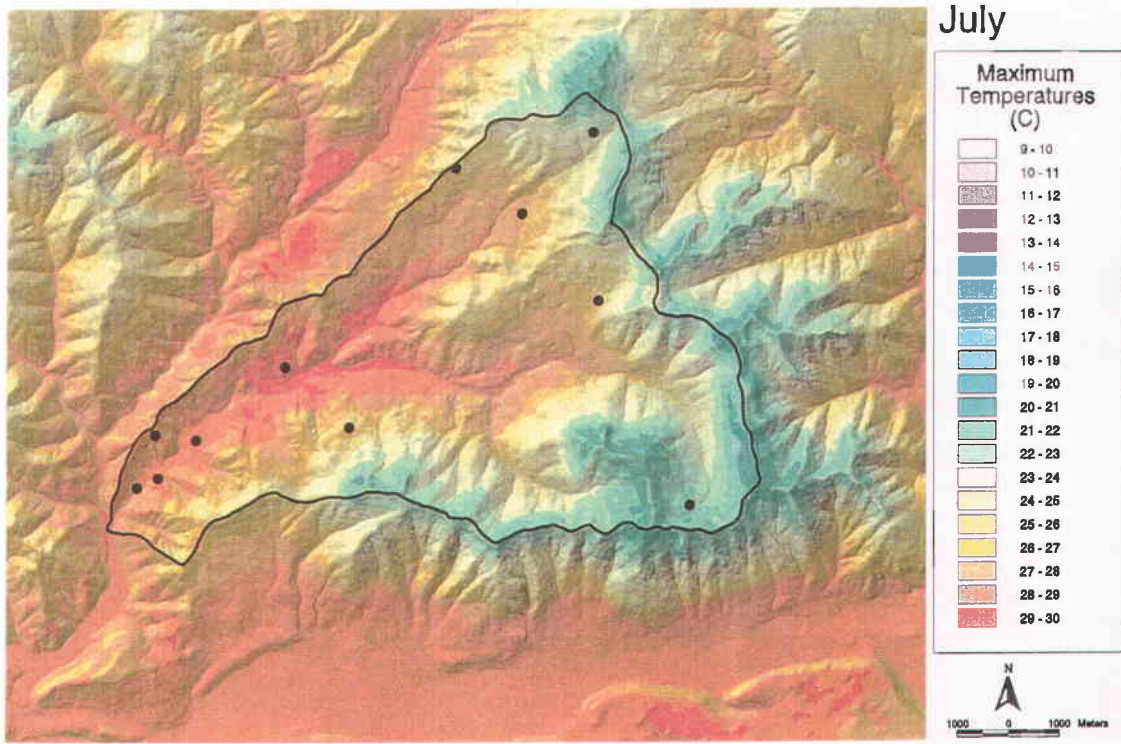


Figure 5.6. (Continued).

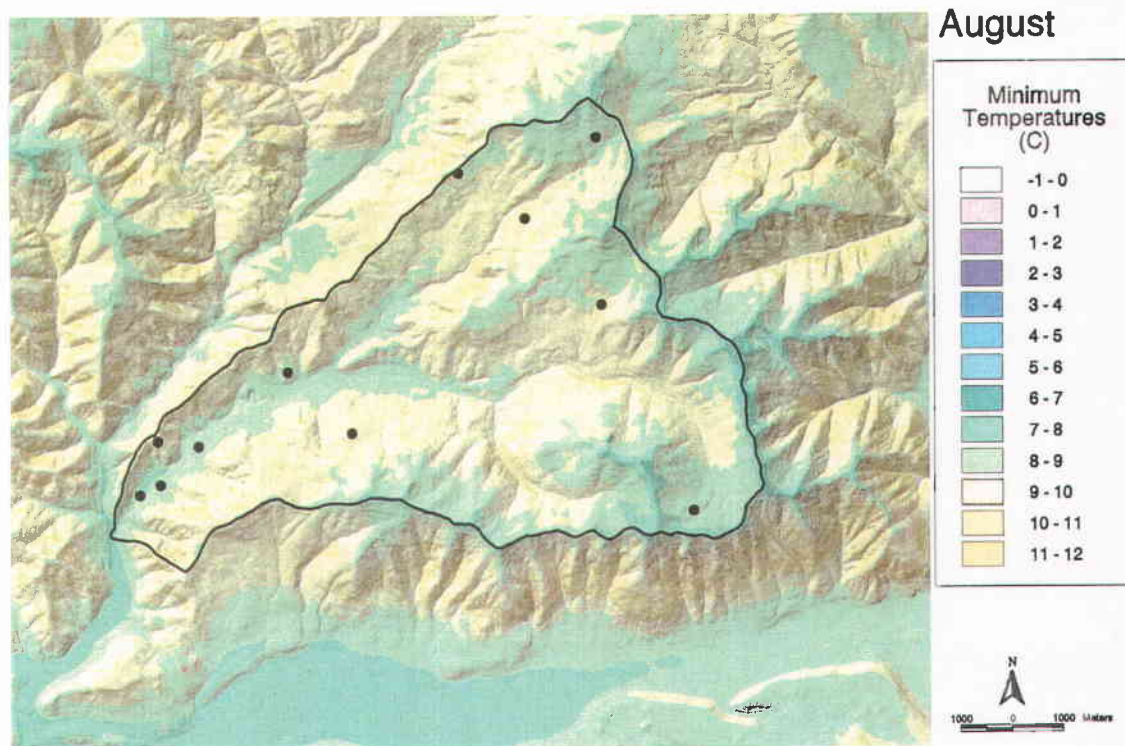
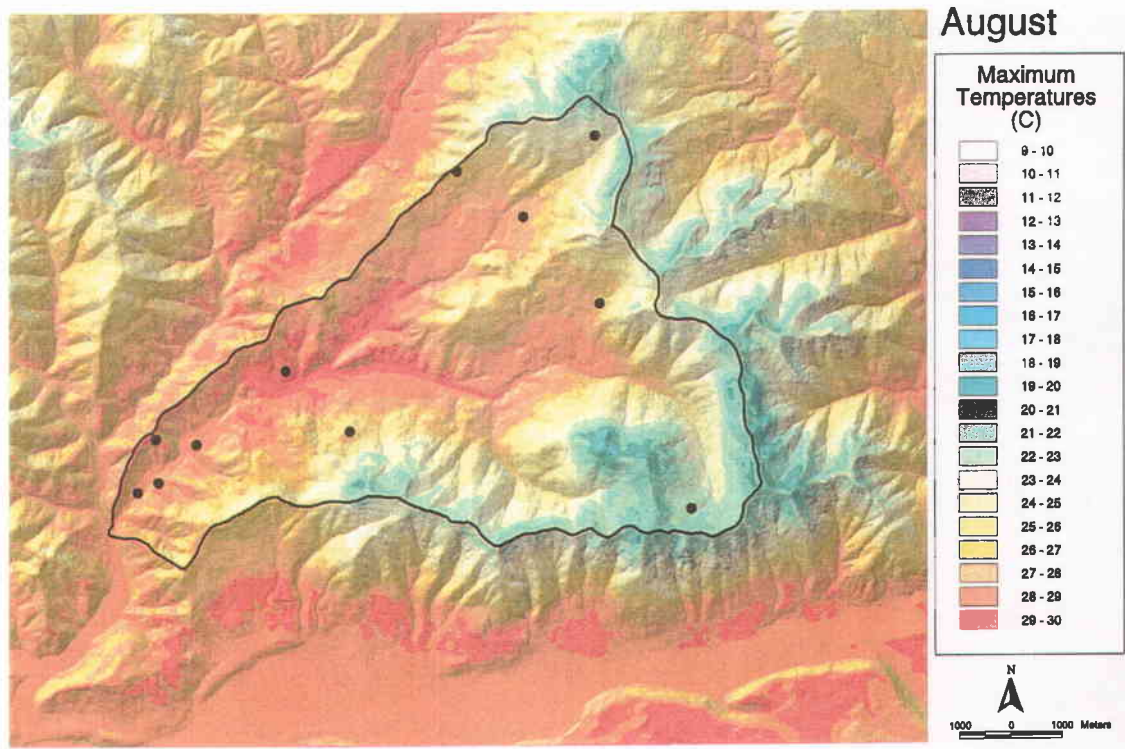


Figure 5.6. (Continued).

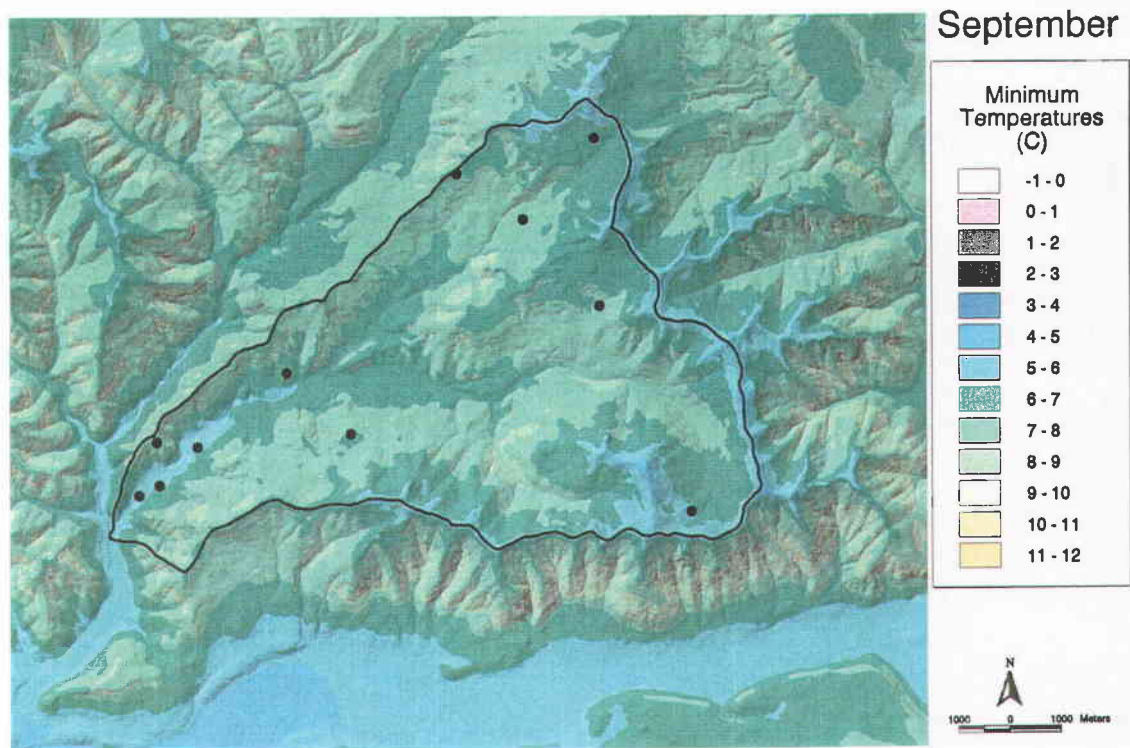
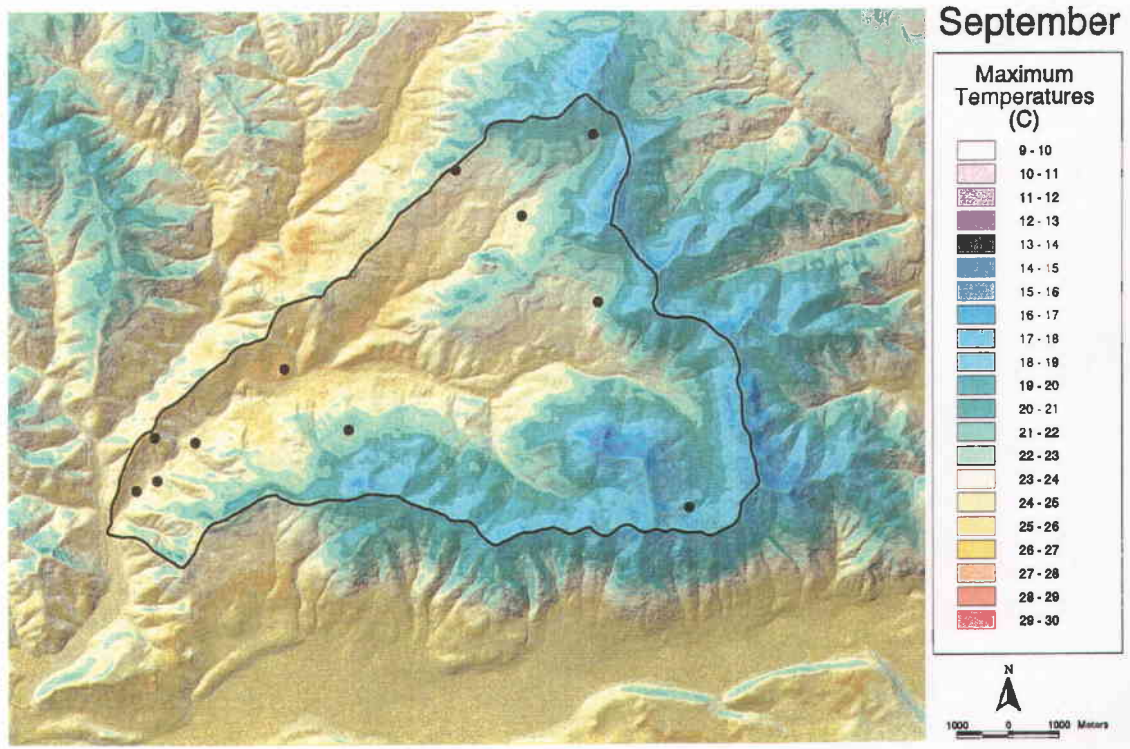


Figure 5.6. (Continued).

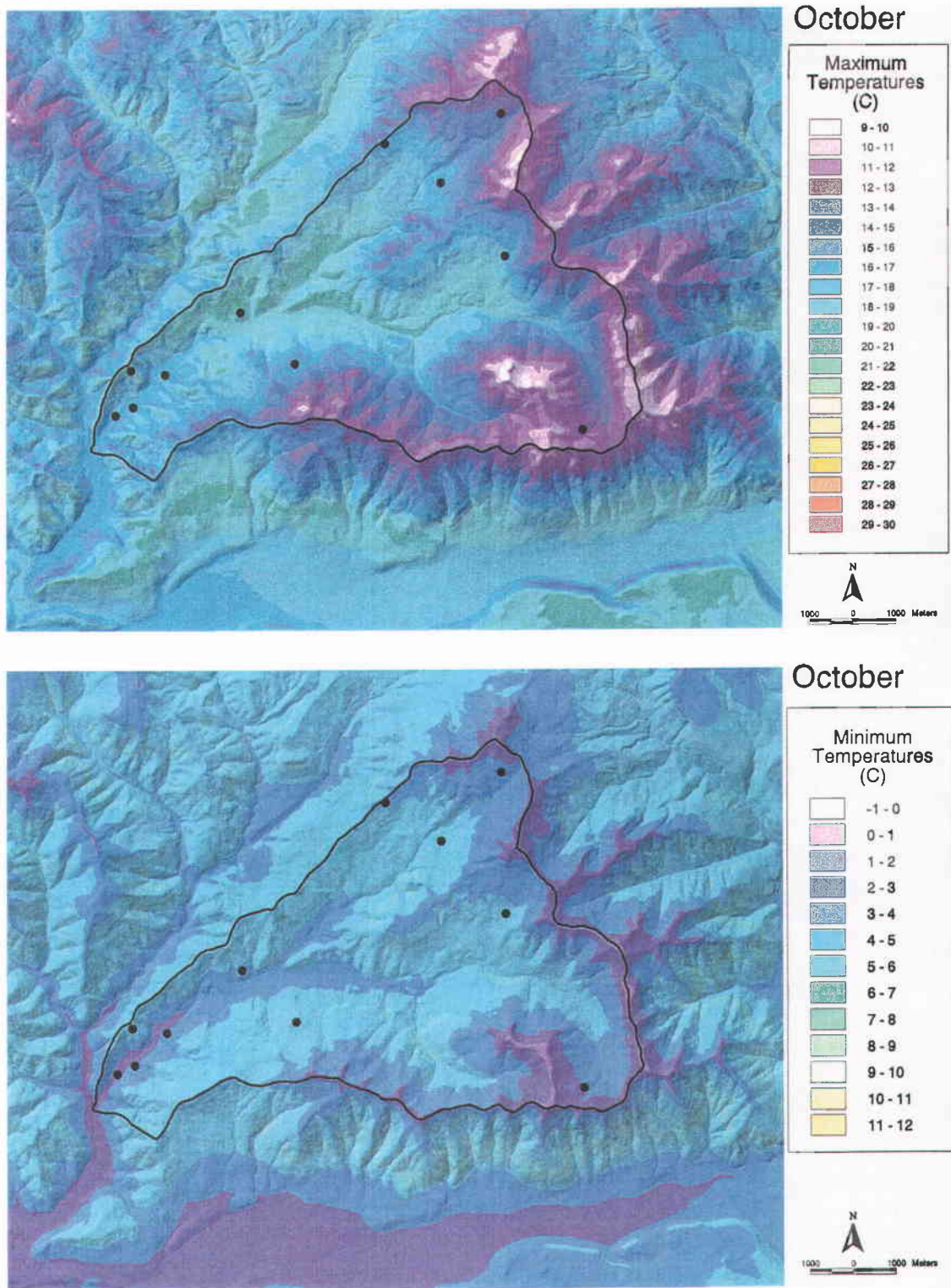


Figure 5.6. (Continued).

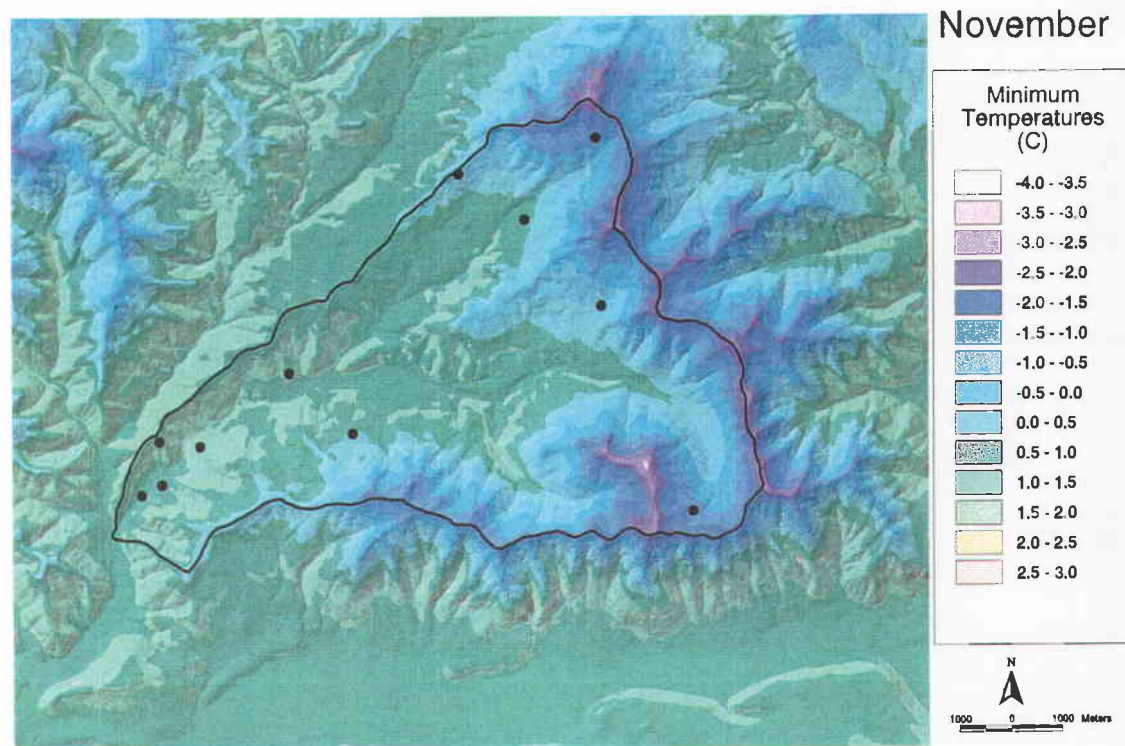
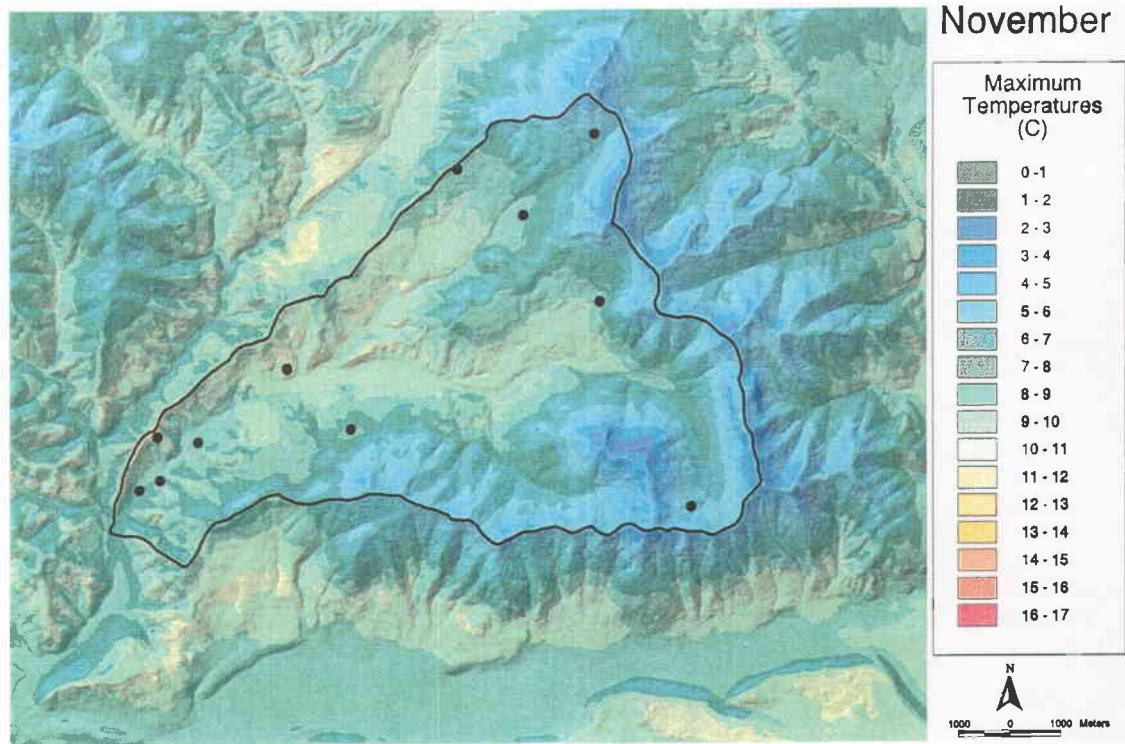


Figure 5.6. (Continued).

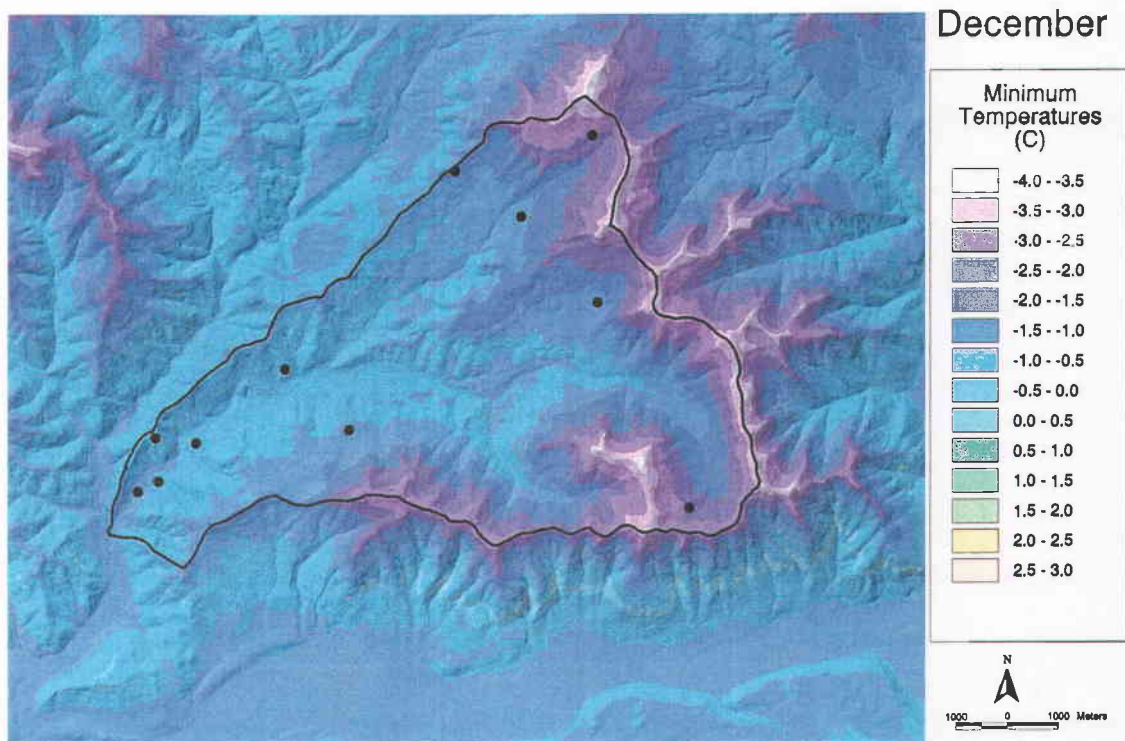
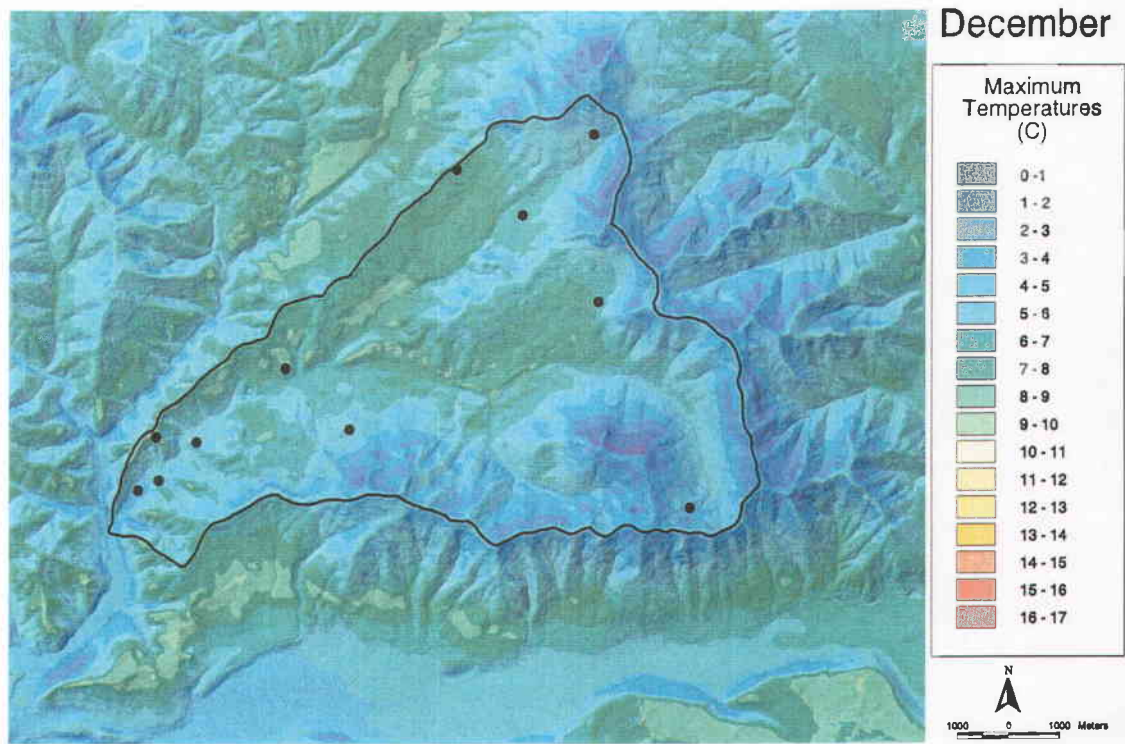


Figure 5.6. (Concluded).

## 6. DISCUSSION

### 6.1 HYPOTHESES BEHIND METHODOLOGY

The methodology behind this study was largely based upon assumptions and hypotheses made regarding the effects of elevation, forest canopy, cloudiness, and topography on mean monthly maximum and minimum temperatures in forested, mountainous terrain. Thus, the maps show hypothetical spatial estimates of temperatures minimizing the effects of vegetation across the HJA, and are not meant to represent 'real' mean monthly temperatures.

Elevation was assumed to be a major determinant of temperature regimes in the HJA. Temperatures generally decrease as elevation increases unless cold-air drainage causes temperature inversions, common throughout the year in the HJA. Elevations of thermal belts were determined by PRISM based on climate station data and specified parameters, with a certain amount of cross-talk between the two atmosphere layers to model the transition from the inversion to the free atmosphere above it as accurately as possible (Section 4.6.2).

Forest canopy was assumed to be another major determinant of temperature regimes in this study because of its effect on incoming shortwave solar radiation during the day and outgoing longwave radiation at night. This project hypothesized that reduction in sky view factor due to vegetation above a temperature sensor attenuated both direct and diffuse shortwave radiation. These radiation reductions lowered maximum temperatures depending upon the total daily radiation load. Tree canopy was assumed to mitigate longwave radiation loss at night by trapping thermal radiation closer

to the surface, thereby incurring a warming effect on minimum temperatures.

This study assumed that cloudiness had a large effect on shortwave and longwave radiation regimes. Clouds reduced total daily shortwave radiation loads and altered direct and diffuse proportions of radiation, which significantly affected topographic shading regimes in our model. Like tree canopy, the presence of clouds at night tended to inhibit longwave radiation loss and kept minimum temperatures warmer, a phenomenon inherent in the temperature observations.

Slope and aspect were assumed to largely determine shortwave radiation regimes, especially on clear days when proportions of direct radiation were relatively large. Other topographic effects on temperatures were thought to exist in the HJA, though they could not be modeled or tested. For example, terrain configurations were assumed to determine cold-air drainage patterns by steering the flow of cold-air pockets through ravines, valleys, and flat areas, and thereby determining inversion and thermal belt characteristics.

Because the project's methodology was based on hypotheses, care should be taken when assessing the spatial and temporal predictive accuracy of the maps, especially at very small scales.

## 6.2 SOURCES OF UNCERTAINTY

In any research project that bases its methodology on hypothesized quantifications of natural phenomena, there can be many sources of uncertainty. In this project, errors were not additive throughout the process because of the way in which the methodology was conducted (for example, the

selective elimination of sites from the analysis at certain stages). Thus, the potential sources of error must be examined at each step independently of one another. Though a formal error analysis could not be done because of low confidence in the historical dataset as a whole, the following discussion attempts to quantify potential sources of uncertainty. Specific recommendations for future research to address some of these issues can be found in Chapter 7.

Historical temperature data at the HJA have been gathered using partially shielded mercury bulb thermometers and thermistors. Instrumentation error for mercury thermometers (used for about two-thirds of the total period of record) was approximately  $\pm 2.0^{\circ}\text{C}$ , with another  $\pm 2.0^{\circ}\text{C}$  error introduced when digitizing the paper charts. Thermistors, installed by the early 1990s at all sites, are accurate to approximately  $\pm 0.4^{\circ}\text{C}$  (J. Moreau, pers. comm.). The inconsistency of sensor heights above the ground may also have been a source of error, though probably a small one. Mean monthly temperatures were less likely to have been affected by these observational errors than the original daily datasets.

In Chapter 4, mean monthly temperatures at sites with short records were adjusted to the full 30-year period using the highest correlated long-term site. For maximum temperature adjustments, mean absolute errors for periods of record ranged from  $1.1^{\circ}\text{C}$  for a one-year period of record to  $0.2^{\circ}\text{C}$  for a 24-year period of record ( $0.6^{\circ}\text{C}$  to  $0.2^{\circ}\text{C}$  for minimum temperatures, from Figures 4.2 and 4.3). The shorter the period of record for a short-term site, the greater the error, but potential temperature errors never exceeded  $0.7^{\circ}\text{C}$  because any site with less than three years of original data was not considered (mean absolute errors for maximum and minimum temperatures were  $0.7^{\circ}\text{C}$  to  $0.6^{\circ}\text{C}$  for three-year

periods of record, respectively). Thus, errors introduced into the procedure by temporal adjustments were likely minimal compared to observational errors.

The most significant source of error in the project probably stems from radiation adjustments to the datasets (adjusting temperatures to simulate flat, open siting conditions for input into PRISM). Monthly cloud factors at UPLMET were taken to be representative of the HJA as a whole. Though the HJA is a small geographic area, it is probable that cloud factors varied somewhat across the watershed. Hemispherical fisheye photographs, which played a major role in our analysis, are temporally unreliable records of radiation and sky view factor attenuation. Canopy characteristics may have changed significantly over the 30-year period of record, and our images documented vegetation conditions at one instant in time only. Given the general trend of increasing canopy closure over time, the probable effect was a bias toward too much canopy correction for the early years of record. Attempts were made to use only climate stations in our analysis for which fisheye images were deemed 'reliable' and most likely to represent long-term canopy characteristics, but this was a significant source of error. We did not account for the role that obstacle distance might play in determining longwave radiation attenuation. For example, clouds, mountain ridges, and nearby trees probably do not mitigate thermal radiation loss equally. It was difficult to quantify fisheye sources of error, but the author's best estimate is 5% uncertainty for very open or closed canopy sites (continuous canopies), and 25% uncertainty for sites with partially open canopies.

The slopes of the regression functions developed in Chapter 4 can be used to estimate the potential effects of

radiation and sky view factor errors on temperature adjustments. The regression functions incorporated many of the potential sources of error in our methodology, so these error estimates give a good idea of the overall effect of several factors on actual temperature estimates.

Consider a  $2.52 \text{ MJ/m}^2 \cdot \text{day}$  radiation difference between site pairs in December, the month with the steepest maximum temperature/radiation regression line slope (Table 4.21). This is the greatest radiation difference between any site pair used to calculate the maximum temperature/radiation regression function for that month (Table 4.20). The 'best and worst case' scenarios assuming 5% and 25% error in the radiation estimates, correspond to margins of error of  $\pm 0.13$  and  $\pm 0.63 \text{ MJ/m}^2 \cdot \text{day}$ , respectively. The resulting uncertainty in maximum temperature adjustment values range from  $\pm 0.18^\circ\text{C}$  to  $\pm 0.89^\circ\text{C}$ . The greatest radiation difference between any site pair in July (the month with the shallowest regression line slope but largest radiation differences) was  $19.91 \text{ MJ/m}^2 \cdot \text{day}$ . The 'best and worst case' scenarios gave radiation difference ranges of  $\pm 1.00$  and  $\pm 4.98 \text{ MJ/m}^2 \cdot \text{day}$ , resulting in ranges in maximum temperature adjustment values from  $\pm 0.2^\circ\text{C}$  to  $\pm 1.0^\circ\text{C}$ , respectively. Thus, even when radiation estimates were made from fisheye photographs having a  $\pm 25\%$  margin of error, maximum temperature adjustment errors never exceeded  $1.0^\circ\text{C}$ , an amount well within the limits of observational error.

A similar analysis performed on minimum temperature adjustments reveals an even lower potential margin of error. Months with the steepest and shallowest minimum temperature/sky view factor regression line slopes were August and January, respectively, and the greatest difference in sky view factor proportions between any site pair was 0.64 (Table

4.22). 'Best and worst case' scenarios assuming 5% and 25% error in the sky view factor estimates correspond to errors of  $\pm 0.03$  and  $\pm 0.16$ , respectively. These values give error ranges in minimum temperature estimates from  $\pm 0.1^{\circ}\text{C}$  to  $\pm 0.6^{\circ}\text{C}$  in August to  $\pm 0.0^{\circ}\text{C}$  to  $\pm 0.2^{\circ}\text{C}$  in January. Thus, errors in minimum temperature adjustments from the minimum temperature/sky view factor regression functions were small.

Error estimates of the temperature interpolation process were made using a jackknife cross-validation procedure within PRISM. At each station location, PRISM was run without that station to estimate the temperature at its location, and the predicted values were compared to the observed station value. Mean absolute errors, which are the average of the absolute value of error, ranged from  $0.5^{\circ}\text{C}$  to  $0.9^{\circ}\text{C}$  for maximum temperatures, and from  $0.1^{\circ}\text{C}$  to  $0.3^{\circ}\text{C}$  for minimum temperatures throughout the year. Biases, which assess how high or low estimates are across the entire grid, ranged from  $+0.1^{\circ}\text{C}$  to  $+0.3^{\circ}\text{C}$  for maximum temperatures, and from  $0.0^{\circ}\text{C}$  to  $+0.1^{\circ}\text{C}$  for minimum temperatures. All of these values are well within observational error, and show that spatial interpolation of temperatures introduced low levels of uncertainty to the process.

There were other possible sources of error in the original temperature datasets. Forest edges (boundary areas between clearings and forests) and streams probably affected long-term monthly temperature values. Many climate stations in the HJA have been and are located within distances that may be affected by edges and streams. These physical features could not be accounted for in this study because necessary datasets did not exist to quantify them. This study also did not quantify scale-dependent temperature advection processes that may affect temperatures in the HJA. For example,

temperature regimes on an even, broad north-facing slope are likely different than those on a small north-facing slope having several slopes of varying orientation nearby.

Caution must be taken when using estimated temperatures for areas outside the HJA boundaries shown in the maps. This is because environmental processes within the Lookout Creek watershed were used to quantify the effects of elevation, canopy, cloudiness, and topography on temperatures, and these effects were extrapolated to other areas, where in fact environmental processes may affect temperatures differently. Because adjustments may have obscured sensitive long-term trends in the datasets, caution should also be taken when using the final dataset to investigate evidence of long-term climatic events in the HJA, such as those associated with PDO (Pacific Decadal Oscillation) or ENSO (El Nino/Southern Oscillation) phenomena.

## 7. CONCLUSIONS

### 7.1 SUMMARY OF PROJECT AND RESULTS

This study attempted to predict the spatial temperature regimes at the H. J. Andrews Experimental Forest at average monthly intervals based on the 1971-2000 30-year record to account for several environmental factors assumed to affect its local microclimates. The 30-year dataset, computer software to analyze radiation effects on temperatures, and an appropriate spatial temperature interpolator, together with GIS capabilities, were used to create high resolution mean monthly maximum and minimum temperature maps of the HJA. In order to make the results as useful as possible, temperatures were modeled to minimize the effects of vegetation, to approximate standard weather station siting conditions and to provide a universal 'starting point' for future projects that may use these data as input.

Besides mean monthly maximum and minimum temperature maps of the HJA, the project had several secondary objectives. Mean monthly radiation maps of the HJA, accounting for topography and cloudiness and their effects on direct and diffuse radiation, were created. Historical temperature datasets and site specifications were quality-checked and inventoried, and site radiation regimes were summarized with hemispherical fisheye photographs. The regression functions developed here for quantifying the effects of topography and canopy on temperatures in complex, forested terrain may be useful in other climate studies.

The final radiation and sky view factor-adjusted temperature maps accounted for many of the microclimatic

patterns thought to exist in the HJA. Major temperature inversions and thermal belts were represented for the months in which they occur. Maximum temperature differences between north- and south-facing slopes and minimum temperature differences between topographically sheltered and open areas reflecting seasonal cloudiness were accounted for in the analysis. It is hoped that the temperature maps created in this study will be useful to a number of scientific disciplines engaging in future research at the HJA.

Datasets from this study are available on the internet as GIS-compatible grids at <http://www.fsl.orst.edu/lter/>. Further information about the project can be found at <http://www.ocs.orst.edu/pub/smithjw/hja/index.html>.

## 7.2 RECOMMENDATIONS FOR FUTURE WORK

This project attempted to account for as many environmental factors affecting microclimates in the HJA as possible, but more research is needed to validate the results and account for other factors not considered in this study. Major weaknesses in the project's methodology were:

- maps incorporate only large-scale effects of cold-air drainage in the HJA
- inability to quantify forest edge effects on temperatures
- inability to investigate topographic scale effects on temperatures
- inability to quantify stream effects on temperatures

The following list contains recommendations for addressing some of these weaknesses, as well as recommendations for future climate research in the HJA and suggestions that may improve the accuracy of further studies.

**1. Expand the climate station network by placing more sites in underrepresented areas.**

Better spatial representation in areas lacking climate stations would be helpful for future climate mapping work. These areas include the middle and lower McRae Creek valley, the area near the confluence of Lookout Creek and McRae Creek, and the broad, high basin to the northwest of CENMET. Additional climate stations along Lookout Ridge, Lookout Mountain, and the east-west ridge between the Lookout and McRae Creek basins would be helpful. Temperature estimates in the Mack Creek drainage could be improved by the addition of non-stream sites. Additional climate stations at elevations near thermal belts (650-850 meters) would help to validate heights of temperature inversions.

**2. Quantify small-scale effects of cold-air drainage in the HJA.**

Although cold air drainage was modeled indirectly, work is needed to accurately assess the specific nature of this phenomenon on temperature inversion regimes in the HJA. The maps presented here incorporate only large-scale effects of cold-air drainage based on temperature/elevation relationships. The proposed cross-sectional network of portable climate stations in drainages (J. Moreau, pers. comm.) would aid greatly in this. Studies estimating the magnitude and geographic scale of stream effects on air temperatures in the HJA also are needed. Accounting for the

cooling effects of water channels might significantly change stream valley temperature patterns, even at the scale of this study.

**3. Add more climate station pairs at similar elevations with different canopy types.**

The accuracy of the radiation and sky view factor-temperature regression functions could be improved with the addition of climate station pairs at similar elevations having different forest canopy or topographic shading regimes. Such site pairing might also allow future HJA researchers to quantify the different effects on minimum temperatures of longwave radiation blockage between nearby vegetation and distant topography.

**4. Manage vegetation around MET sites and future climate stations to maintain standard siting conditions.**

Given the high spatial and temporal variabilities of air temperatures at the HJA, and their critical role in ecosystem processes, some vegetation modification around temperature monitoring sites seems justified to bring them up to NWS standards. Future climate stations in the HJA should be located on relatively flat, topographically-open sites that are regularly cleared of vegetation.

**5. Develop a historical database of vegetation changes at each climate station site.**

A weakness of the mapping model presented here is the temporal unreliability of fisheye photographs. Images portraying canopies at one instant in time were archived for this project, but do not incorporate canopy changes over time, which can be significant. If fisheye photographs could be

taken at each climate station at regular time intervals (1-2 years), an image database could be established from which long-term and short-term vegetation changes could be quantified.

**6. Test maximum temperature/radiation and minimum temperature/sky view factor regression functions elsewhere.**

The methodology applied in this study to adjust air temperature to account for radiation effects might be useful in other studies. However, care should be taken if the radiation and sky view factor-temperature regression functions are to be applied elsewhere. Climate controls specific to the HJA may exist, giving the area unique temperature regimes that may make these regression functions inappropriate in other forested, mountainous areas. It would be useful to test these regression functions on data obtained elsewhere.

**7. Reintroduce vegetation effects by creating canopy-sensitive maps with remotely-sensed canopy coverages.**

It would be possible to take the temperature adjustment sequence one step further by reintroducing the effects of vegetation into the analysis. Regression functions in this study relied on hemispherical fisheye images, so any attempts to adjust for the effects of forest canopy would require such images at every pixel in the HJA. A possible solution to this problem might be a function relating existing high-resolution leaf-area index (LAI) coverages (C. Daly, pers. comm.) to proportions of solar radiation blocked by forest canopy, so that the LAI coverage itself could be used as a temperature-adjustment tool.

**8. Investigate the effects of different instrumentation shielding on temperatures.**

Thermistors at HJA climate stations are shielded above with PVC pipes cut length-wise, and open beneath. It is possible that thermistors would record different temperature values if bottom shielding were used because of longwave radiation emission from the earth's surface below them. Temperature sensors in other station networks are often completely enclosed or shielded differently than those in the HJA. These differences could be significant, especially in open areas, and should be studied in order to ascertain the accuracy of long-term HJA temperature datasets.

This project is one step in a coordinated effort to map HJA thermal climate regimes. It is hoped that future climate studies at the HJA will build upon it.

BIBLIOGRAPHY

Alsop, T.J., 1989. The natural seasons of Oregon and Washington. *Journal of Climate*, 2, 888-896.

Barry, R.G., Chorley, R.J., 1992. *Atmosphere, Weather, and Climate*. New York, Routledge.

Bergen, J.D., 1969. Cold air drainage on a forested mountain slope. *Journal of Applied Meteorology*, 8, 884-895.

Bierlmaier, F.A., and McKee, A. 1989. Climatic Summaries and Documentation for the Primary Meteorological Station, H.J. Andrews Experimental Forest, 1972 to 1984. USDA Forest Service, Pacific Northwest Research Station, Portland, OR.

Black, A.T., Chen, J.M., Lee, X., Sagar, R.M., 1991. Characteristics of shortwave and longwave irradiances under a Douglas-fir forest stand. *Canadian Journal of Forest Research*, 21, 1020-1028.

Bolstad, P.V., Swift, L., Collins, F., Regniere, J., 1998. Measured and predicted air temperatures at basin to regional scales in the southern Appalachian mountains. *Agricultural and Forest Meteorology*, 91, 161-176.

Bootsma, A., 1976. Estimating minimum temperature and climatological freeze risk in hilly terrain. *Agricultural Meteorology*, 16, 425-443.

Boyer, D.G., 1984. Estimation of daily temperature means using elevation and latitude in mountainous terrain. *Water Resources Bulletin*, 20(4), 583-588.

Bristow, K.L, Campbell, G.S., 1984. On the relationship between incoming solar radiation and daily maximum and minimum temperature. *Agricultural and Forest Meteorology*, 31, 159-166.

Geiger, R., 1965. *The Climate Near the Ground*. Harvard University, Cambridge, MA.

Bristow, K.L., Campbell, G.S., 1985. An equation for separating daily solar irradiation into direct and diffuse components. *Agricultural and Forest Meteorology*, 35, 123-131.

Brokofske, K.D., Chen, J., Naiman, R.J., Franklin, J.F., 1997. Harvesting effects on microclimatic gradients from small streams to uplands in western Washington. *Ecological Applications*, 7(4), 1188-1200.

Cadenasso, M.L., Traynor, M.M., Pickett, S.T.A., 1997. Functional location of forest edges: gradients of multiple physical factors. *Canadian Journal of Forest Research*, 27, 774-782.

Caissie, D., El-Jabi, N., Satish, M.G., 2001. Modeling of maximum daily water temperatures in a small stream using air temperatures. *Journal of Hydrology*, 251, 14-28.

Carlson, D.W., Groot, A., 1997. Microclimate of clear-cut, forest interior, and small openings in trembling aspen forest. *Agricultural and Forest Meteorology*, 87, 313-329.

Chan, S.S., McCreight, R.W., Walstad, J.D., Spies, T.A., 1986. Evaluating forest vegetative cover with computerized analysis of fisheye photographs. *Forest Science*, 32(4), 1085-1091.

Chen, J., Franklin, J.F., 1990. Microclimate pattern and basic biological responses at the clearcut edges of old-growth Douglas-fir stands. *The Northwest Environmental Journal*, 6, 424-425.

Chen, J., Franklin, J.F., Spies, T.A., 1993. An empirical model for predicting diurnal air-temperature gradients from edge into old-growth Douglas-fir forest. *Ecological Modelling*, 67, 179-198.

Chen, J., Franklin, J.F., Spies, T.A., 1995. Growing season microclimate gradients from clearcut edges into old-growth Douglas-fir forests. *Ecological Applications*, 5(1), 74-86.

Coulter, R.L., Martin, T.J., Porch, W.M., 1991. A comparison of nocturnal drainage flow in three tributaries. *Journal of Applied Meteorology*, 30, 157-169.

Daly, C., 2002. Personal communication. Director, Spatial Climate Analysis Service, Corvallis, OR.

Daly, C., Neilson, R.P., Phillips, D.L., 1994. A statistical-topographic model for mapping climatological precipitation over mountainous terrain. *Journal of Applied Meteorology*, 33, 140-158.

Daly, C., 1996. Precipitation study of HJA 1994-1995, letter to D. Henshaw.

Daly, C., Taylor, G., Gibson, W., 1997. The PRISM approach to mapping precipitation and temperature. 10<sup>th</sup> Conference on Applied Climatology, American Meteorological Society, 20-23 October, Reno NV, 10-12.

Daly, C., Johnson, G.L., 1999. PRISM spatial climate layers: their development and use. Short Course on Topics in Applied Climatology, 79<sup>th</sup> Annual Meeting of the American Meteorological Society, 10-15 January, Dallas, TX.

Daly, C., Taylor, G.H., Gibson, W.P., Parzybok, T.W., Johnson, G.L., Pasteris, P.A., 2000. High-quality spatial climate data sets for the United States and beyond. *American Society of Agricultural Engineers*, 43(6), 1957-1962.

Daly, C., Gibson, W.P., Taylor, G.H., 2002. A knowledge-based approach to the statistical mapping of climate. *Climate Research*, in press.

DeGaetano, A.T., Eggleston, K.L., Knapp, W.W., 1995. A method to estimate missing daily maximum and minimum temperature Observations. *Journal of Applied Meteorology*, 34, 371-380.

Delta-T Devices Ltd, HemiView Canopy Analysis Software, Version 2.1, 1999.

Dodson, R., Marks, D., 1995. Interpolating air temperature over large mountainous regions at high spatial and temporal resolution. US Environmental Protection Agency, National Health and Environmental Effects Research Laboratory, Corvallis, OR.

Dong, J., Chen, J., Brosofske, K.D., Naiman, R.J., 1998. Modelling air temperature gradients across managed small streams in western Washington. *Journal of Environmental Management*, 53, 309-321.

Dozier, J., Frew, J., 1990. Rapid calculation of terrain parameters for radiation modeling from digital elevation data. *IEEE Transactions on Geoscience and Remote Sensing*, 28(5), 963-969.

Dubayah, R.C., Dozier, J., Davis, F.W., 1990. Topographic distribution of clear-sky radiation over the Konza prairie, Kansas. *Water Resources Research*, 26(4), 679-690.

Dubayah, R.C., 1994. Modeling a solar radiation topoclimatology for the Rio Grande Basin. *Journal of Vegetation Science*, 5, 627-640.

Dyrness, C.T., 1973. Early stages of plant succession following logging and burning in the western Cascades of Oregon. *Ecology*, 54(1), 57-69.

Easter, M.J., Spies, T.A., 1994. Using hemispherical photography for estimating photosynthetic photon flux density under canopies and in gaps in Douglas-fir forests of the Pacific Northwest. *Canadian Journal of Forest Research*, 24, 2050-2058.

Environmental Systems Research Institute (ESRI), Inc., ArcView GIS Software, Version 3.2a, 2000.

Garen, D.C., Marks, D., 2001. Spatial fields of meteorological input data including forest canopy corrections for an energy budget snow simulation model. *Soil-Vegetation-Atmosphere Transfer Schemes and Large-Scale Hydrological Models*, Proceedings of Sixth IAHS Scientific Assembly, July 2001, Maastricht, The Netherlands.

Glassy, J.M., Running, S.W., 1994. Validating diurnal climatology logic of the MT-CLIM model across a climatic gradient in Oregon. *Ecological Applications*, 4(2), 248-257.

Goodale, C.L., Aber, J.D., Ollinger, S.V., 1998. Mapping monthly precipitation, temperature, and solar radiation for Ireland with polynomial regression and a digital elevation model. *Climate Research*, 10, 35-49.

Greenland, D., 1994a. Potential radiation maps of the H.J. Andrews Experimental Forest. USDA Forest Service, Pacific Northwest Research Station, Portland, OR.

Greenland, D., 1994b. The Pacific northwest regional context of the climate of the H.J. Andrews Experimental Forest. *Northwest Science*, 69(2), 81-96.

Gustavsson, T., Karlsson, M., Bogren, J., Lindkvist, S., 1998. Development of temperature patterns during clear nights. *Journal of Applied Meteorology*, 37, 559-571.

Hawk, G.M., Franklin, J.F., McKee, W.A., Brown, R.B., 1978. H.J. Andrews Experimental Forest Reference Stand System: Establishment and Use History. Seattle, University of Washington.

Henshaw, D., 2002. Personal communication. USDA Forest Service Statistician and Information Manager, Corvallis, OR.

H. J. Andrews Long-Term Ecological Research Website, <http://www.fsl.orst.edu/lter/> , 2002.

Hocevar, A., Martsolf, J.D., 1971. Temperature distribution under radiation frost conditions in a central Pennsylvania valley. *Agricultural Meteorology*, 8, 371-383.

Holbo, H.R., Childs, S.W., 1987. Summertime radiation balances of clearcut and shelterwood slopes in southwest Oregon. *Forest Science*, 33(2), 504-516.

Jarvis, C.H., Stuart, N., 2001a. A comparison among strategies for interpolating maximum and minimum daily air temperatures. Part I: The selection of "guiding" topographic and land cover variables. *Journal of Applied Meteorology*, 40, 1060-1074.

Jarvis, C.H., Stuart, N., 2001b. A comparison among strategies for interpolating maximum and minimum daily air temperatures. Part II: The interaction between number of guiding variables and the type of interpolation method. *Journal of Applied Meteorology*, 40, 1075-1084.

Jones, J., Grant, G., 1996. Peak flow responses to clear-cutting and roads in small and large basins, western Cascades, Oregon. *Water Resources Research*, 32(4), 959-974.

Karlsson, I.M., 2000. Nocturnal air temperature variations between forest and open areas. *Journal of Applied Meteorology*, 39, 851-862.

Laughlin, G.P., 1982. Minimum temperature and lapse rate in complex terrain: influencing factors and prediction. *Archives for Meteorology, Geophysics, and Bioclimatology*, 30, 141-152.

Lee, R., 1978. *Forest Microclimatology*. New York, Columbia University Press.

Lindkvist, L., Gustavsson, T., Bogren, J., 2000. A frost assessment method for mountainous areas. *Agricultural and Forest Meteorology*, 102, 51-67.

Link, T., Marks, D., 1999. Distributed simulation of snowcover mass- and energy-balance in the boreal forest. *Hydrological Processes*, 13, 2439-2452.

Malcolm, J.R., 1998. A model of conductive heat flow in forest edges and fragmented landscapes. *Climate Change*, 39, 487-502.

McCutchan, M.H. and Fox, D.G., 1997. Effect of elevation and aspect on wind, temperature and humidity. *Journal of Climate and Applied Meteorology*, 25, 1996-2013.

Miller, D.R., Bergen, J.D., Neuroth, G., 1983. Cold air drainage in a narrow forested valley. *Forest Science*, 29(2), 357-370.

Mohseni, O., Stefan, H.G., 1999. Stream temperature/air relationship: a physical interpretation. *Journal of Hydrology*, 218, 128-141.

Moreau, J., 2002. Personal communication. H. J. Andrews/LTER Bioscience Research Technician, Blue River, OR.

Morecroft, M.D., Taylor, M.E., Oliver, H.R., 1998. Air and soils microclimates of deciduous woodland compared to an open site. *Agricultural and Forest Meteorology*, 90, 141-156.

Nalder, I.A., Wein, R.W., 1998. Spatial interpolation of climatic normals: test of a new method in the Canadian boreal forest. *Agricultural and Forest Meteorology*, 92, 211-225.

National Climatic Data Center (NCDC)/National Weather Service (NWS) Cooperative Observers Network, 2000.

Oke, T.R., 1987. *Boundary Layer Climates*. New York, Routledge.

Pielke, R.A., Mehring, P., 1977. Use of mesoscale climatology in mountainous terrain to improve the spatial representation of mean monthly temperatures. *Monthly Weather Review*, 105, 108-112.

Raynor, G.S., 1971. Wind and temperature structure in a coniferous forest and a contiguous field. *Forest Science*, 17(3), 351-363.

Richardson, C.W., 1981. Stochastic simulation of daily precipitation, temperature, and solar radiation. *Water Resources Research*, 17(1), 182-190.

Richardson, C.W., 1982. Dependence structure of daily temperature and solar radiation. *Transactions of the American Society of Agricultural Engineers*, 25, 736-739.

Rosentrater, L., 1997. *The Thermal Climate of the H.J. Andrews Experimental Forest, Oregon*. Master's Thesis, University of Oregon, Eugene, OR.

Running, S.W., Nemani, R., 1985. Topographic and microclimate control of simulated photosynthesis and transpiration in coniferous forests. *Establishment and Tending of Subalpine Forest: Research and Management, Proceedings of the 3<sup>rd</sup> IUFRO Ecology of Subalpine Zones Project Group Workshop, September 1984, Riederalp, Switzerland*, 53-60.

- Running, S.W., Nemani, R., 1987. Extrapolation of synoptic meteorological data in mountainous terrain and its use for simulating forest evapotranspiration and photosynthesis. *Canadian Journal of Forest Research*, 17, 472-482.
- Saunders, S.C., Chen, J., Drummer, T.D., Crow, T.R., 1999. Modeling temperature gradients across edges over time in a managed landscape. *Forest Ecology and Management*, 117, 17-31.
- Tabony, R.C., 1983. The estimation of missing climatological data. *Journal of Climatology*, 3, 297-314.
- Tabony, R.C., 1985. Relations between minimum temperature and topography in Great Britain. *Journal of Climatology*, 5, 503-520.
- Taylor, G.H., Hannan, C., 1999. *The Climate of Oregon*. Oregon State University Press, Corvallis, OR.
- Thornton, P.E., Running, S.W., White, M.A., 1997. Generating surfaces of daily meteorological variables over large regions of complex terrain. *Journal of Hydrology*, 190, 214-251.
- Thornton, P.E., Running, S.W., 1999. An improved algorithm for estimating incident daily solar radiation from measurements of temperature, humidity, and precipitation. *Agricultural and Forest Meteorology*, 93, 211-228.
- Thornton, P.E., Hasenauer, H., White, M.A., 2000. Simultaneous estimation of daily solar radiation and humidity from observed temperature and precipitation: an application over complex terrain in Austria. *Agricultural and Forest Meteorology*, 104, 255-271.
- United States Army - Construction Engineering Research Laboratory (USA-CERL), Geographic Resources Analysis Support System (GRASS) GIS Software, Version 4.1, 1992.

United States Department of Agriculture (USDA)/National Resources Conservation Service (NRCS) Snow-Telemetry Network, 2000.

Vales, D.J., Bunnell, F.L., 1988. Relationships between transmission of solar radiation and coniferous forest stand characteristics. *Agricultural and Forest Meteorology*, 43, 201-223.

Waring, R.H., Holbo, H.R., Bueb, R.P., and Fredriksen R.L., 1978. Documentation of Meteorological Data from the Coniferous Biome Primary Station in Oregon. USDA Forest Service, Pacific Northwest Research Station, Portland, OR.

Williams, L.D., Barry, R.G., Andrews, J.T. 1972. Application of computed global radiation for areas of high relief. *Journal of Applied Meteorology*, 11, 526-533.

Xia, Y., Fabian, P., Stohl, A., Winterhalter, M., 1999. Forest climatology: reconstruction of mean climatological data for Bavaria, Germany. *Agricultural and Forest Meteorology*, 96, 117-129.

APPENDICES

APPENDIX A

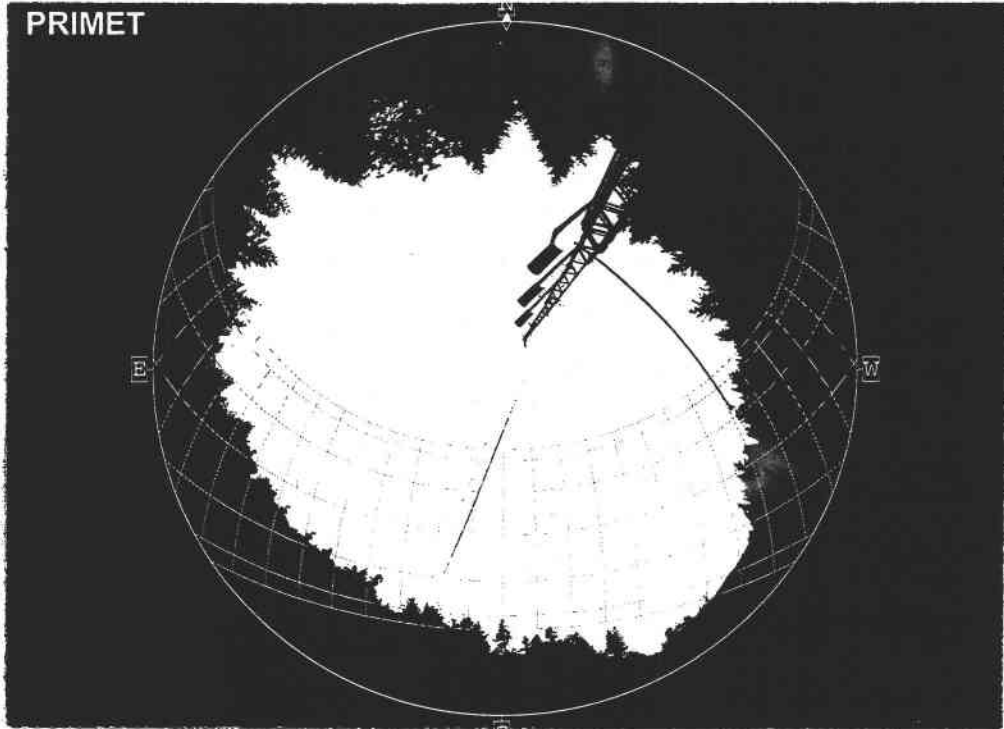
Table A.1. Maximum temperature correlation coefficients between long-term sites.

	RS02	CSCDIA	PRIMET	BKSPGS	CS2MET	RS86	RS04	RS10	RS13	RS12	RS05	RS14	RS89	RS01	RS38	RS07
RS02	1.000	.9947	.9973	.9972	.9915	.9975	.9864	.9978	.9771	.9924	.9966	.9821	.9992	.9956	.9937	.9997
CSCDIA		1.000	.9972	.9987	.9751	.9976	.9812	.9974	.9752	.9812	.9927	.9794	.9928	.9984	.9942	.9944
PRIMET			1.000	.9981	.9838	.9968	.9764	.9957	.9666	.9815	.9909	.9725	.9968	.9966	.9908	.9962
BKSPGS				1.000	.9809	.9984	.9834	.9984	.9770	.9858	.9952	.9815	.9951	.9984	.9943	.9969
CS2MET					1.000	.9810	.9724	.9827	.9578	.9896	.9850	.9643	.9936	.9765	.9748	.9918
RS86						1.000	.9892	.9995	.9832	.9893	.9971	.9869	.9956	.9996	.9983	.9975
RS04							1.000	.9910	.9981	.9942	.9954	.9991	.9817	.9864	.9946	.9881
RS10								1.000	.9853	.9917	.9986	.9889	.9955	.9989	.9981	.9982
RS13									1.000	.9878	.9904	.9995	.9708	.9811	.9908	.9794
RS12										1.000	.9964	.9906	.9909	.9854	.9901	.9941
RS05											1.000	.9934	.9939	.9954	.9972	.9977
RS14												1.000	.9763	.9847	.9933	.9840
RS89													1.000	.9936	.9907	.9990
RS01														1.000	.9976	.9957
RS38															1.000	.9943
RS07																1.000

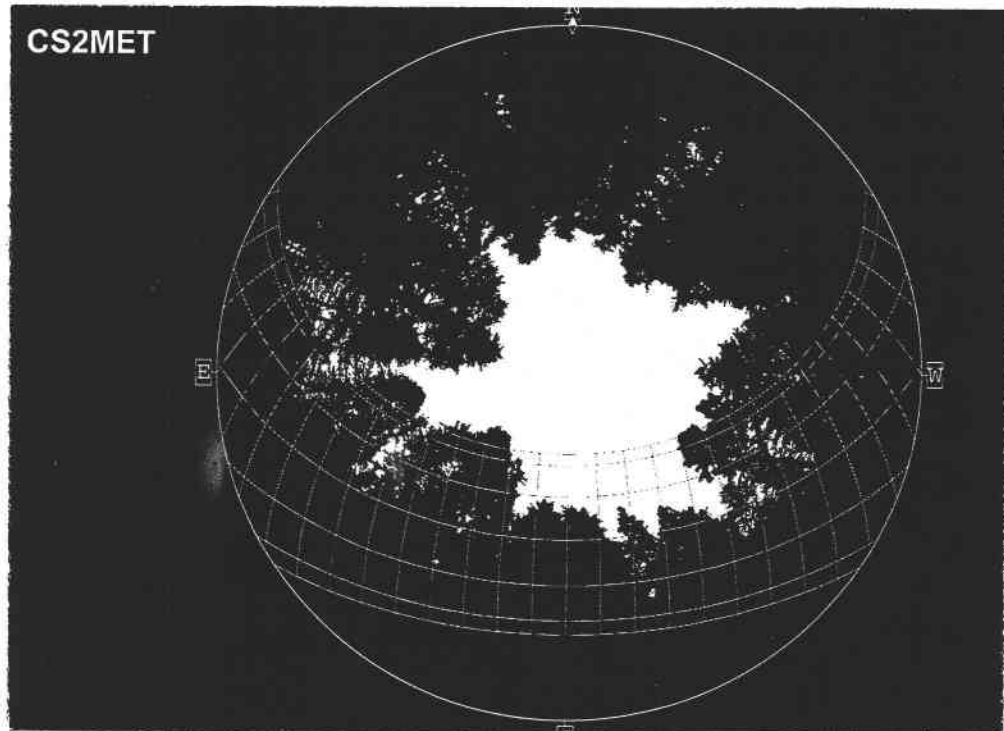
APPENDIX B

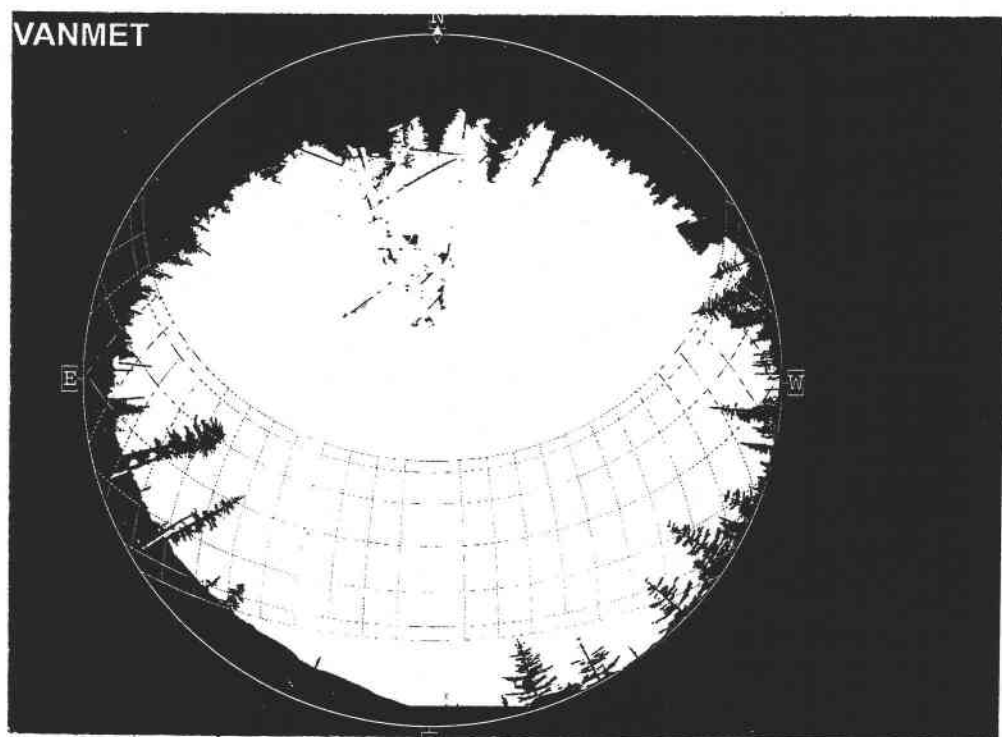
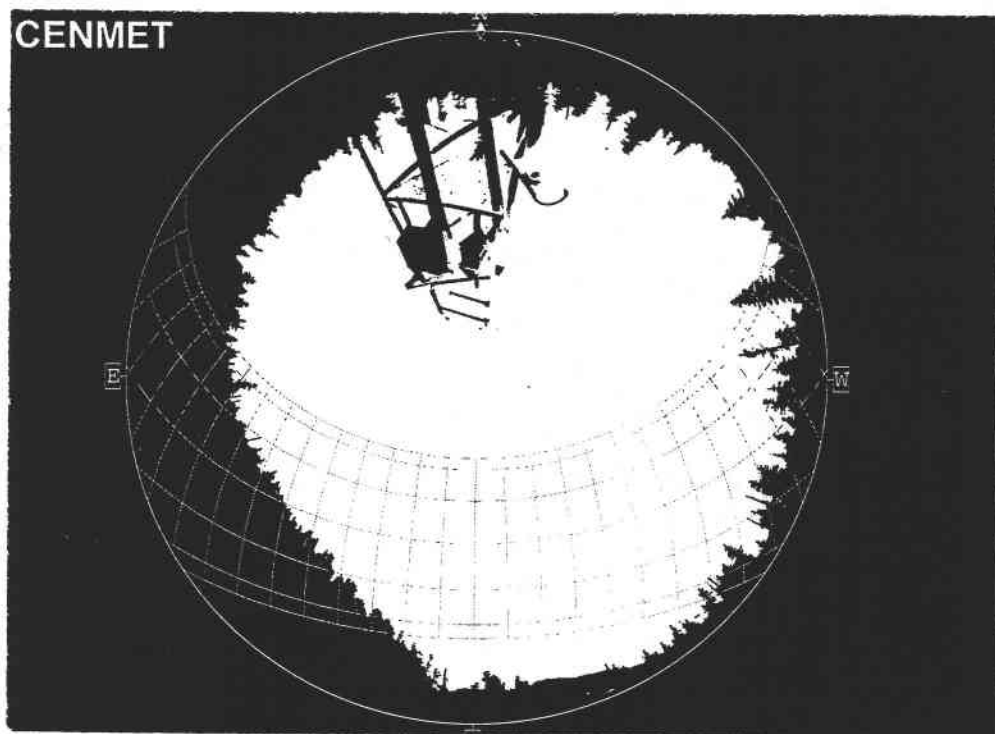
Figure B.1. Processed hemispherical fisheye images with suntracks at each climate station used in the study.

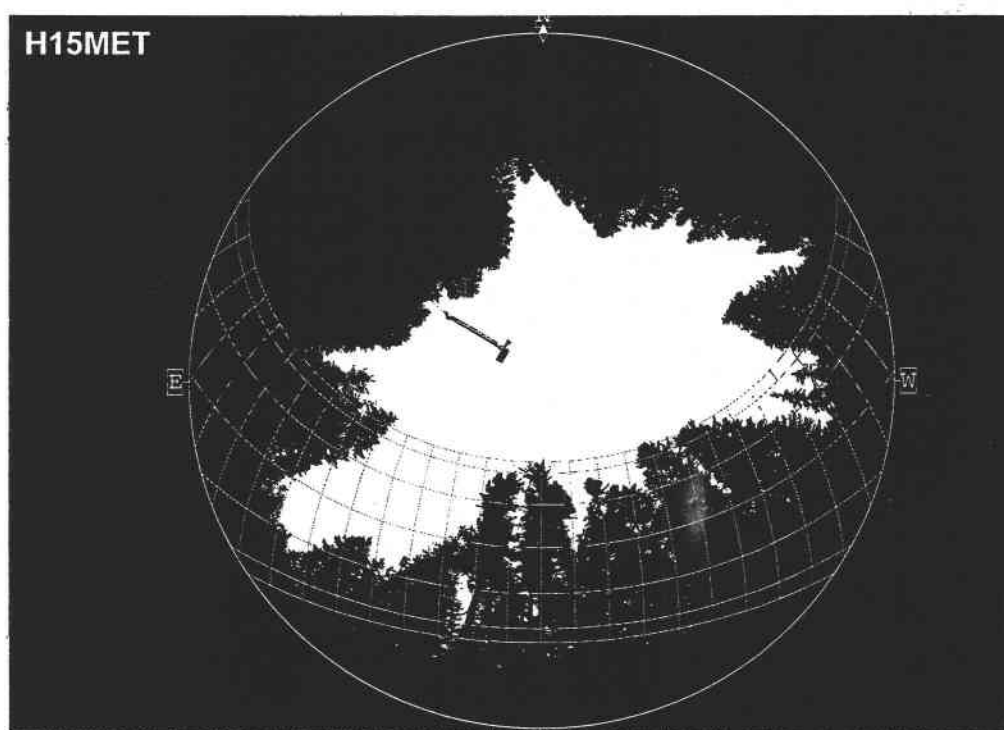
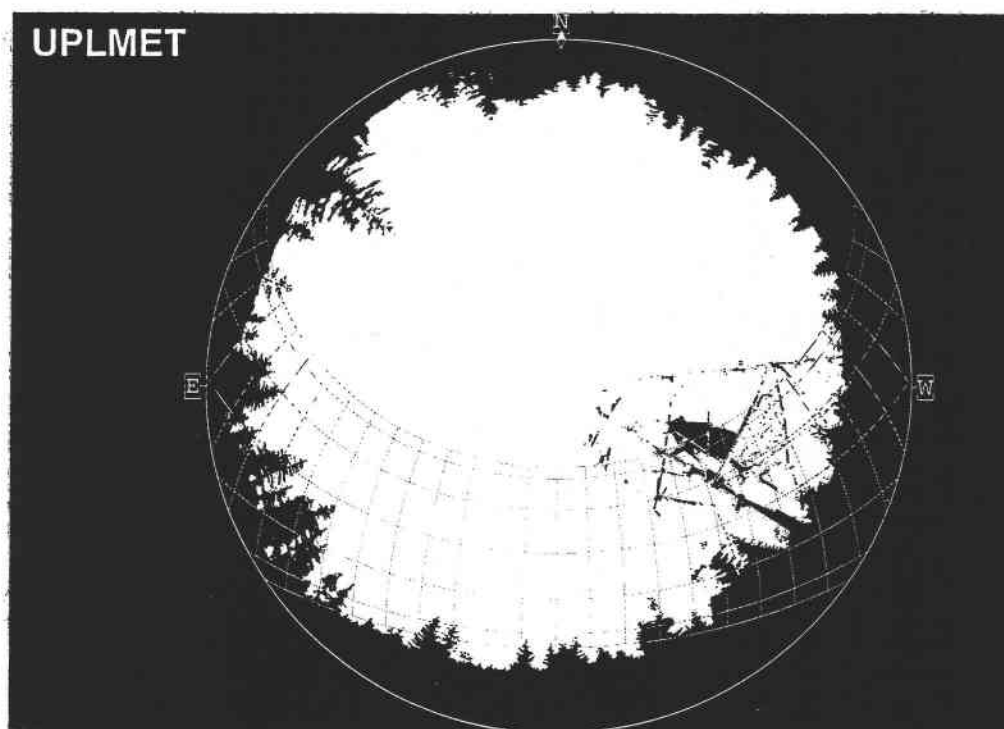
PRIMET

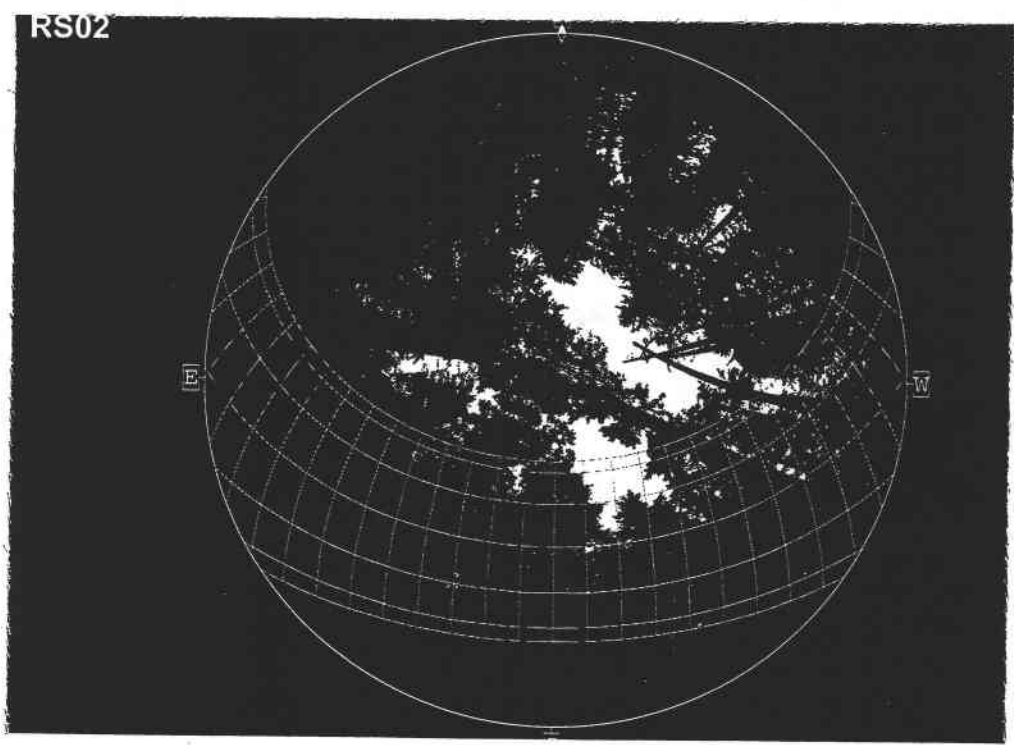
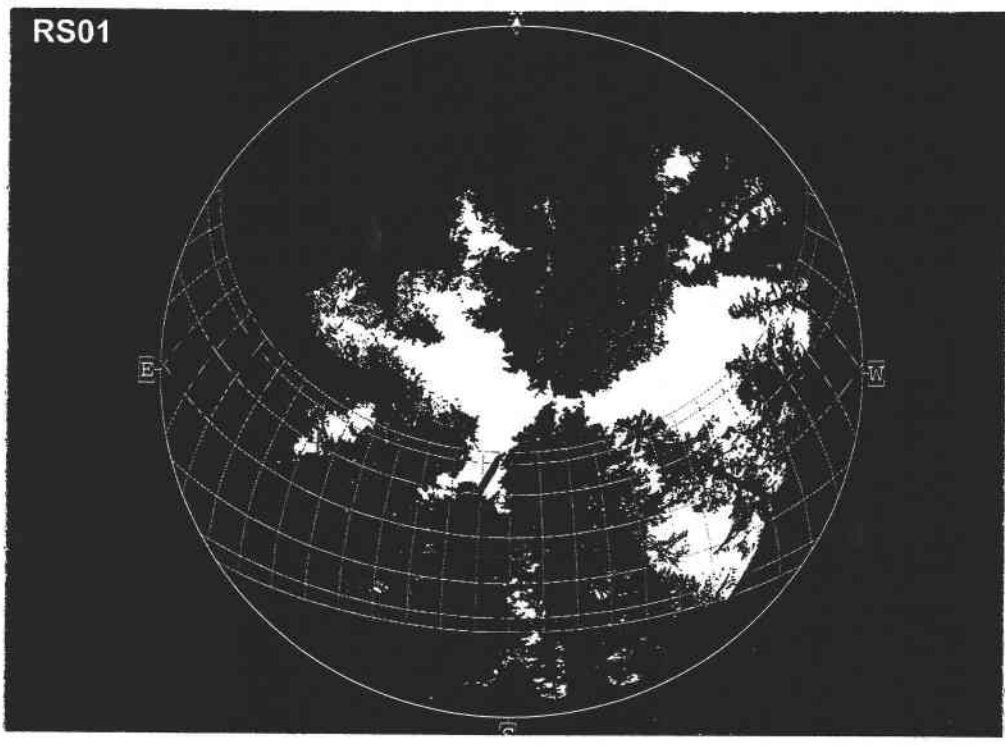


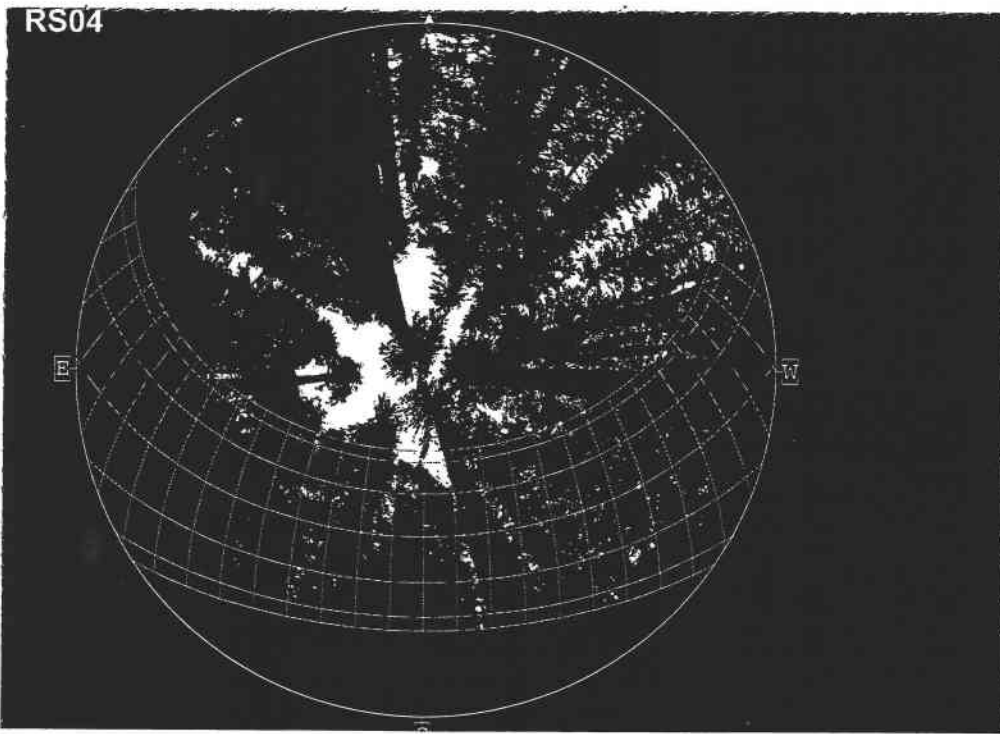
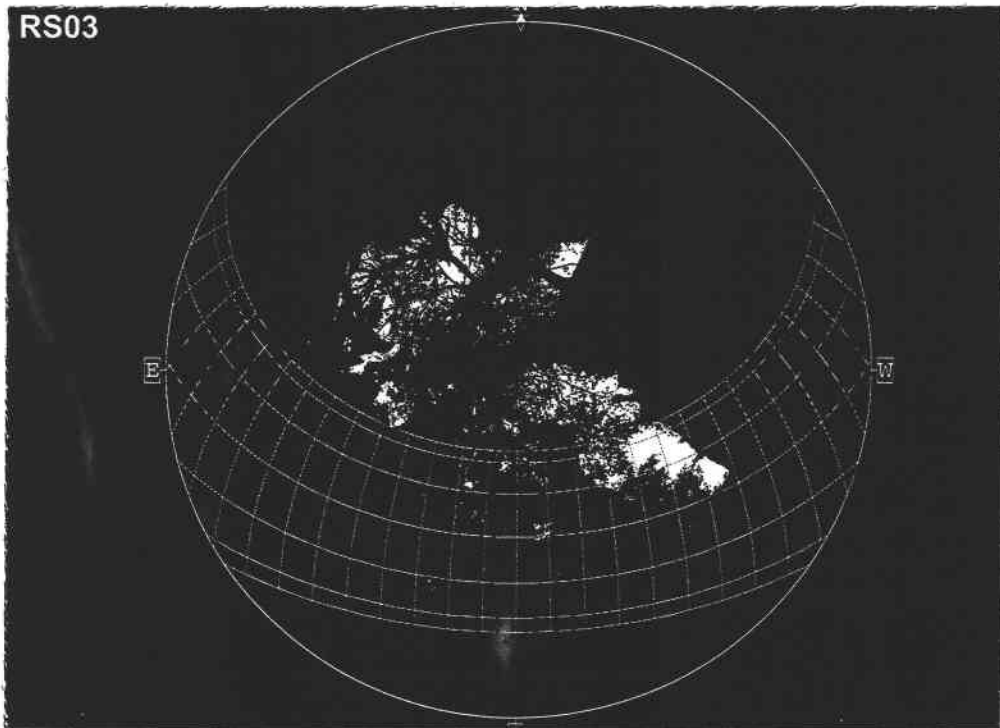
CS2MET

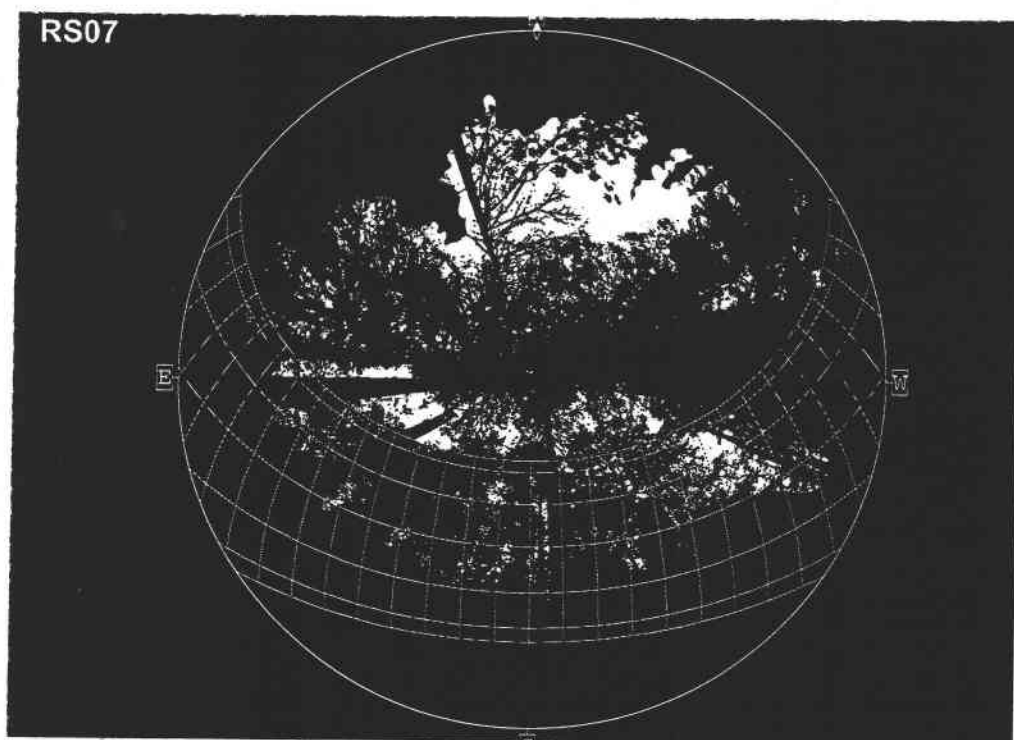
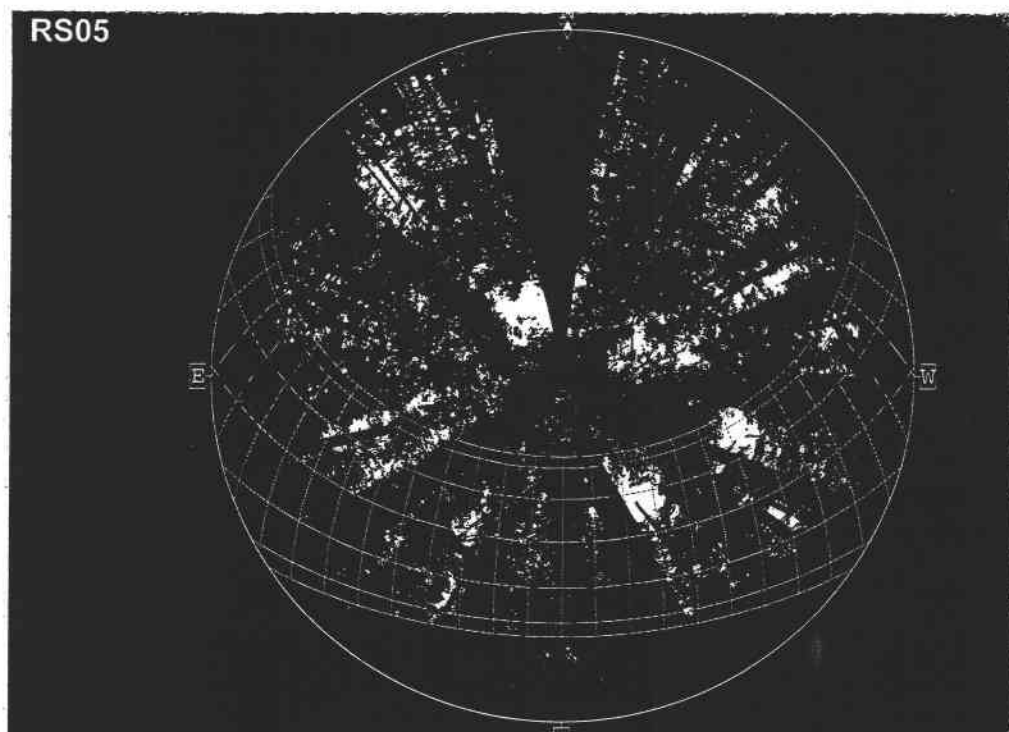


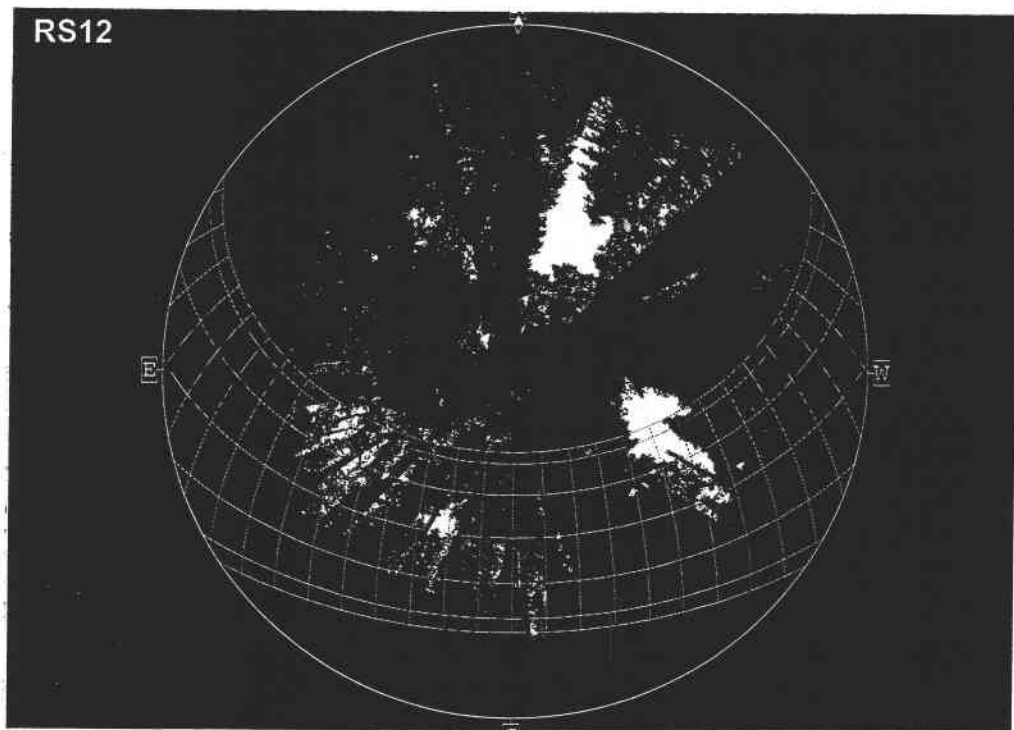
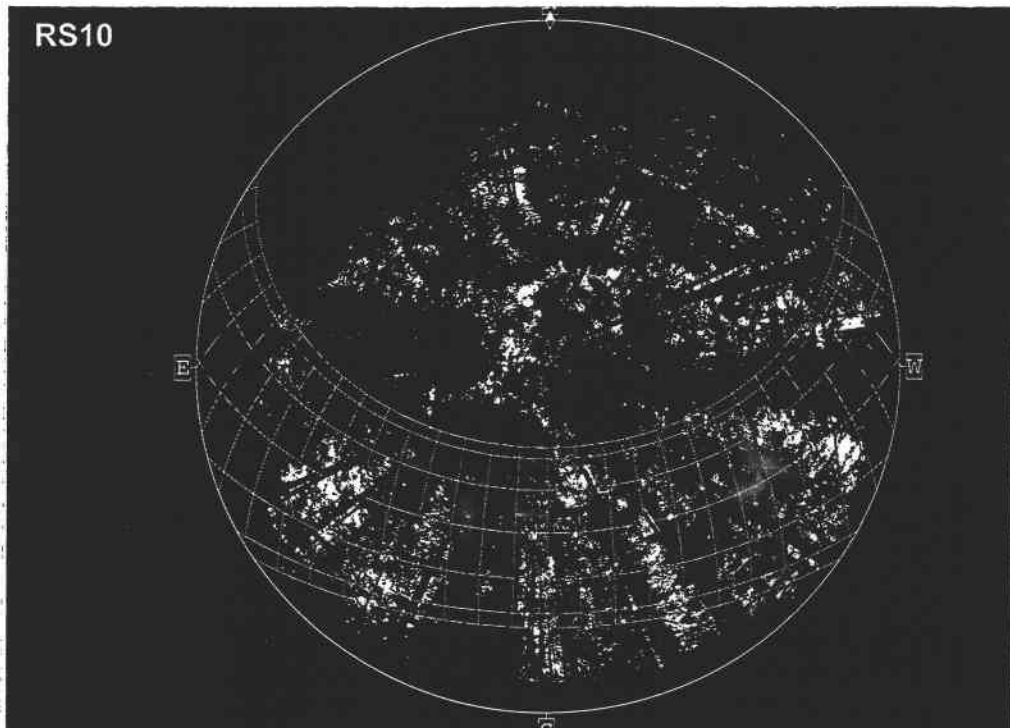


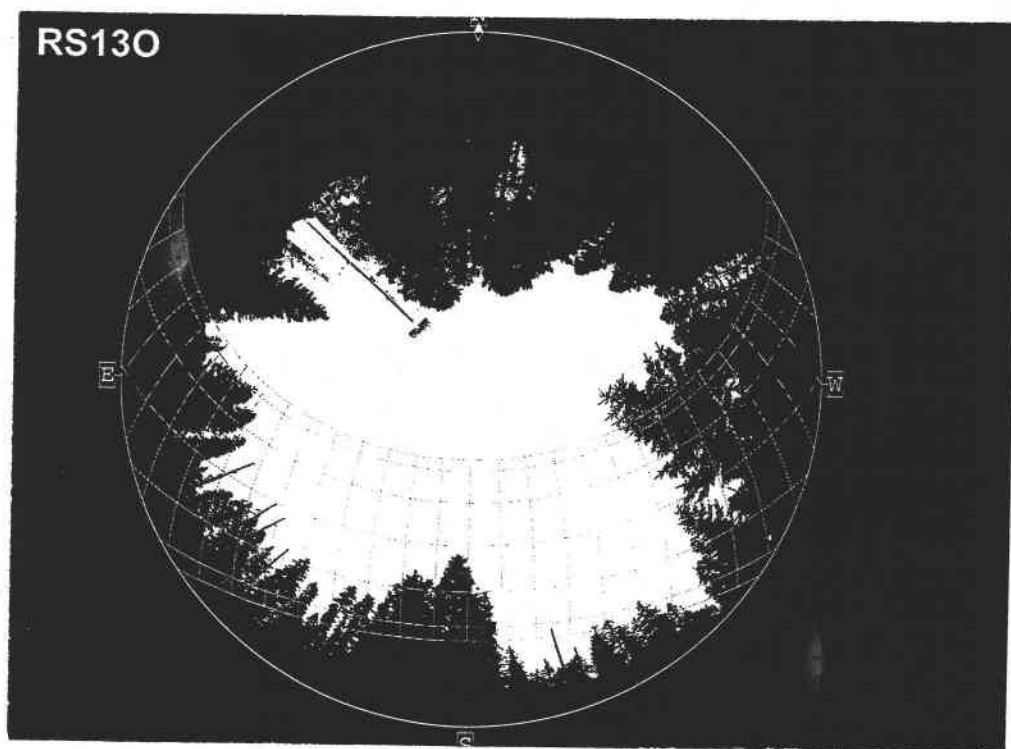
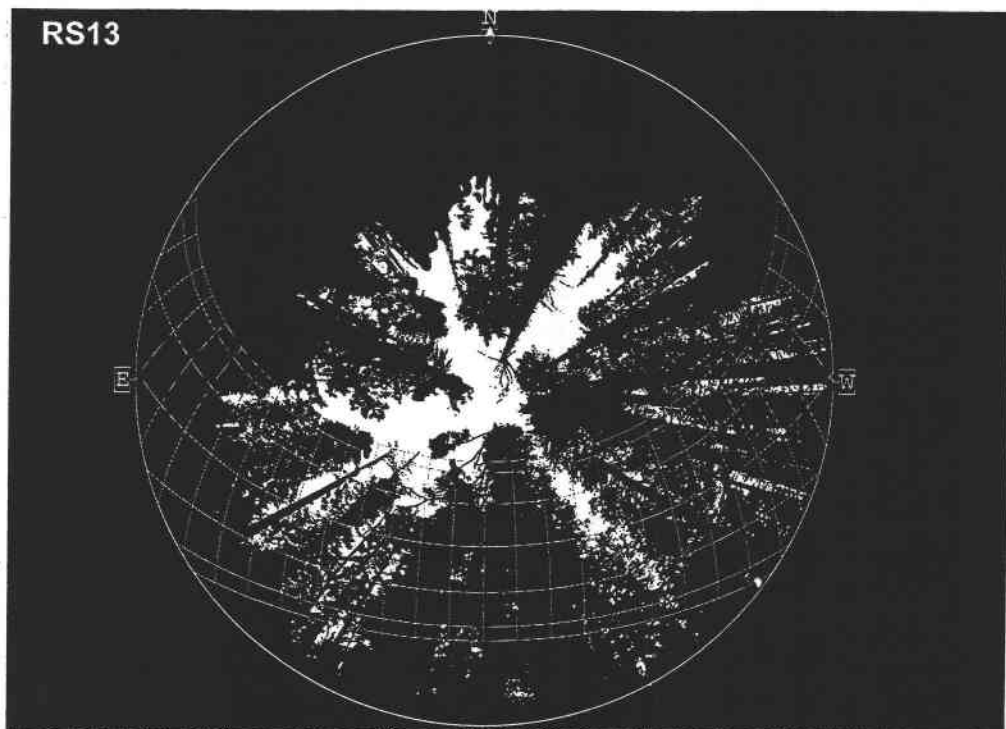


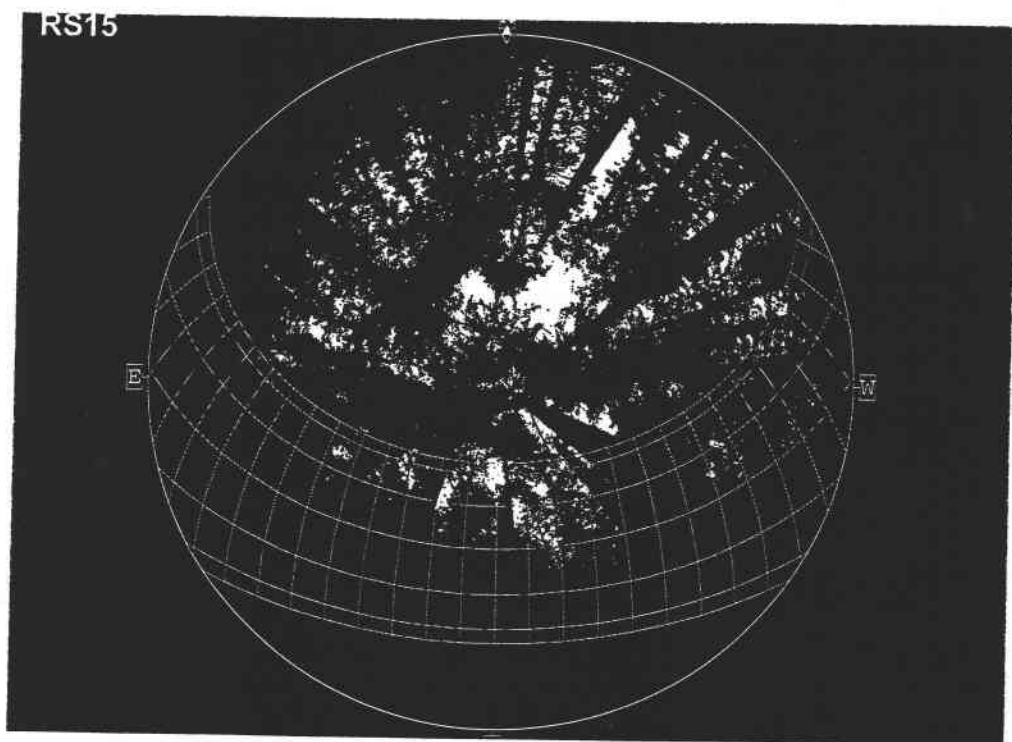
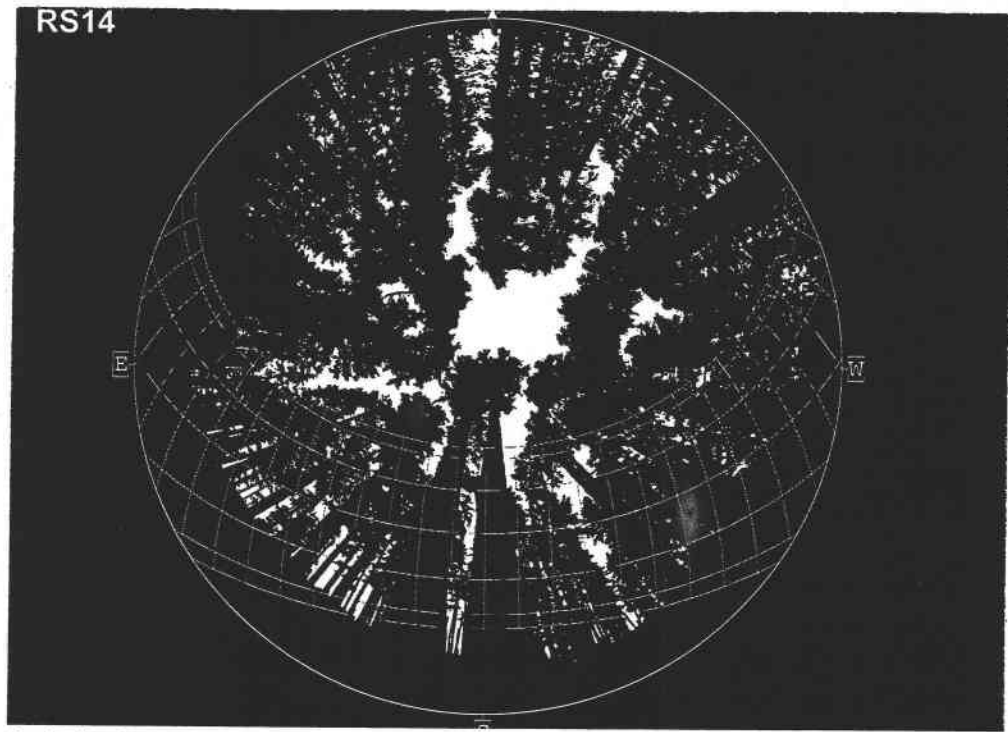


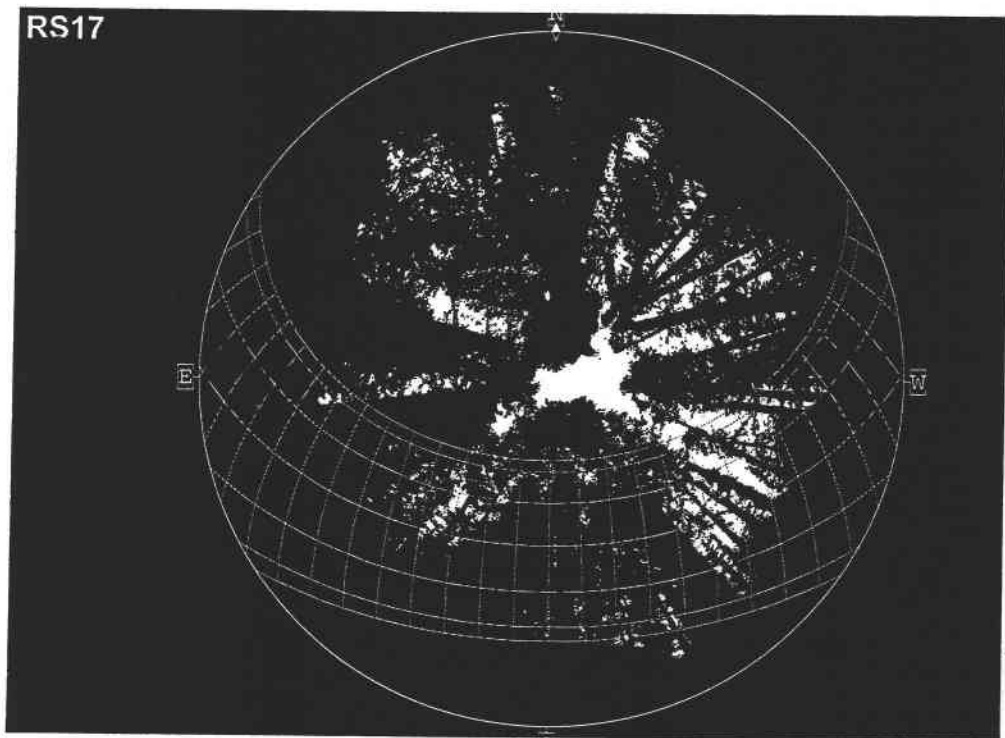
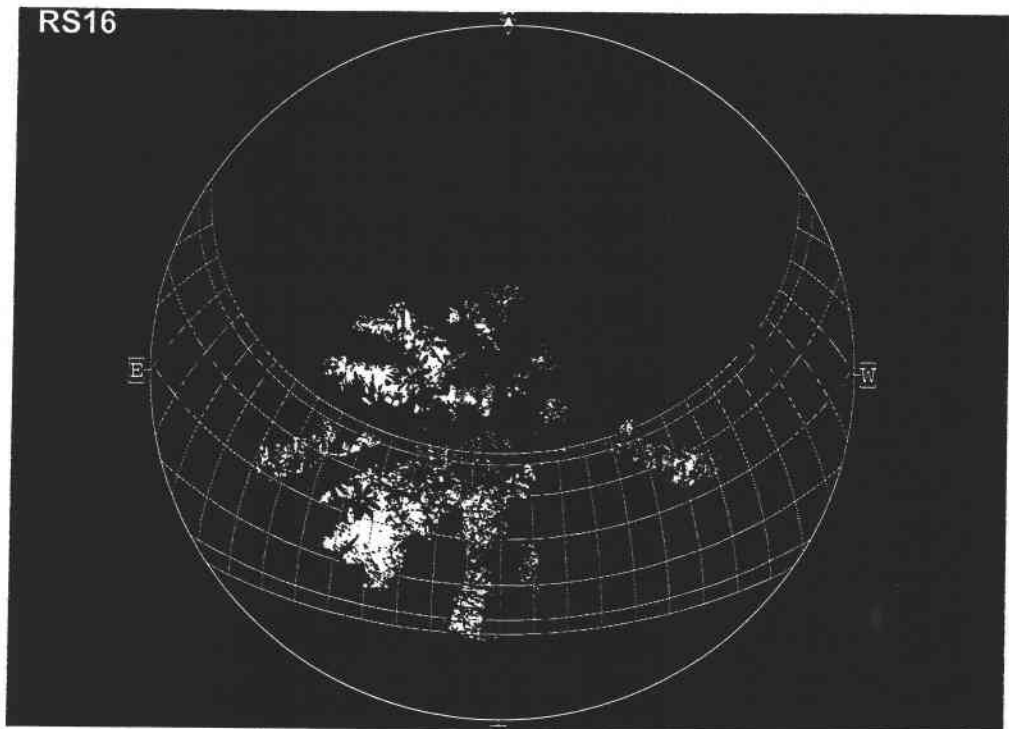


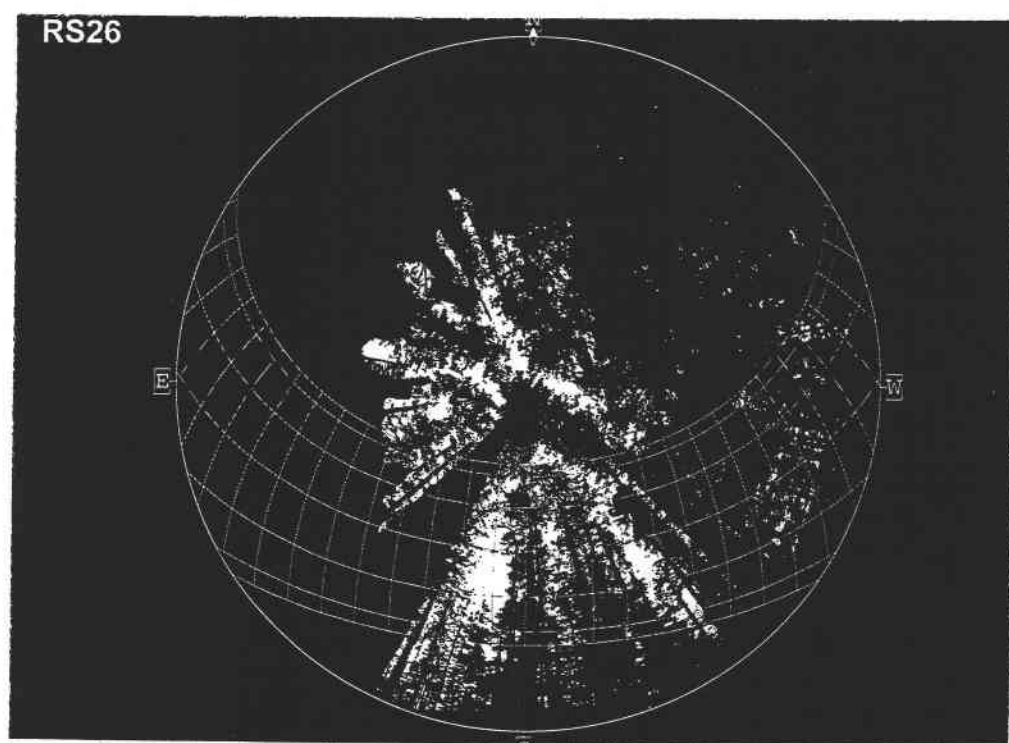
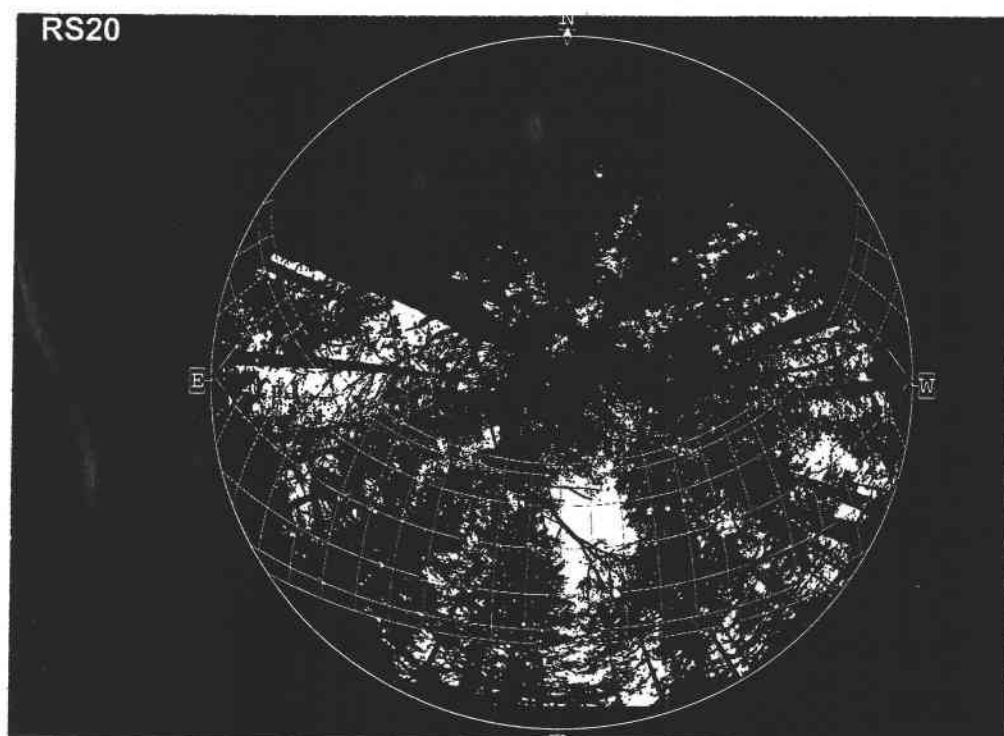


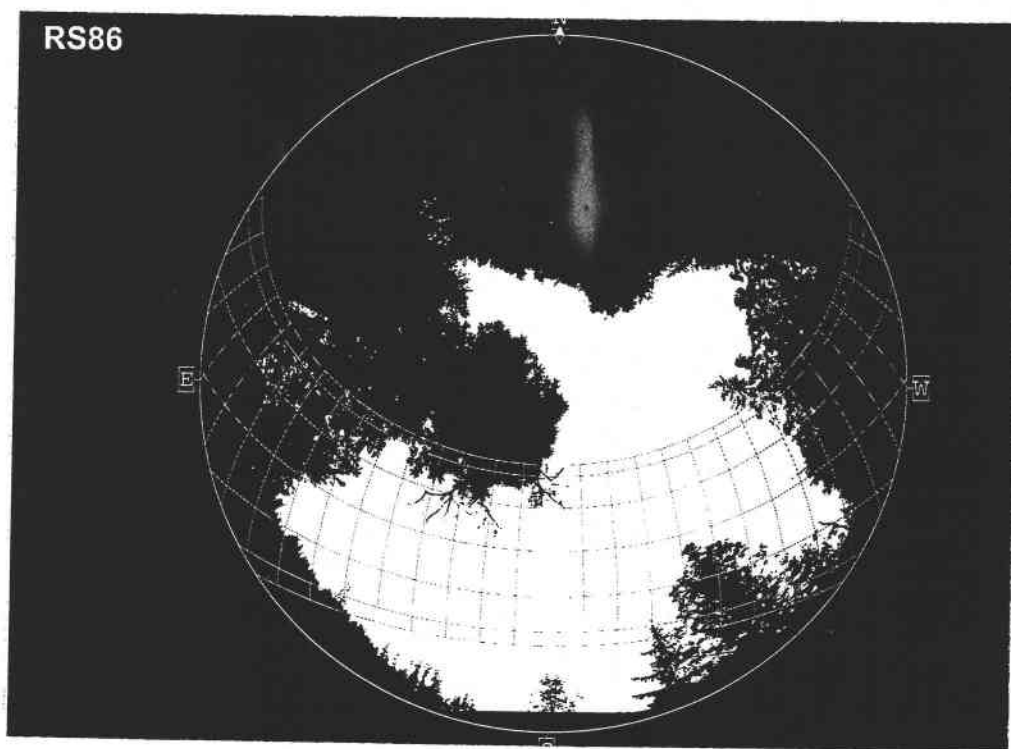
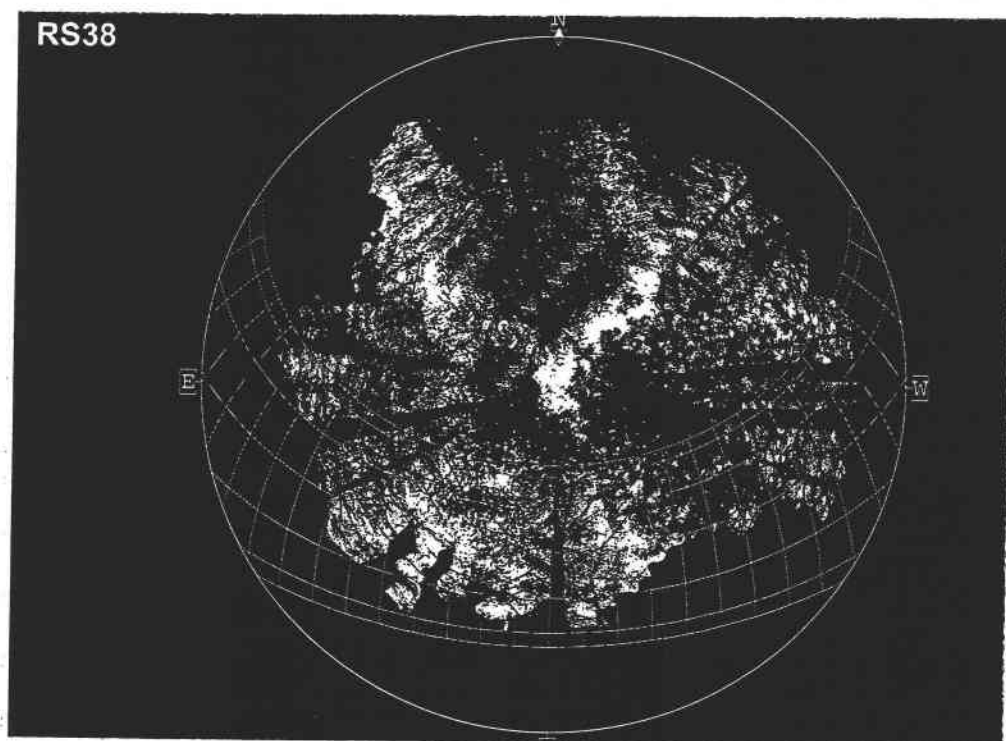


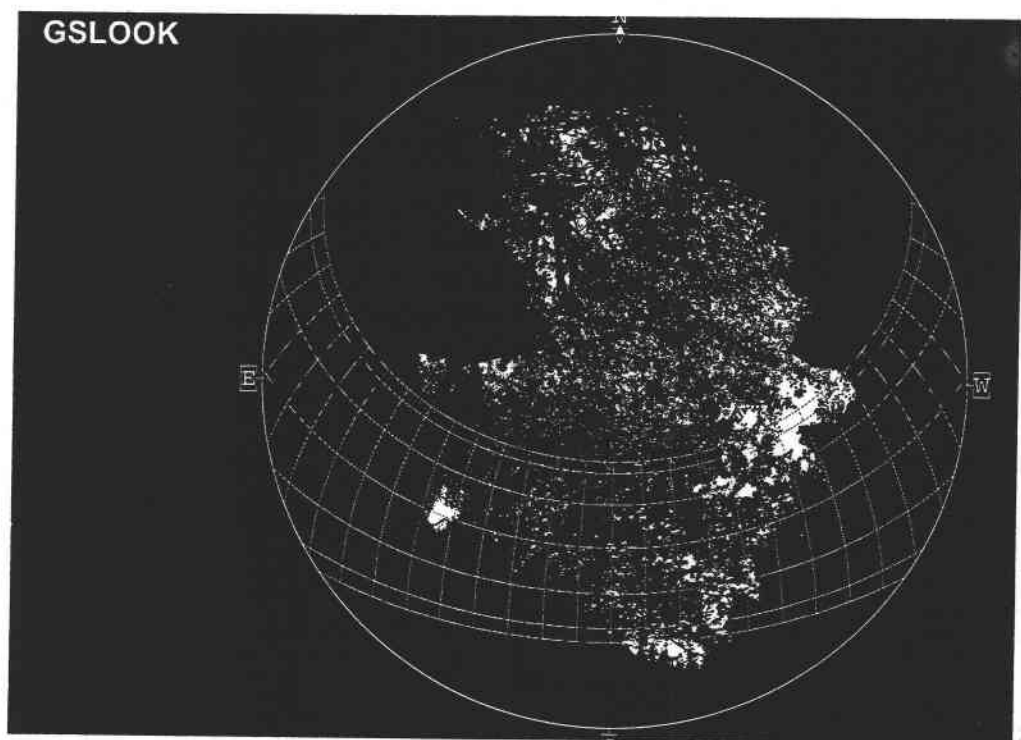
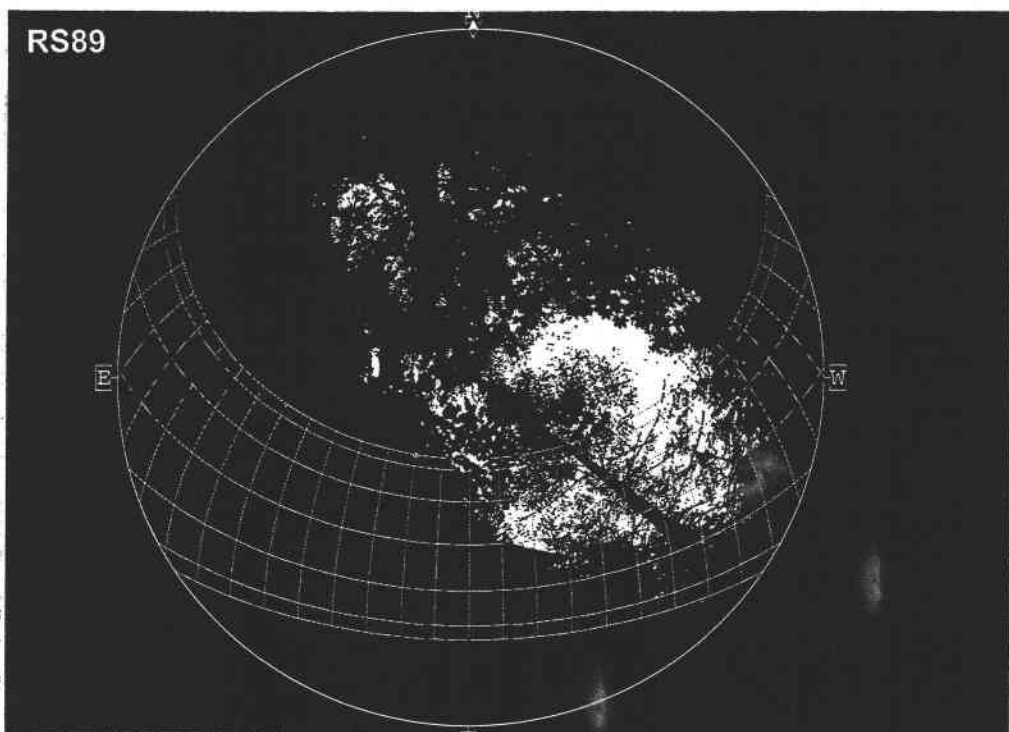


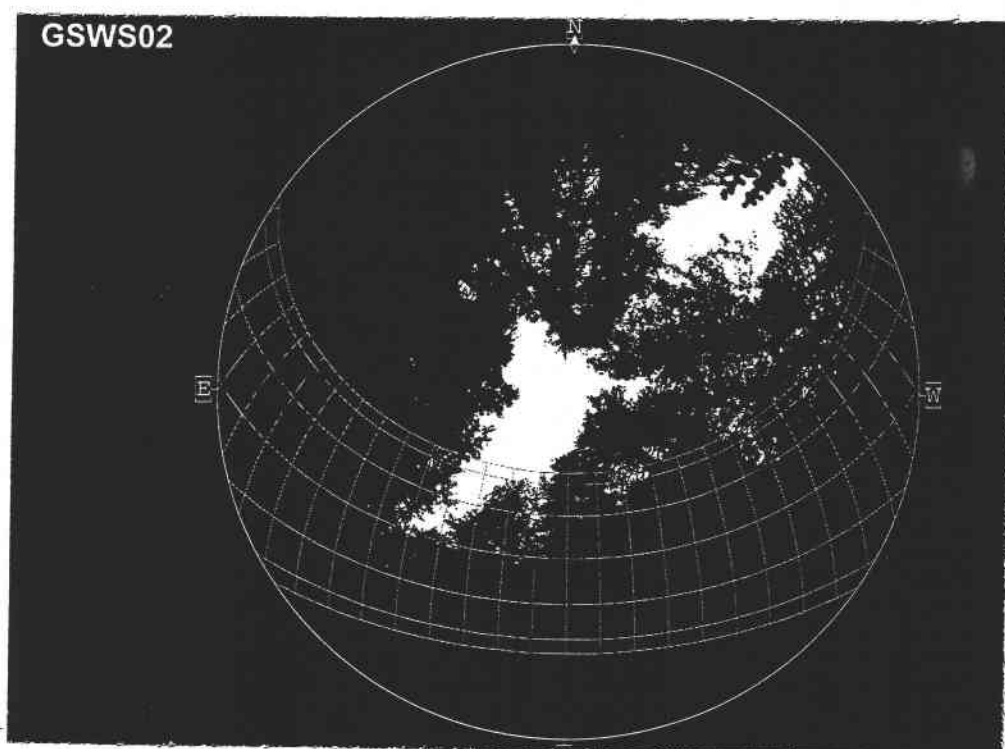
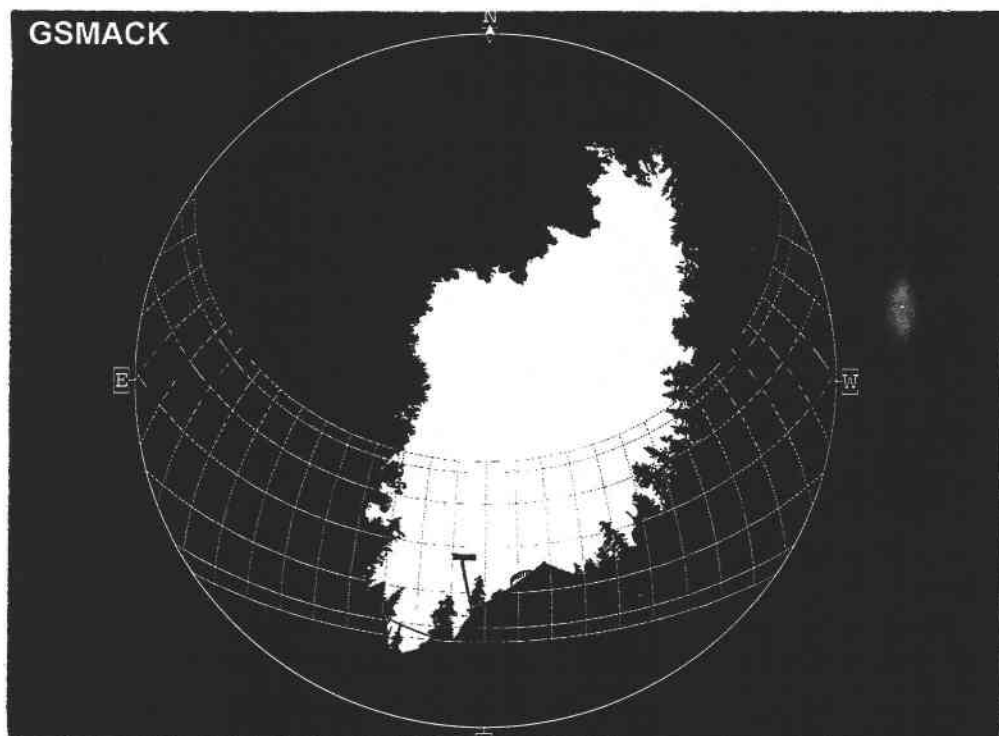


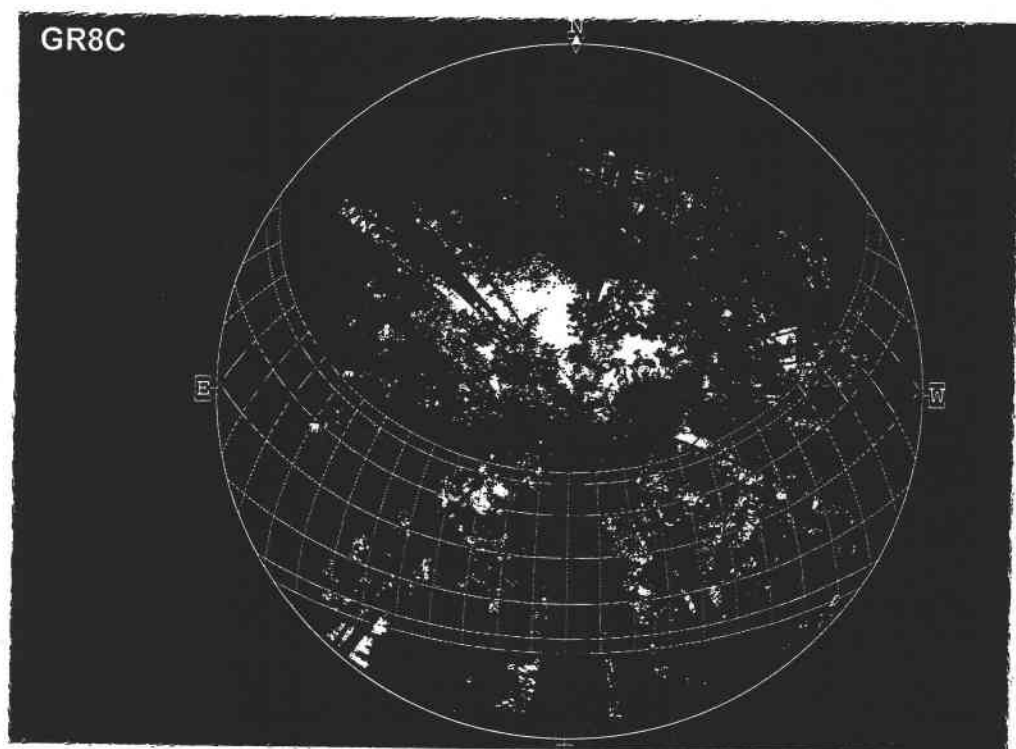
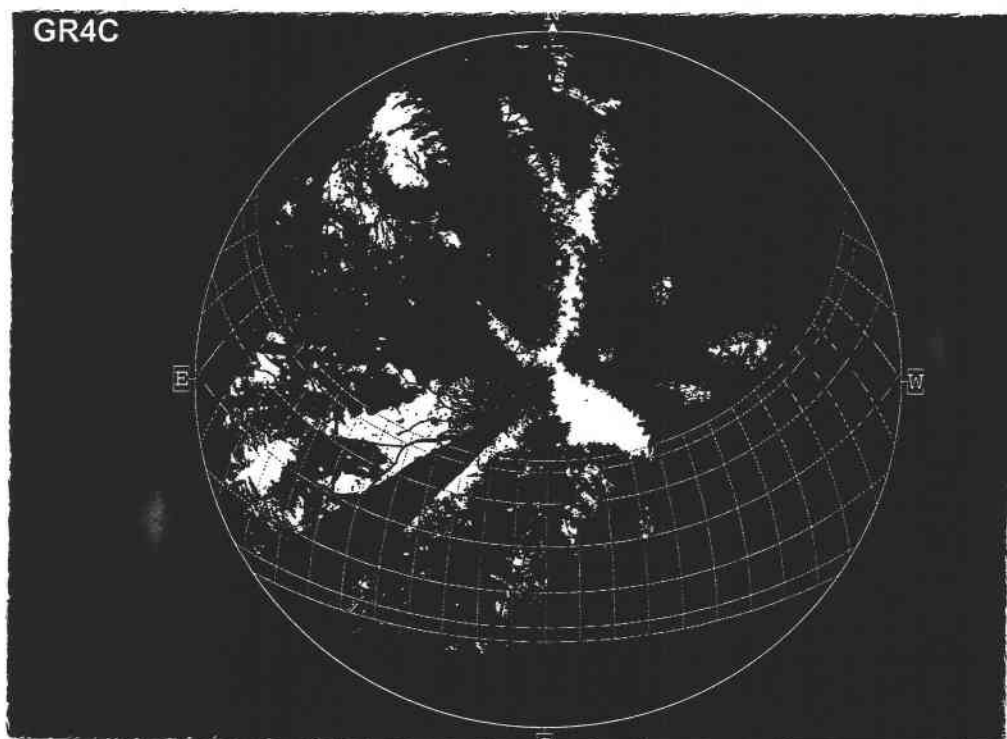


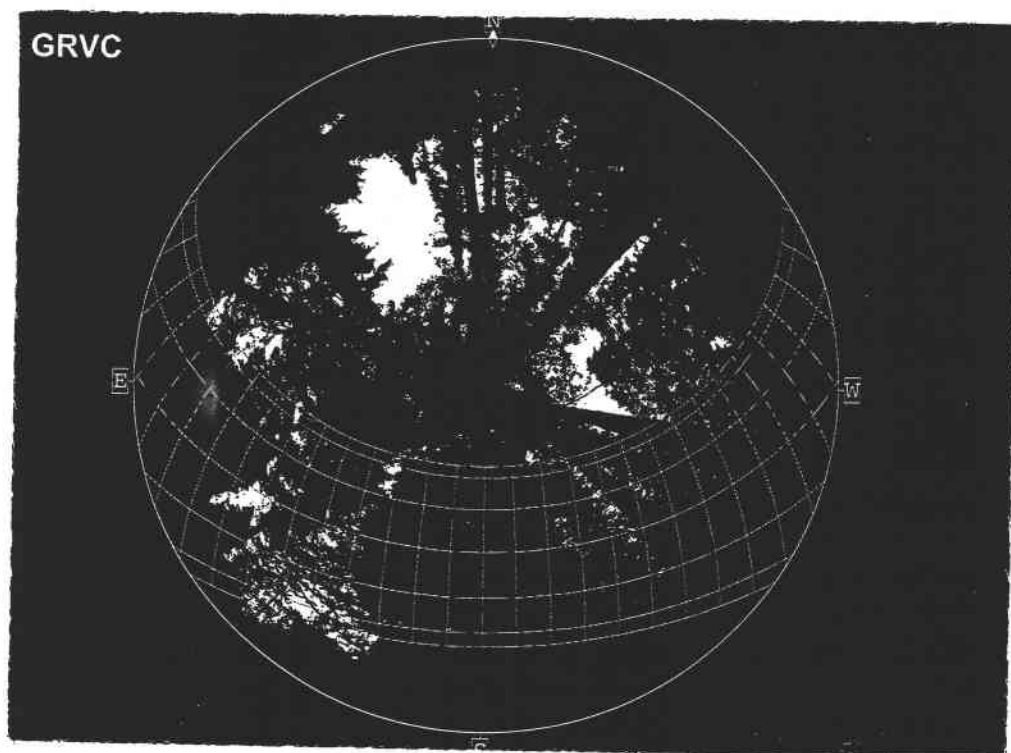
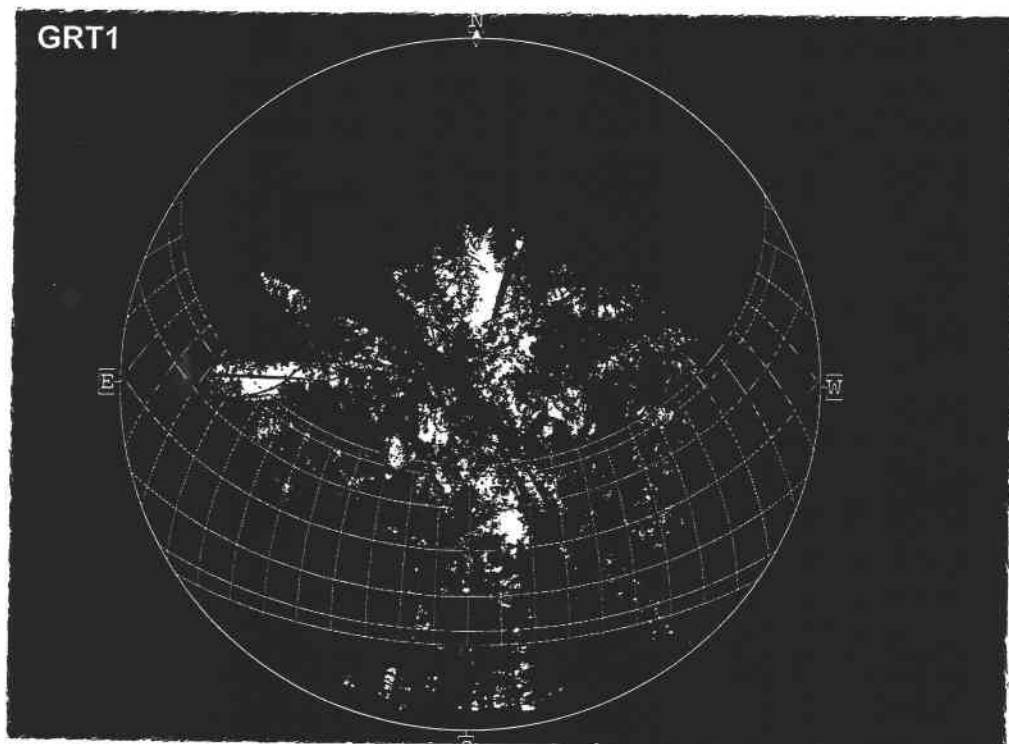


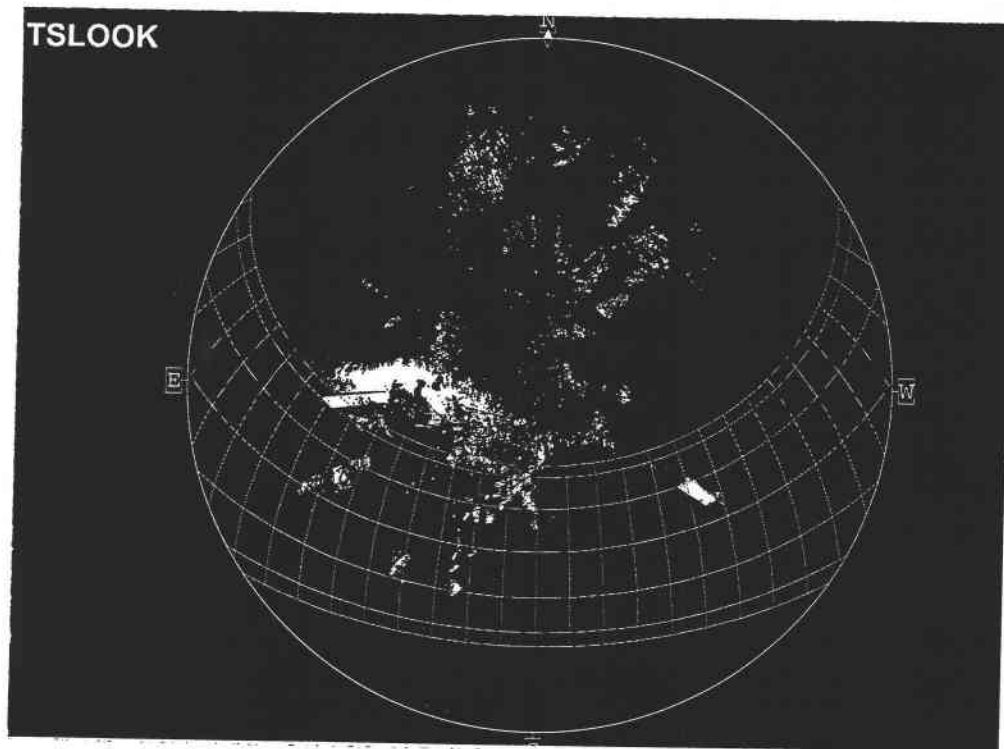
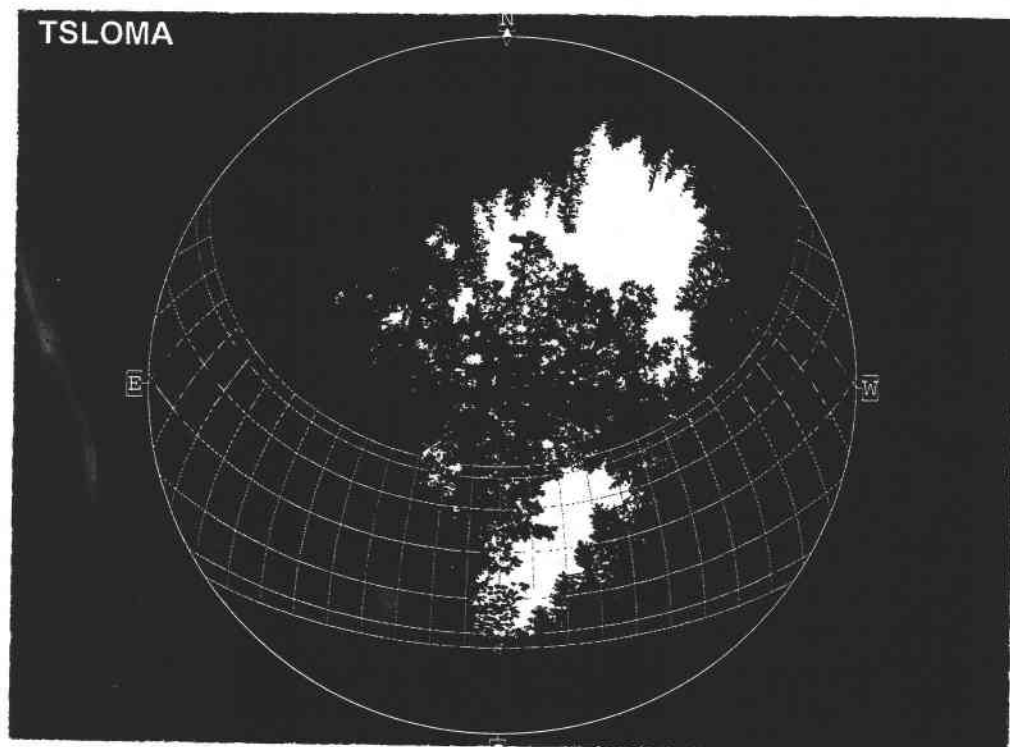


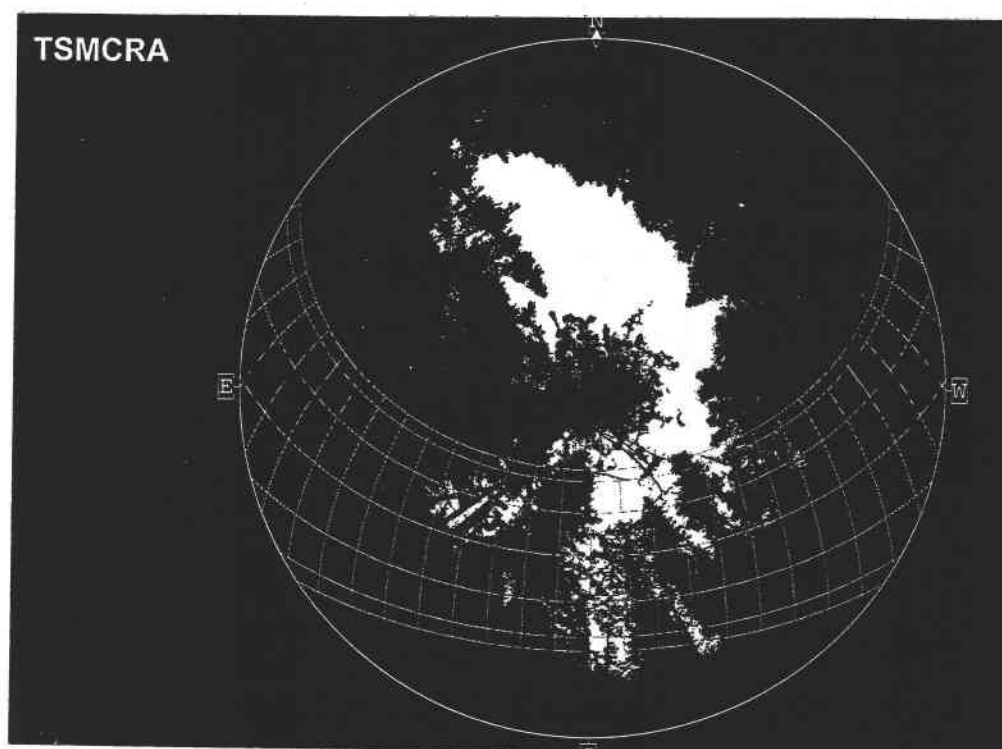
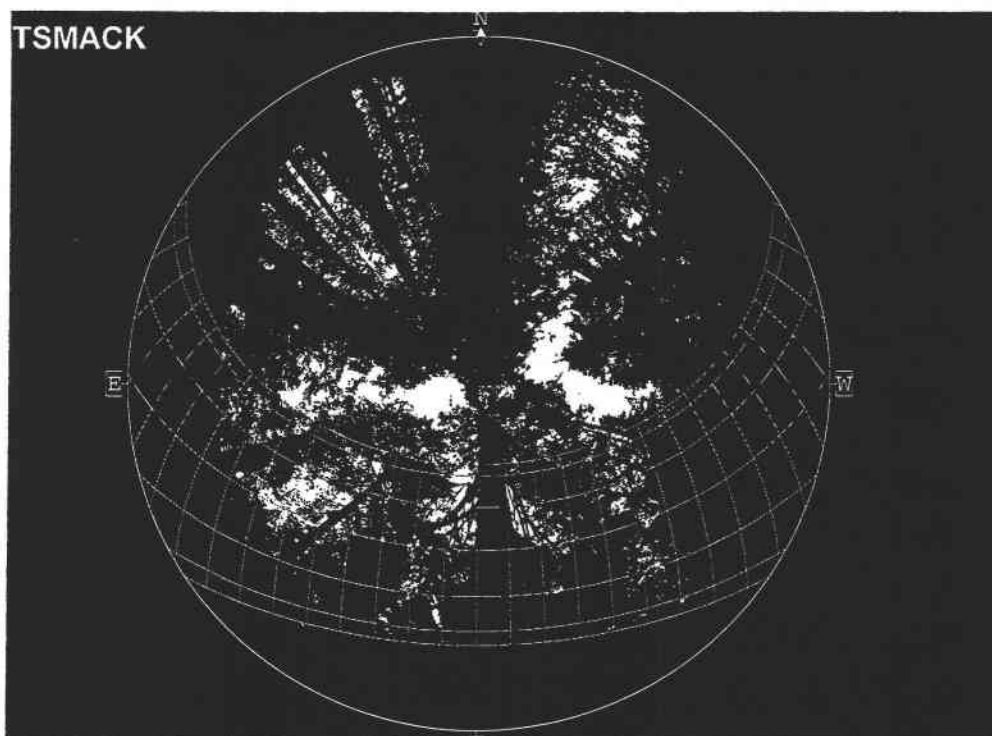








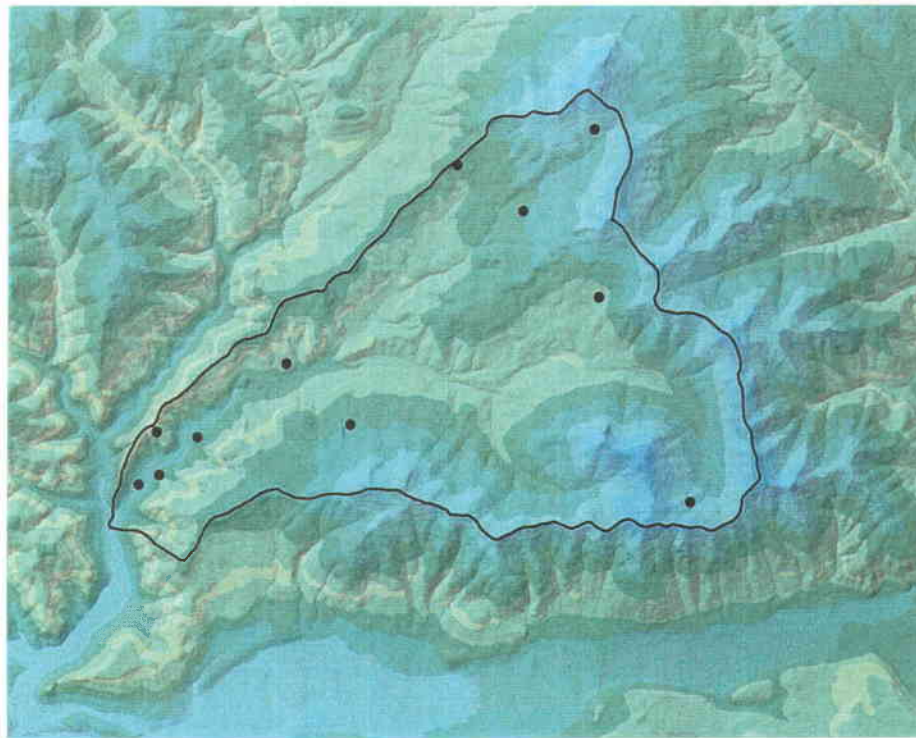




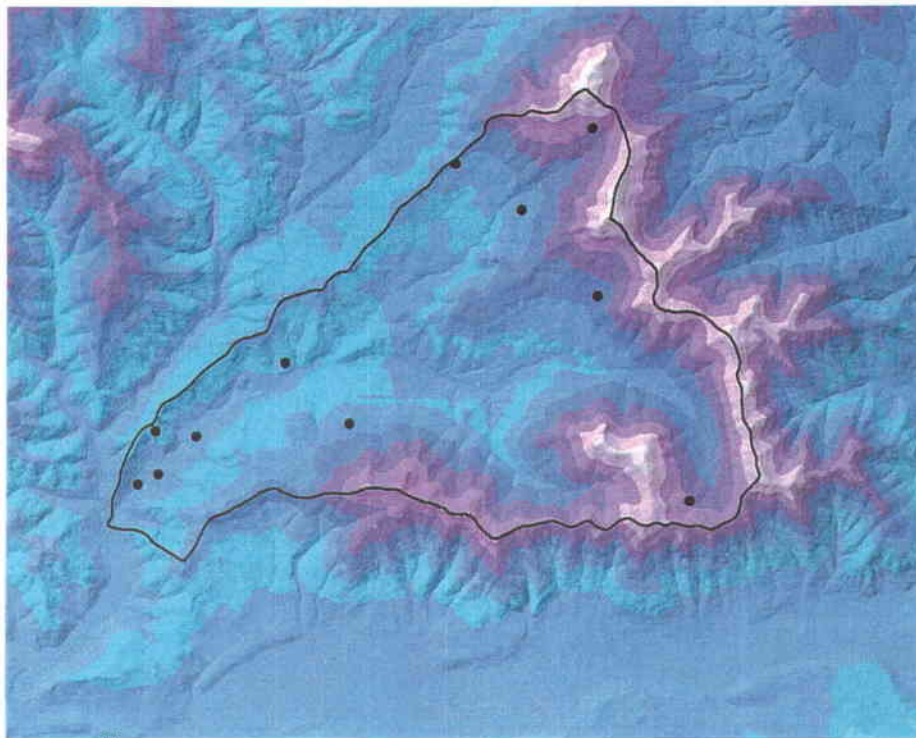
APPENDIX C

Figure C.1. PRISM estimated mean monthly maximum and minimum temperature maps for all months with no radiation or sky view factor effects.

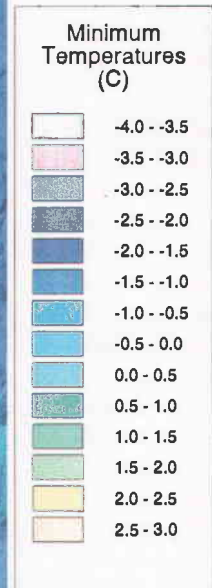
Note: Maps show hypothesized patterns of temperatures assuming unvegetated, topographically-open (flat and unshaded) surfaces.

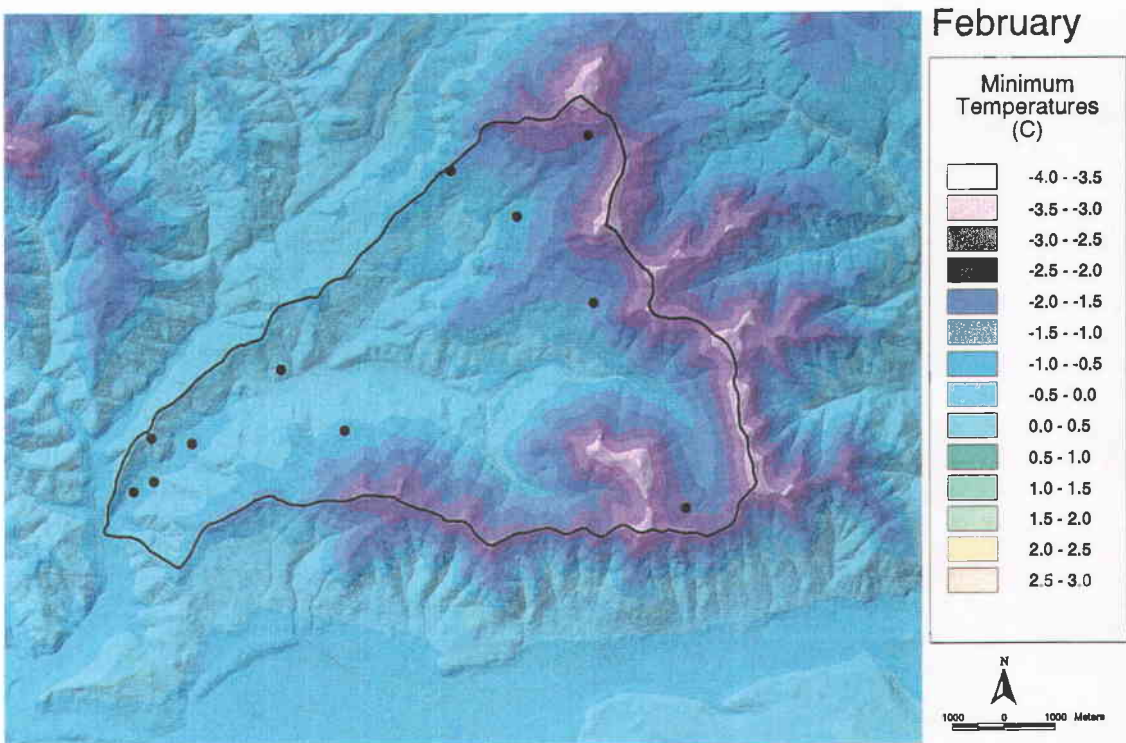


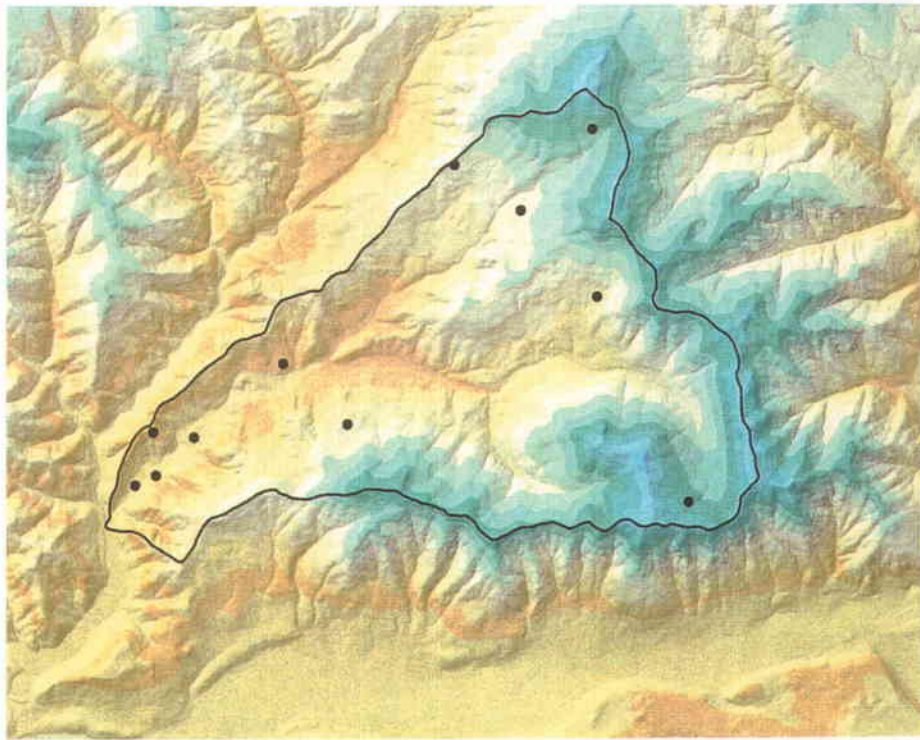
January



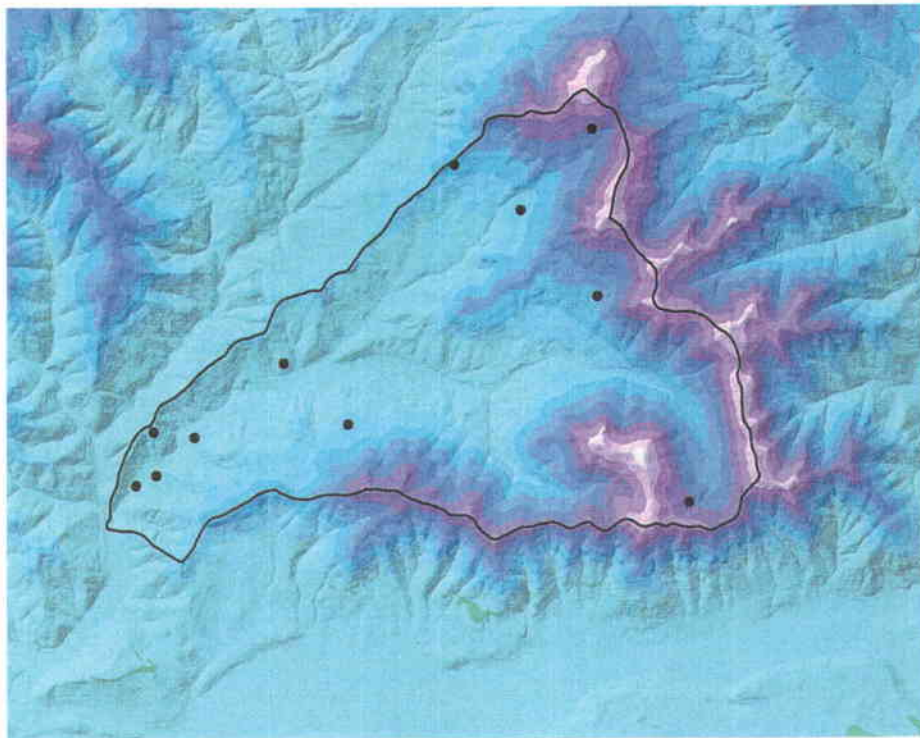
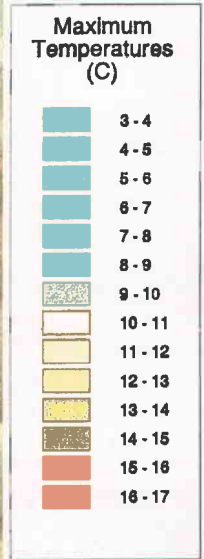
January



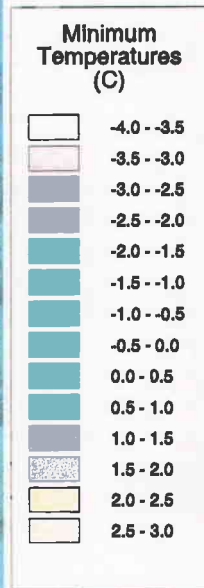


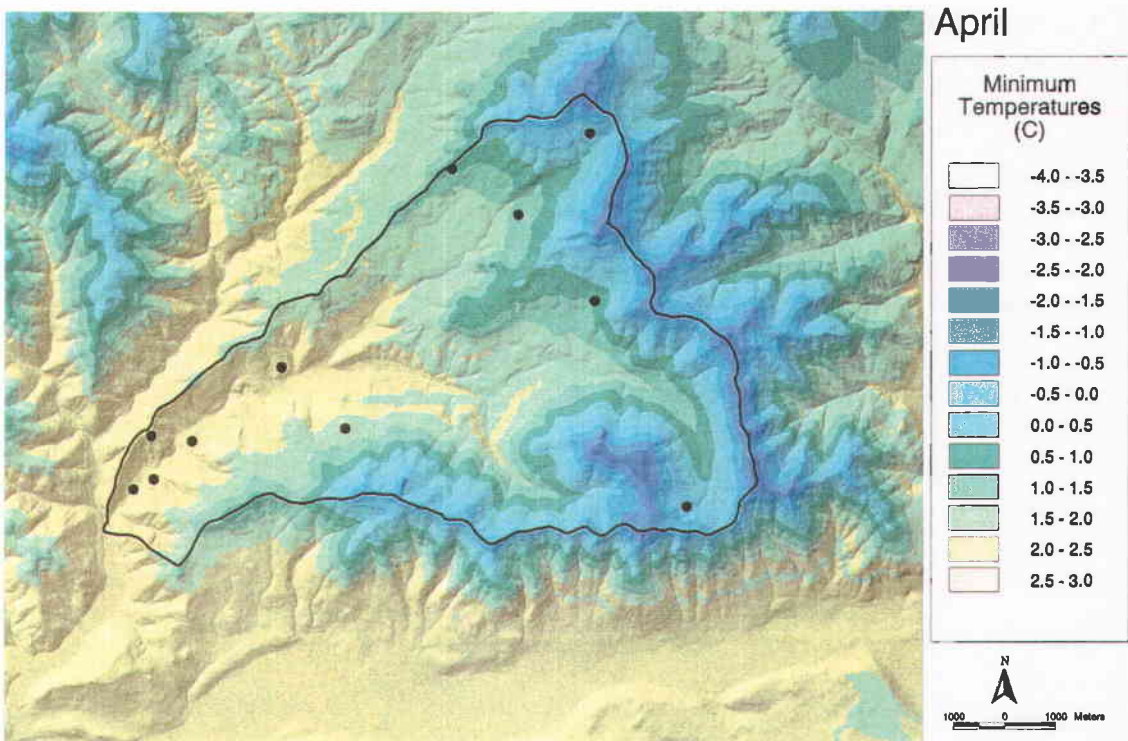
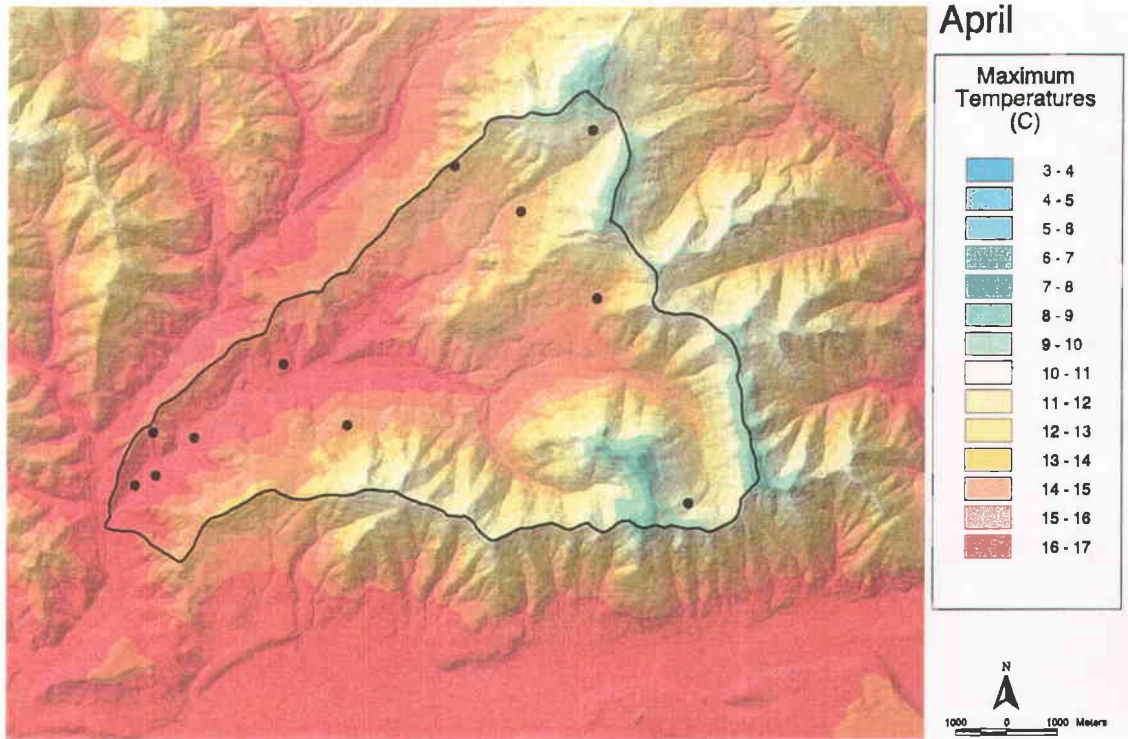


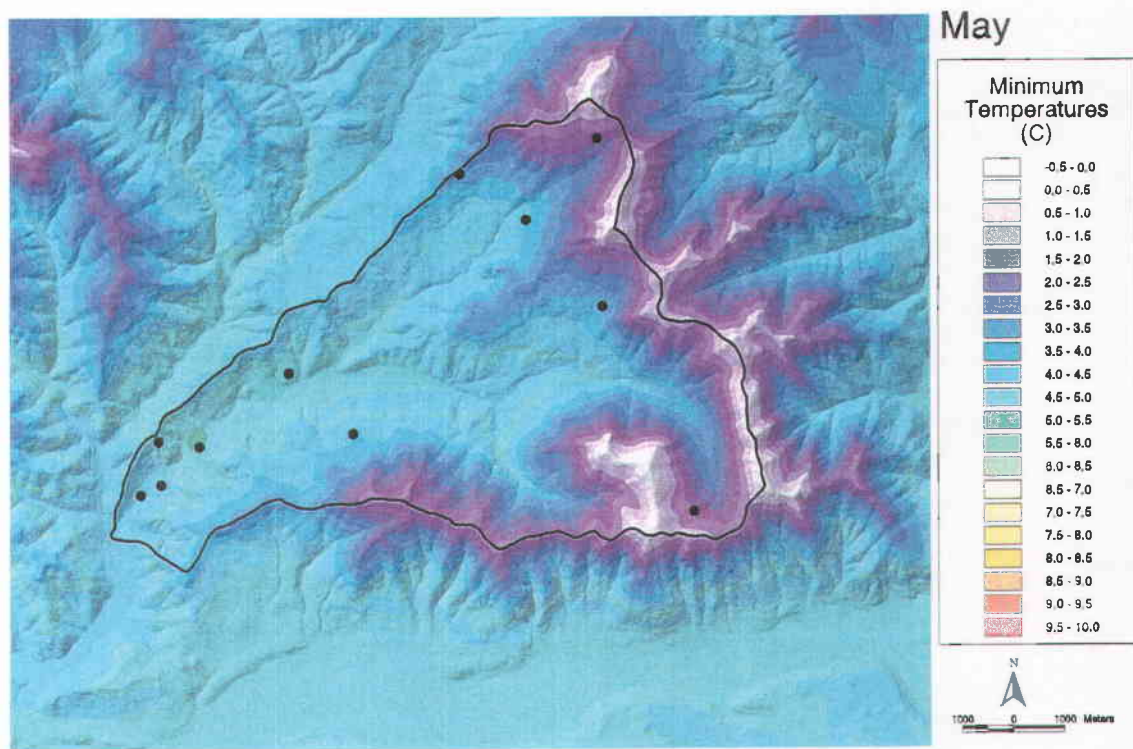
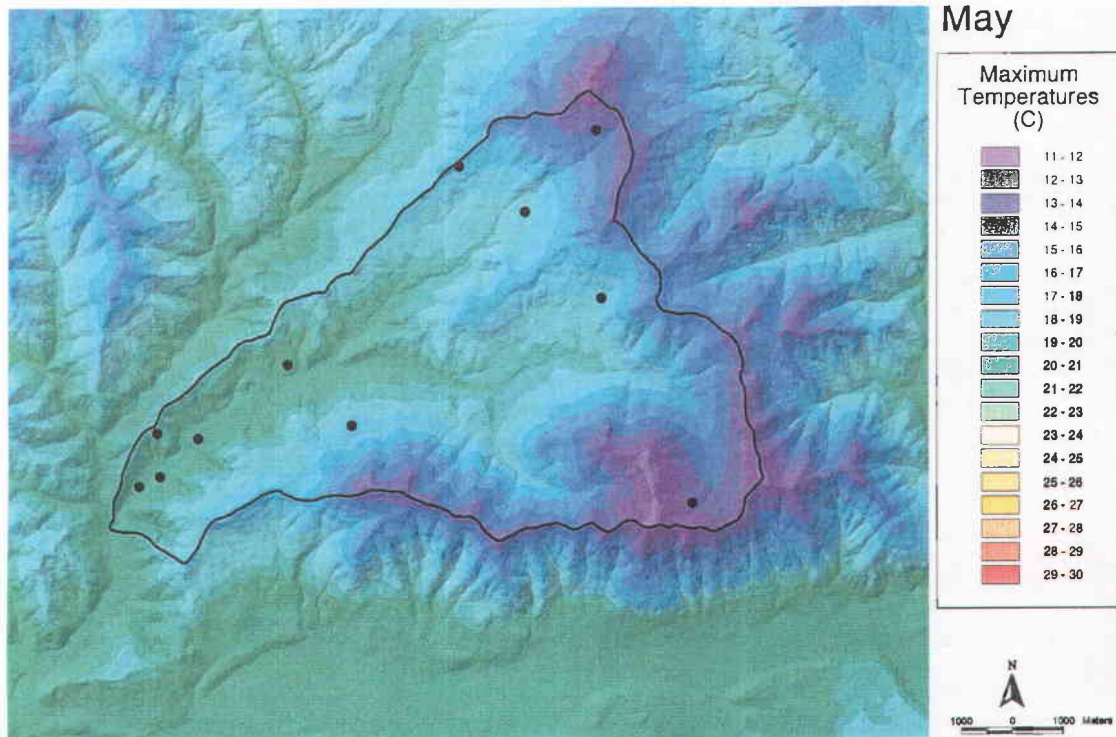
March

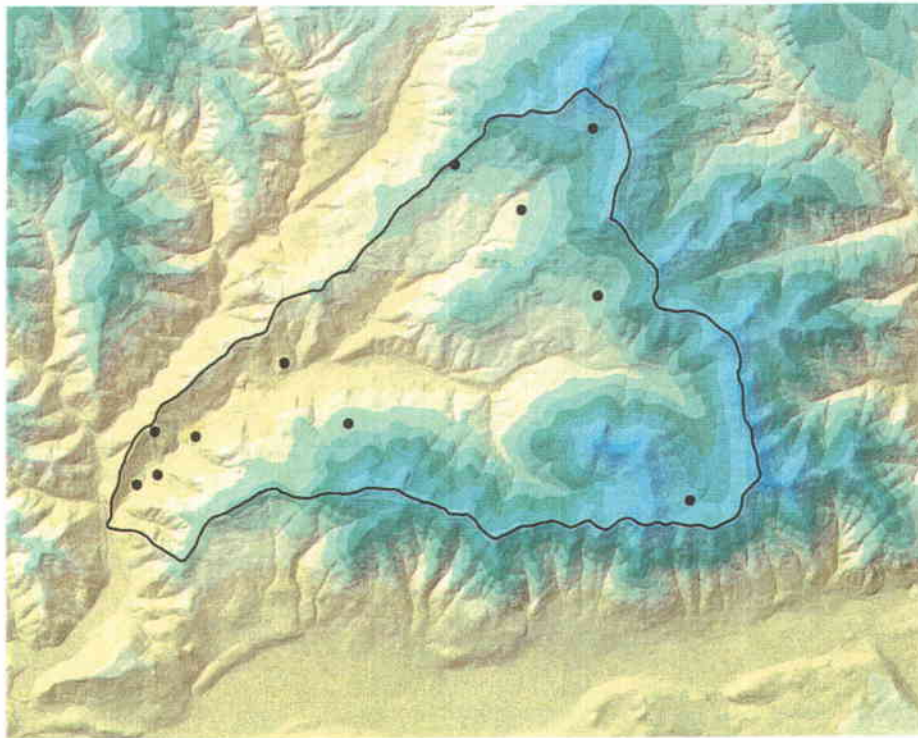


March

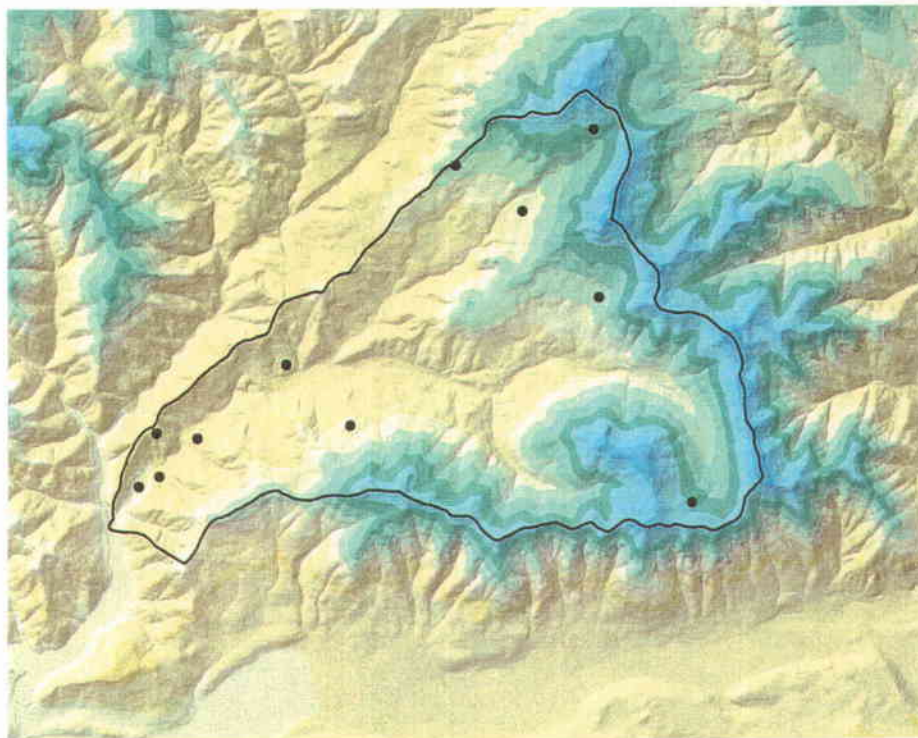
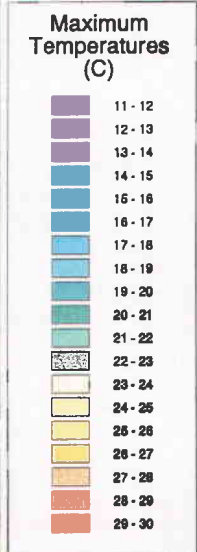




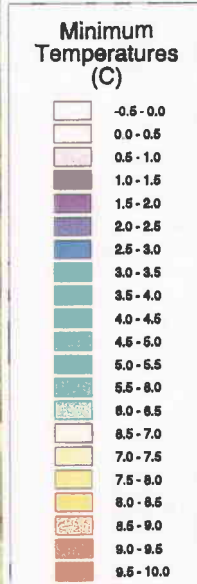


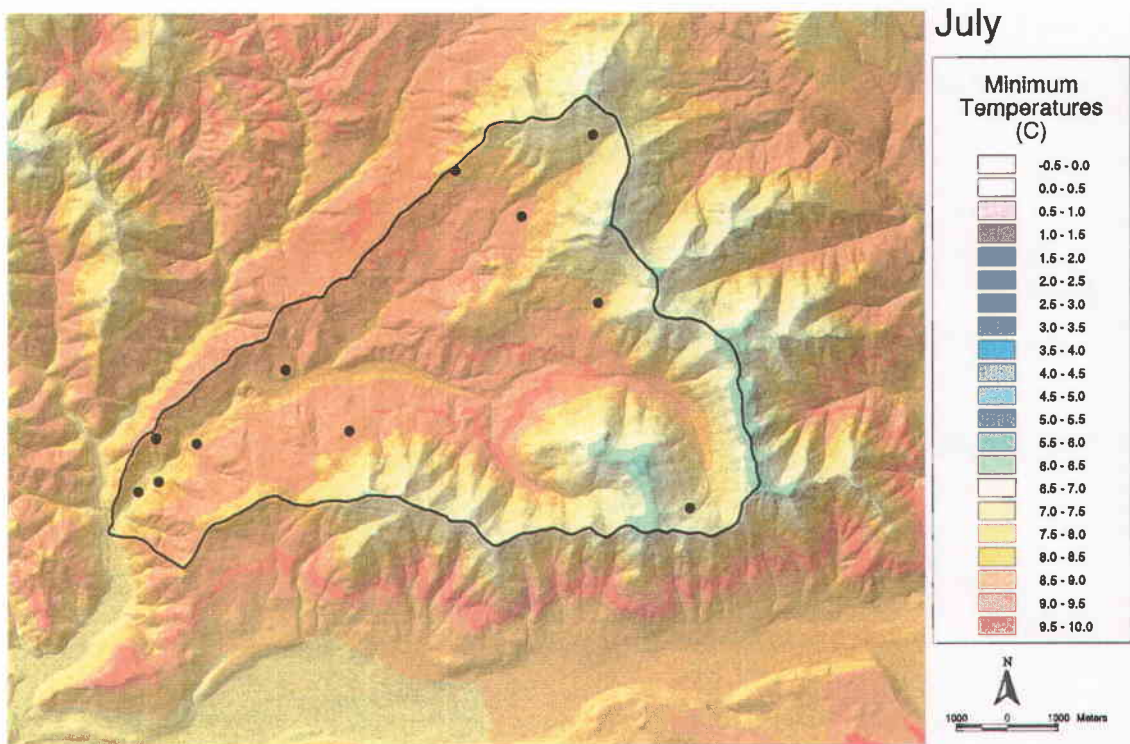
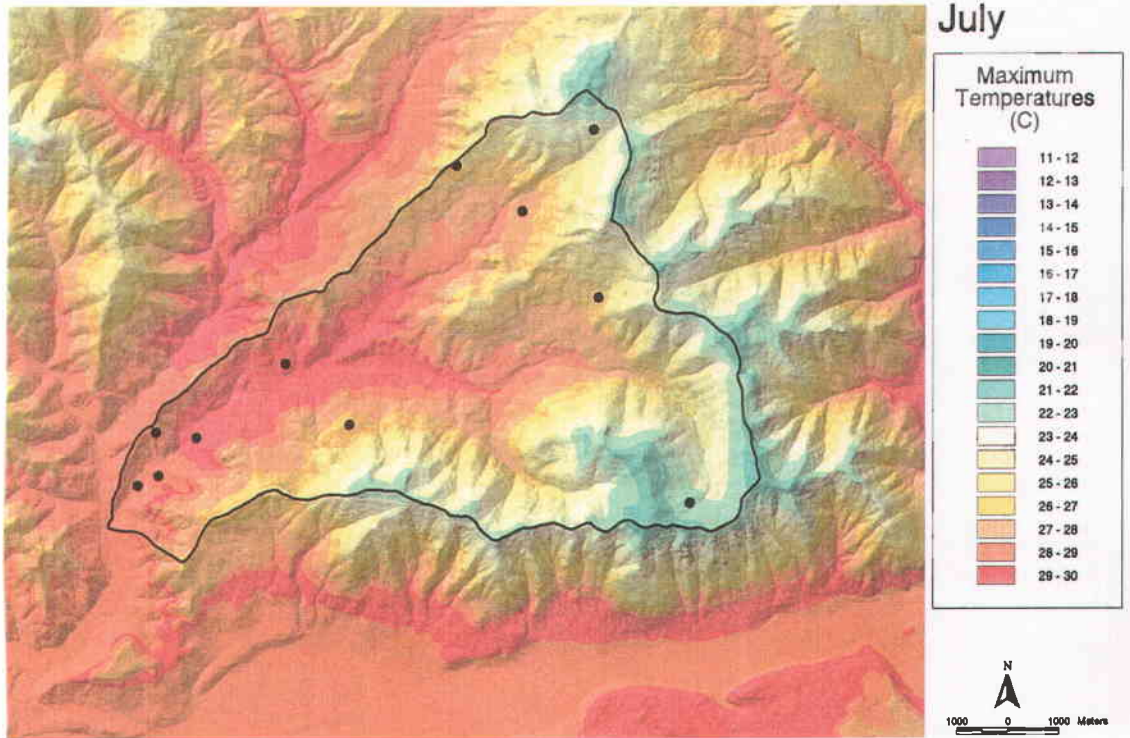


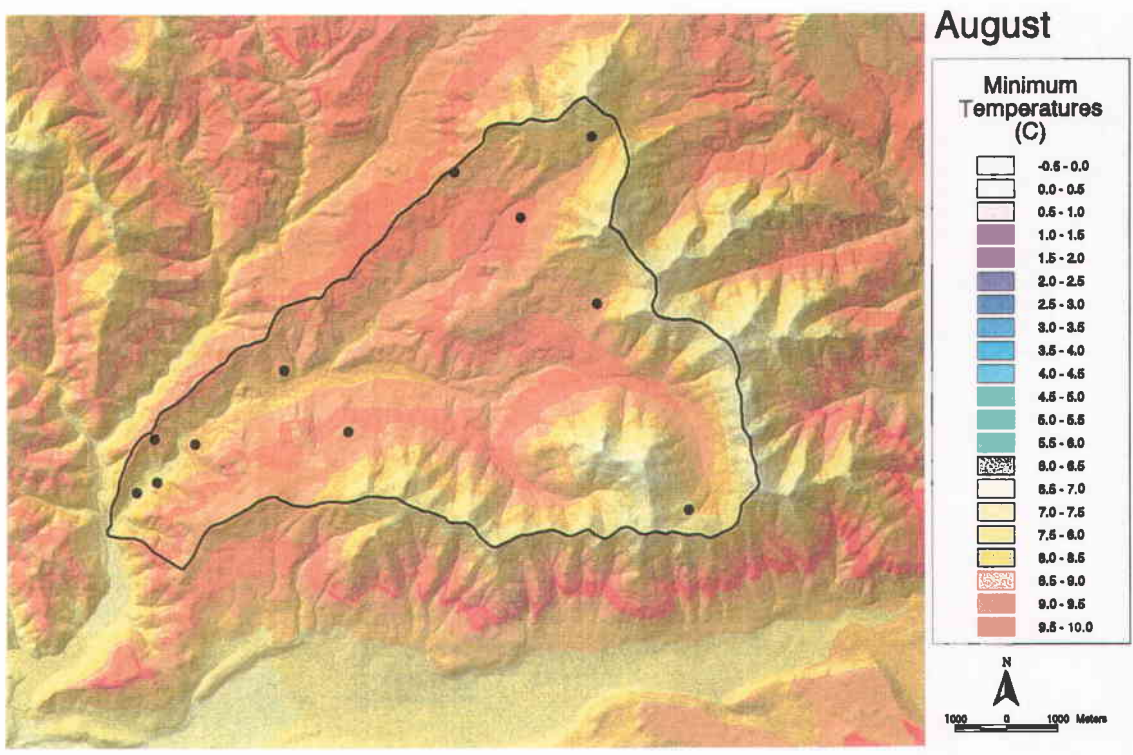
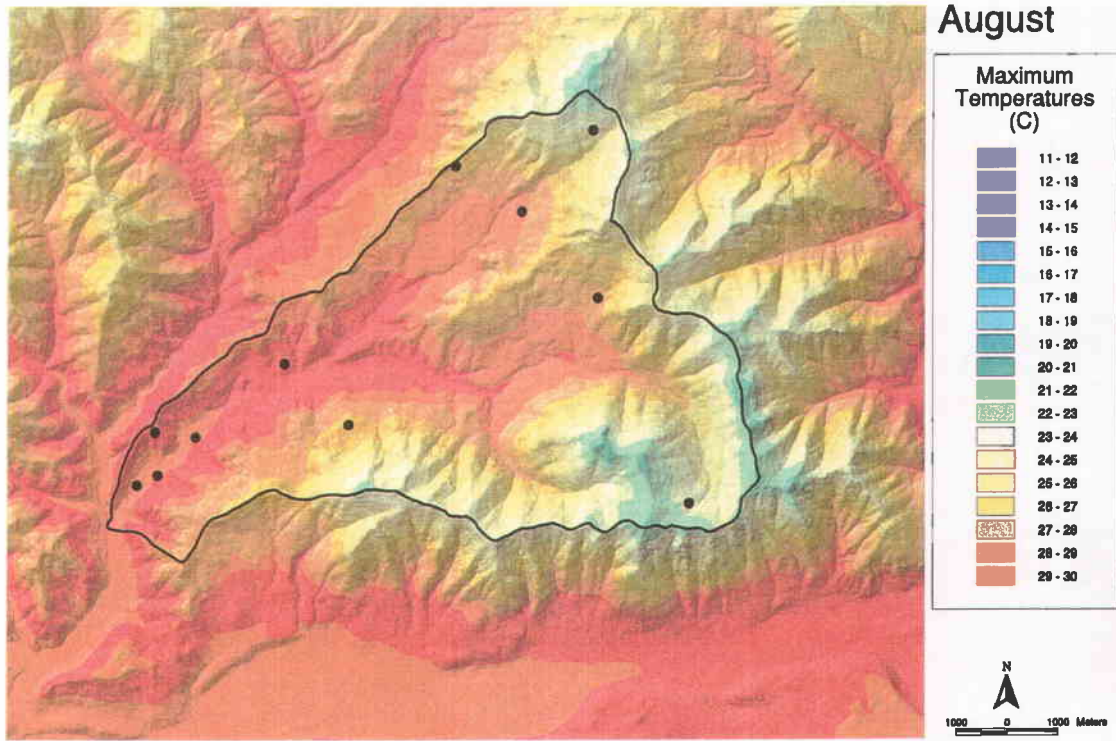
June

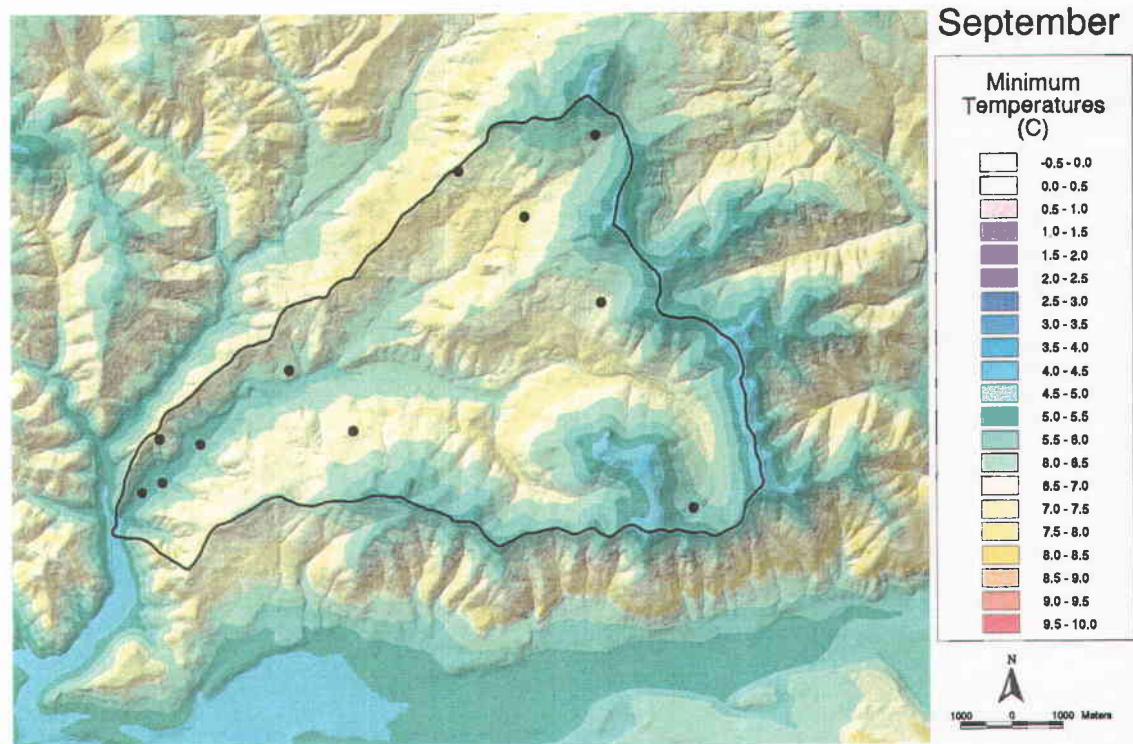
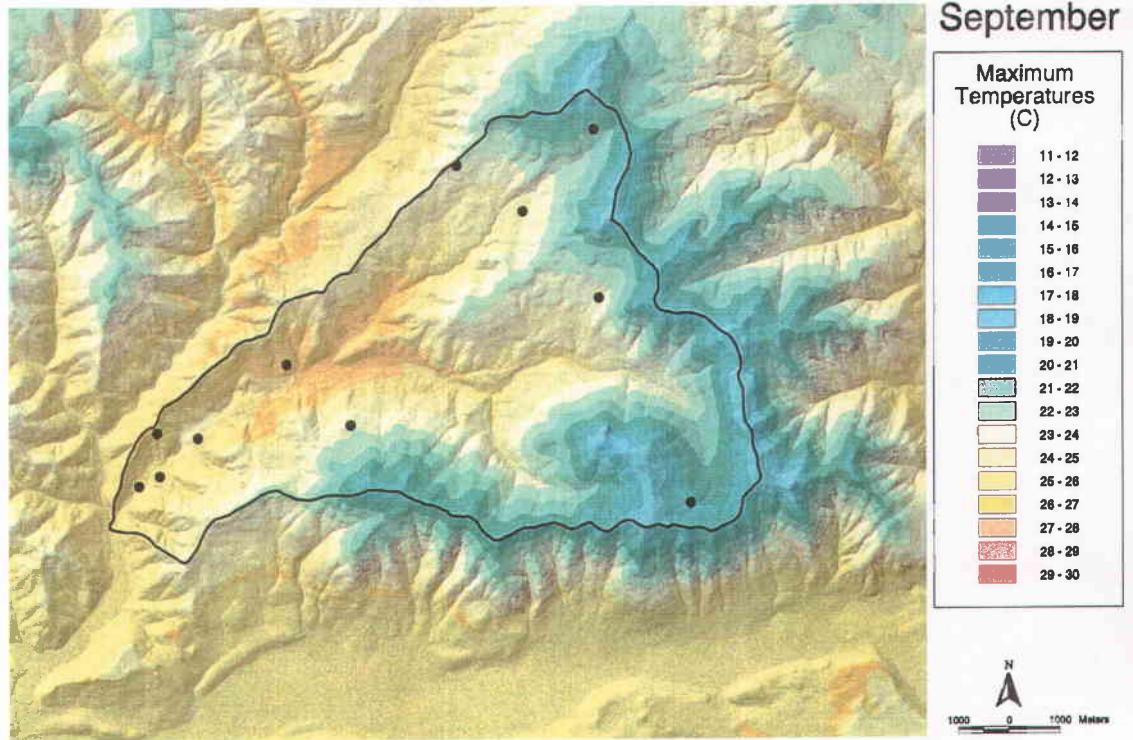


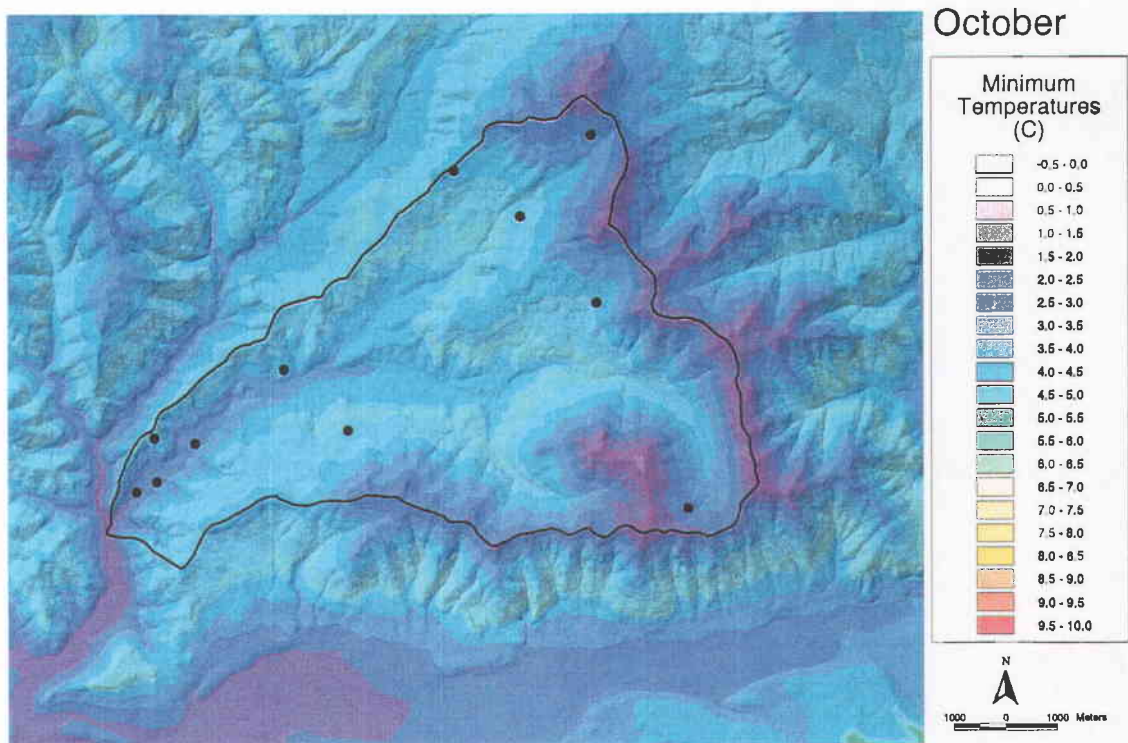
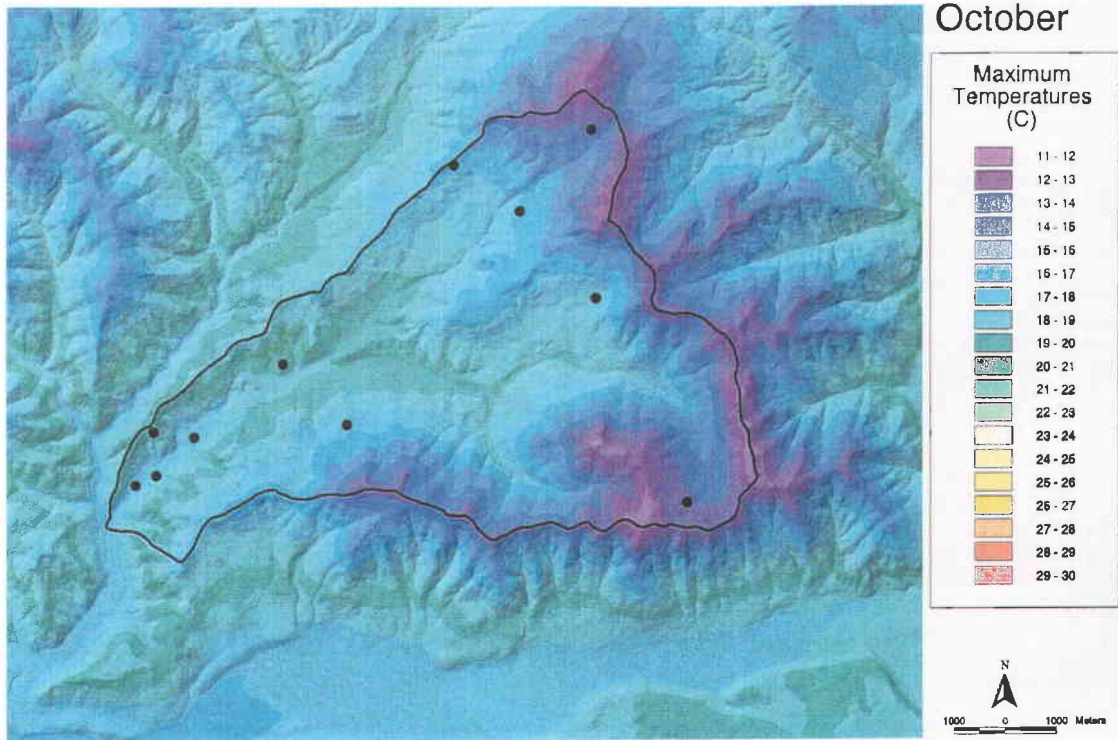
June

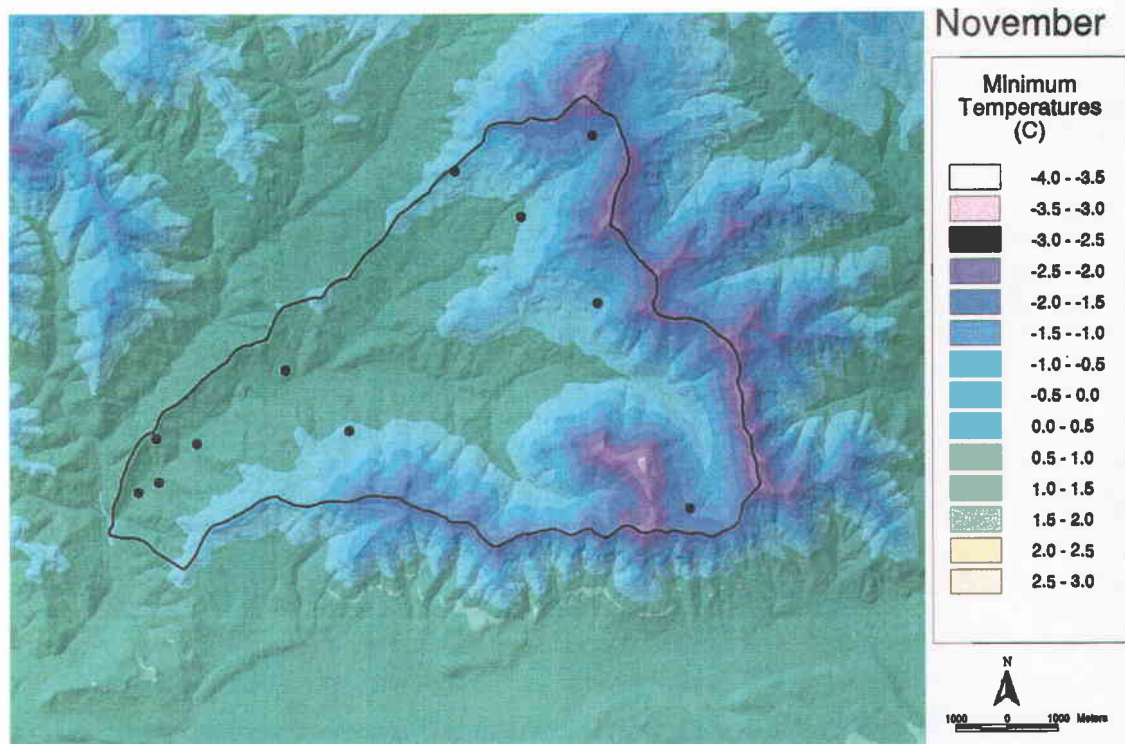








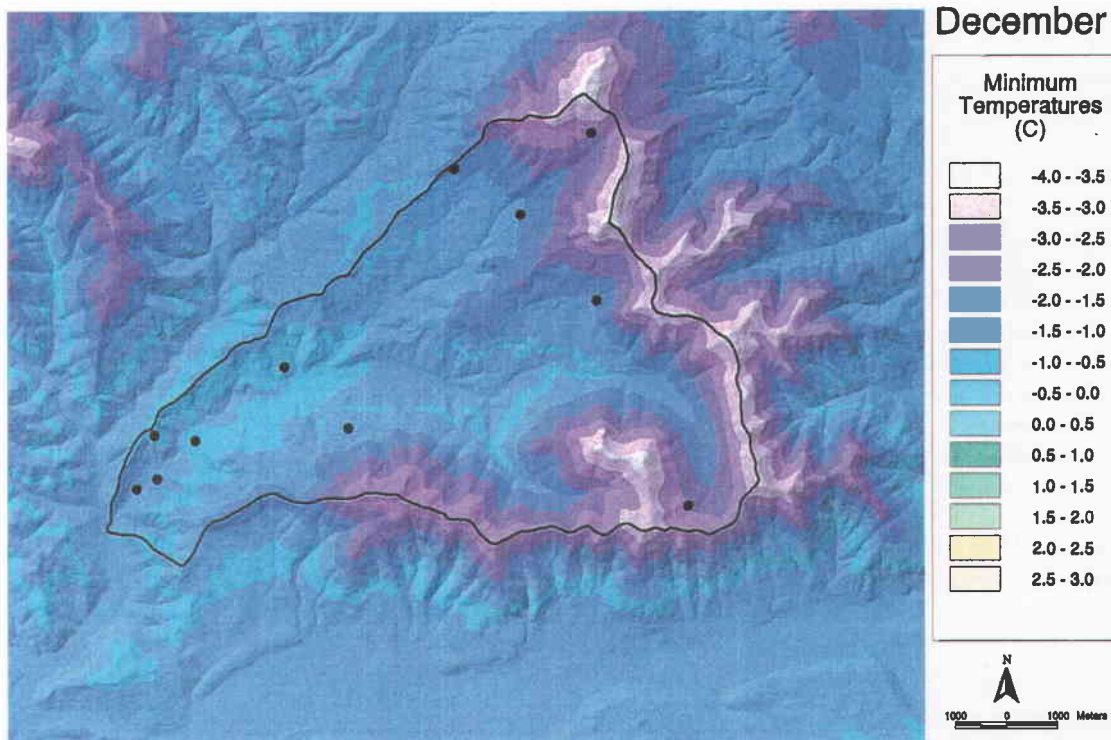




### December



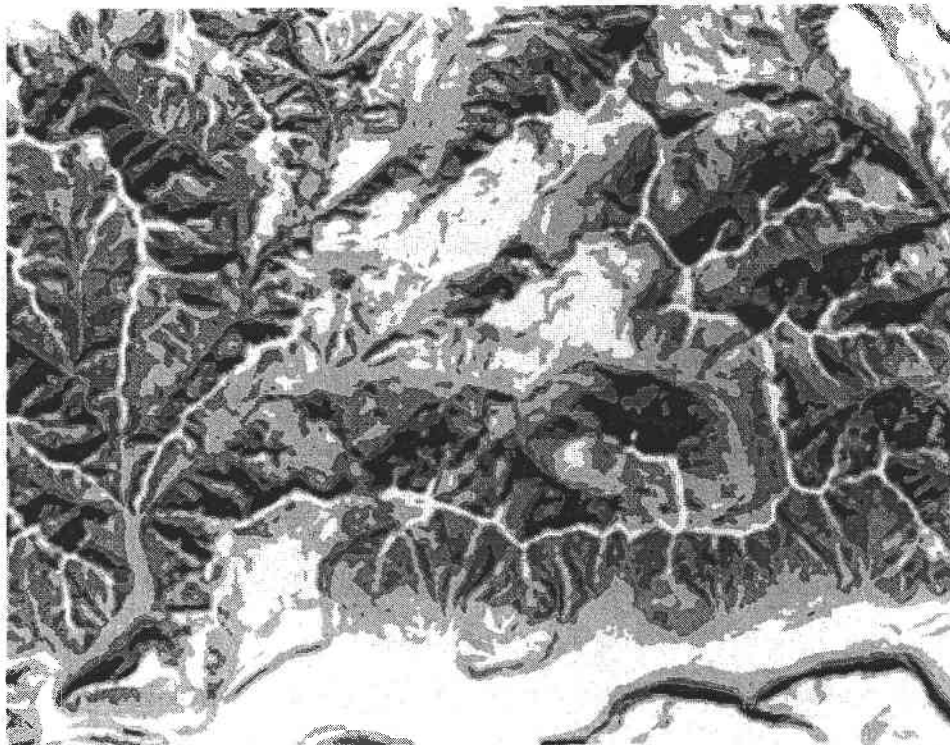
### December



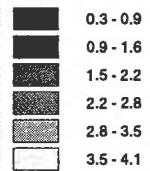
APPENDIX D

Figure D.1. IPW mean daily solar radiation maps for each month.

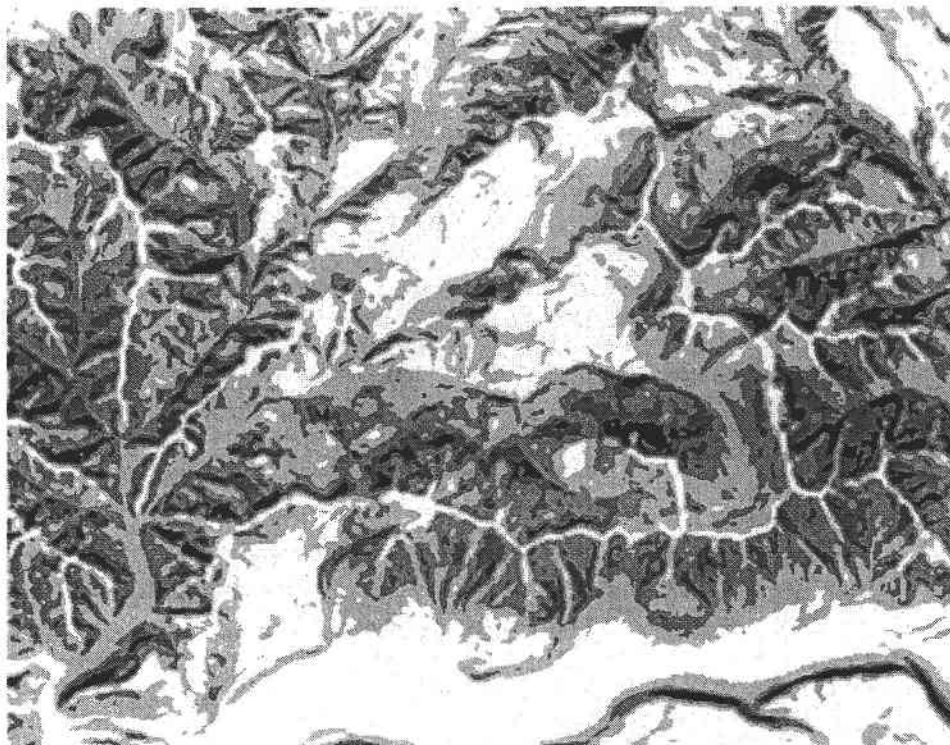
### January



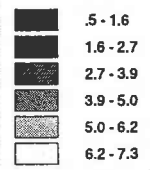
MJ/m<sup>2</sup>.day

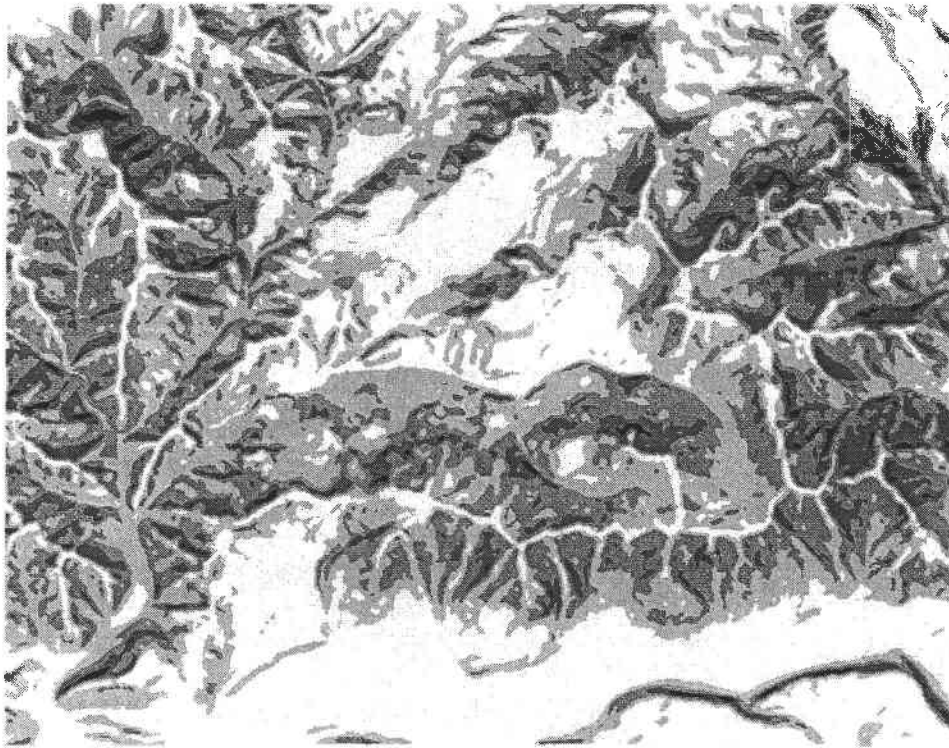


### February



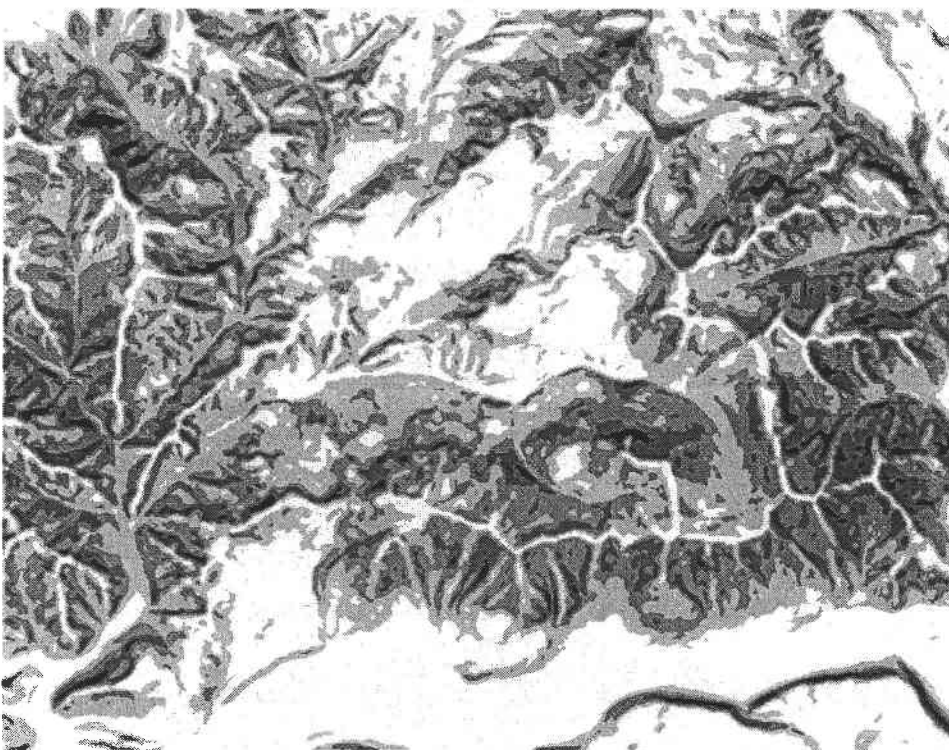
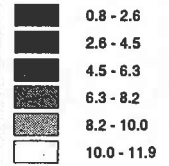
MJ/m<sup>2</sup>.day





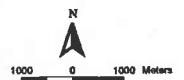
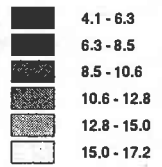
March

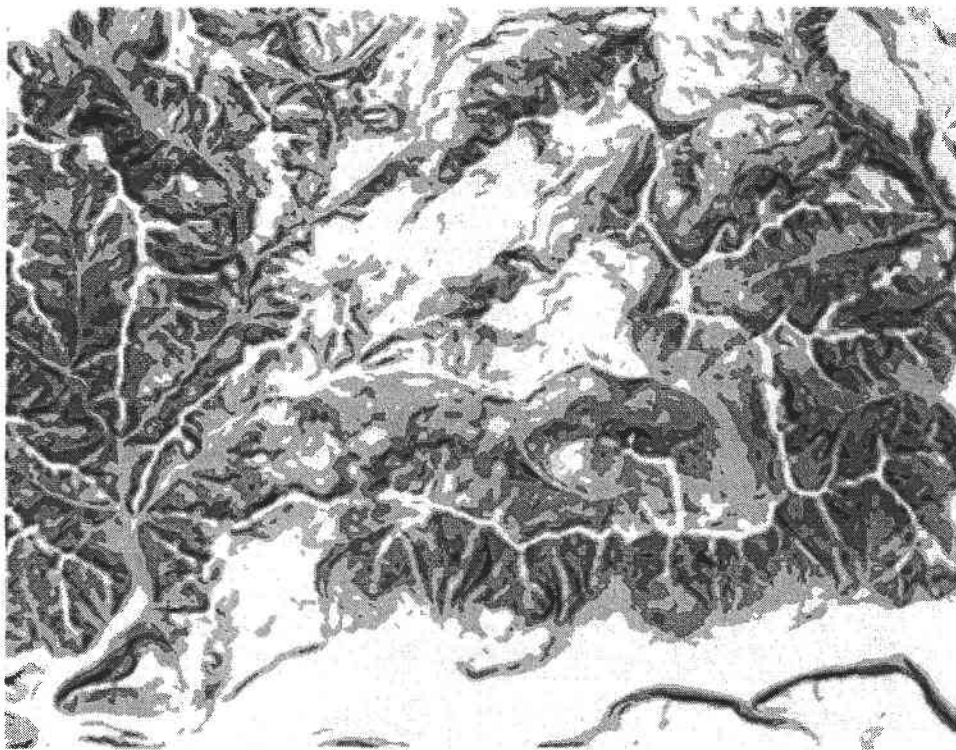
MJ/m<sup>2</sup>.day



April

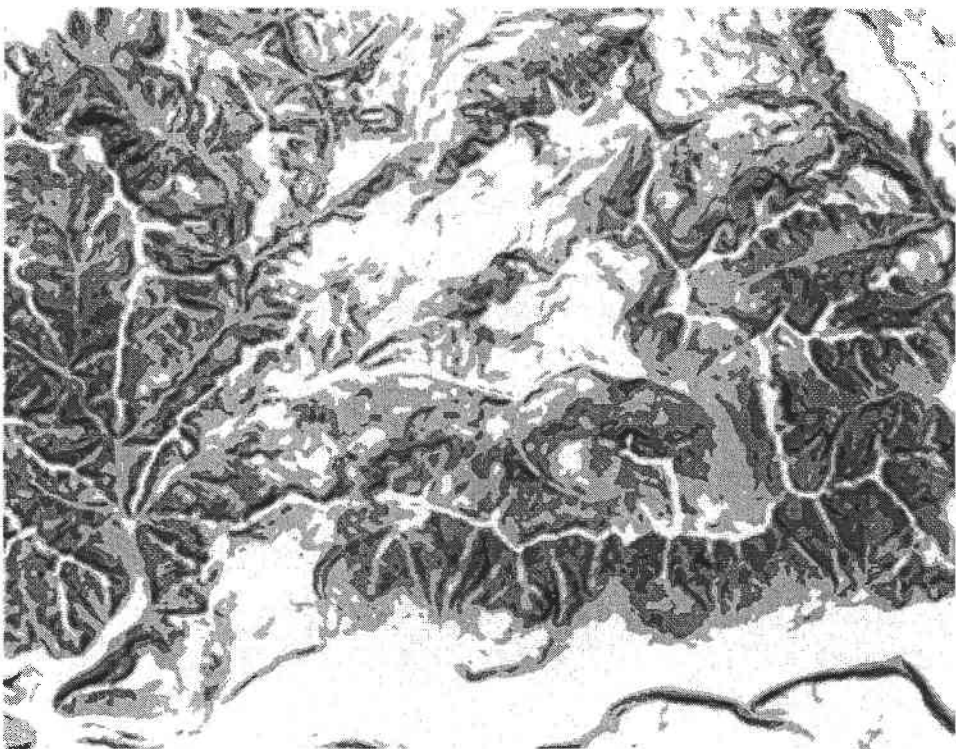
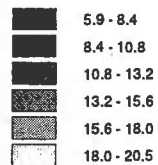
MJ/m<sup>2</sup>.day





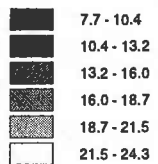
May

MJ/m<sup>2</sup>.day

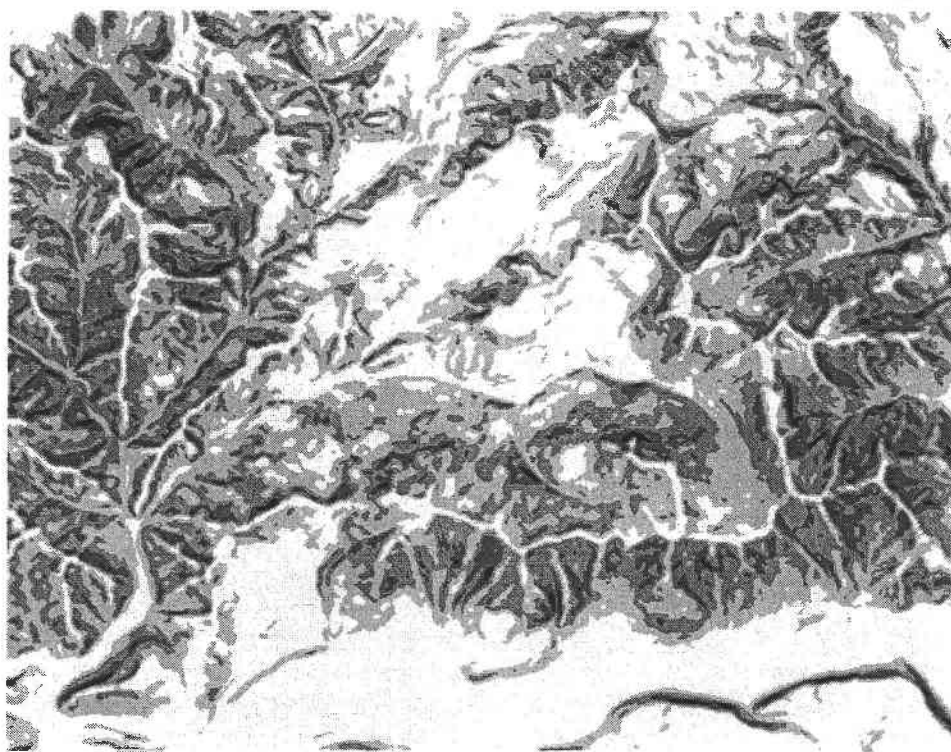


June

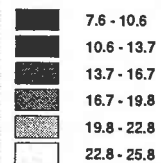
MJ/m<sup>2</sup>.day



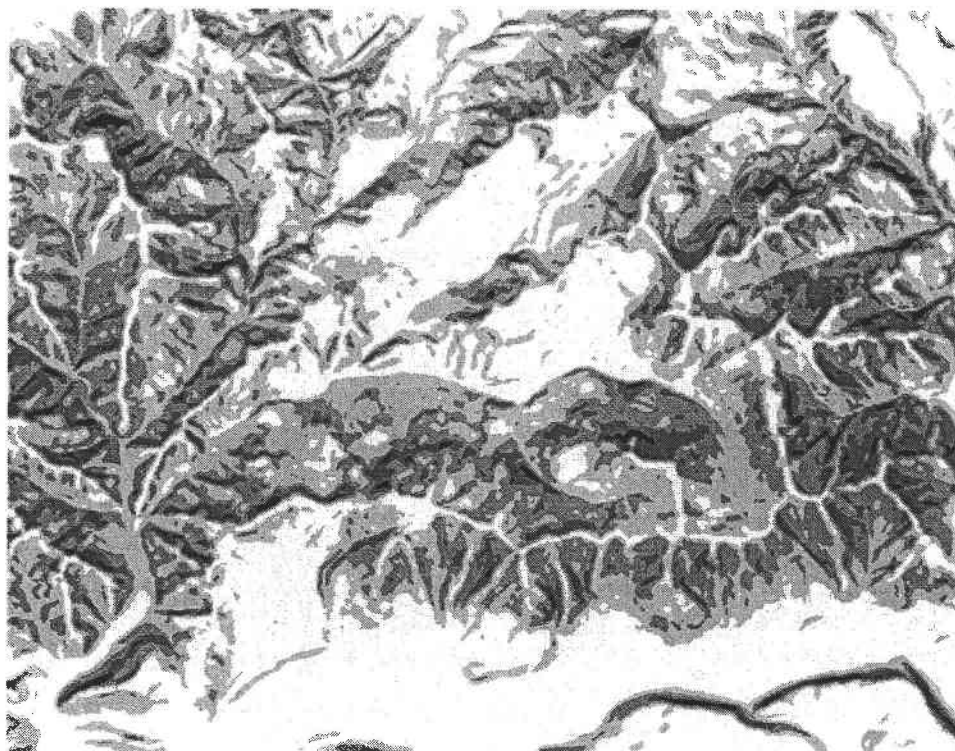
### July



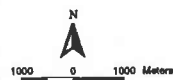
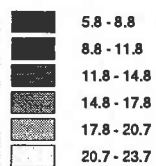
MJ/m<sup>2</sup>.day



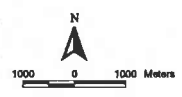
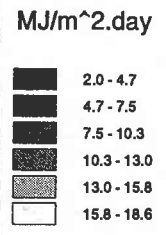
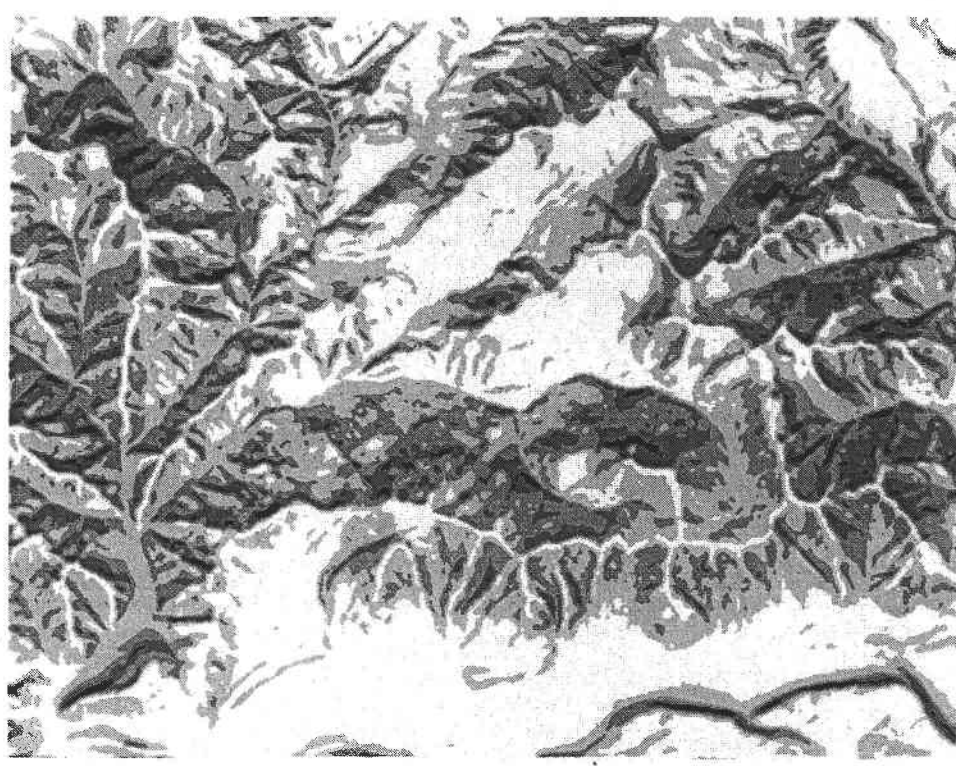
### August



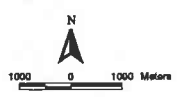
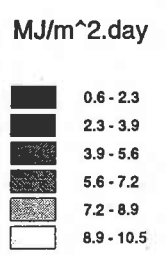
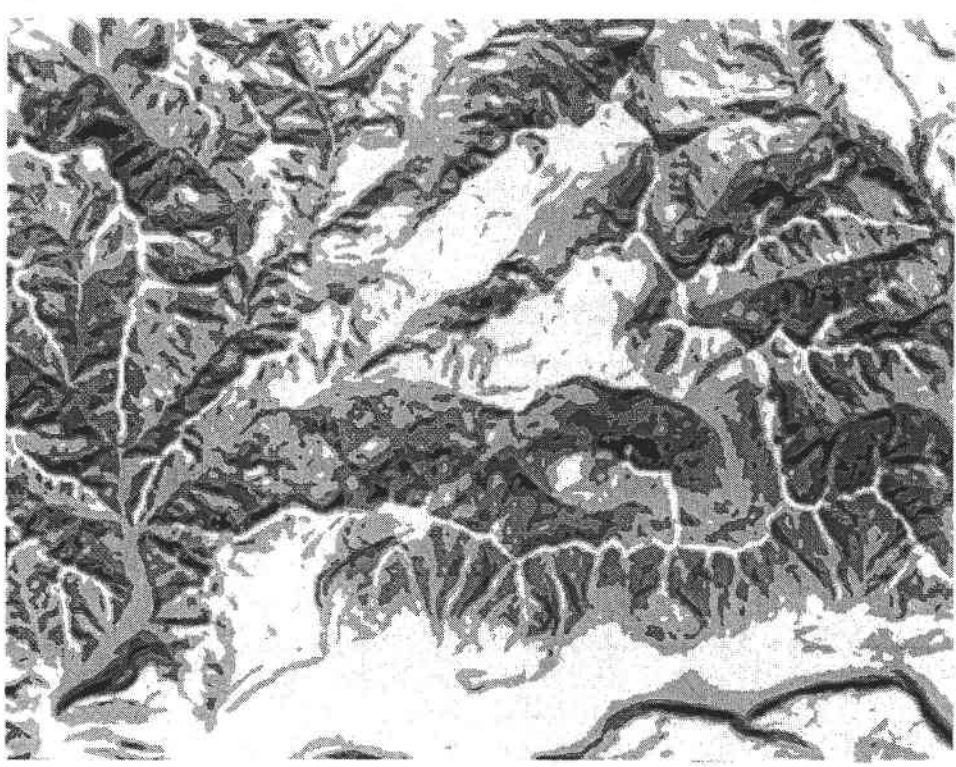
MJ/m<sup>2</sup>.day



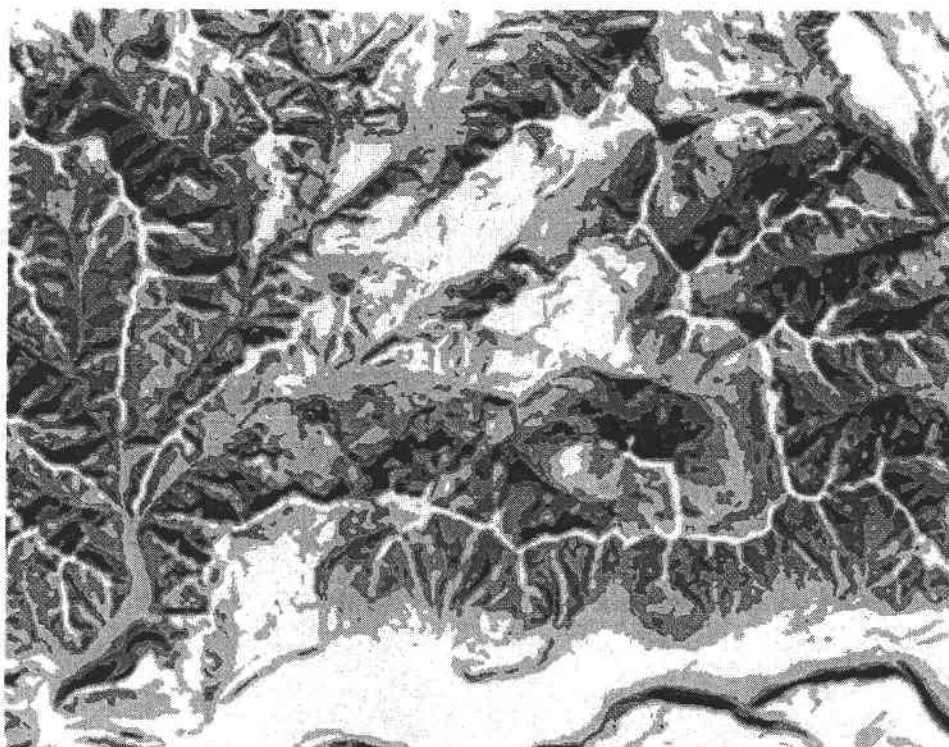
### September



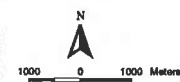
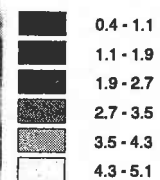
### October



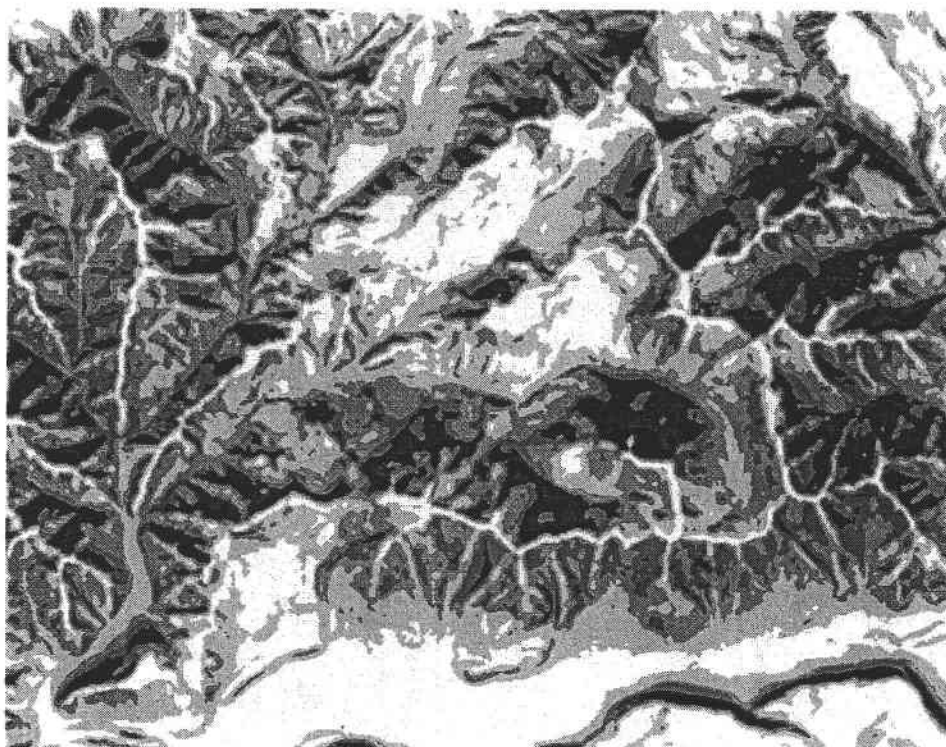
### November



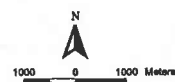
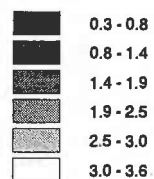
MJ/m<sup>2</sup>.day



### December



MJ/m<sup>2</sup>.day



APPENDIX E



Figure E.1. Sky view factor map.

APPENDIX F

Table F.1. Detailed site descriptions of climate stations used in the study.

SITE: PRIMET  
 EASTING: 559563  
 NORTHING: 4895461  
 ELEV: 430  
 SLOPE: 0  
 ASPECT: -

MODELED RADIATION REGIME:

	J	F	M	A	M	J	J	A	S	O	N	D
TOTAL RADIATION*	2.86	5.37	9.31	14.15	17.18	20.61	22.06	19.79	14.65	7.93	3.56	2.50
BLKD BY TOPO**	0.245	0.190	0.124	0.102	0.100	0.088	0.082	0.081	0.102	0.138	0.211	0.232
BLKD BY CANOPY**	0.010	0.024	0.050	0.049	0.042	0.047	0.046	0.045	0.037	0.032	0.004	0.024

\*DIFFUSE & DIRECT ON SLOPED SURFACE, MJ/m<sup>2</sup>.day  
 (INCLUDING CLOUDINESS, TOPOGRAPHY, AND CANOPY)

\*\*PROPORTIONS OF TOTAL INCOMING RADIATION AT SURFACE

CANOPY: None overhead, though insolation affected slightly from trees on adjacent hillsides.  
 CONTINUOUS, OPEN CANOPY TYPE.

SURFACE: Short grass/dirt, generally clear of vegetation.

SENSOR: Cotton shelter, enclosed sensor (1.5 m). Also a thermister tower (1.5, 2.5, 3.5, 4.5 m),  
 but long-term sensor is enclosed one.

GENERAL SITE CHARACTERISTICS:

Level, open MET site at HJA headquarters, one of the long-term benchmark sites in the HJ Andrews.  
 Long-term temperature measurements are from an enclosed sensor in a cotton shelter. Site is close  
 to Lookout Creek, at the bottom of the valley; cold-air drainage possibly influences this site.  
 Little difference between topographic and canopy insolation blocking, except during winter months.  
 Trees to north much closer than trees to the south. Along with CS2MET, appears have cooler and  
 somewhat unusual long-term temperature trends compared to the rest of the HJ Andrews.

DATES OF OPERATION: 05/70-present

SITE USED FOR MAPPING? yes

SITE: CS2MET  
EASTING: 560044  
NORTHING: 4895780  
ELEV: 460  
SLOPE: 5  
ASPECT: 355

MODELED RADIATION REGIME:

	J	F	M	A	M	J	J	A	S	O	N	D
TOTAL RADIATION*	1.18	1.76	2.45	4.84	7.19	8.46	8.78	7.70	4.37	1.93	1.26	1.08
BLKD BY TOPO**	0.194	0.129	0.092	0.072	0.071	0.059	0.053	0.055	0.075	0.105	0.157	0.263
BLKD BY CANOPY**	0.537	0.631	0.704	0.625	0.556	0.570	0.575	0.563	0.637	0.705	0.603	0.471

\*DIFFUSE & DIRECT ON SLOPED SURFACE, MJ/m<sup>2</sup>.day  
(INCLUDING CLOUDINESS, TOPOGRAPHY, AND CANOPY)

\*\*PROPORTIONS OF TOTAL INCOMING RADIATION AT SURFACE

CANOPY: Closest site to having 45 degree cone overhead. Canopy slightly more open to the east than other directions. CONTINUOUS, OPEN CANOPY TYPE.

SURFACE: Tends to be bushy with thick short shrubbery and grass.

SENSOR: 1.3 m thermister, shielded above with PVC.

GENERAL SITE CHARACTERISTICS:

The longest running site in the HJ Andrews. Surrounded on all sides by thick forest with tall trees, located directly in middle of clearing (15-20m from trees). Located in a clearing up and across the main road from Lookout Creek, with cold-air drainage possibly affecting temperature regime. Surrounding forest plays a major role in insolation regime, though site is completely open directly above. Along with PRIMET, , appears have cooler and somewhat unusual long-term temperature trends compared to the rest of the HJ Andrews.

DATES OF OPERATION: 10/49-present

SITE USED FOR MAPPING? no

SITE: CENMET  
EASTING: 586680  
NORTHING: 4899065  
ELEV: 1018  
SLOPE: 12  
ASPECT: 260

MODELED RADIATION REGIME:

	J	F	M	A	M	J	J	A	S	O	N	D
TOTAL RADIATION*	2.95	5.30	9.09	13.92	17.09	20.59	22.21	20.05	14.63	7.74	3.62	2.56
BLKD BY TOPO**	0.114	0.107	0.104	0.093	0.075	0.063	0.061	0.071	0.090	0.102	0.103	0.110
BLKD BY CANOPY**	0.062	0.063	0.050	0.032	0.027	0.028	0.025	0.020	0.030	0.053	0.069	0.067

\*DIFFUSE & DIRECT ON SLOPED SURFACE, MJ/m<sup>2</sup>.day  
(INCLUDING CLOUDINESS, TOPOGRAPHY, AND CANOPY)

\*\*PROPORTIONS OF TOTAL INCOMING RADIATION AT SURFACE

CANOPY: None overhead, open site, though insolation affected slightly from trees on adjacent hillsides. CONTINUOUS, OPEN CANOPY TYPE.

SURFACE: Short grass, dirt.

SENSOR: 1.5 m thermister, shielded above with PVC, on thermister tower (1.5, 2.5, 3.5, 4.5 m sensors).

GENERAL SITE CHARACTERISTICS:

One of the benchmark MET sites. Insolation topographically blocked to east and southeast, with closest forest in those directions, on top of clear-cut hill. This prominent forest wall possibly affects temperature regime and wind patterns. In a large clear-cut.

DATES OF OPERATION: 08/95-present

SITE USED FOR MAPPING? yes

SITE: VANMET  
 EASTING: 567832  
 NORTHING: 4902239  
 ELEV: 1273  
 SLOPE: 13  
 ASPECT: 180

MODELED RADIATION REGIME:

	J	F	M	A	M	J	J	A	S	O	N	D
TOTAL RADIATION*	3.57	6.44	10.75	15.64	18.52	22.08	23.92	22.16	17.23	9.58	4.50	3.15
BLKD BY TOPO**	0.043	0.032	0.032	0.024	0.024	0.020	0.019	0.018	0.021	0.029	0.046	0.053
BLKD BY CANOPY**	0.025	0.030	0.022	0.028	0.019	0.016	0.014	0.020	0.026	0.023	0.016	0.016

\*DIFFUSE & DIRECT ON SLOPED SURFACE, MJ/m<sup>2</sup>.day  
 (INCLUDING CLOUDINESS, TOPOGRAPHY, AND CANOPY)

\*\*PROPORTIONS OF TOTAL INCOMING RADIATION AT SURFACE

CANOPY: The most open site in the HJ Andrews. Horizon visible east-south-west. Trees not a factor for insolation. CONTINUOUS, OPEN CANOPY TYPE.

SURFACE: Mixed short grass, brush, dirt

SENSOR: 1.5 m thermister, shielded above with PVC, on thermister tower (1.5, 2.5, 3.5, 4.5 m sensors). Recording sensor height varied during operating period between .5 and 2.5 m.

GENERAL SITE CHARACTERISTICS:

One of the benchmark MET sites. On a south-facing slope with horizon fully visible in that direction. Sparse forest begins 20-30 m to the north. In a large clear-cut with an expansive view.

DATES OF OPERATION: 06/87-present

SITE USED FOR MAPPING? no

SITE: UPLMET  
EASTING: 570331  
NORTHING: 4895053  
ELEV: 1292  
SLOPE: 13  
ASPECT: 72

MODELED RADIATION REGIME:

	J	F	M	A	M	J	J	A	S	O	N	D
TOTAL RADIATION*	3.22	5.75	9.73	14.80	17.78	20.61	21.91	20.29	15.23	8.14	4.01	2.77
BLKD BY TOPO**	0.056	0.045	0.049	0.036	0.035	0.031	0.027	0.029	0.036	0.042	0.059	0.065
BLKD BY CANOPY**	0.085	0.075	0.060	0.044	0.049	0.082	0.086	0.050	0.039	0.069	0.062	0.078

\*DIFFUSE & DIRECT ON SLOPED SURFACE, MJ/m<sup>2</sup>.day  
(INCLUDING CLOUDINESS, TOPOGRAPHY, AND CANOPY)

\*\*PROPORTIONS OF TOTAL INCOMING RADIATION AT SURFACE

CANOPY: None overhead, open site, though insolation affected slightly from trees on adjacent hillsides. CONTINUOUS, OPEN CANOPY TYPE.

SURFACE: Mixed short grass, brush, dirt.

SENSOR: 1.5 m thermister, shielded above with PVC, on thermister tower (1.5, 2.5, 3.5, 4.5 m sensors).

GENERAL SITE CHARACTERISTICS:

The highest of the benchmark MET sites. On gentle east-facing slope, with horizon visible in all directions, though slight topographic shading to the southwest in winter. Very open, in a large clear-cut. Presence of young trees growing in clearcut provides some insolation blockage; nearest forest starts due east 70-80 m. Due to openness and reliability of insolation and temperature data, this site was used to determine percentages of diffuse and direct radiation for each month in the study.

DATES OF OPERATION: 10/94-present

SITE USED FOR MAPPING? yes

SITE: H15MET  
EASTING: 565859  
NORTHING: 4901219  
ELEV: 922  
SLOPE: 15  
ASPECT: 240

MODELED RADIATION REGIME:

	J	F	M	A	M	J	J	A	S	O	N	D
TOTAL RADIATION*	1.57	2.62	4.40	7.09	9.34	13.46	14.46	10.76	7.49	3.72	1.82	1.39
BLKD BY TOPO**	0.065	0.055	0.055	0.043	0.045	0.045	0.031	0.032	0.040	0.050	0.062	0.074
BLKD BY CANOPY**	0.539	0.580	0.577	0.537	0.483	0.374	0.382	0.505	0.555	0.596	0.573	0.534

\*DIFFUSE & DIRECT ON SLOPED SURFACE, MJ/m<sup>2</sup>.day  
(INCLUDING CLOUDINESS, TOPOGRAPHY, AND CANOPY)

\*\*PROPORTIONS OF TOTAL INCOMING RADIATION AT SURFACE

CANOPY: None directly overhead, but site surrounded by moderate forest.  
CONTINUOUS, OPEN CANOPY TYPE.

SURFACE: Gravel and dirt.

SENSOR: 1.5 m thermister, shielded above with PVC. Recording sensor height varied during period of operation between 1.5 m (6 years) and 4.8 m (1.5 years).

GENERAL SITE CHARACTERISTICS:

At the confluence of 2 roads in moderate forest. Site is thus unusual by having large open areas radiating out from it through the surrounding forest. Attenuation is completely by surrounding trees, about 20 m from sensor in each direction. More open to direct radiation from the southwest for most months (direct sun in the mornings). During June and July site receives direct radiation through much of the day but during other months sun is blocked by forest wall to the south.

DATES OF OPERATION: 03/92-present

SITE USED FOR MAPPING? no

SITE: RS01  
EASTING: 559434  
NORTHING: 4894296  
ELEV: 490  
SLOPE: 41  
ASPECT: 200

MODELED RADIATION REGIME:

	J	F	M	A	M	J	J	A	S	O	N	D
TOTAL RADIATION*	0.76	1.43	2.27	3.07	4.58	5.93	6.47	5.17	2.99	1.93	0.97	0.69
BLKD BY TOPO**	0.138	0.135	0.117	0.108	0.105	0.089	0.087	0.088	0.096	0.118	0.138	0.159
BLKD BY CANOPY**	0.679	0.674	0.703	0.734	0.672	0.651	0.649	0.692	0.760	0.705	0.671	0.660

\*DIFFUSE & DIRECT ON SLOPED SURFACE, MJ/m<sup>2</sup>.day  
(INCLUDING CLOUDINESS, TOPOGRAPHY, AND CANOPY)

\*\*PROPORTIONS OF TOTAL INCOMING RADIATION AT SURFACE

CANOPY: Sparse, moderately high. DISCONTINUOUS, with numerous open and shaded areas.

SURFACE: Scrubby bushes, grasses, small felled timber.

SENSOR: 1.0 m and .8 m mercury bulb thermometers.

GENERAL SITE CHARACTERISTICS:

Site is on southwest-facing steep slope with open views of Blue River Res. and ridges to the south and west. Canopy coverage very discontinuous, from severe insolation blockage to no direct insolation blockage for every month of the year. Most blockage from canopy, not topography. Direct sun in late afternoon for every month.

DATES OF OPERATION: 4/70-7/95

SITE USED FOR MAPPING? no

SITE: RS02  
EASTING: 560513  
NORTHING: 4896132  
ELEV: 490  
SLOPE: 22  
ASPECT: 285

MODELED RADIATION REGIME:

	J	F	M	A	M	J	J	A	S	O	N	D
TOTAL RADIATION*	0.81	1.08	1.51	2.31	3.75	4.93	5.18	4.13	1.98	1.22	0.87	0.76
BLKD BY TOPO**	0.215	0.123	0.098	0.088	0.076	0.070	0.063	0.068	0.071	0.098	0.175	0.257
BLKD BY CANOPY**	0.687	0.790	0.829	0.828	0.775	0.754	0.757	0.779	0.854	0.833	0.738	0.647

\*DIFFUSE & DIRECT ON SLOPED SURFACE, MJ/m<sup>2</sup>.day  
(INCLUDING CLOUDINESS, TOPOGRAPHY, AND CANOPY)

\*\*PROPORTIONS OF TOTAL INCOMING RADIATION AT SURFACE

CANOPY: High/low mix, sparse forest, DISCONTINUOUS CANOPY TYPE; mostly closed, with two significant open areas.

SURFACE: Soft forest floor, thick low ferns and shrubs, amongst fallen tree trunks.

SENSOR: 1.0, 2.25 m mercury bulb thermometer and thermister shielded above with PVC.

GENERAL SITE CHARACTERISTICS:

In sparse forest of mixed-aged trees. Near total attenuation of direct radiation from Oct. through Feb. In summer, direct radiation just after midday for 2-3 hours.

DATES OF OPERATION: 5/70-present

SITE USED FOR MAPPING? no

SITE: RS03  
 EASTING: 567175  
 NORTHING: 4900777  
 ELEV: 945  
 SLOPE: 5  
 ASPECT: 315

MODELED RADIATION REGIME:

	J	F	M	A	M	J	J	A	S	O	N	D
TOTAL RADIATION*	0.37	0.60	0.85	1.43	2.53	2.38	2.61	2.86	1.28	0.70	0.44	0.38
BLKD BY TOPO**	0.060	0.054	0.047	0.042	0.037	0.029	0.029	0.031	0.034	0.047	0.062	0.080
BLKD BY CANOPY**	0.892	0.903	0.917	0.907	0.865	0.894	0.891	0.865	0.918	0.920	0.895	0.872

\*DIFFUSE & DIRECT ON SLOPED SURFACE, MJ/m<sup>2</sup>.day  
 (INCLUDING CLOUDINESS, TOPOGRAPHY, AND CANOPY)

\*\*PROPORTIONS OF TOTAL INCOMING RADIATION AT SURFACE

CANOPY: Shady, thick, low canopy. Much low evergreen vegetation. CONTINUOUS, CLOSED CANOPY TYPE.

SURFACE: Thick vegetation (grasses and shrubs), and fallen tree trunks.

SENSOR: 1.0 and 2.35 m mercury bulb thermometers.

GENERAL SITE CHARACTERISTICS:

Site is tucked away in thick grove in thick forest. Little direct sun except during mid-afternoon in summer. Site has very little topographic attenuation but great amount of canopy attenuation. Directly south just beyond near trees is a large clearing (edge effects?). Site is defunct; canopy photo a best estimate.

DATES OF OPERATION: 4/70-7/95

SITE USED FOR MAPPING? yes

SITE: RS04  
EASTING: 568985  
NORTHING: 4902368  
ELEV: 1310  
SLOPE: 27  
ASPECT: 270

MODELED RADIATION REGIME:

	J	F	M	A	M	J	J	A	S	O	N	D
TOTAL RADIATION*	0.68	1.07	1.52	1.97	2.73	3.63	4.01	2.59	2.00	1.40	0.72	0.63
BLKD BY TOPO**	0.151	0.124	0.096	0.076	0.087	0.060	0.067	0.067	0.086	0.121	0.118	0.173
BLKD BY CANOPY**	0.753	0.789	0.828	0.854	0.834	0.819	0.812	0.864	0.853	0.807	0.795	0.732

\*DIFFUSE & DIRECT ON SLOPED SURFACE, MJ/m<sup>2</sup>.day  
(INCLUDING CLOUDINESS, TOPOGRAPHY, AND CANOPY)

\*\*PROPORTIONS OF TOTAL INCOMING RADIATION AT SURFACE

CANOPY: High and sparse; CONTINUOUS, CLOSED CANOPY TYPE with some small clearings directly overhead.

SURFACE: Soft forest floor, pine needles and light vegetation.

SENSOR: Mercury bulb thermometers and open thermistors shielded above with PVC; varied in height from 1.0 to 4.0 m during period of operation.

GENERAL SITE CHARACTERISTICS:

Highest site in the HJ Andrews, facing due west on a steep slope. Little topographic attenuation. No significant periods of uninterrupted sunlight.

DATES OF OPERATION: 6/70-present

SITE USED FOR MAPPING? no

SITE: RS05  
EASTING: 563769  
NORTHING: 4896670  
ELEV: 880  
SLOPE: 12  
ASPECT: 10

MODELED RADIATION REGIME:

	J	F	M	A	M	J	J	A	S	O	N	D
TOTAL RADIATION*	0.65	0.70	0.97	1.89	2.66	2.61	2.79	3.02	1.88	0.86	0.61	0.73
BLKD BY TOPO**	0.127	0.043	0.027	0.021	0.023	0.019	0.019	0.016	0.020	0.035	0.077	0.212
BLKD BY CANOPY**	0.803	0.890	0.909	0.882	0.863	0.887	0.887	0.862	0.884	0.904	0.856	0.719

\*DIFFUSE & DIRECT ON SLOPED SURFACE, MJ/m<sup>2</sup>.day  
(INCLUDING CLOUDINESS, TOPOGRAPHY, AND CANOPY)

\*\*PROPORTIONS OF TOTAL INCOMING RADIATION AT SURFACE

CANOPY: Mixed high/medium height, sparse; CONTINUOUS, CLOSED CANOPY TYPE.

SURFACE: Soft forest floor, bed of pine needles and leaves.

SENSOR: 1.0, 2.0 m mercury bulb thermometer and thermister shielded above with PVC.

GENERAL SITE CHARACTERISTICS:

In sparse to moderate forest of mostly older trees, on a broad flat area on the north-facing side of Lookout Ridge. Virtually no topographic attenuation in summer, but shady site due almost exclusively to presence of canopy.

DATES OF OPERATION: 1/71-present

SITE USED FOR MAPPING? yes

SITE: RS07  
 EASTING: 560023  
 NORTHING: 4895655  
 ELEV: 460  
 SLOPE: 19  
 ASPECT: 1

MODELED RADIATION REGIME:

	J	F	M	A	M	J	J	A	S	O	N	D
TOTAL RADIATION*	0.71	0.86	1.13	1.71	2.39	2.32	2.31	2.31	1.46	0.99	0.78	0.57
BLKD BY TOPO**	0.230	0.115	0.067	0.053	0.050	0.041	0.038	0.038	0.050	0.094	0.209	0.201
BLKD BY CANOPY**	0.665	0.791	0.846	0.851	0.838	0.870	0.877	0.853	0.861	0.824	0.697	0.695

\*DIFFUSE & DIRECT ON SLOPED SURFACE, MJ/m<sup>2</sup>.day  
 (INCLUDING CLOUDINESS, TOPOGRAPHY, AND CANOPY)

\*\*PROPORTIONS OF TOTAL INCOMING RADIATION AT SURFACE

CANOPY: Low and dense; CONTINUOUS, CLOSED CANOPY TYPE.

SURFACE: Thick shrubs and ferns.

SENSOR: .65, 1.0 m mercury bulb thermometers and thermister shielded above with PVC.

GENERAL SITE CHARACTERISTICS:

Site is in a dense forest of mixed-aged trees, on a steep northwest-facing slope just above CS2MET. Canopy relatively open due north. Not far from Lookout Creek, so possible is susceptible to cold-air drainage issues.

DATES OF OPERATION: 5/70-present

SITE USED FOR MAPPING? yes

SITE: RS10  
 EASTING: 562474  
 NORTHING: 4897908  
 ELEV: 610  
 SLOPE: 6  
 ASPECT: 170

MODELED RADIATION REGIME:

	J	F	M	A	M	J	J	A	S	O	N	D
TOTAL RADIATION*	0.45	0.87	1.38	1.81	1.90	1.63	1.56	2.12	1.93	1.20	0.62	0.50
BLKD BY TOPO**	0.040	0.039	0.032	0.023	0.024	0.022	0.016	0.019	0.020	0.029	0.048	0.076
BLKD BY CANOPY**	0.878	0.870	0.875	0.889	0.902	0.929	0.937	0.906	0.888	0.876	0.862	0.842

\*DIFFUSE & DIRECT ON SLOPED SURFACE, MJ/m<sup>2</sup>.day  
 (INCLUDING CLOUDINESS, TOPOGRAPHY, AND CANOPY)

\*\*PROPORTIONS OF TOTAL INCOMING RADIATION AT SURFACE

CANOPY: Low, dense; CONTINUOUS, CLOSED CANOPY TYPE.

SURFACE: Mossy, soft bed of pine needles and decomposing logs.

SENSOR: 1.0, 1.9, 2.0 m mercury bulb thermometer and thermister shielded above with PVC.

GENERAL SITE CHARACTERISTICS:

In thick forest of mostly young-middle-aged trees, low canopy. Very little radiation ever reaches site; canopy very thick. On a south-facing slope. Virtually no topographic shading during any months.

DATES OF OPERATION: 4/71-present

SITE USED FOR MAPPING? yes

SITE: RS12  
EASTING: 570409  
NORTHING: 4897130  
ELEV: 1007  
SLOPE: 11  
ASPECT: 282

MODELED RADIATION REGIME:

	J	F	M	A	M	J	J	A	S	O	N	D
TOTAL RADIATION*	0.76	1.27	1.83	2.70	3.63	4.29	4.42	4.00	2.74	1.51	0.90	0.69
BLKD BY TOPO**	0.210	0.186	0.141	0.116	0.116	0.109	0.096	0.095	0.103	0.134	0.201	0.220
BLKD BY CANOPY**	0.733	0.763	0.807	0.810	0.787	0.791	0.801	0.804	0.823	0.816	0.748	0.724

\*DIFFUSE & DIRECT ON SLOPED SURFACE, MJ/m<sup>2</sup>.day  
(INCLUDING CLOUDINESS, TOPOGRAPHY, AND CANOPY)

\*\*PROPORTIONS OF TOTAL INCOMING RADIATION AT SURFACE

CANOPY: Sparse and high; CONTINUOUS, CLOSED CANOPY TYPE

SURFACE: Sparse small bushes and grass.

SENSOR: 1.0 to 3.0 m mercury bulb thermometers and thermister shielded above with PVC.

GENERAL SITE CHARACTERISTICS:

In a moderate forest of middle to older-aged trees. Near Lookout Creek at its upper reaches, just uphill from TSLOOK; susceptible to cold-air drainage. Significant topographic attenuation during winter months. In summer, direct radiation briefly during mid-afternoon.

DATES OF OPERATION: 7/71-present

SITE USED FOR MAPPING? no

SITE: RS15  
 EASTING: 560821  
 NORTHING: 4895184  
 ELEV: 760  
 SLOPE: 33  
 ASPECT: 350

MODELED RADIATION REGIME:

	J	F	M	A	M	J	J	A	S	O	N	D
TOTAL RADIATION*	0.53	0.97	1.25	1.56	2.28	2.44	2.45	2.13	1.35	1.09	0.68	0.47
BLKD BY TOPO**	0.568	0.326	0.188	0.110	0.100	0.078	0.070	0.073	0.111	0.246	0.514	0.548
BLKD BY CANOPY**	0.356	0.606	0.754	0.822	0.801	0.832	0.839	0.828	0.827	0.700	0.418	0.377

\*DIFFUSE & DIRECT ON SLOPED SURFACE, MJ/m<sup>2</sup>.day  
 (INCLUDING CLOUDINESS, TOPOGRAPHY, AND CANOPY)

\*\*PROPORTIONS OF TOTAL INCOMING RADIATION AT SURFACE

CANOPY: Sparse and high; CONTINUOUS, CLOSED CANOPY TYPE.

SURFACE: Soft bed of pine needles and decaying logs.

SENSOR: 1.0, 1.8 m mercury bulb thermometers.

GENERAL SITE CHARACTERISTICS:

Site is on a very steep north-facing slope; great solar attenuation in winter due to topographic shading to south. Midday in summer site receives the most direct insolation of the year. Site is defunct; canopy photos a best estimate.

DATES OF OPERATION: 7/72-10/94

SITE USED FOR MAPPING? no

SITE: RS16  
 EASTING: 560694  
 NORTHING: 4895527  
 ELEV: 640  
 SLOPE: 29  
 ASPECT: 202

MODELED RADIATION REGIME:

	J	F	M	A	M	J	J	A	S	O	N	D
TOTAL RADIATION*	0.78	1.10	1.85	2.65	2.52	2.67	2.46	2.90	2.97	1.75	0.96	0.72
BLKD BY TOPO**	0.316	0.180	0.143	0.112	0.111	0.113	0.090	0.098	0.109	0.166	0.305	0.416
BLKD BY CANOPY**	0.635	0.773	0.782	0.795	0.836	0.856	0.879	0.845	0.789	0.758	0.649	0.535

\*DIFFUSE & DIRECT ON SLOPED SURFACE, MJ/m<sup>2</sup>.day  
 (INCLUDING CLOUDINESS, TOPOGRAPHY, AND CANOPY)

\*\*PROPORTIONS OF TOTAL INCOMING RADIATION AT SURFACE

CANOPY: Low, dense; CONTINUOUS, CLOSED CANOPY TYPE.

SURFACE: Fallen logs and thick vegetation (rhododendron bushes).

SENSOR: 1.0, 1.8 m mercury bulb thermometers.

GENERAL SITE CHARACTERISTICS:

Site is on a steep west-facing slope; receives direct solar radiation mid-mornings in spring and fall. Vegetation is thick and mixture of rhododendrons and evergreens.

Site is defunct; canopy photos a best estimate. Extremely unsure of fisheye photo accuracy.

DATES OF OPERATION: 7/72-10/94

SITE USED FOR MAPPING? no

SITE: RS17  
EASTING: 560767  
NORTHING: 4896468  
ELEV: 490  
SLOPE: 14  
ASPECT: 315

MODELED RADIATION REGIME:

	J	F	M	A	M	J	J	A	S	O	N	D
TOTAL RADIATION*	0.61	0.89	1.40	2.21	2.89	3.20	3.26	3.03	2.10	1.09	0.66	0.58
BLKD BY TOPO**	0.103	0.075	0.066	0.040	0.039	0.034	0.030	0.031	0.042	0.064	0.092	0.134
BLKD BY CANOPY**	0.794	0.834	0.843	0.842	0.834	0.848	0.853	0.841	0.843	0.849	0.817	0.765

\*DIFFUSE & DIRECT ON SLOPED SURFACE, MJ/m<sup>2</sup>.day  
(INCLUDING CLOUDINESS, TOPOGRAPHY, AND CANOPY)

\*\*PROPORTIONS OF TOTAL INCOMING RADIATION AT SURFACE

CANOPY: High, sparse; CONTINUOUS, CLOSED CANOPY TYPE with one significant opening directly overhead.

SURFACE: Soft forest floor, pine needles and ferns.

SENSOR: .6, 1.0 m mercury bulb thermometers.

GENERAL SITE CHARACTERISTICS:

Site is on northwest-facing slope not far from Lookout Creek; cold-air drainage may affect temperature regimes. In a thick forest with high canopy, sparse to the west.  
Site is defunct; canopy photo a best estimate. Unsure of fisheye photo accuracy.

DATES OF OPERATION: 6/72-7/95

SITE USED FOR MAPPING? yes

SITE: RS20  
 EASTING: 559997  
 NORTHING: 4896597  
 ELEV: 683  
 SLOPE: 34  
 ASPECT: 180

MODELED RADIATION REGIME:

	J	F	M	A	M	J	J	A	S	O	N	D
TOTAL RADIATION*	0.43	0.79	1.55	2.85	3.17	3.38	3.68	4.00	3.42	1.41	0.54	0.41
BLKD BY TOPO**	0.029	0.027	0.024	0.019	0.022	0.018	0.016	0.015	0.018	0.024	0.028	0.042
BLKD BY CANOPY**	0.871	0.872	0.849	0.810	0.818	0.836	0.836	0.812	0.798	0.849	0.871	0.858

\*DIFFUSE & DIRECT ON SLOPED SURFACE, MJ/m<sup>2</sup>.day  
 (INCLUDING CLOUDINESS, TOPOGRAPHY, AND CANOPY)

\*\*PROPORTIONS OF TOTAL INCOMING RADIATION AT SURFACE

CANOPY: Low and sparse; DISCONTINUOUS CANOPY TYPE.

SURFACE: Pine needles, dirt, and sticks.

SENSOR: 1.0, 2.2 m mercury bulb thermometers and thermister shielded above with PVC.

GENERAL SITE CHARACTERISTICS:

On a steep south-facing slope near the top of the lower Blue River Ridge. Sparse and discontinuous canopy to east, south, and west. Though canopy is thin, attenuation due to it is significant; very little topographic attenuation due to position near top of ridge. In a moderate forest of young to middle-aged evergreens.

DATES OF OPERATION: 1/79-present

SITE USED FOR MAPPING? yes

SITE: RS26  
 EASTING: 565992  
 NORTHING: 4901852  
 ELEV: 1040  
 SLOPE: 20  
 ASPECT: 180

MODELED RADIATION REGIME:

	J	F	M	A	M	J	J	A	S	O	N	D
TOTAL RADIATION*	0.58	1.12	2.16	2.71	3.13	3.28	3.50	3.71	3.07	1.94	0.78	0.53
BLKD BY TOPO**	0.031	0.025	0.027	0.020	0.020	0.019	0.016	0.015	0.017	0.023	0.030	0.039
BLKD BY CANOPY**	0.834	0.826	0.798	0.826	0.828	0.848	0.851	0.832	0.823	0.798	0.821	0.827

\*DIFFUSE & DIRECT ON SLOPED SURFACE, MJ/m<sup>2</sup>.day  
 (INCLUDING CLOUDINESS, TOPOGRAPHY, AND CANOPY)

\*\*PROPORTIONS OF TOTAL INCOMING RADIATION AT SURFACE

CANOPY: High, thick; CONTINUOUS, CLOSED CANOPY TYPE, though thin to south.

SURFACE: Pine needles, sticks, small plants.

SENSOR: 1.0, 2.0 m mercury bulb thermometers and thermister shielded above with PVC.

GENERAL SITE CHARACTERISTICS:

In thick forest of young, middle, and old-aged trees. On a slope facing due south, with very little topographic attenuation throughout the year.

DATES OF OPERATION: 1/78-present

SITE USED FOR MAPPING? yes

SITE: RS38  
EASTING: 565480  
NORTHING: 4901379  
ELEV: 977  
SLOPE: 15  
ASPECT: 170

MODELED RADIATION REGIME:

	J	F	M	A	M	J	J	A	S	O	N	D
TOTAL RADIATION*	0.61	1.23	2.55	3.90	3.75	3.50	3.76	4.38	4.45	2.31	0.84	0.60
BLKD BY TOPO**	0.034	0.040	0.030	0.027	0.028	0.021	0.022	0.020	0.024	0.034	0.038	0.060
BLKD BY CANOPY**	0.830	0.807	0.761	0.752	0.797	0.841	0.842	0.803	0.742	0.758	0.809	0.805

\*DIFFUSE & DIRECT ON SLOPED SURFACE, MJ/m<sup>2</sup>.day  
(INCLUDING CLOUDINESS, TOPOGRAPHY, AND CANOPY)

\*\*PROPORTIONS OF TOTAL INCOMING RADIATION AT SURFACE

CANOPY: Thin, low; CONTINUOUS, CLOSED CANOPY TYPE, though site used to be clear-cut.

SURFACE: Leaves, shrubs, and dirt.

SENSOR: 1.0 m mercury bulb thermometers and thermister shielded above with PVC.

GENERAL SITE CHARACTERISTICS:

Site is in south-facing slope amongst young dense evergreen forest. Historically an unusually warm site due to thin low canopy, southern exposure, and fact that it used to be clear-cut (has since grown back). Canopy appears to act as a sort of magnifier of solar radiation, keeping site inordinately warm.

DATES OF OPERATION: 6/75-present

SITE USED FOR MAPPING? no

SITE: RS86  
EASTING: 559377  
NORTHING: 4896330  
ELEV: 653  
SLOPE: 28  
ASPECT: 215

MODELED RADIATION REGIME:

	J	F	M	A	M	J	J	A	S	O	N	D
TOTAL RADIATION*	1.58	3.14	6.03	9.05	9.11	8.93	9.70	11.53	10.74	5.45	2.09	1.42
BLKD BY TOPO**	0.018	0.024	0.024	0.016	0.021	0.016	0.015	0.013	0.021	0.022	0.030	0.033
BLKD BY CANOPY**	0.432	0.395	0.319	0.313	0.413	0.521	0.523	0.394	0.268	0.306	0.389	0.414

\*DIFFUSE & DIRECT ON SLOPED SURFACE, MJ/m<sup>2</sup>.day  
(INCLUDING CLOUDINESS, TOPOGRAPHY, AND CANOPY)

\*\*PROPORTIONS OF TOTAL INCOMING RADIATION AT SURFACE

CANOPY: Open site except for bushy deciduous tree directly overhead and to east; CONTINUOUS, OPEN CANOPY TYPE.

SURFACE: Fallen leaves and dirt.

SENSOR: 1.0, 1.6, 2.35 m mercury bulb thermometers and thermister shielded above with PVC.

GENERAL SITE CHARACTERISTICS:

Site located at the top of large clear-cut, almost completely open to south. On a southwest-facing slope near the top of lower Blue River Ridge. Horizon and distant ridges clearly visible from east-south-west. Direct insolation blocked until noon in summer due to fact that sensor is located directly to the west of tall bushy deciduous tree. Almost no topographic attenuation; virtually all blockage of insolation due to canopy and surrounding trees.

DATES OF OPERATION: 9/75-present

SITE USED FOR MAPPING? no

SITE: RS89  
 EASTING: 559227  
 NORTHING: 4896106  
 ELEV: 475  
 SLOPE: 37  
 ASPECT: 315

MODELED RADIATION REGIME:

	J	F	M	A	M	J	J	A	S	O	N	D
TOTAL RADIATION*	0.59	0.94	1.58	3.02	3.28	3.88	4.09	3.49	2.83	1.27	0.73	0.50
BLKD BY TOPO**	0.246	0.207	0.183	0.166	0.135	0.120	0.114	0.114	0.141	0.192	0.305	0.251
BLKD BY CANOPY**	0.656	0.706	0.719	0.662	0.717	0.729	0.733	0.732	0.677	0.715	0.607	0.652

\*DIFFUSE & DIRECT ON SLOPED SURFACE, MJ/m<sup>2</sup>.day  
 (INCLUDING CLOUDINESS, TOPOGRAPHY, AND CANOPY)

\*\*PROPORTIONS OF TOTAL INCOMING RADIATION AT SURFACE

CANOPY: Low, thick evergreen ; CONTINUOUS, CLOSED CANOPY TYPE.

SURFACE: Very bushy vegetation.

SENSOR: .85, 1.0, 2.85 m mercury bulb thermometers and thermister shielded above with PVC.

GENERAL SITE CHARACTERISTICS:

Site is located near bottom of narrow east-west gully with small creek. On a very steep north-facing slope. Just beyond near trees to north and west is a large open area. Site receives direct sun late on summer afternoons. Historical temperature trends appear unusually high. Just uphill from GSWS10. Dark and shady every morning of year until noon.

DATES OF OPERATION: 9/75-present

SITE USED FOR MAPPING? no

SITE: GSLOOK  
EASTING: 559438  
NORTHING: 4895195  
ELEV: 436  
SLOPE: 1  
ASPECT: 230

MODELED RADIATION REGIME:

	J	F	M	A	M	J	J	A	S	O	N	D
TOTAL RADIATION*	0.92	1.51	2.15	2.75	3.42	4.83	4.88	3.71	2.90	1.84	1.11	0.85
BLKD BY TOPO**	0.239	0.214	0.160	0.120	0.104	0.109	0.089	0.092	0.131	0.164	0.247	0.278
BLKD BY CANOPY**	0.682	0.714	0.770	0.810	0.808	0.770	0.786	0.818	0.803	0.768	0.681	0.643

\*DIFFUSE & DIRECT ON SLOPED SURFACE, MJ/m<sup>2</sup>.day  
(INCLUDING CLOUDINESS, TOPOGRAPHY, AND CANOPY)

\*\*PROPORTIONS OF TOTAL INCOMING RADIATION AT SURFACE

CANOPY: Low, deciduous; CONTINUOUS, CLOSED CANOPY TYPE.

SURFACE: On edge of wide stream bed, water/rocks/leaves.

SENSOR: Thermister shielded above with PVC.

GENERAL SITE CHARACTERISTICS:

Site is over lower Lookout Creek, next to deep pool. Forest clearing for creek 5-10 m wide, oriented northeast-southwest. Though site is under continuous canopy, is immediately adjacent to large clearing. Most direct sun from early to mid-afternoon throughout year. Susceptible to cold-air drainage and stream effects.

DATES OF OPERATION: 03/95-present

SITE USED FOR MAPPING? no

SITE: GSMACK  
EASTING: 566590  
NORTHING: 4896416  
ELEV: 756  
SLOPE: 7  
ASPECT: 350

MODELED RADIATION REGIME:

	J	F	M	A	M	J	J	A	S	O	N	D
TOTAL RADIATION*	1.68	2.87	5.23	8.49	10.41	12.79	13.62	11.87	8.73	4.38	2.00	1.43
BLKD BY TOPO**	0.341	0.228	0.168	0.122	0.104	0.086	0.078	0.093	0.128	0.200	0.252	0.410
BLKD BY CANOPY**	0.293	0.419	0.413	0.393	0.400	0.395	0.395	0.399	0.378	0.385	0.396	0.227

\*DIFFUSE & DIRECT ON SLOPED SURFACE, MJ/m<sup>2</sup>.day  
(INCLUDING CLOUDINESS, TOPOGRAPHY, AND CANOPY)

\*\*PROPORTIONS OF TOTAL INCOMING RADIATION AT SURFACE

CANOPY: None directly overhead, though radiation heavily affected by surrounding trees. CONTINUOUS, OPEN CANOPY TYPE.

SURFACE: Sensor directly over large deep pool.

SENSOR: Thermister shielded above with PVC.

GENERAL SITE CHARACTERISTICS:

Stream site halfway up Mack Creek watershed. Sensor is high above water level of deep, large pool. Canopy plays more of a role in radiation attenuation than topography for all months except December and January. Susceptible to cold-air drainage and stream effects.

DATES OF OPERATION: 8/87-present

SITE USED FOR MAPPING? no

SITE: GSWS02  
 EASTING: 560444  
 NORTHING: 4895513  
 ELEV: 561  
 SLOPE: 13  
 ASPECT: 340

MODELED RADIATION REGIME:

	J	F	M	A	M	J	J	A	S	O	N	D
TOTAL RADIATION*	0.98	1.65	2.14	3.09	4.30	6.17	6.39	4.32	2.93	1.95	1.21	0.89
BLKD BY TOPO**	0.588	0.276	0.170	0.127	0.123	0.115	0.100	0.094	0.131	0.227	0.547	0.573
BLKD BY CANOPY**	0.288	0.614	0.739	0.762	0.732	0.683	0.694	0.764	0.768	0.687	0.343	0.305

\*DIFFUSE & DIRECT ON SLOPED SURFACE, MJ/m<sup>2</sup>.day  
 (INCLUDING CLOUDINESS, TOPOGRAPHY, AND CANOPY)

\*\*PROPORTIONS OF TOTAL INCOMING RADIATION AT SURFACE

CANOPY: Open above, solid elsewhere. DISCONTINUOUS CANOPY TYPE.

SURFACE: Water, ferns, moss, concrete (gaging station).

SENSOR: Thermister shielded above with PVC.

GENERAL SITE CHARACTERISTICS:

Site is a gaging station above CS2MET. Directly above site canopy is open, but solid walls of trees to north and south. Large clearing and pool/road to south; stream clearing narrow. Only significant direct sun late morning spring/summer. Susceptible to cold-air drainage, stream effects.

DATES OF OPERATION: 6/95-present

SITE USED FOR MAPPING? no

SITE: GR4C  
EASTING: 570404  
NORTHING: 4895251  
ELEV: 1268  
SLOPE: 13  
ASPECT: 60

MODELED RADIATION REGIME:

	J	F	M	A	M	J	J	A	S	O	N	D
TOTAL RADIATION*	0.61	0.81	1.17	1.78	2.95	3.93	4.19	3.13	1.64	0.97	0.66	0.54
BLKD BY TOPO**	0.125	0.074	0.054	0.043	0.041	0.035	0.033	0.034	0.042	0.059	0.108	0.129
BLKD BY CANOPY**	0.785	0.844	0.868	0.870	0.828	0.810	0.808	0.834	0.876	0.866	0.810	0.782

\*DIFFUSE & DIRECT ON SLOPED SURFACE, MJ/m<sup>2</sup>.day  
(INCLUDING CLOUDINESS, TOPOGRAPHY, AND CANOPY)

\*\*PROPORTIONS OF TOTAL INCOMING RADIATION AT SURFACE

CANOPY: High, DISCONTINUOUS CANOPY TYPE.

SURFACE: Thick ferns, plants, limbs.

SENSOR: Mercury bulb thermometer.

GENERAL SITE CHARACTERISTICS:

Site located near UPLMET in thick forest, near small clearings with discontinuous canopy. One of 5 sites operated for Bob Griffith study in early-mid 90s. On east-facing slope, with most direct radiation coming from that direction in early morning. Precise location of site unknown; canopy image a best guess. Sensor characteristics unknown.

DATES OF OPERATION: 11/92-9/95

SITE USED FOR MAPPING? no

SITE: GR8C  
 EASTING: 560999  
 NORTHING: 4897637  
 ELEV: 756  
 SLOPE: 25  
 ASPECT: 135

MODELED RADIATION REGIME:

	J	F	M	A	M	J	J	A	S	O	N	D
TOTAL RADIATION*	0.59	1.06	1.83	2.57	3.29	3.18	3.27	3.69	2.75	1.52	0.73	0.53
BLKD BY TOPO**	0.061	0.058	0.058	0.049	0.051	0.054	0.048	0.038	0.052	0.051	0.058	0.063
BLKD BY CANOPY**	0.814	0.817	0.813	0.822	0.809	0.845	0.853	0.821	0.825	0.823	0.817	0.812

\*DIFFUSE & DIRECT ON SLOPED SURFACE, MJ/m<sup>2</sup>.day  
 (INCLUDING CLOUDINESS, TOPOGRAPHY, AND CANOPY)

\*\*PROPORTIONS OF TOTAL INCOMING RADIATION AT SURFACE

CANOPY: Low, both young and old trees; CONTINUOUS, CLOSED CANOPY TYPE.

SURFACE: Decomposing logs, twigs, few plants.

SENSOR: Mercury bulb thermometer.

GENERAL SITE CHARACTERISTICS:

Site fairly isolated from others in thick forest, on south-facing slope just on south side of Blue River Ridge crest. One of 5 sites operated for Bob Griffith study in early-mid 90s. Little topographic shading of radiation throughout year; almost all canopy shading. Precise location of site unknown; canopy image a best guess. Sensor characteristics unknown.

DATES OF OPERATION: 11/92-9/95

SITE USED FOR MAPPING? no

SITE: GRT1  
 EASTING: 567437  
 NORTHING: 4902252  
 ELEV: 1277  
 SLOPE: 12  
 ASPECT: 190

MODELED RADIATION REGIME:

	J	F	M	A	M	J	J	A	S	O	N	D
TOTAL RADIATION*	0.36	0.52	0.85	1.45	2.09	2.71	2.88	2.36	1.46	0.72	0.38	0.29
BLKD BY TOPO**	0.028	0.018	0.021	0.017	0.016	0.014	0.011	0.012	0.013	0.022	0.023	0.024
BLKD BY CANOPY**	0.908	0.924	0.925	0.912	0.893	0.883	0.884	0.898	0.918	0.927	0.918	0.913

\*DIFFUSE & DIRECT ON SLOPED SURFACE, MJ/m<sup>2</sup>.day  
 (INCLUDING CLOUDINESS, TOPOGRAPHY, AND CANOPY)

\*\*PROPORTIONS OF TOTAL INCOMING RADIATION AT SURFACE

CANOPY: High and thick; CONTINUOUS, CLOSED CANOPY TYPE.

SURFACE: Soft forest floor, twigs, needles, fallen timber.

SENSOR: Mercury bulb thermometer.

GENERAL SITE CHARACTERISTICS:

Site located near VANMET on southwest side of Carpenter Mountain. On south-facing slope, but with heavy canopy coverage; one of the most topographically open sites in the HJ Andrews. One of 5 sites operated for Bob Griffith study in early-mid 90s. Precise location of site unknown; canopy image a best guess. Sensor characteristics unknown.

DATES OF OPERATION: 11/92-9/95

SITE USED FOR MAPPING? no

SITE: GRVC  
 EASTING: 566366  
 NORTHING: 4896704  
 ELEV: 805  
 SLOPE: 17  
 ASPECT: 90

MODELED RADIATION REGIME:

	J	F	M	A	M	J	J	A	S	O	N	D
TOTAL RADIATION*	0.65	0.99	1.38	1.62	1.89	2.12	2.09	1.79	1.54	1.15	0.71	0.85
BLKD BY TOPO**	0.110	0.089	0.069	0.050	0.044	0.037	0.033	0.036	0.052	0.072	0.097	0.280
BLKD BY CANOPY**	0.796	0.827	0.858	0.890	0.896	0.902	0.910	0.912	0.895	0.858	0.819	0.627

\*DIFFUSE & DIRECT ON SLOPED SURFACE, MJ/m<sup>2</sup>.day  
 (INCLUDING CLOUDINESS, TOPOGRAPHY, AND CANOPY)

\*\*PROPORTIONS OF TOTAL INCOMING RADIATION AT SURFACE

CANOPY: High, DISONCONTINUOUS CANOPY TYPE. Fairly open and thin to north.

SURFACE: Thick bushes and other vegetation.

SENSOR: Mercury bulb thermometer.

GENERAL SITE CHARACTERISTICS:

Site located on west side of Mack Creek drainage near GSMACK gaging station. Significant topographic radiation shading in winter but very little in summer. One of 5 sites operated for Bob Griffith study in early-mid 90s. Precise location of site unknown; canopy image a best guess. Sensor characteristics unknown.

DATES OF OPERATION: 11/92-9/95

SITE USED FOR MAPPING? no

SITE: TSLOMA  
EASTING: 566547  
NORTHING: 4897293  
ELEV: 652  
SLOPE: 0  
ASPECT: -

MODELED RADIATION REGIME:

	J	F	M	A	M	J	J	A	S	O	N	D
TOTAL RADIATION*	0.93	1.63	2.66	3.53	4.09	3.22	3.15	4.58	3.69	2.43	1.29	0.78
BLKD BY TOPO**	0.156	0.131	0.096	0.067	0.055	0.049	0.041	0.043	0.066	0.123	0.205	0.142
BLKD BY CANOPY**	0.716	0.729	0.742	0.774	0.783	0.857	0.870	0.792	0.776	0.716	0.656	0.731

\*DIFFUSE & DIRECT ON SLOPED SURFACE, MJ/m<sup>2</sup>.day  
(INCLUDING CLOUDINESS, TOPOGRAPHY, AND CANOPY)

\*\*PROPORTIONS OF TOTAL INCOMING RADIATION AT SURFACE

CANOPY: One deciduous tree overhead, otherwise open; DISCONTINUOUS, OPEN CANOPY TYPE.

SURFACE: Water, rocks, moss.

SENSOR: 3.5m thermister shielded above with PVC.

GENERAL SITE CHARACTERISTICS:

Stream site at confluence of Lookout and Mack Creeks. Site is on east edge of large open clearing, so is hemmed in by thick canopy wall in that direction. Directly above is deciduous tree which is bushy in summer (affects radiation regime) and bare in winter. Sensor receives direct sun throughout year in early-mid afternoon. Due to location at confluence of two major streams, temperature regime likely strongly influenced by cold-air drainage and stream effects.

DATES OF OPERATION: 5/95-present

SITE USED FOR MAPPING? no

SITE: TSLOOK  
 EASTING: 570293  
 NORTHING: 4897091  
 ELEV: 988  
 SLOPE: 5  
 ASPECT: 315

MODELED RADIATION REGIME:

	J	F	M	A	M	J	J	A	S	O	N	D
TOTAL RADIATION*	0.89	1.44	1.79	2.32	2.65	3.46	3.64	2.84	2.37	1.79	1.07	0.78
BLKD BY TOPO**	0.288	0.250	0.158	0.120	0.107	0.099	0.096	0.098	0.123	0.208	0.291	0.292
BLKD BY CANOPY**	0.673	0.715	0.809	0.841	0.852	0.838	0.841	0.861	0.840	0.760	0.675	0.670

\*DIFFUSE & DIRECT ON SLOPED SURFACE, MJ/m<sup>2</sup>.day  
 (INCLUDING CLOUDINESS, TOPOGRAPHY, AND CANOPY)

\*\*PROPORTIONS OF TOTAL INCOMING RADIATION AT SURFACE

CANOPY: High, thick; CONTINUOUS, CLOSED CANOPY TYPE.

SURFACE: Wet, mossy rocks.

SENSOR: 1.0, 2.4 m mercury bulb thermometers and thermister shielded above with PVC.

GENERAL SITE CHARACTERISTICS:

Stream site in upper Lookout Creek Basin. Cold, shady site, radiation topographically blocked year-round to east, southwest and west. Very little direct radiation reaches sensor. Since site is over stream, susceptible to cold-air drainage and stream effects.

DATES OF OPERATION: 1/77-present

SITE USED FOR MAPPING? no

SITE: TSMACK  
EASTING: 566697  
NORTHING: 4896231  
ELEV: 780  
SLOPE: 7  
ASPECT: 330

MODELED RADIATION REGIME:

	J	F	M	A	M	J	J	A	S	O	N	D
TOTAL RADIATION*	1.16	1.76	2.72	4.43	4.57	5.01	5.23	4.91	4.53	2.20	1.38	0.99
BLKD BY TOPO**	0.448	0.244	0.214	0.171	0.146	0.123	0.118	0.125	0.167	0.200	0.412	0.521
BLKD BY CANOPY**	0.443	0.654	0.688	0.675	0.731	0.759	0.765	0.752	0.676	0.707	0.487	0.371

\*DIFFUSE & DIRECT ON SLOPED SURFACE, MJ/m<sup>2</sup>.day  
(INCLUDING CLOUDINESS, TOPOGRAPHY, AND CANOPY)

\*\*PROPORTIONS OF TOTAL INCOMING RADIATION AT SURFACE

CANOPY: High, mostly old trees; CONTINUOUS, CLOSED CANOPY TYPE.

SURFACE: Water, mossy rocks.

SENSOR: 1.0, 2.0 m mercury bulb thermometers.

GENERAL SITE CHARACTERISTICS:

Site located just upstream from gaging station GSMACK, over Mack Creek. Canopy continuous but thin relative to other canopied sites in the HJ Andrews. Radiation highly blocked by topography during winter months; this section of Mack Creek watershed narrow and steep. Site no longer operational so canopy image a best guess. Likely susceptible to cold-air drainage and stream effects.

DATES OF OPERATION: 8/76-9/95

SITE USED FOR MAPPING? no

SITE: TSMCRA  
 EASTING: 566568  
 NORTHING: 4900583  
 ELEV: 829  
 SLOPE: 3  
 ASPECT: 225

MODELED RADIATION REGIME:

	J	F	M	A	M	J	J	A	S	O	N	D
TOTAL RADIATION*	1.28	1.67	2.47	3.73	5.13	5.59	5.85	5.60	3.68	2.13	1.25	1.10
BLKD BY TOPO**	0.272	0.108	0.090	0.066	0.064	0.054	0.050	0.049	0.066	0.101	0.142	0.249
BLKD BY CANOPY**	0.534	0.720	0.756	0.756	0.723	0.749	0.755	0.738	0.766	0.749	0.686	0.557

\*DIFFUSE & DIRECT ON SLOPED SURFACE, MJ/m<sup>2</sup>.day  
 (INCLUDING CLOUDINESS, TOPOGRAPHY, AND CANOPY)

\*\*PROPORTIONS OF TOTAL INCOMING RADIATION AT SURFACE

CANOPY: Thin, high, at base of old pine tree; otherwise open; DISCONTINUOUS, OPEN SITE.

SURFACE: Water, mossy rocks.

SENSOR: 1.0, 2.0 m mercury bulb thermometer and thermister shielded above with PVC.

GENERAL SITE CHARACTERISTICS:

Site located over McRae Creek. Directly above is thin canopy from old pine tree, but site is open. On east side of creek, so thick wall of trees to east, open all other directions. Susceptible to cold-air drainage and stream effects.

DATES OF OPERATION: 8/76-present

SITE USED FOR MAPPING? no